Maintenance of the root stem cell niche homeostasis through the formation of transcription factor complexes in *Arabidopsis thaliana*

Inaugural-Dissertation

zur Erlangung des Doktorgrades
der Mathematisch-Naturwissenschaftlichen Fakultät
der Heinrich-Heine-Universität Düsseldorf

vorgelegt von

Rebecca Burkart (geb. Drisch)
aus Heidelberg

Düsseldorf, Oktober 2020

aus dem Institut für Entwicklungsgenetik
der Heinrich-Heine-Universität Düsseldorf

Gedruckt mit der Genehmigung der
Mathematisch-Naturwissenschaftlichen Fakultät der
Heinrich-Heine-Universität Düsseldorf

Berichterstatter:

1. PD Dr. Yvonne Stahl

2. Prof. Georg Groth

Tag der mündlichen Prüfung: 07.12.2020

Eidesstaatliche Erklärung

Eidesstattliche Erklärung zur Dissertation mit dem Titel:

„Maintenance of the root stem cell niche homeostasis through the formation of transcription factor complexes in *Arabidopsis thaliana*"

Ich versichere an Eides statt, dass die Dissertation von mir selbständig und ohne unzulässige fremde Hilfe unter Beachtung der „Grundsätze zur Sicherung guter wissenschaftlicher Praxis an der Heinrich-Heine-Universität Düsseldorf" erstellt worden ist. Außerdem versichere ich, dass ich diese Dissertation nur in diesem und keinem anderen Promotionsverfahren eingereicht habe und dass diesem Promotionsverfahren kein gescheitertes Promotionsverfahren vorausgegangen ist.

Düsseldorf, 30.3.2020

Ort, Datum

Unterschrift

Content

Eidesstaatliche Erklärung ... 3
Content ... 4
Aims of this study ... 7
I. Function and regulation of transcription factors involved in root apical meristem and stem cell maintenance ... 9
II. Dynamic complexity: plant receptor complexes at the plasma membrane ... 18
III. Precise transcriptional control of cellular quiescence by BRAVO/WOX5 complex in Arabidopsis roots ... 26
1. Summary ... 27
2. Keywords ... 27
3. Introduction ... 27
4. Results ... 28
4.1 BRAVO and WOX5 control QC division and lateral root density ... 28
4.2 *BRAVO* and *WOX5* reinforce each other at the root stem cell niche ... 30
4.3 *WOX5* induces *BRAVO*, which alleviates *WOX5* self-inhibition ... 32
4.4 BRAVO and WOX5 directly interact forming a transcriptional complex ... 35
4.5 BRAVO-WOX5 complex is relevant for the control of QC divisions ... 36
5. Discussion ... 38
6. Acknowledgments ... 41
7. Methods ... 42
7.1 Plant Material and Root Measurement ... 42
7.2 Confocal Microscopy and Quantification of Fluorescence Signal ... 42
7.3 RT-qPCR assay ... 43
7.4 Yeast two-hybrid assay ... 43
7.5 Transient expression in *Nicotiana benthamiana* for FLIM measurements ... 43
7.6 Acquisition of FLIM data ... 43
7.7 Analyses and presentation of FLIM data ... 44
7.8 Bimolecular fluorescence complementation assay (BiFC) ... 44
7.9 Mathematical model of BRAVO and WOX5 effective regulations ... 44
8. References ... 51
9. Supplementary information ... 54
9.1 Supplementary figures ... 54
9.2 Supplementary tables ... 61
9.3 Supplementary text ... 63
IV. PLETHORA and WOX5 interaction and subnuclear localisation regulates *Arabidopsis* root stem cell maintenance ... 66

1. Abstract 67
2. Introduction 67
3. Results 68
4. Discussion 82
5. Methods 85
   5.1 Cloning 85
   5.2 plant work 86
   5.3 Cell wall and plasma membrane staining 86
   5.4 *N. benthamiana* infiltration 86
   5.5 SCN staining 87
   5.6 RNA staining 88
   5.7 Microscopy 88
   5.8 Image deconvolution 89
   5.9 Analyses of expression patterns and levels in *Arabidopsis* 89
   5.10 FLIM measurements 89
   5.11 Correlation of PLT3-NBs and PLT3-mVenus fluorescence intensity 90
   5.12 Prediction of protein domains 91
   5.13 Figure assembly 91
6. References 92
7. Supplementary information 96
   7.1 Supplementary figures 96
   7.2 Supplementary movie 101
   7.3 Supplementary tables 102

V. A novel role for EARLY FLOWERING 3 (ELF3) links circadian/light signalling and root stem cell maintenance by microdomain formation 110

1. Abstract 111
2. Introduction 111
3. Results 113
   3.1 *PLT3* and *ELF3* are both expressed in the RAM of *Arabidopsis thaliana* .. 113
   3.2 *plt3* and *elf3* mutants show defects in the *Arabidopsis* root stem cell niche (SCN) 115
   3.3 PLT3 and ELF3 proteins co-localise upon co-expression 118
   3.4 ELF3 and PLT3 localise to bodies with different behaviour 123
   3.5 ELF3 and PLT3 interaction is mediated by the PrDs 125
   3.6 PIFs as mediators for ELF3 translocation and PLT3-ELF3 complex formation 127
   3.7 PIF3 and PIF4 co-localise and interact with PLT3 *in planta* 129
4. Discussion 132
5. Methods 137

5.1 Cloning ... 137
5.2 Plant work ... 138
5.3 Hypocotyl length measurements ... 138
5.4 Quantification of leaf area and leaf number ... 138
5.5 *N. benthamiana* infiltration ... 139
5.6 SCN staining ... 139
5.7 Cell culture ... 139
5.8 Microscopy ... 139
5.9 Intensity measurements ... 140
5.10 Body-tracking ... 140
5.11 FLIM measurements ... 140
5.12 Prediction of protein domains ... 140
5.13 Figure assembly ... 141
6. References ... 142
7. Supplementary information ... 148
7.1 Supplementary figures ... 148
7.2 Supplementary tables ... 150
Summary ... 157
Zusammenfassung ... 159
Appendix ... 161
1. Abbreviations ... 161
2. Exemplary plasmid maps ... 169
3. List of figures ... 177
4. List of tables ... 178
5. List of supplementary figures ... 178
6. List of supplementary tables ... 179
7. List of supplementary movies ... 180
Acknowledgements - Danksagung ... 181

Aims of this study

The primary aim of this study is to elucidate the function of complex formation of specific transcription factors (TFs) and their subcellular localisation to microdomains in the regulation of root stem cell niche (SCN) homeostasis in *Arabidopsis thaliana*.

As plant roots provide access to water and nutrients and anchor the plant in the soil, root growth and development have a great impact on all above-ground tissues and are essential for an overall healthy plant. Further, the urgent need for healthy, efficient, and high yield crops is growing because of an increasing world population, while at the same time food security is being threatened by climate change. In research, *Arabidopsis thaliana* serves as a model plant because of its comparably fast generation time, small genome and simplicity in structure. Due to the homology that exists between plant species, knowledge gained from *A. thaliana* research can in many cases serve as a basis for crop plant research.

In *A. thaliana* the root SCN is located at the root tip within the so-called root apical meristem and harbours the stem cells that give rise to all kind of root tissues. Notably, in the centre of the SCN a small group of slowly dividing cells, the quiescent centre (QC) cells, regulate the fate of a single layer of directly surrounding stem cells, including the distally located columella stem cells (CSCs). Sustaining the QC quiescence is important for robust stem cell fate regulation over a plants' lifetime as the QC maintains and replenishes the stem cell population. Stem cell maintenance is in turn important for balanced root growth, which is critical as plants must adapt to an ever changing and often challenging environment.

In this study a novel connection between root stem cell maintenance and environmental signals is uncovered on a subcellular level, integrating the formation of potentially phase-separated microdomains as a fast read-out mechanism for cell fate. Microdomains are known regulatory elements, e.g. in light-signalling, but as shown in this study, they also occur at positions inaccessible to light, like the root meristem. Still, little is known about their function although phase-separation is of great interest because it could represent a fast and reversible mechanism to regulate a variety of cellular processes. Remarkably, this study reveals a function of microdomain-forming TF-complexes in root SCN homeostasis, possibly integrating a regulatory mechanism through environmental stimuli.

The present work is divided into five parts:

Chapter I gives an overview of currently known TFs involved in root stem cell fate and RAM maintenance of *Arabidopsis* and their potential regulation through complex formation and subcellular translocation is discussed. This serves as a basis for further investigations and identifies WUSCHEL-RELATED HOMEOBOX5 (WOX5) as a key TF in stem cell maintenance and QC quiescence.

Chapter II focuses on a possible function of subcellular microdomains in *Arabidopsis*, comparable to the observed TF-localisations. Here, plasma membrane localized plant receptors are taken as an example for cluster-forming complexes, where the reversible formation of microdomains provides spatio-temporal separation of signalling processes.

Chapter III investigates the control of *Arabidopsis* QC quiescence. Here, with mathematical modelling and protein interaction experiments, the importance of mutual regulation as well as protein interaction of the brassinosteroid-regulated TFs BRAVO (BRASSINOSTEROIDS AT VASCULAR AND ORGANIZING CENTER) and WOX5 is revealed.

In chapter IV, expression analysis and a new staining method for *Arabidopsis* SCN phenotyping reveal the concerted mutual regulation of WOX5 and PLETHORAs (PLTs) and their control of QC quiescence and CSC maintenance in an interdependent manner. Prion-like domains (PrDs) in PLT3 are identified as domains responsible for its localisation to nuclear microdomains and the recruitment of WOX5. Furthermore, a function for the microdomains as markers for stem cell fate determination is hypothesized.

Chapter V uncovers the involvement of the clock-related transcriptional regulator EARLY FLOWERING3 (ELF3) in PLT3-dependent *Arabidopsis* root SCN regulation, revealing a new link to the integration of environmental stimuli. (Co)-localisation and interaction experiments and the identification of PrDs in ELF3 reveal a regulatory mechanism occurring through a PrD-dependent TF-interaction and translocation to microdomains.

In summary, the results of this study highlight the delicate regulation of *Arabidopsis* root SCN homeostasis through TF-complexes and their localisation to subcellular microdomains, thereby leading to a better understanding of root stem cell fate regulation as basis for future research also in consideration of the need for more adaptive crops in light of a changing planet.

I. Function and regulation of transcription factors involved in root apical meristem and stem cell maintenance

The following manuscript was published in frontiers in Plant Science in July 2015 (doi: https://doi.org/10.3389/fpls.2015.00505).

Authors:

Rebecca C. Drisch[1] and Yvonne Stahl[1]

Affiliations:

[1]Institute for Developmental Genetics, Heinrich-Heine-University, Universitätsstr. 1, D-40225 Düsseldorf, Germany

Contributions:

Rebecca C. Drisch and Yvonne Stahl wrote the manuscript.

frontiers in Plant Science

MINI REVIEW
published: 06 July 2015
doi: 10.3389/fpls.2015.00505

Function and regulation of transcription factors involved in root apical meristem and stem cell maintenance

*Rebecca C. Drisch and Yvonne Stahl**

Institute for Developmental Genetics, Heinrich-Heine-University, Düsseldorf, Germany

Plant roots are essential for overall plant development, growth, and performance by providing anchorage in the soil and uptake of nutrients and water. The primary root of higher plants derives from a group of pluripotent, mitotically active stem cells residing in the root apical meristem (RAM) which provides the basis for growth, development, and regeneration of the root. The stem cells in the *Arabidopsis thaliana* RAM are surrounding the quiescent center (QC), which consists of a group of rarely dividing cells. The QC maintains the stem cells in a non-cell-autonomous manner and prevents them from differentiation. The necessary dynamic but also tight regulation of the transition from stem cell fate to differentiation most likely requires complex regulatory mechanisms to integrate external and internal cues. Transcription factors play a central role in root development and are regulated by phytohormones, small signaling molecules, and miRNAs. In this review we give a comprehensive overview about the function and regulation of specific transcription factors controlling stem cell fate and root apical meristem maintenance and discuss the possibility of TF complex formation, subcellular translocations and cell-to-cell movement functioning as another level of regulation.

Keywords: stem cells, differentiation, root apical meristem, quiescent center, transcription factors

OPEN ACCESS

Edited by:
Ikram Blilou,
Wageningen University, Netherlands

Reviewed by:
Jian Xu,
National University of Singapore, Singapore
Tom Bennett,
University of Cambridge, UK

***Correspondence:**
Yvonne Stahl,
Institute for Developmental Genetics, Heinrich-Heine-University, Universitätsstrasse 1, Düsseldorf, NRW, Germany
yvonne.stahl@hhu.de

Specialty section:
This article was submitted to Plant Cell Biology, a section of the journal Frontiers in Plant Science

Received: *29 April 2015*
Accepted: *23 June 2015*
Published: *06 July 2015*

Citation:
Drisch RC and Stahl Y (2015) Function and regulation of transcription factors involved in root apical meristem and stem cell maintenance. Front. Plant Sci. 6:505. doi: 10.3389/fpls.2015.00505

Introduction

Terrestrial plants are sessile organisms and have to adapt to different environmental stimuli by coordinating their growth and development accordingly. Because of these needs plants have evolved a high degree of developmental and morphological plasticity, which is only possible due to the continuity of plant development (Bradshaw, 1965; Palmer et al., 2012). Plants, in contrast to animals, have to produce most of their organs post-embryonically. Therefore, plants possess structures called meristems that contain pluripotent stem cells, which are maintained during the whole lifespan of the plant. There are two main meristems in plants, the shoot apical meristem (SAM) generating above-ground tissues and organs and the root apical meristem (RAM) giving rise to the primary root of the plant. The RAM and the SAM show different structural organizations, but both meristems harbor stem cells, which continuously generate new cells (Benfey and Scheres, 2000). In *Arabidopsis*, on average four slowly dividing cells, the quiescent center (QC), maintain the adjacent stem cells (or initials) and act as a long-term reservoir for the surrounding shorter-lived stem cells (van den Berg et al., 1997). The stem cells continuously divide asymmetrically generating new stem cells still in contact with the QC cells and daughter cells, undergoing further cell divisions, are shifted further away from the QC and finally differentiate.

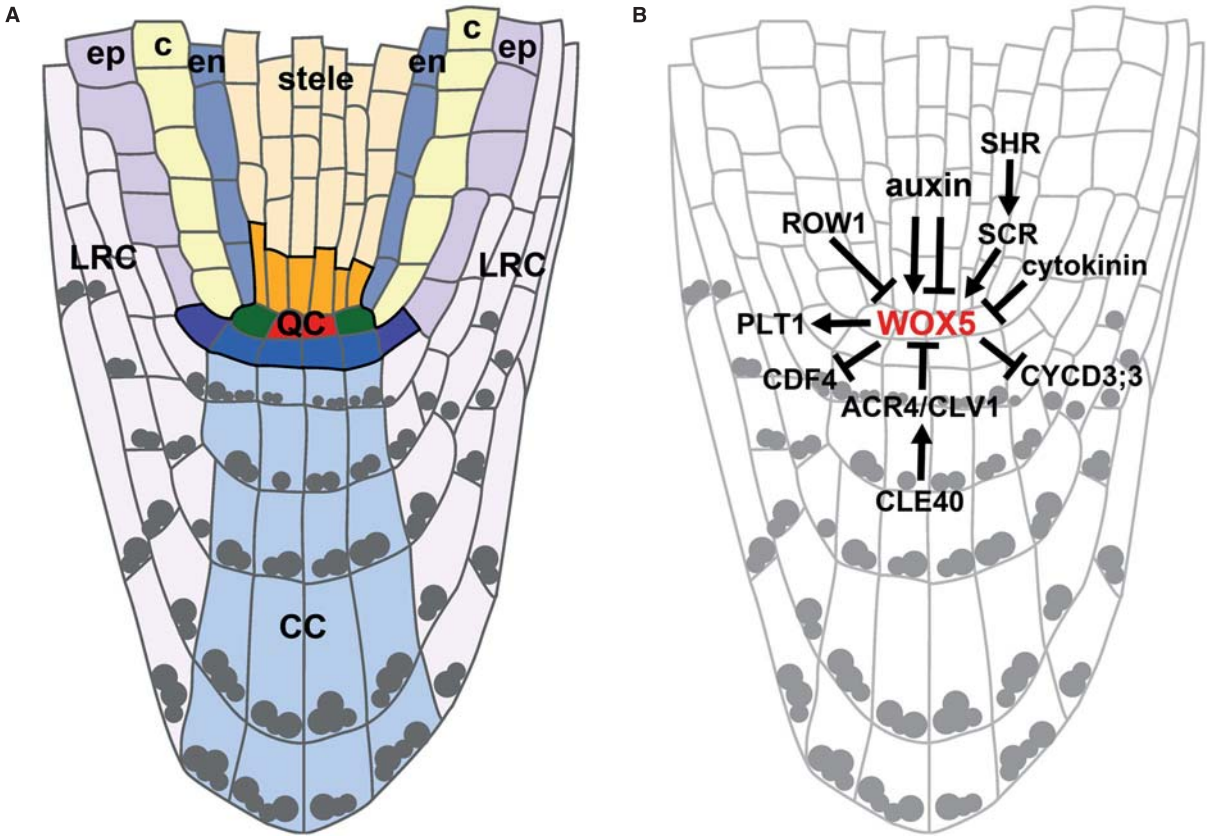

FIGURE 1 | *Arabidopsis* meristematic zone organization and regulation of *WOX5* expression in the QC. (A) Schematic representation of an *Arabidopsis* meristematic zone. The stem cell niche (outlined in black) contains the QC cells (red), the cortex/endodermis initials (green), stele initials (orange), lateral root cap/epidermis initials (purple), and CSCs (blue). ep, epidermis; c, cortex; en, endodermis; LRC, lateral root cap; CC, columella cells. Gray dots indicate starch granules. **(B)** Regulational model highlighting the complex interplay of phytohormones, TFs and signaling peptides on *WOX5* expression levels and domain. Arrows indicate positive, barred lines indicate negative regulations.

The RAM can be divided into three main zones: (a) the meristematic zone at the root tip containing the stem cell niche, (b) the elongation zone, containing the cells that after cell divisions have left the meristematic zone and are now elongating, and (c) the differentiation zone, containing cells that have acquired their destined cell fates. The beginning of the differentiation zone is marked by the appearance of root hairs (Dolan et al., 1993). The position of the stem cells remains the same throughout development and defines the cell fates of their descendants. Thereby concentrically organized clonal cell lineages are generated representing a spatio-temporal developmental gradient. From the outside to the inside of the root these cell layers are the epidermis, cortex, endodermis, pericycle, and vasculature. Cortex and endodermis together are also referred to as ground tissue. Stem cells for the lateral root cap (LRC)/epidermis and the columella are positioned distal to the QC. The columella stem cells (CSCs) give rise to the differentiated columella cells (CCs) which contain starch granules for graviperception (see **Figure 1A**).

Apart from phytohormones, intercellular signaling processes mediated by small peptide ligands and their respective receptors in interplay with specific transcription factors (TFs) play important roles in maintaining stem cell homeostasis in the root. In this review we will focus on the function and regulation of known TFs important for stem cell regulation in the RAM (summarized in **Table 1**).

TFs Involved in RAM Development

One of the most important TF regulating stem cell fate in the root is the homeodomain containing WUSCHEL-RELATED HOMEOBOX5 (WOX5). *WOX5* is expressed in the QC in embryos and mature roots and maintains the surrounding stem cells in a largely unknown non-cell autonomous way. WOX5 is necessary for the maintenance of CSCs as in *wox5* mutant roots, cells in the CSC position acquire starch granules like differentiated CCs (Sarkar et al., 2007). Furthermore, it has been shown that WOX5 is necessary to prevent cell divisions in the QC by repressing *CYCD3;3* expression thereby establishing quiescence in the embryonic root and maintaining it in the mature root (Forzani et al., 2014; **Figure 1B**). WOX5 homologs have been identified in a number of plant species (Nardmann et al., 2009; Zhao et al., 2014) and were shown to be expressed in the QC in rice and maize (Kamiya et al., 2003b; Nardmann et al., 2007).

TABLE 1 | Transcription factor (TFs) in RAM maintenance.

Name	Class/type	Expression domain	Function	Mobile	Interaction	Reference
WOX5	Homeodomain	QC	Maintains surrounding stem cells; represses QC divisions	Yes		Sarkar et al. (2007), Forzani et al. (2014), Pi et al. (2015)
PLT1-4	AP2/ERF	RAM, mainly QC	Necessary and sufficient for RAM maintenance	Yes (PLT2)		Aida et al. (2004), Galinha et al. (2007)
SHR	GRAS	Stele	QC fate specification and maintenance, asymmetric cell divisions, cortex, and endodermis specification	yes	SCR SIEL JKD MGP BIB	Di Laurenzio et al. (1996), Helariutta et al. (2000), Wysocka-Diller et al. (2000), Nakajima et al. (2001), Welch et al. (2007), Long et al. (2015b)
SCR	GRAS	QC, CEI, endodermis	QC fate specification and maintenance; asymmetric cell divisions, cortex, and endodermis specification		SHR JKD MGP BIB	Scheres et al. (1995), Di Laurenzio et al. (1996), Sabatini et al. (2003), Welch et al. (2007), Long et al. (2015b)
SPT	bHLH	Epidermal initial and CSC, stele	Regulates RAM size and QC cell number		ALC IND	Groszmann et al. (2010), Girin et al. (2011), Makkena and Lamb (2013)
TMO7	bHLH	Adjacent to hypophysis	Embryonic root initiation	Yes	SIEL	Schlereth et al. (2010)
MYC2	bHLH	Ground tissue, vasculature, epidermis, LRC	JA-mediated inhibition of root growth and meristem development; repressing PLT expression			Boter et al. (2004), Chini et al. (2007), Chen et al. (2011), Fernández-Calvo et al. (2011)
UPB1	bHLH	LRC, vasculature	Modulates the balance between cell proliferation and differentiation by controlling ROS production	Yes		Tsukagoshi et al. (2010)
NTT	Zinc finger	Hypophysis and lens-shaped cell (embryo); QC, CEI, CSC, CC	Initiation of the root meristem; confers CSC fate			Crawford et al. (2015)
BRX	BRX family	Vasculature	Regulates RAM size by mediating BR and auxin signaling	Yes	NGA1	Mouchel et al. (2004, 2006a,b), Scacchi et al. (2009)
FEZ	NAC-domain	CSC and LRC/epidermis stem cells	Stimulates periclinal divisions in the LRC/epidermis initials and CSCs			Willemsen et al. (2008), Bennett et al. (2010, 2014)
SMB	NAC-domain	Maturing root cap cells	Constrains CSC-like activity and promotes differentiation; activation of root cap maturation together with BRN1&2			Willemsen et al. (2008), Bennett et al. (2010, 2014), Fendrych et al. (2014)
BRAVO	R2R3-MYB	QC, vascular initials, CEI	Repressor of QC divisions; counteracting BR signaling		BES1	Vilarrasa-Blasi et al. (2014)
BES1	BZR1-like	RAM	Activates QC divisions; represses BRAVO		BRAVO	Vilarrasa-Blasi et al. (2014)
ERF115	ERF	Dividing QC cells	Regulates QC divisions			Heyman et al. (2013)

Summary of the function, interaction, and mobility of key TFs involved in RAM development and maintenance.

Members of the AINTEGUMENTA-LIKE (AIL) family of APETALA2/ETHYLENE RESPONSE FACTOR (AP2/ERF) domain TFs, like PLETHORA1–3 (PLT1–3) and BABYBOOM (BBM/PLT4) have been described as master regulators of root meristem initiation and maintenance. The *PLT*s are expressed in the embryonic and adult root meristem, overlapping in their expression domains mainly in and around the QC building a developmentally instructive protein gradient, where protein levels decrease the more differentiated the cells are (Aida et al., 2004; Galinha et al., 2007). *plt1 plt2* double mutants show a severe reduction in root meristem size and loss of QC markers (Aida et al., 2004). Ectopic over-expression of *PLT* leads to accumulation of stem cells in the root meristem and can also lead to the production of ectopic roots from the shoot apex (Galinha et al., 2007). The AIL genes are conserved throughout the plant kingdom and play important roles in meristem development, e.g., in adventitious rooting in poplar (Rigal et al., 2012) and gametophore stem cell formation in the moss *Physcomitrella patens* (Aoyama et al., 2012).

The GRAS-transcription factors SHORTROOT (SHR) and SCARECROW (SCR) are required for QC specification and the formative asymmetric cell divisions that are necessary for the

formation of distinct cortex and endodermal cell layers (Sabatini et al., 2003). *SHR* is expressed in the stele of the *Arabidopsis* root and the protein moves one cell layer outwards into the endodermis, cortex/endodermis initial, and QC cells where it activates *SCR* expression. Loss of SHR and SCR results in a short root phenotype and abnormal QC cells indicating the importance of theses TFs in maintaining the root stem cell niche (Di Laurenzio et al., 1996; Helariutta et al., 2000; Wysocka-Diller et al., 2000; Nakajima et al., 2001). SHR/SCR act in parallel with PLT to maintain QC identity and stem cell homeostasis in the *Arabidopsis* root (Aida et al., 2004). TFs act by regulating the expression of downstream genes and some of these direct transcriptional targets have been reported. CYCD6;1 has been identified as downstream target of SHR/SCR transcriptional regulation, directly linking the asymmetric cell division in the cortex/endodermis initials with activation of cell cycle genes (Sozzani et al., 2010). Furthermore, *WOX5* expression requires SHR and SCR (Sarkar et al., 2007). The RETINOBLASTOMA-RELATED (RBR) protein has been found to physically bind to SCR and together with the cell cycle regulator CYCD6;1 and proteins of the BIRD family defines the position of the asymmetric cell divisions in the stem cell area of the root (Cruz-Ramírez et al., 2012; Long et al., 2015b). SHR and SCR regulate *CYCD6;1* expression and also expression of the BIRD family members *MAGPIE* (*MGP*) and *NUTCRACKER* (*NUT*, Levesque et al., 2006; Cui et al., 2007; Welch et al., 2007). In the monocot rice, which has a different morphology and number of cortical tissue layers, two SHR and SCR homologs each have been identified and might play a similar role in cortex and endodermis specification than in *Arabidopsis* (Kamiya et al., 2003a; Cui et al., 2007).

Other TFs have been described to play important roles in root stem cell maintenance, e.g., the R2R3-MYB transcription factor BRASSINOSTEROIDS AT VASCULAR AND ORGANIZING CENTER (BRAVO). BRAVO is acting as a cell-specific repressor of QC divisions by counteracting brassinosteroid (BR)-mediated cell divisions in QC cells (Vilarrasa-Blasi et al., 2014). Recently, the putative zinc finger TF NO TRANSMITTING TRACT (NTT) and two closely related paralogs have been described to be necessary for root meristem initiation and conferring distal stem cell fate. *nww* triple mutants fail to develop the progenitor of the QC, the lens-shaped cell, in the embryo and therefore do not develop a root. Furthermore, NTT is both necessary and sufficient to confer distal stem cell identities in the root meristem (Crawford et al., 2015). The bHLH TF UPBEAT1 (UPB1) regulates the concentration of reactive oxygen species (ROS) in the *Arabidopsis* RAM. *upb1* loss-of-function mutants show an increased RAM size and therefore UPB1 is thought to keep the balance between cell proliferation and differentiation by controlling ROS production (Tsukagoshi et al., 2010). NAC domain TFs acting in LRC development have also been identified. FEZ and SOMBRERO (SMB) antagonistically control the frequency and division plane orientation of LRC/epidermis initials and CSCs (Willemsen et al., 2008; Bennett et al., 2014). SMB, together with BEARSKIN1 and 2 (BRN1,2), is also necessary for the final differentiation steps of LRC cells and regulates programmed cell death (Bennett et al., 2010; Fendrych et al., 2014). Another bHLH TF named SPATULA (SPT) has been found to regulate root meristem size. Loss of SPT results in a larger RAM due to an increased QC size as well as supernumerary divisions in initials. SPT is thought to act independently of gibberellic acid, but might regulate auxin transport or accumulation (Makkena and Lamb, 2013).

Phytohormonal Regulation of TFs in the RAM

Phytohormones like auxin, cytokinin, brassinosteroids, ethylene, jasmonate, and gibberellic acid play fundamental roles in specification, development, and maintenance of the RAM in *Arabidopsis*. Considerable crosstalk between different hormonal pathways is necessary for integrating external and internal cues into the dynamic developmental processes of stem cell maintenance, proliferation, and differentiation. Also transcriptional regulation is controlled by phytohormones and several TFs have been shown to be regulated by and act in concert with them.

The phytohormone auxin plays a dominant role in root initiation and development. An auxin gradient is build up by local biosynthesis and polar auxin transport in the root and has its maximum in the QC (Blilou et al., 2005; Petersson et al., 2009). The PINFORMED (PIN) auxin efflux carriers control auxin distribution and thereby regulate elongation and differentiation of root cells in a complex interplay with the PLT proteins. The expression of *PLT* TFs is auxin inducible and their expression domains are defined by local auxin accumulation (Aida et al., 2004; Blilou et al., 2005; Mähönen et al., 2014). Auxin has also been proposed to act upstream of WOX5 and PLT1 as *WOX5* expression was reported to be restricted to the QC cells by auxin via AUXIN RESPONSE FACTOR (ARF) 10 and 16 (Ding and Friml, 2010), but later WOX5 and ARF 10 and 16 were suggested to act in parallel instead (Bennett et al., 2014). Furthermore, *WOX5* expression was reported to be auxin inducible and responsible for the establishment of an auxin maximum in the root tip (Gonzali et al., 2005). The specific expression of *WOX5* in the QC is not only confined by auxin, but also by a PHD domain-containing protein, REPRESSOR OF WUSCHEL1 (ROW1), that binds tri-methylated histone H3 lysine 4 (H3K4me3) in the WOX5 promoter thereby repressing *WOX5* transcription in the more proximal cells (Zhang et al., 2015; **Figure 1B**). Cytokinins also play a pivotal role in root meristem balance and act antagonistically to auxin. They control the switch from meristematic to differentiated cell fates by suppressing auxin signaling and transport where cells leave the meristematic zone (transition zone). This is mediated by the AUX/IAA SHORT HYPOCOTYL2 (SHY2), which is activated by cytokinin via ARABIDOPSIS RESPONSE REGULATOR1 (ARR1), but negatively influences auxin signaling and is itself negatively regulated by auxin (Dello Ioio et al., 2007, 2008). SCR has been found to suppress cytokinin signaling via ARR1 thereby also influencing auxin accumulation in the QC (Moubayidin et al., 2013). Furthermore, cytokinins have been shown to negatively regulate *WOX5* expression possibly by modulating the auxin flux in the root and promote cell divisions in the QC (Zhang et al., 2013). The rarely dividing QC cells are thought to be

less stress sensitive and protected from DNA damage and can therefore maintain their longevity. Contrariwise, the surrounding stem cells seem to be more sensitive to DNA damage. It has been proposed that the QC serves as a "safe haven" for the surrounding stem cells and if stress is occurring, driven by hormonal signals like cytokinin, BR, ethylene, and JA, the QC will divide to replenish the lost stem cells (Curtis and Hays, 2007; Fulcher and Sablowski, 2009; Cruz-Ramírez et al., 2013). Brassinosteroids (BRs) have been described to act antagonistically to auxin in *Arabidopsis* RAM maintenance (Chaiwanon and Wang, 2015). BR-mediated QC divisions are repressed by the R2R3-MYB TF BRAVO. The BR-activated TF BES1 (BRI1- EMS SUPRESSOR1) can physically interact with and repress BRAVO thereby modulating QC divisions (Vilarrasa-Blasi et al., 2014). Additionally, the TF BREVIS RADIX (BRX) has been shown to mediate a feedback between auxin and BR signaling, influencing RAM size (Mouchel et al., 2006a). Ethylene has also been shown to induce QC cell divisions (Ortega-Martínez et al., 2007). Recently, the ETHYLENE RESPONSE FACTOR115 (ERF115) TF was found to act as a rate-limiting factor of QC divisions. Here, ERF115 is positively regulated by BR, but is not involved in ethylene signaling. *ERF115* is expressed in dividing QC cells and ERF115 protein abundance is negatively regulated by proteolysis leading to a convergence of BR and ethylene signaling in the RAM (Heyman et al., 2013). Jasmonate inhibits primary root growth by reducing RAM activity and results in irregular QC divisions and CSC differentiation. This is mediated by the function of MYC2/JASMONATE INSENSITIVE1 (MYC2), a bHLH TF. MYC2 has been shown to directly bind to PLT1 and 2 promoters and to repress their transcription, thereby integrating jasmonate and auxin pathways in RAM maintenance (Chen et al., 2011).

Regulation of TFs in the RAM by Peptides and microRNAs

Phytohormones act mostly as long-range signals, other more short-range signals mediating TF regulations include small peptides, microRNAs, and movement of TFs. Small signaling peptides are also known to regulate *Arabidopsis* root development (Delay et al., 2013) and some of them have been shown to regulate TFs involved in root stem cell homeostasis. In both shoot and root meristem maintenance CLAVATA3/EMBRYO SURROUNDING REGION (CLE) peptides are known to play important roles. In the *Arabidopsis* root, *CLE40* is expressed from differentiated columella cells and regulates CSC fate via the receptor-like kinases ARABIDOPSIS CRINKLY4 (ACR4) and CLAVATA1 (CLV1). This signaling pathway influences the expression level and positioning of *WOX5* RNA (Stahl et al., 2009, 2013). The ROOT MERISTEM GROWTH FACTOR (RGF) peptide family also known as GOLVEN (GLV) or CLE-like (CLEL) possesses a conserved 14 aa domain containing the tyrosine sulfation motif Asp-Tyr (Matsuzaki et al., 2010; Meng et al., 2012; Whitford et al., 2012). RGF1 has been demonstrated to positively regulate and define *PLT* expression and protein stability (Matsuzaki et al., 2010).

MicroRNAs (miRNAs) have been shown to generate a gradient defining vascular cell types in the root. miRNA165a and miRNA166b are transcriptionally activated by SHR in the endodermis and then move through plasmodesmata to the stele regulating the expression of the homeodomain leucine zipper (HD-ZIP) TF PHABULOSA (PHB), that determines vascular cell fates (Carlsbecker et al., 2010; Miyashima et al., 2011; Vatén et al., 2011).

Mobile TFs in RAM Regulation

Due to their rigid cell walls, plant cells are not able to move and need to communicate with each other non-cell autonomously in order to integrate external and internal cues with development and growth. About 17–29% of TFs are predicted to move either targeted or non-targeted from cell to cell (Lee et al., 2006; Rim et al., 2011). This TF movement is proposed to occur by transit through plasmodesmata, membrane-lined channels that interconnect plant cells symplastically, and thereby propagate signaling outputs.

A prominent example of a mobile TF is SHR, which is expressed in the stele of the *Arabidopsis* root, but moves one layer further where it interacts with and activates SCR. SHR is not only a mobile TF, but it notably also alters its subcellular localization. In the stele it localizes to the nucleus and cytoplasm, whereas in the endodermis it is localized mostly in the nucleus (Nakajima et al., 2001). The cytoplasmic localization of SHR is important for its movement to the outer cell layer via plasmodesmata and is regulated by phosphorylation of a specific tyrosine residue (Gallagher et al., 2004; Vatén et al., 2011). SHR movement is dependent on microtubules and is mediated by SHORT ROOT INTERACTING EMBRYONIC LETHAL (SIEL), an endosomal protein, which needs SHR and SCR for its own expression suggesting a potential feedback for SHR regulating its own directional movement (Koizumi et al., 2011, 2012; Wu and Gallagher, 2013). Furthermore, members of the BIRD family like JACKDAW (JKD) and its close homolog BALD IBIS (BIB) constrain SHR movement by nuclear retention and complex formation (Welch et al., 2007; Long et al., 2015b).

In the *Arabidopsis* embryo, the mobile bHLH TF TARGET OF MONOPTEROS7 (TMO7) is required for embryonic root initiation and also interacts with SIEL (Schlereth et al., 2010). The TF BRX translocates from the basal plasma membrane in the vasculature to the nucleus in response to auxin (Scacchi et al., 2009). But also other TFs important for root development have been shown to be able to move, like WOX5 and PLT2 (Daum et al., 2014; Mähönen et al., 2014). Recently, it was shown that WOX5 movement from the QC to the CSCs is necessary to maintain the undifferentiated state of these cells by chromatin-mediated repression of the TF CYCLING DOF FACTOR4 (CDF4) in the CSCs (Pi et al., 2015).

The TF UPB1 has been proposed to act as a mobile non-cell-autonomous signal. It is supposed to move from its expression domain in the LRC to cells of the transition and elongation zones. Here it localizes predominantly to the nucleus and positions the location of the transition zone (Tsukagoshi et al., 2010). Nevertheless, it has not yet been completely clarified how TF movement regulates stem cell and RAM maintenance.

Outlook and Perspectives

In the *Arabidopsis* root over 300 differentially regulated TFs have been found to be expressed, but only some have an assigned function in meristem maintenance (Birnbaum et al., 2003). TFs are regulating the expression of other genes, but information on direct targets of TFs involved in RAM regulation are scarce, except for the above mentioned examples. Regulation of the TF WOX5 alone includes phytohormones, small signaling peptides, histone modifications, and cell-to-cell movement, demonstrating the diversity of control mechanisms (**Figure 1B**). Although, e.g., root cap development is mainly regulated by parallel pathways, also a regulatory connection between WOX5 and SMB has been described (Bennett et al., 2014). Therefore, it is tempting to speculate that there might be complex regulatory networks involved, but that some important links have not been found yet. One could speculate that not only transcriptional regulations or TF protein stability are important but that, e.g., the interaction of TFs with other TFs or proteins create differential outputs. Also, the described subcellular translocations of some TFs might represent mechanisms to regulate TF function. Movement of TFs via plasmodesmata for short-range signaling could represent yet another level of regulation (Long et al., 2015a), but if this is directional and how it is exactly controlled remains to be elucidated.

The future challenge is to develop methods that will help to analyze and consolidate the supposed complex regulatory mechanisms. Here the rise of sequencing and bioinformatic tools together with sophisticated imaging techniques will be a prerequisite to enable the necessary modeling approaches.

Acknowledgments

We would like to thank Rüdiger Simon and Peter Welters for critical reading of the manuscript and gratefully acknowledge funding by the DFG to YS. We apologize to all colleagues whose relevant work could not be mentioned due to space restrictions.

References

Aida, M., Beis, D., Heidstra, R., Willemsen, V., Blilou, I., Galinha, C., et al. (2004). The PLETHORA genes mediate patterning of the *Arabidopsis* root stem cell niche. *Cell* 119, 109–120. doi: 10.1016/j.cell.2004.09.018

Aoyama, T., Hiwatashi, Y., Shigyo, M., Kofuji, R., Kubo, M., Ito, M., et al. (2012). AP2-type transcription factors determine stem cell identity in the moss *Physcomitrella patens*. *Development* 139, 3120–3129. doi: 10.1242/dev.076091

Benfey, P. N., and Scheres, B. (2000). Root development. *Curr. Biol.* 10, R813–R815. doi: 10.1016/S0960-9822(00)00814-9

Bennett, T., van den Toorn, A., Sanchez-Perez, G. F., Campilho, A., Willemsen, V., Snel, B., et al. (2010). SOMBRERO, BEARSKIN1, and BEARSKIN2 regulate root cap maturation in *Arabidopsis*. *Plant Cell* 22, 640–654. doi: 10.1105/tpc.109.072272

Bennett, T., van den Toorn, A., Willemsen, V., and Scheres, B. (2014). Precise control of plant stem cell activity through parallel regulatory inputs. *Development* 141, 4055–4064. doi: 10.1242/dev.110148

Birnbaum, K., Shasha, D. E., Wang, J. Y., Jung, J. W., Lambert, G. M., Galbraith, D. W., et al. (2003). A gene expression map of the *Arabidopsis* root. *Science* 302, 1956–1960. doi: 10.1126/science.1090022

Blilou, I., Xu, J., Wildwater, M., Willemsen, V., Paponov, I., Heidstra, R., et al. (2005). The PIN auxin efflux facilitator network controls growth and patterning in *Arabidopsis* roots. *Nature* 433, 39–44. doi: 10.1038/nature03184

Boter, M., Ruíz-Rivero, O., Abdeen, A., and Prat, S. (2004). Conserved MYC transcription factors play a key role in jasmonate signaling\nboth in tomato and *Arabidopsis*. *Genes Dev.* 18, 1577–1591. doi: 10.1101/gad.297704

Bradshaw, A. D. (1965). Evolutionary significance of phenotypic plasticity in plants. *Adv. Genet.* 13, 115–155.

Carlsbecker, A., Lee, J.-Y., Roberts, C. J., Dettmer, J., Lehesranta, S., Zhou, J., et al. (2010). Cell signalling by microRNA165/6 directs gene dose-dependent root cell fate. *Nature* 465, 316–321. doi: 10.1038/nature08977

Chaiwanon, J., and Wang, Z.-Y. (2015). Spatiotemporal Brassinosteroid signaling and antagonism with auxin pattern stem cell dynamics in *Arabidopsis* roots. *Curr. Biol.* 25, 1031–1042. doi: 10.1016/j.cub.2015.02.046

Chen, Q., Sun, J., Zhai, Q., Zhou, W., Qi, L., Xu, L., et al. (2011). The basic helix-loop-helix transcription factor MYC2 directly represses PLETHORA expression during jasmonate-mediated modulation of the root stem cell niche in *Arabidopsis*. *Plant Cell* 23, 3335–3352. doi: 10.1105/tpc.111.089870

Chini, A., Fonseca, S., Fernández, G., Adie, B., Chico, J. M., Lorenzo, O., et al. (2007). The JAZ family of repressors is the missing link in jasmonate signalling. *Nature* 448, 666–671. doi: 10.1038/nature06006

Crawford, B., Sewell, J., Golembeski, G., Roshan, C., Long, J., and Yanofsky, M. (2015). Genetic control of distal stem cell fate within root and embryonic meristems. *Science* 347, 655–659. doi: 10.1126/science.aaa0196

Cruz-Ramírez, A., Díaz-Triviño, S., Blilou, I., Grieneisen, V. A., Sozzani, R., Zamioudis, C., et al. (2012). A bistable circuit involving SCARECROW-RETINOBLASTOMA integrates cues to inform asymmetric stem cell division. *Cell* 150, 1002–1015. doi: 10.1016/j.cell.2012.07.017

Cruz-Ramírez, A., Díaz-Triviño, S., Wachsman, G., Du, Y., Arteága-Vázquez, M., Zhang, H., et al. (2013). A SCARECROW-RETINOBLASTOMA protein network controls protective quiescence in the *Arabidopsis* root stem cell organizer. *PLoS Biol.* 11:e1001724. doi: 10.1371/journal.pbio.1001724

Cui, H., Levesque, M. P., Vernoux, T., Jung, J. W., Paquette, A. J., Gallagher, K. L., et al. (2007). An evolutionarily conserved mechanism delimiting SHR movement defines a single layer of endodermis in plants. *Science* 316, 421–425. doi: 10.1126/science.1139531

Curtis, M. J., and Hays, J. B. (2007). Tolerance of dividing cells to replication stress in UVB-irradiated *Arabidopsis* roots: requirements for DNA translesion polymerases Eta and Zeta. *DNA Repair* (*Amst.*) 6, 1341–1358. doi: 10.1016/j.dnarep.2007.03.004

Daum, G., Medzihradszky, A., Suzaki, T., and Lohmann, J. U. (2014). A mechanistic framework for noncell autonomous stem cell induction in *Arabidopsis*. *Proc. Natl. Acad. Sci. U.S.A.* 111, 14619–14624. doi: 10.1073/pnas.1406446111

Delay, C., Imin, N., and Djordjevic, M. A. (2013). Regulation of *Arabidopsis* root development by small signaling peptides. *Front. Plant Sci.* 4:352. doi: 10.3389/fpls.2013.00352

Dello Ioio, R., Linhares, F. S., Scacchi, E., Casamitjana-Martinez, E., Heidstra, R., and Costantino, P. (2007). Cytokinins determine *Arabidopsis* root-meristem size by controlling cell differentiation. *Curr. Biol.* 17, 678–682. doi: 10.1016/j.cub.2007.02.047

Dello Ioio, R., Nakamura, K., Moubayidin, L., Perilli, S., Taniguchi, M., Morita, M. T., et al. (2008). A genetic framework for the control of cell division and differentiation in the root meristem. *Science* 322, 1380–1384. doi: 10.1126/science.1164147

Ding, Z., and Friml, J. (2010). Auxin regulates distal stem cell differentiation in *Arabidopsis* roots. *Proc. Natl. Acad. Sci. U.S.A.* 107, 12046–12051. doi: 10.1073/pnas.1000672107

Di Laurenzio, L., Wysocka-Diller, J., Malamy, J. E., Pysh, L., Helariutta, Y., Freshour, G., et al. (1996). The SCARECROW gene regulates an asymmetric cell division that is essential for generating the radial organization of the *Arabidopsis* root. *Cell* 86, 423–433. doi: 10.1016/S0092-8674(00)80115-4

Dolan, L., Janmaat, K., Willemsen, V., Linstead, P., Poethig, S., Roberts, K., et al. (1993). Cellular organisation of the *Arabidopsis thaliana* root. *Development* 84, 71–84.

Fendrych, M., Van Hautegem, T., Van Durme, M., Olvera-Carrillo, Y., Huysmans, M., Karimi, M., et al. (2014). Programmed cell death controlled by ANAC033/SOMBRERO determines root cap organ size in *Arabidopsis*. *Curr. Biol.* 24, 931–940. doi: 10.1016/j.cub.2014.03.025

Fernández-Calvo, P., Chini, A., Fernández-Barbero, G., Chico, J.-M., Gimenez-Ibanez, S., Geerinck, J., et al. (2011). The *Arabidopsis* bHLH transcription factors MYC3 and MYC4 are targets of JAZ repressors and act additively with MYC2 in the activation of jasmonate responses. *Plant Cell* 23, 701–715. doi: 10.1105/tpc.110.080788

Forzani, C., Aichinger, E., Sornay, E., Willemsen, V., Laux, T., Dewitte, W., et al. (2014). WOX5 suppresses CYCLIN D activity to establish quiescence at the center of the root stem cell niche. *Curr. Biol.* 24, 1939–1944. doi: 10.1016/j.cub.2014.07.019

Fulcher, N., and Sablowski, R. (2009). Hypersensitivity to DNA damage in plant stem cell niches. *Proc. Natl. Acad. Sci. U.S.A.* 106, 20984–20988. doi: 10.1073/pnas.0909218106

Galinha, C., Hofhuis, H., Luijten, M., Willemsen, V., Blilou, I., Heidstra, R., et al. (2007). PLETHORA proteins as dose-dependent master regulators of *Arabidopsis* root development. *Nature* 449, 1053–1057. doi: 10.1038/nature06206

Gallagher, K. L., Paquette, A. J., Nakajima, K., and Benfey, P. N. (2004). Mechanisms regulating SHORT-ROOT intercellular movement. *Curr. Biol.* 14, 1847–1851. doi: 10.1016/j.cub.2004.09.081

Girin, T., Paicu, T., Stephenson, P., Fuentes, S., Körner, E., O'Brien, M., et al. (2011). INDEHISCENT and SPATULA interact to specify carpel and valve margin tissue and thus promote seed dispersal in *Arabidopsis*. *Plant Cell* 23, 3641–3653. doi: 10.1105/tpc.111.090944

Gonzali, S., Novi, G., Loreti, E., Paolicchi, F., Poggi, A., Alpi, A., et al. (2005). A turanose-insensitive mutant suggests a role for WOX5 in auxin homeostasis in *Arabidopsis thaliana*. *Plant J.* 44, 633–645. doi: 10.1111/j.1365-313X.2005.02555.x

Groszmann, M., Bylstra, Y., Lampugnani, E. R., and Smyth, D. R. (2010). Regulation of tissue-specific expression of SPATULA, a bHLH gene involved in carpel development, seedling germination, and lateral organ growth in *Arabidopsis*. *J. Exp. Bot.* 61, 1495–1508. doi: 10.1093/jxb/erq015

Helariutta, Y., Fukaki, H., Wysocka-Diller, J., Nakajima, K., Jung, J., Sena, G., et al. (2000). The SHORT-ROOT gene controls radial patterning of the *Arabidopsis* root through radial signaling. *Cell* 101, 555–567. doi: 10.1016/S0092-8674(00)80865-X

Heyman, J., Cools, T., Vandenbussche, F., Heyndrickx, K. S., Van Leene, J., Vercauteren, I., et al. (2013). ERF115 controls root quiescent center cell division and stem cell replenishment. *Science* 342, 860–863. doi: 10.1126/science.1240667

Kamiya, N., Itoh, J. I., Morikami, A., Nagato, Y., and Matsuoka, M. (2003a). The SCARECROW gene's role in asymmetric cell divisions in rice plants. *Plant J.* 36, 45–54. doi: 10.1046/j.1365-313X.2003.01856.x

Kamiya, N., Nagasaki, H., Morikami, A., Sato, Y., and Matsuoka, M. (2003b). Isolation and characterization of a rice WUSCHEL-type homeobox gene that is specifically expressed in the central cells of a quiescent center in the root apical meristem. *Plant J.* 35, 429–441. doi: 10.1046/j.1365-313X.2003.01816.x

Koizumi, K., Hayashi, T., Wu, S., and Gallagher, K. L. (2012). The SHORT-ROOT protein acts as a mobile, dose-dependent signal in patterning the ground tissue. *Proc. Natl. Acad. Sci. U.S.A.* 109, 13010–13015. doi: 10.1073/pnas.1205579109

Koizumi, K., Wu, S., MacRae-Crerar, A., and Gallagher, K. L. (2011). An essential protein that interacts with endosomes and promotes movement of the SHORT-ROOT transcription factor. *Curr. Biol.* 21, 1559–1564. doi: 10.1016/j.cub.2011.08.013

Lee, J.-Y., Colinas, J., Wang, J. Y., Mace, D., Ohler, U., and Benfey, P. N. (2006). Transcriptional and posttranscriptional regulation of transcription factor expression in *Arabidopsis* roots. *Proc. Natl. Acad. Sci. U.S.A.* 103, 6055–6060. doi: 10.1073/pnas.0510607103

Levesque, M. P., Vernoux, T., Busch, W., Cui, H., Wang, J. Y., and Blilou, I. (2006). Whole-genome analysis of the SHORT-ROOT developmental pathway in *Arabidopsis*. *PLoS Biol.* 4:e143. doi: 10.1371/journal.pbio.0040143

Long, Y., Scheres, B., and Blilou, I. (2015a). The logic of communication: roles for mobile transcription factors in plants. *J. Exp. Bot.* 66, 1133–1144. doi: 10.1093/jxb/eru548

Long, Y., Smet, W., Cruz-Ramírez, A., Castelijns, B., de Jonge, W., and Mähönen, P. (2015b). *Arabidopsis* BIRD zinc finger proteins jointly stabilize tissue boundaries by confining the cell fate regulator SHORT-ROOT and contributing to fate specification. *Plant Cell* 27, 1185–1199. doi: 10.1105/tpc.114.132407

Mähönen, A. P., ten Tusscher, K., Siligato, R., Smetana, O., Diaz-Trivino, S., Salojärvi, J., et al. (2014). PLETHORA gradient formation mechanism separates auxin responses. *Nature* 515, 125–129. doi: 10.1038/nature13663

Makkena, S., and Lamb, R. S. (2013). The bHLH transcription factor SPATULA regulates root growth by controlling the size of the root meristem. *BMC Plant Biol.* 13:1. doi: 10.1186/1471-2229-13-1

Matsuzaki, Y., Ogawa-Ohnishi, M., Mori, A., and Matsubayashi, Y. (2010). Secreted peptide signals required for maintenance of root stem cell niche in *Arabidopsis*. *Science* 329, 1065–1067. doi: 10.1126/science.1191132

Meng, L., Buchanan, B. B., Feldman, L. J., and Luan, S. (2012). CLE-like (CLEL) peptides control the pattern of root growth and lateral root development in *Arabidopsis*. 109. doi: 10.1073/pnas.1119864109

Miyashima, S., Koi, S., Hashimoto, T., and Nakajima, K. (2011). Non-cell-autonomous microRNA165 acts in a dose-dependent manner to regulate multiple differentiation status in the *Arabidopsis* root. *Development* 138, 2303–2313. doi: 10.1242/dev.060491

Moubayidin, L., Di Mambro, R., Sozzani, R., Pacifici, E., Salvi, E., Terpstra, I., et al. (2013). Spatial coordination between stem cell activity and cell differentiation in the root meristem. *Dev. Cell* 26, 405–415. doi: 10.1016/j.devcel.2013.06.025

Mouchel, C. F., Briggs, G. C., and Hardtke, C. S. (2004). Natural genetic variation in *Arabidopsis* identifies BREVIS RADIX, a novel regulator of cell proliferation and elongation in the root. *Genes Dev.* 18, 700–714. doi: 10.1101/gad.1187704

Mouchel, C. F., Osmont, K. S., and Hardtke, C. S. (2006a). BRX mediates feedback between brassinosteroid levels and auxin signalling in root growth. *Nature* 443, 458–461. doi: 10.1038/nature05130

Mouchel, F., Hardtke, C. S., and Briggs, G. C. (2006b). Characterization of the plant-specific BREVIS RADIX gene family reveals limited genetic redundancy despite high sequence conservation 1. *Plant Physiol.* 140, 1306–1316. doi: 10.1104/pp.105.075382

Nakajima, K., Sena, G., Nawy, T., and Benfey, P. N. (2001). Intercellular movement of the putative transcription factor SHR in root patterning. *Nature* 413, 307–311. doi: 10.1038/35095061

Nardmann, J., Reisewitz, P., and Werr, W. (2009). Discrete shoot and root stem cell-promoting WUS/WOX5 functions are an evolutionary innovation of angiosperms. *Mol. Biol. Evol.* 26, 1745–1755. doi: 10.1093/molbev/msp084

Nardmann, J., Zimmermann, R., Durantini, D., Kranz, E., and Werr, W. (2007). WOX gene phylogeny in Poaceae: a comparative approach addressing leaf and embryo development. *Mol. Biol. Evol.* 24, 2474–2484. doi: 10.1093/molbev/msm182

Ortega-Martínez, O., Pernas, M., Carol, R. J., and Dolan, L. (2007). Ethylene modulates stem cell division in the *Arabidopsis thaliana* root. *Science* 317, 507–511. doi: 10.1126/science.1143409

Palmer, C. M., Bush, S. M., and Maloof, J. N. (2012). *Phenotypic and Developmental Plasticity in Plants*. eLS. Chichester: John Wiley & Sons Ltd. doi: 10.1002/9780470015902.a0002092.pub2

Petersson, S. V., Johansson, A. I., Kowalczyk, M., Makoveychuk, A., Wang, J. Y., Moritz, T., et al. (2009). An auxin gradient and maximum in the *Arabidopsis* root apex shown by high-resolution cell-specific analysis of IAA distribution and synthesis. *Plant Cell* 21, 1659–1668. doi: 10.1105/tpc.109.066480

Pi, L., Aichinger, E., van der Graaff, E., Llavata-Peris, C. I., Weijers, D., Hennig, L., et al. (2015). Organizer-derived WOX5 signal maintains root columella stem cells through chromatin-mediated repression of CDF4 expression. *Dev. Cell* 33, 576–588. doi: 10.1016/j.devcel.2015.04.024

Rigal, A., Yordanov, Y., Perrone, I., Karlberg, A., Tisserant, E., Bellini, C., et al. (2012). The Populus AINTEGUMENTA LIKE 1 homeotic transcription factor PtAIL1 controls the formation of adventitious root primordia. *Plant Physiol.* 160, 1996–2006. doi: 10.1104/pp.112.204453

Rim, Y., Huang, L., Chu, H., Han, X., Cho, W. K., Jeon, C. O., et al. (2011). Analysis of *Arabidopsis* transcription factor families revealed extensive capacity for cell-to-cell movement as well as discrete trafficking patterns. *Mol. Cells* 32, 519–526. doi: 10.1007/s10059-011-0135-2

Sabatini, S., Heidstra, R., Wildwater, M., and Scheres, B. (2003). SCARECROW is involved in positioning the stem cell niche in the *Arabidopsis* root meristem service SCARECROW is involved in positioning the stem cell niche in the *Arabidopsis* root meristem. *Genes Dev.* 17, 354–358. doi: 10.1101/gad.252503

Sarkar, A. K., Luijten, M., Miyashima, S., Lenhard, M., Hashimoto, T., Nakajima, K., et al. (2007). Conserved factors regulate signalling in *Arabidopsis thaliana* shoot and root stem cell organizers. *Nature* 446, 811–814. doi: 10.1038/nature05703

Scacchi, E., Osmont, K. S., Beuchat, J., Salinas, P., Navarrete-gómez, M., Trigueros, M., et al. (2009). Dynamic, auxin-responsive plasma membrane-to-nucleus movement of *Arabidopsis* BRX. *Development* 2067, 2059–2067. doi: 10.1242/dev.035444

Scheres, B., Dilaurenzio, L., Willemsen, V., Hauser, M. T., Janmaat, K., Weisbeek, P., et al. (1995). Mutations affecting the radial organisation of the *Arabidopsis* root display specific defects throughout the embryonic axis. *Development* 121, 53–62.

Schlereth, A., Möller, B., Liu, W., Kientz, M., Flipse, J., Rademacher, E. H., et al. (2010). MONOPTEROS controls embryonic root initiation by regulating a mobile transcription factor. *Nature* 464, 2–6. doi: 10.1038/nature08836

Sozzani, R., Cui, H., Moreno-Risueno, M. A., Busch, W., Van Norman, J. M., Vernoux, T., et al. (2010). Spatiotemporal regulation of cell-cycle genes by SHORTROOT links patterning and growth. *Nature* 466, 128–132. doi: 10.1038/nature09143

Stahl, Y., Grabowski, S., Bleckmann, A., Kühnemuth, R., Weidtkamp-Peters, S., Pinto, K. G., et al. (2013). Moderation of *Arabidopsis* root stemness by CLAVATA1 and ARABIDOPSIS CRINKLY4 receptor kinase complexes. *Curr. Biol.* 23, 362–371. doi: 10.1016/j.cub.2013.01.045

Stahl, Y., Wink, R. H., Ingram, G. C., and Simon, R. (2009). A signaling module controlling the stem cell niche in *Arabidopsis* root meristems. *Curr. Biol.* 19, 909–914. doi: 10.1016/j.cub.2009.03.060

Tsukagoshi, H., Busch, W., and Benfey, P. N. (2010). Transcriptional regulation of ROS controls transition from proliferation to differentiation in the root. *Cell* 143, 606–616. doi: 10.1016/j.cell.2010.10.020

van den Berg, C., Willemsen, V., Hendriks, G., and Scheres, B. (1997). Short-range control of cell differentiation in the *Arabidopsis* root meristem. *Nature* 390, 287–289. doi: 10.1038/36856

Vatén, A., Dettmer, J., Wu, S., Stierhof, Y. D., Miyashima, S., Yadav, S. R., et al. (2011). Callose biosynthesis regulates symplastic trafficking during root development. *Dev. Cell* 21, 1144–1155. doi: 10.1016/j.devcel.2011.10.006

Vilarrasa-Blasi, J., González-García, M.-P., Frigola, D., Fàbregas, N., Alexiou, K. G., López-Bigas, N., et al. (2014). Regulation of plant stem cell quiescence by a brassinosteroid signaling module. *Dev. Cell* 30, 36–47. doi: 10.1016/j.devcel.2014.05.020

Welch, D., Hassan, H., Blilou, I., Immink, R., Heidstra, R., and Scheres, B. (2007). Restricting SHORT-ROOT action *Arabidopsis* JACKDAW and MAGPIE zinc finger proteins delimit asymmetric cell division and stabilize tissue boundaries by restricting SHORT-ROOT action. *Genes Dev.* 21, 2196–2204. doi: 10.1101/gad.440307

Whitford, R., Fernandez, A., Tejos, R., Perez, A. C., Kleine-Vehn, J., Vanneste, S., et al. (2012). GOLVEN secretory peptides regulate auxin carrier turnover during plant gravitropic responses. *Dev. Cell* 22, 678–685. doi: 10.1016/j.devcel.2012.02.002

Willemsen, V., Bauch, M., Bennett, T., Campilho, A., Wolkenfelt, H., Xu, J., et al. (2008). The NAC domain transcription factors FEZ and SOMBRERO control the orientation of cell division plane in *Arabidopsis* root stem cells. *Dev. Cell* 15, 913–922. doi: 10.1016/j.devcel.2008.09.019

Wu, S., and Gallagher, K. L. (2013). Intact microtubules are required for the intercellular movement of the SHORT-ROOT transcription factor. *Plant J.* 74, 148–159. doi: 10.1111/tpj.12112

Wysocka-Diller, J. W., Helariutta, Y., Fukaki, H., Malamy, J. E., and Benfey, P. N. (2000). Molecular analysis of SCARECROW function reveals a radial patterning mechanism common to root and shoot. *Dev. Biol.* 603, 595–603.

Zhang, W., Swarup, R., Bennett, M., Schaller, G. E., and Kieber, J. J. (2013). Cytokinin induces cell division in the quiescent center of the *Arabidopsis* root apical meristem. *Curr. Biol.* 23, 1979–1989. doi: 10.1016/j.cub.2013.08.008

Zhang, Y., Jiao, Y., Liu, Z., and Zhu, Y. (2015). ROW1 maintains quiescent centre identity by confining WOX5 expression to specific cells. *Nat. Commun.* 6, 1–8. doi: 10.1038/ncomms7003

Zhao, S., Jiang, Q. T., Ma, J., Zhang, X. W., Zhao, Q. Z., Wang, X. Y., et al. (2014). Characterization and expression analysis of WOX5 genes from wheat and its relatives. *Gene* 537, 63–69. doi: 10.1016/j.gene.2013.12.022

Conflict of Interest Statement: The authors declare that the research was conducted in the absence of any commercial or financial relationships that could be construed as a potential conflict of interest.

II. Dynamic complexity: plant receptor complexes at the plasma membrane

The following manuscript was published in Current Opinion in Plant Biology in July 2017 (doi: https://doi.org/10.1016/j.pbi.2017.06.016).

Authors:

Rebecca C. Burkart[1] and Yvonne Stahl[1]

Affiliations:

[1]Institute for Developmental Genetics, Heinrich-Heine-University, Universitätsstr. 1, D-40225 Düsseldorf, Germany

Contributions:

Rebecca C. Burkart and Yvonne Stahl wrote the manuscript.

Available online at www.sciencedirect.com

ScienceDirect

Current Opinion in Plant Biology

Dynamic complexity: plant receptor complexes at the plasma membrane

Rebecca C Burkart and Yvonne Stahl

Plant receptor complexes at the cell surface perceive many different external and internal signalling molecules and relay these signals into the cell to regulate development, growth and immunity. Recent progress in the analyses of receptor complexes using different live cell imaging approaches have shown that receptor complex formation and composition are dynamic and take place at specific microdomains at the plasma membrane. In this review we focus on three prominent examples of *Arabidopsis thaliana* receptor complexes and how their dynamic spatio-temporal distribution at the PM has been studied recently. We will elaborate on the newly emerging concept of plasma membrane microdomains as potential hubs for specific receptor complex assembly and signalling outputs.

Address
Institute for Developmental Genetics, Heinrich-Heine University, Universitätsstr. 1, D-40225 Düsseldorf, Germany

Corresponding author: Stahl, Yvonne (Yvonne.Stahl@hhu.de)

Current Opinion in Plant Biology 2017, **40**:15–21

This review comes from a themed issue on **Cell biology**

Edited by **Eugenia Russinova** and **Karin Schumacher**

For a complete overview see the Issue and the Editorial

Available online 14th July 2017

http://dx.doi.org/10.1016/j.pbi.2017.06.016

Introduction

Plants as sessile organisms have to adapt to a variety of environmental and internal stimuli by coordinating their growth, development and reproduction accordingly and therefore show a high degree of developmental and morphological plasticity. In order to perceive external and internal signalling molecules, plants have evolved a high number of plasma membrane (PM)-localized receptor-like kinases (RLKs) and receptor-like proteins (RLPs) (more than 600 in Arabidopsis) [1]. RLKs usually consist of a distinct extracellular domain (ED) that can specifically sense signals (e.g. phytohormones, proteins, small peptides, polysaccharides, etc.), a single transmembrane domain (TMD) and an intracellular kinase domain (KD) transmitting the signal into the cell for the necessary differential outputs, for example, regulation of development, growth, and immunity. In Arabidopsis the largest group of RLKs with more than 200 predicted members contains leucine rich repeats (LRRs) in the ED [1]. RLPs, in contrast to RLKs are lacking an intracellular kinase domain and often act as co-receptors together with RLKs. In many cases the binding of the ligand to the extracellular domain of the PM-localized RLK triggers the formation of specific receptor complexes and downstream signalling events.

The plant PM is a highly organized but also dynamic structure and consists of a phospholipid bilayer and integral (like RLKs) or peripheral proteins. The PM is further sub-compartmentalized dependent on lipid composition, protein–protein or protein–lipid interactions, and possibly interactions with components of the cytoskeleton and/or the cell wall into different nanoclusters or microdomains (hereafter for simplification called microdomains). The existence of distinct microdomains at the PM has been observed in Arabidopsis and *Nicotiana benthamiana* and their patterns and dynamics characterized using different marker proteins [2,3]. A novel proposed definition of PM microdomains and nanodomains can be found in [4].

How signalling specificity is achieved is one of the most urging questions as many different RLKs are present in the confined space of the same PM, yet they have to react to distinct signals requiring differential signalling outputs. Recent findings suggest that receptor complex partitioning to PM microdomains could specify signalling outputs as some PM microdomains were found to be temporally stable structures and could therefore provide a 'scaffold' for spatio-temporal partitioning of protein interactions, thereby specifying differential signalling outputs [2,3]. In this review we focus on three key receptor complexes involved in the perception of phytohormones, pathogen associated molecular patterns (PAMPs) or small peptides, and on recent findings on their dynamic localization to specific PM microdomains.

Brassinosteroid perception by the BRI1/BAK1 (SERK3) complex

One of the best studied phytohormone sensing receptor complexes is the one sensing brassinosteroids (BRs). BRs are plant steroid hormones that control cell expansion, division and differentiation [5]. BRs are mainly perceived by the extracellular domains of the LRR-RLK BRASSINOSTEROID INSENSITIVE1 (BRI1), BRI1-LIKE1 (BRL1) or BRL3. Heteromeric complexes of BRI1, BRL1 or BRL3 with another LRR-RLK named BRI1 ASSOCIATED KINASE1 (BAK1) (also known as SOMATIC EMBRYOGENESIS RECEPTOR

KINASE3 (SERK3)) or other members of the SERK family [6–11] are formed after ligand perception and the subsequent dissociation of the BRI1 KINASE INHIBITOR 1 (BKI1) from the BRI1 kinase domain [12,13]. Generally, SERK RLKs have a smaller extracellular domain containing only five LRRs and interact with many ligand-binding RLKs for example, involved in phytohormone perception, developmental decisions and plant defence (recently reviewed in [14]). The following trans-phosphorylation of the BRI1 and BAK1 (SERK3) kinase domains initiates an intracellular signalling cascade regulating numerous aspects of plant growth and development (for more details see these latest reviews [15–17]).

Recently, the use of advanced fluorescence techniques like variable angle total internal reflection microscopy (VA-TIRFM, Table 1) allowed the examination of the long and short distance mobility of BRI1-GFP molecules at the PM by single particle tracking (SPT). This aided the observation that BRI1 is not homogenously distributed at the PM but localizes as a mixture of monomers and dimers in PM microdomains, which may be involved in BR-regulated BRI1 partitioning [18•]. The application of fluorescence cross correlation spectroscopy (FCCS, Table 1) showed the close correlation of BRI1 diffusion with the PM microdomain marker Arabidopsis FLOTILLIN1 (AtFlot1) but also with CLATHRIN-LIGHT-CHAIN (CLC), a marker for clathrin-dependent endocytosis indicating that clathrin-dependent and PM microdomain-dependent endocytosis of BRI1 coexist [18•].

The BRI1/BAK1(SERK3) complexes were already shown to be at least to some extent preassembled at the PM [10], whereas the BRI1/SERK1 complex only forms in a ligand-induced manner [19]. BRI1/BAK1(SERK3) complexes are also found in microdomains at the PM which has recently been shown using variable angle epifluorescence microscopy (VAEM, Table 1) on Arabidopsis root cells in the elongation zone [20••]. The density and mobility of the observed microdomains was not influenced by ligand-availability or BRI1 or SERK concentrations [20••].

Furthermore, in a more detailed analysis measuring Förster Resonance Energy Transfer (FRET, Table 1) by fluorescence lifetime imaging microscopy (FLIM, Table 1) at the surface of the PM in roots using Selected Surface Observation FLIM (SSO-FLIM, Table 1), the

Table 1

Live cell imaging techniques used to study receptor complexes at the PM.

Technique	Description	Receptors analysed	References
VA-TIRFM/VAEM	Both techniques use an evanescence wave for illuminating only a very thin layer of the sample in close proximity (~100 nm) to the coverslip, which allows for reduction of background from out-of-focus regions by total internal reflection of the illuminating laser light using a critical angle (TIRFM = total internal reflection fluorescence microscopy). Variable angle (VA)-TIRFM or variable angle epifluorescence microscopy (VAEM) use subcritical angles for creating the evanescence wave in order to compensate diffractions caused by the plant cell wall. Single fluorescently labelled molecules can be resolved if their distance is greater than the diffraction limit (~200 nm). This technique is often used for dynamic co-localization studies.	BRI1/BAK1(SERK3) BRI1 FLS2	[18•,20••] [47••] [47••]
SPT	Single particle tracking (SPT) is often combined with VA-TIRM/VAEM because of the improved signal to noise ratio.	BRI1/BAK1(SERK3) BRI1 FLS2	[18•] [47••] [47••]
FCCS	Fluorescence cross correlation spectroscopy (FCCS) of two different fluorophore-labelled molecules over time reflects their interaction, mobility and concentration.	BRI1/BAK1(SERK3)	[18•]
FRET FLIM	This technique allows for studying protein–protein interactions as the donor and acceptor molecules must be in close proximity (<10 nm) for Förster resonance energy transfer (FRET) to occur. The energy transfer from a donor to an acceptor fluorophore can be measured by the reduction of the fluorescence lifetime of the donor (FLIM = fluorescence lifetime imaging microscopy).	BRI1/BAK1(SERK3)	[20••]
SSO-FLIM	In order to omit signals from the underlying structures in the cell the confocal spot is positioned perpendicular to the PM and FLIM measurements are acquired (selective surface observation = SSO).	BRI1/BAK1(SERK3)	[20••]
MFIS	With multiparameter fluorescence imaging spectroscopy (MFIS), a combination of fluorescence parameters can be acquired at once, for example, fluorescence lifetime and anisotropy. This can be used to measure protein–protein interactions and to distinguish homomeric and heteromeric complex composition.	CLV1/CLV2/CRN CLV1/ACR4	[51••] [52]

This table highlights only some of the techniques that have been recently used to study composition, dynamics and localization of the three described receptor complexes at the PM *in vivo*.

Figure 1

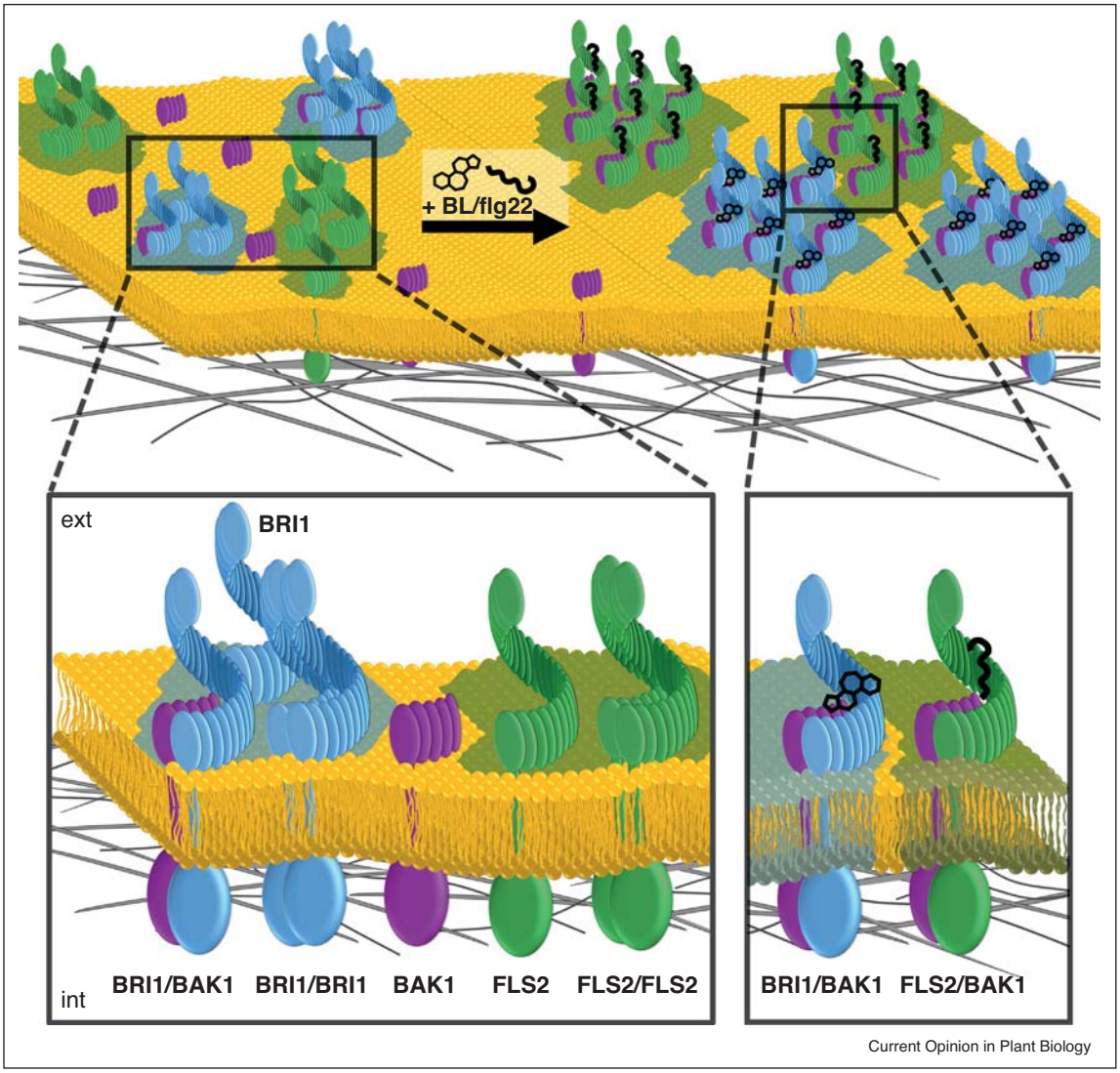

BRI1/BAK1(SERK3) and FLS2/BAK1(SERK3) receptor complexes in PM microdomains. BRI1 localizes as a mixture of monomers and dimers at the PM in microdomains. BRI1/BAK1(SERK3) complexes are at least partially preformed before BL perception, but after BL perception higher order BRI1/BAK1(SERK3) complexes are formed in larger microdomains. FLS2 is also present in microdomains at the PM, but only forms complexes with BAK1(SERK3) after binding of flagellin or flg22. Over time higher order complexes of FLS2/BAK1(SERK3) are formed in larger microdomains spatially separated from the BRI1/BAK1(SERK3) complexes. BRI1 (blue), BAK1(SERK3) (magenta), FLS2 (green), PM phospholipid bilayer (yellow), cytoskeleton (grey), BL = brassinolide, PM = plasma membrane, shaded areas = microdomains, ext = extracellular space, int = intracellular space.

existence of a certain amount of pre-formed BRI1/BAK1 (SERK3) complexes was confirmed independently of ligand-availability [20••]. The general mobility of BRI1-GFP at the PM is relatively low [18•,20••], suggesting that BRI1/SERK complexes might be transported to the PM already as preassembled units, which has also been observed previously [10] (Figure 1).

Flg22 perception by the FLS2/BAK1(SERK3) complex

All organisms must defend themselves against pathogens to survive and one way to do this is via the perception of environmental signals that induce an immune response. Plants have an innate immunity that perceives such signals through surface-localized pattern recognition receptors (PRRs) which results in PRR-triggered immunity (PTI). Plant PRRs are surface localized RLKs or RLPs, that contain extracellular motifs like LRR domains, lysin motifs (LysM), lectin motifs or epidermal growth factor (EGF)-like domains (as recently reviewed in [21]).

One of the most studied receptor complexes in plant defence is the FLAGELLIN SENSITIVE2 (FLS2)/

BAK1(SERK3) complex [22]. FLS2 is activated upon flagellin (or the elicitor-active epitope flg22) binding, which also triggers complex formation with BAK1 (SERK3) and results in an early PAMP response and PTI [22–26]. The downstream signalling pathway consists of different components and results in a reactive oxygen species (ROS) burst, calcium accumulation and stomatal closure [27–33]. Before binding of flg22, in the pre-active state, FLS2 as well as BAK1/SERK3 can be found within different independent complexes. FLS2 forms a complex with the PM-localized protein kinase, BOTRYTIS-INDUCED KINASE1 (BIK1) that gets phosphorylated, dissociates and activates G-protein signalling after complex formation with BAK1, resulting in ROS production [29,34–36]. BAK1 in turn forms a complex with the LRR-RLKs BAK1-INTERACTING RLK1 (BIR1), BIR2 and BIR3. BIR1 controls the activation of G-protein signalling cascades after the activation of the FLS2/BAK1 complex, once again leading to changes in ROS and calcium levels [33,37,38]. BIR2 prevents the interaction of BAK1 with FLS2 and is released from BAK1 upon PAMP perception which consequently enables BAK1-FLS2 association [36,39,40]. Upon flg22 binding and activation of FLS2, BAK1 instantly interacts with FLS2 and leaves BIR1 [33]. Later after flg22 perception, a flagellin-induced degradation of FLS2 takes place, where FLS2 is poly-ubiquitinated and gets internalized into intracellular mobile vesicles which is followed by its degradation [41] (for more details see [42]). This flagellin-induced degradation is time-dependent and dose-dependent and leads to a desensitizing of the host cells to the stimulus. Resensitization takes place upon *de novo* synthesis of FLS2 [43]. Additionally, BR-SIGNALLING KINASE1 (BSK1), a PM-localized kinase normally involved in BR-signalling, mediates signal transduction by acting as a substrate of the receptor kinase BRI1 [44], physically interacts with FLS2 and is required for flg22-induced responses [45]. Further information on membrane nano-domains and microdomains involved in plant-microbe interactions is reviewed in [4].

BRI1 and FLS2 signalling pathways show many similarities, for example, they share the same co-receptor BAK1 (SERK3), the protein kinase BIK1 and can both be found as monomers and dimers at the PM [18•,22,26,34]. Many BAK1-interacting PRRs share a common internalization and intracellular trafficking pathway similar to that of the hormone receptor BRI1. In case of FLS2, clathrin-dependent endocytosis mediates immune responses like stomatal closure and callose deposition [46]. In a recent study using VAEM and SPT, the spatial partitioning and dynamics of both receptors into separate microdomains was observed. This partitioning at the PM is suggested to result in the spatio-temporal separation of immune signalling and brassinosteroid signal transduction and could explain how the specificity of the two pathways is ensured even though they share some of the same signalling components [47••] (Figure 1). Recently, the malectin-like RLK FERONIA (FER) which perceives the immune response dampending RAPID ALKALINIZATION FACTOR (RALF) peptides was found to act as a 'scaffold' for the assembly of FLS2 or ELONGATION FACTOR-TU (EF-Tu) RECEPTOR (EFR) complexes with BAK1(SERK3). This could indicate that FER also resides at PM microdomains as part of a potential signalling hub, but this hypothesis still has to be verified [48•].

CLE peptide perception by CLV1/CLV2/CRN or CLV1/ACR4 receptor complexes

Another prominent example of a LRR-RLK involved in the maintenance of stem cell homeostasis in floral and shoot apical meristems is CLAVATA1 (CLV1). CLV1 perceives the small signalling peptide CLV3 and acts together with the LRR-RLP CLAVATA2 (CLV2) which lacks an intracellular kinase domain and the RLK CORYNE (CRN) which lacks a functional extracellular domain but contains a pseudo-kinase domain. This signalling pathway results in a negative feedback loop involving the homeodomain transcription factor WUSCHEL, which is a key component in stem cell maintenance (as reviewed in [49]).

CLV2 and CRN interact at the PM via their TMDs and form complexes with CLV1 dimers which was revealed measuring FRET [50]. Recently, a comparative, dynamic analysis of FLS2/BAK1(SERK3) and CLV1/CLV2/CRN complex formation in response to flg22 and CLV3, respectively, using multiparameter fluorescence imaging spectroscopy (MFIS, Table 1) uncovered a fundamental difference of the two signalling pathways [50]. The FLS2/BAK1(SERK3) heteromeric complex formation only occurs shortly after binding of the ligand flg22, whereas the CLV1/CLV2/CRN complex already exists ligand-independently as a preformed complex at the PM. Both receptor complexes then form, in response to their respective ligands, higher order complexes in clusters (microdomains) at the PM over time which was also described for BR-activated BRI1/BAK1(SERK3) complexes [10,51••] (Figure 2).

An explanation for ligand-independent receptor complex formation could be that signalling responses of the described BRI1/BAK1(SERK3) and CLV1/CLV2/CRN complexes are required continuously for maintaining plant growth and stem cell homeostasis and receptor complex pre-formation may facilitate this task. In contrast, FLS2/BAK1(SERK3) signalling interferes with plant growth and development and it is therefore advantageous for the plant to only activate this signalling upon pathogen attack. Therefore, the FLS2/BAK1(SERK3) complexes only form when a pathogen signal (like flagellin or flg22) is actually perceived [50]. The following formation of higher order complexes in larger PM microdomains that occurs after

Figure 2

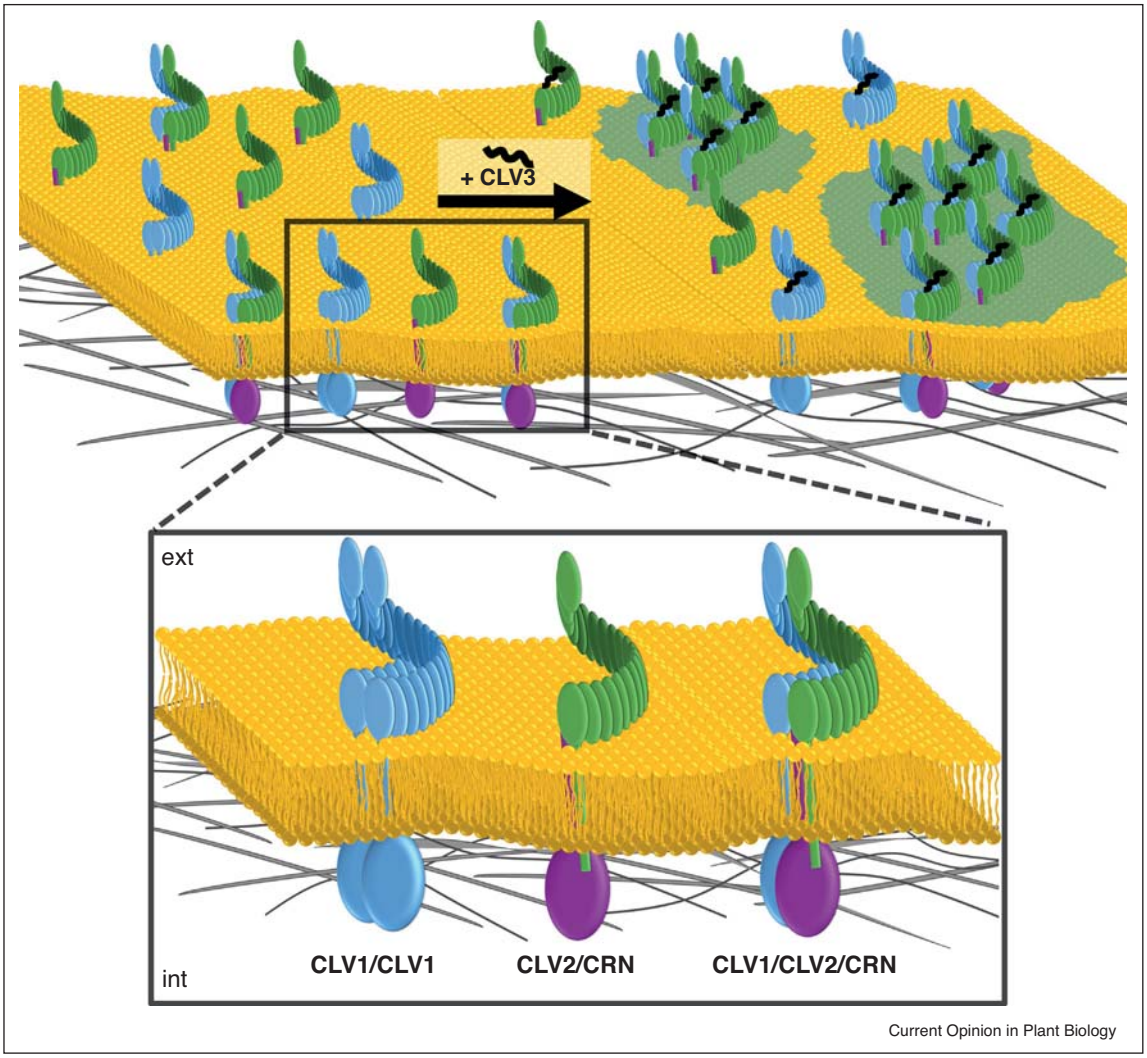

CLV1/CLV2/CRN receptor complexes in PM microdomains. CLV1 homomers, CLV2/CRN heteromers, and CLV1/CLV2/CRN receptor complexes are already preformed before binding of CLV3. After ligand perception higher order CLV1/CLV2/CRN complexes are formed in larger microdomains at the PM. CLV1 (blue), CLV2 (green), CRN (magenta), PM phospholipid bilayer (yellow), cytoskeleton (grey), PM = plasma membrane, shaded areas = microdomains, ext = extracellular space, int = intracellular space.

ligand perception in all three described receptor complexes may serve to reinforce and/or to further separate differential signalling events.

Further specialized PM domains, like the PM lining the plasmodesmal pore (PD PM), might also provide yet another specific domain necessary for differential signalling outputs. Receptor complexes involved in root stem cell signalling, like CLV1 and ARABIDOPSIS CRINKLY4 (ACR4) show differential complex composition at the PM compared to the PD PM as analysed by MFIS [52]. Also other RLKs involved in development and immune signalling have been observed to localize at plasmodesmata, implicating a specific role of these PD PM domains for signal perception and/or integration of extracellular and intracellular signalling events [53,54].

Conclusions and outlook

Various state-of-the-art live cell imaging techniques (as reviewed in [55,56]) have been successfully applied to observe microdomain (co-)localization and receptor complex formation in a ligand-dependent manner over time at the PM (summarized in Table 1). These techniques provide applicable measures to tackle urgent questions that still need to be answered, like what are the concentrations of receptors, what is the stoichiometry of receptor complexes, how dynamic is receptor complex formation and how stable are receptor complexes at PM microdomains.

Further research is needed to show if receptor complexes are formed *de novo* in the potentially functionally distinct PM microdomains or if they are brought to the PM in an already preassembled state as suggested for CLV1/CLV/CRN and BRI1/BAK1(SERK3) [10,20••,51••]. It will also be necessary to investigate which types of phospholipids (e.g. sterols or sphingolipids [18•]) are necessary for PM microdomain formation and if receptor complex formation is dependent on a specific lipid composition [57]. Furthermore, it has to be analysed if components of the cytoskeleton or the cell wall are also involved in PM microdomain formation or stabilization by further biochemical approaches [47••]. Receptor complex localization to distinct microdomains at the PM or plasmodesmata could also define entry sites to differential clathrin-dependent or independent endocytic pathways and thereby may serve as hubs for differential signal transduction. Furthermore, other plant organelles also show sub-compartmentalization (e.g. dynamic microdomains within the nucleus or cytosol) and it will be interesting to compare if these may as well function as potential signalling hubs in a similar manner as PM microdomains.

Taken together, the recent observations of specific RLK complex formation at distinct PM microdomains suggests that rapid PM compartmentalization following a signalling stimulus might be crucial for an appropriate and specific signalling response, for example, by enabling the assembly of specific signalling clusters by the separation of shared co-receptors to avoid signalling crosstalk. It remains to be elucidated whether PM microdomain association of RLK complexes is critical for their function and activity in the different signalling pathways (e.g. on the level of stimuli perception, kinase activity, differential phosphorylation of KDs or ubiquitination). Therefore, it will be important to unravel the molecular mechanisms underlying the dynamic partitioning of receptor complexes into the various PM microdomain compartments [57].

Acknowledgements

We thank Stefanie Weidtkamp-Peters and Rüdiger Simon for critical reading of the manuscript. We apologize to all colleagues whose relevant work could not be mentioned because of space restrictions. This work was funded by the Deutsche Forschungsgesellschaft (DFG, Sta 1212/1-1).

References and recommended reading

Papers of particular interest, published within the period of review, have been highlighted as:

- • of special interest
- • of special interest

1. Shiu SH, Bleecker AB: **Expansion of the receptor-like kinase/Pelle gene family and receptor-like proteins in Arabidopsis**. *Plant Physiol* 2003, **132**:530-543.

2. Konrad SSA, Ott T: **Molecular principles of membrane microdomain targeting in plants**. *Trends Plant Sci* 2015, **20**:351-361.

3. Jarsch IK, Konrad SSA, Stratil TF, Urbanus SL, Szymanski W, Braun P, Braun K-H, Ott T: **Plasma membranes are subcompartmentalized into a plethora of coexisting and diverse microdomains in Arabidopsis and *Nicotiana benthamiana***. *Plant Cell* 2014, **26**:1698-1711.

4. Ott T: **Membrane nano- and microdomains in plant-microbe interactions**. *Curr Opin Plant Biol* 2017.

5. Clouse S: **Brassinosteroids**. *Curr Biol* 2001, **11**:R904.

6. Nam KH, Li J: **BRI1/BAK1, a receptor kinase pair mediating brassinosteroid signaling**. *Cell* 2002:203-212.

7. Li J, Wen J, Lease KA, Doke JT, Tax FE, Walker JC: **BAK1, an Arabidopsis LRR receptor-like protein kinase, interacts with BRI1 and modulates brassinosteroid signaling**. *Cell* 2002:213-222.

8. Wang X, Kota U, He K, Blackburn K, Li J, Goshe MB, Huber SC, Clouse SD: **Sequential transphosphorylation of the BRI1/BAK1 receptor kinase complex impacts early events in brassinosteroid signaling**. *Dev Cell* 2008, **15**:220-235.

9. Russinova E, Borst JW, Kwaaitaal M, Cano-Delgado A, Yin Y, Chory J, de Vries SC: **Heterodimerization and endocytosis of Arabidopsis brassinosteroid receptors BRI1 and AtSERK3 (BAK1)**. *Plant Cell* 2004, **16**:3216-3229.

10. Bücherl CA, van Esse GW, Kruis A, Luchtenberg J, Westphal AH, Aker J, van Hoek A, Albrecht C, Borst JW, de Vries SC: **Visualization of BRI1 and BAK1(SERK3) membrane receptor heterooligomers during brassinosteroid signaling**. *Plant Physiol* 2013, **162**:1911-1925.

11. Li J, Chory J: **A putative leucine-rich repeat receptor kinase involved in brassinosteroid signal transduction**. *Cell* 1997, **90**:929-938.

12. Wang X, Chory J: **Brassinosteroids regulate dissociation of BKI1, a negative regulator of BRI1 signaling, from the plasma membrane**. *Science* 2006, **313**:1118-1122.

13. Jaillais Y, Hothorn M, Belkhadir Y, Dabi T, Nimchuk ZL, Meyerowitz EM, Chory J: **Tyrosine phosphorylation controls brassinosteroid receptor activation by triggering membrane release of its kinase inhibitor**. *Genes Dev* 2011, **25**:232-237.

14. Ma X, Xu G, He P, Shan L: **SERKing coreceptors for receptors**. *Trends Plant Sci* 2016, **21**:1017-1033.

15. Jaillais Y, Vert G: **Brassinosteroid signaling and BRI1 dynamics went underground**. *Curr Opin Plant Biol* 2016, **33**:92-100.

16. Belkhadir Y, Jaillais Y: **The molecular circuitry of brassinosteroid signaling**. *New Phytol* 2015, **206**:522-540.

17. Singh AP, Savaldi-Goldstein S: **Growth control, brassinosteroid activity gets context**. *J Exp Bot* 2015, **66**:1123-1132.

18. • Wang L, Li H, Lv X, Chen T, Li R, Xue Y, Jiang J, Jin B, Baluska F, Samaj J *et al.*: **Spatiotemporal dynamics of the BRI1 receptor and its regulation by membrane microdomains in living Arabidopsis cells**. *Mol Plant* 2015, **8**:1334-1349.
In this article VA-TIRF and FCCS were used to study BRI1 mobility in Arabidopsis. The authors found that BR promotes the partitioning of BRI1 into functional membrane microdomains to activate BR signalling.

19. Santiago J, Henzler C, Hothorn M: **Molecular mechanism for plant steroid receptor activation by somatic embryogenesis co-receptor kinases**. *Science* 2013, **341**:889-892.

20. •• Hutten SJ, Hamers DS, Aan den Toorn M, van Esse W, Nolles A, Bücherl CA, de Vries SC, Hohlbein J, Borst JW: **Visualization of BRI1 and SERK3/BAK1 nanoclusters in Arabidopsis roots**. *PLOS ONE* 2017, **12**:e0169905.
In this study the authors observed hetero-oligomerisation of BRI1 and BAK1 (SERK3) in ligand-independent nanoclusters by using SSO-FLIM. Active BR signalling induced the reduction of BRI1/BAK1(SERK3) heteromers at the PM possibly indicating endocytosis of active signalling complexes.

21. Couto D, Zipfel C: **Regulation of pattern recognition receptor signalling in plants**. *Nat Rev Immunol* 2016, **16**:537-552.

22. Chinchilla D, Zipfel C, Robatzek S, Kemmerling B, Nürnberger T, Jones JDG, Felix G, Boller T: **A flagellin-induced complex of the receptor FLS2 and BAK1 initiates plant defence**. *Nature* 2007, **448**:497-500.

23. Gómez-Gómez L, Bauer Z, Boller T: **Both the extracellular leucine-rich repeat domain and the kinase activity of FSL2 are required for flagellin binding and signaling in Arabidopsis**. *Plant Cell* 2001, **13**:1155-1163.

24. Heese A, Hann DR, Gimenez-Ibanez S, Jones AME, He K, Li J, Schroeder JI, Peck SC, Rathjen JP: **The receptor-like kinase SERK3/BAK1 is a central regulator of innate immunity in plants**. *PNAS* 2007, **104**:12217-12222.

25. Gómez-Gómez L, Boller T: **FLS2: an LRR receptor-like kinase involved in the perception of the bacterial elicitor flagellin in Arabidopsis**. *Mol Cell* 2000, **5**:1003-1011.

26. Sun W, Cao Y, Jansen Labby K, Bittel P, Boller T, Bent AF: **Probing the Arabidopsis flagellin receptor. FLS2-FLS2 association and the contributions of specific domains to signaling function**. *Plant Cell* 2012, **24**:1096-1113.

27. Boutrot F, Segonzac C, Chang KN, Qiao H, Ecker JR, Zipfel C, Rathjen JP: **Direct transcriptional control of the Arabidopsis immune receptor FLS2 by the ethylene-dependent transcription factors EIN3 and EIL1**. *PNAS* 2010, **107**:14502-14507.

28. Jeworutzki E, Roelfsema MRG, Anschütz U, Krol E, Elzenga JTM, Felix G, Boller T, Hedrich R, Becker D: **Early signaling through the Arabidopsis pattern recognition receptors FLS2 and EFR involves Ca2+-associated opening of plasma membrane anion channels**. *Plant J* 2010, **62**:367-378.

29. Liang X, Ding P, Lian K, Wang J, Ma M, Li L, Li L, Li M, Zhang X, Chen S *et al.*: **Arabidopsis heterotrimeric G proteins regulate immunity by directly coupling to the FLS2 receptor**. *eLife* 2016, **5**:e13568.

30. Melotto M, Underwood W, Koczan J, Nomura K, He SY: **Plant stomata function in innate immunity against bacterial invasion**. *Cell* 2006, **126**:969-980.

31. Mersmann S, Bourdais G, Rietz S, Robatzek S: **Ethylene signaling regulates accumulation of the FLS2 receptor and is required for the oxidative burst contributing to plant immunity**. *Plant Physiol* 2010, **154**:391-400.

32. Spallek T, Beck M, Ben Khaled S, Salomon S, Bourdais G, Schellmann S, Robatzek S: **ESCRT-I mediates FLS2 endosomal sorting and plant immunity**. *PLOS Genet* 2013, **9**.

33. Tunc-Ozdemir M, Jones AM: **Ligand-induced dynamics of heterotrimeric G protein-coupled receptor-like kinase complexes**. *PLOS ONE* 2017, **12**:e0171854.

34. Lu D, Wu S, Gao X, Zhang Y, Shan L, He P: **A receptor-like cytoplasmic kinase, BIK1, associates with a flagellin receptor complex to initiate plant innate immunity**. *PNAS* 2010, **107**:496-501.

35. Zhang J, Li W, Xiang T, Liu Z, Laluk K, Ding X, Zou Y, Gao M, Zhang X, Chen S *et al.*: **Receptor-like cytoplasmic kinases integrate signaling from multiple plant immune receptors and are targeted by a *Pseudomonas syringae* effector**. *Cell Host Microbe* 2010, **7**:290-301.

36. Halter T, Imkampe J, Blaum BS, Stehle T, Kemmerling B: **BIR2 affects complex formation of BAK1 with ligand binding receptors in plant defense**. *Plant Signal Behav* 2014:9.

37. Gao M, Wang X, Wang D, Xu F, Ding X, Zhang Z, Bi D, Cheng YT, Chen S, Li X *et al.*: **Regulation of cell death and innate immunity by two receptor-like kinases in Arabidopsis**. *Cell Host Microbe* 2009, **6**:34-44.

38. Tunc-Ozdemir M, Urano D, Jaiswal DK, Clouse SD, Jones AM: **Direct modulation of heterotrimeric G protein-coupled signaling by a receptor kinase complex**. *J Biol Chem* 2016, **291**:13918-13925.

39. Blaum BS, Mazzotta S, Nöldeke ER, Halter T, Madlung J, Kemmerling B, Stehle T: **Structure of the pseudokinase domain of BIR2, a regulator of BAK1-mediated immune signaling in Arabidopsis**. *J Struct Biol* 2014, **186**:112-121.

40. Halter T, Imkampe J, Mazzotta S, Wierzba M, Postel S, Bücherl C, Kiefer C, Stahl M, Chinchilla D, Wang X *et al.*: **The leucine-rich repeat receptor kinase BIR2 is a negative regulator of BAK1 in plant immunity**. *Curr Biol* 2014, **24**:134-143.

41. Lu D, Lin W, Gao X, Wu S, Cheng C, Avila J, Heese A, Devarenne TP, He P, Shan L: **Direct ubiquitination of pattern recognition receptor FLS2 attenuates plant innate immunity**. *Science* 2011, **332**:1439-1442.

42. Li B, Lu D, Shan L: **Ubiquitination of pattern recognition receptors in plant innate immunity**. *Mol Plant Pathol* 2014, **15**:737-746.

43. Smith JM, Salamango DJ, Leslie ME, Collins CA, Heese A: **Sensitivity to Flg22 is modulated by ligand-induced degradation and *de novo* synthesis of the endogenous flagellin-receptor FLAGELLIN-SENSING2**. *Plant Physiol* 2014, **164**:440-454.

44. Tang W, Kim T-W, Oses-Prieto JA, Sun Y, Deng Z, Zhu S, Wang R, Burlingame AL, Wang Z-Y: **BSKs mediate signal transduction from the receptor kinase BRI1 in Arabidopsis**. *Science* 2008, **321**:557-560.

45. Shi H, Shen Q, Qi Y, Yan H, Nie H, Chen Y, Zhao T, Katagiri F, Tang D: **BR-SIGNALING KINASE1 physically associates with FLAGELLIN SENSING2 and regulates plant innate immunity in Arabidopsis**. *Plant Cell* 2013, **25**:1143-1157.

46. Mbengue M, Bourdais G, Gervasi F, Beck M, Zhou J, Spallek T, Bartels S, Boller T, Ueda T, Kuhn H *et al.*: **Clathrin-dependent endocytosis is required for immunity mediated by pattern recognition receptor kinases**. *PNAS* 2016, **113**:11034-11039.

47. •• Bücherl CA, Jarsch IK, Schudoma C, Segonzac C, Mbengue M, Robatzek S, MacLean D, Ott T, Zipfel C: **Plant immune and growth receptors share common signalling components but localise to distinct plasma membrane nanodomains**. *eLife* 2017, **6**:e25114.
In this study FLS2 and BRI1 were found to localize at distinct PM nanodomains marked by specific remorin proteins and differential co-localisation with the cytoskeleton using VAEM and SPT.

48. • Stegmann M, Monaghan J, Smakowska-Luzan E, Rovenich H, Lehner A, Holton N, Belkhadir Y, Zipfel C: **The receptor kinase FER is a RALF-regulated scaffold controlling plant immune signaling**. *Science* 2017, **355**:287-289.
The RLK FER perceiving the immune response dampending RALF peptides was found to act as a scaffold for the assembly of FLS2 or EF-Tu complexes with BAK1(SERK3), which might also involve FER localization to PM microdomains.

49. Stahl Y, Simon R: **Plant primary meristems: shared functions and regulatory mechanisms**. *Curr Opin Plant Biol* 2010:53-58.

50. Bleckmann A, Weidtkamp-Peters S, Seidel CAM, Simon R: **Stem cell signaling in Arabidopsis requires CRN to localize CLV2 to the plasma membrane**. *Plant Physiol* 2010, **152**:166-176.

51. •• Somssich M, Ma Q, Weidtkamp-Peters S, Stahl Y, Felekyan S, Bleckmann A, Seidel CAM, Simon R: **Real-time dynamics of peptide ligand-dependent receptor complex formation in planta**. *Sci Signal* 2015, **8**:ra76.
In this article MFIS was used to compare the dynamics of receptor complex formation upon ligand-binding to FLS2/BAK1(SERK3) and CLV1/CLV2/CRN. The CLV1/CLV2/CRN receptor complex was found, in contrast to the FLS2/BAK1(SERK3) complex, to be preformed.

52. Stahl Y, Grabowski S, Bleckmann A, Kühnemuth R, Weidtkamp-Peters S, Pinto KG, Kirschner GK, Schmid JB, Wink RH, Hülsewede A *et al.*: **Moderation of Arabidopsis root stemness by CLAVATA1 and ARABIDOPSIS CRINKLY4 receptor kinase complexes**. *Curr Biol* 2013, **23**:362-371.

53. Stahl Y, Simon R: **Gated communities: apoplastic and symplastic signals converge at plasmodesmata to control cell fates**. *J Exp Bot* 2013, **64**:5237-5241.

54. Stahl Y, Faulkner C: **Receptor complex mediated regulation of symplastic traffic**. *Trends Plant Sci* 2016, **21**:450-459.

55. Truong-Quang B-A, Lenne P-F: **Membrane microdomains. From seeing to understanding**. *Front Plant Sci* 2014, **18**:18.

56. Li X, Luu D-T, Maurel C, Lin J: **Probing plasma membrane dynamics at the single-molecule level**. *Trends Plant Sci* 2013, **18**:617-624.

57. Keinath NF, Kierszniowska S, Lorek J, Bourdais G, Kessler SA, Shimosato-Asano H, Grossniklaus U, Schulze WX, Robatzek S, Panstruga R: **PAMP (pathogen-associated molecular pattern)-induced changes in plasma membrane compartmentalization reveal novel components of plant immunity**. *J Biol Chem* 2010, **285**:39140-39149.

III. Precise transcriptional control of cellular quiescence by BRAVO/WOX5 complex in Arabidopsis roots

This chapter is a manuscript under review in Molecular Systems Biology and was uploaded on bioRxiv (doi: https://doi.org/10.1101/2020.07.15.203638).

Authors:

Isabel Betegón-Putze[1], Josep Mercadal[2,3], Nadja Bosch[1], Ainoa Planas-Riverola[1], Mar Marquès-Bueno[1], Josep Vilarrasa-Blasi[1,4], David Frigola[2], Rebecca Corinna Burkart[5], Cristina Martínez[6], Yvonne Stahl[5], Salomé Prat[6], Marta Ibañes[2,3], and Ana I. Caño-Delgado[1]

Affiliations:

[1]Department of Molecular Genetics, Centre for Research in Agricultural Genomics (CRAG) CSIC-IRTA-UAB-UB, Campus UAB (Cerdanyola del Vallès), 08193 Barcelona, Spain.

[2]Departament de Matèria Condensada, Facultat de Física, Universitat de Barcelona, 08028 Barcelona, Spain.

[3]Universitat de Barcelona Institute of Complex Systems (UBICS), Barcelona, Spain

[4]Present address: Department of Biology, Stanford University, 371 Serra Mall, Stanford, CA94305, USA.

[5]Institute for Developmental Genetics, Heinrich Heine University, Universitätsstr. 1, D-40225 Düsseldorf, Germany

[6]Department of Plant Molecular Genetics, Centro Nacional de Biotecnología (CNB), Darwin 3, Madrid E-28049, Spain.

Contributions:

Ana I. Caño-Delgado and Marta Ibañes designed and supervised the study. Isabel Betegón-Putze, Nadja Bosch, Ainoa Planas-Riverola, Josep Vilarrasa-Blasi and Mar Marquès-Bueno performed the experiments. Josep Mercadal, David Frigola and Marta Ibañes performed the mathematical modelling. Yvonne Stahl and Rebecca Corinna Burkart performed and analysed the FRET-FLIM assays. Salomé Prat and Cristina Martínez collaborated in the Y2H and BiFC assays. Isabel Betegón-Putze, Josep Mercadal, Nadja Bosch, Marta Ibañes and Ana I. Caño-Delgado wrote the manuscript, and all authors revised the manuscript.

1. Summary

Root growth and development are essential features for plant survival and the preservation of terrestrial ecosystems. In Arabidopsis primary root apex, stem-cell specific transcription factors BRAVO and WOX5 co-localise at the Quiescent Centre (QC) cells, where they repress cell division so it can act as a reservoir to replenish surrounding stem cells, yet their molecular connection remains unknown. Here, by using empirical evidence and mathematical modelling, we establish the regulatory and molecular interactions between BRAVO and WOX5. We found that BRAVO and WOX5 regulate each other and form a transcription factor complex in the QC to preserve overall root growth and architecture. The results unveil the importance of transcriptional regulatory circuits at the quiescent and stem cells to control organ initiation and growth of plant tissues.

2. Keywords

Root growth, Brassinosteroids, BRAVO, WOX5, root growth, stem cell, quiescent centre, mathematical modelling.

3. Introduction

Roots are indispensable organs to preserve plant life and terrestrial ecosystems under normal and adverse environmental conditions. In *Arabidopsis thaliana* (Arabidopsis), the primary root derives from the activity of the stem cells located at the base of the meristem in the root apex (Dolan et al., 1993; van den Berg, Willemsen, Hage, Weisbeek, & Scheres, 1995). The root stem cell niche (SCN) is composed of a set of proliferative stem cells that surround the mitotically less active cells, named the quiescent centre (QC) (Scheres, 2007). Proximally to the QC, the vascular stem cells (VSC, also called vascular initial cells) give rise to functional procambial, xylem and phloem conductive vessels in the plant (De Rybel, Mahonen, Helariutta, & Weijers, 2016). Distally to the QC, the columella stem cells (CSC) give rise to the columella cells (Supplementary figure III-1, Gonzalez-Garcia et al., 2011; Stahl, Wink, Ingram, & Simon, 2009). The QC prevents the differentiation of the surrounding stem cells (van den Berg, Willemsen, Hendriks, Weisbeek, & Scheres, 1997), and its low proliferation rate provides a way to preserve the genome from replication errors, acting as a reservoir of the root stem cells, having the ability of promoting its division rate to replenish the stem cells when they are

damaged (Fulcher & Sablowski, 2009; Lozano-Elena, Planas-Riverola, Vilarrasa-Blasi, Schwab, & Cano-Delgado, 2018).

BRASSINOSTEROIDS AT VASCULAR AND ORGANIZING CENTER (BRAVO) and WUSCHEL RELATED HOMEOBOX 5 (WOX5) are two transcription factors that are expressed at the QC and control its quiescence, as mutation of either BRAVO or WOX5 promotes QC cell division (Forzani et al., 2014; Pi et al., 2015; Vilarrasa-Blasi et al., 2014). BRAVO is an R2R3-MYB transcription factor and besides being expressed at the QC it is also present at the vascular initials (Vilarrasa-Blasi et al., 2014). It was identified as a target of Brassinosteroid (BR) hormone signalling, being directly repressed by BRI1-EMS-SUPPRESSOR 1 (BES1), one of the main effectors of the BR signalling pathway, altogether with its co-repressor TOPLESS (TPL) (Espinosa-Ruiz et al., 2017; Vilarrasa-Blasi et al., 2014). WOX5 is a member of the WUSCHEL homeodomain transcription factor family and localises mainly at the QC and to a lesser extent at surrounding CSC and vascular initials (Pi et al., 2015; Sarkar et al., 2007). WOX5 can repress QC divisions by repressing CYCLIN D3;3 (Forzani et al., 2014), and in contrast to BRAVO it is also involved in CSC differentiation, as in *wox5* mutant CSCs differentiate prematurely (Sarkar et al., 2007).

Although BRAVO and WOX5 are well-studied plant cell-specific repressors of QC division, their molecular connection and the biological relevance in proper SCN functioning has not yet been established. In this study, we set the regulatory and molecular interactions between BRAVO and WOX5 at the SCN and disclose a common role as regulators of primary and lateral root growth and development. Our results show that BRAVO and WOX5 promote each other expressions and can directly bind to form a protein complex. The BRAVO/WOX5 protein complex underlies their functions as QC repressors to maintain stem cell development, that is essential for root growth and adaptation to the environment.

4. Results

4.1 BRAVO and WOX5 control QC division and lateral root density

We have previously shown that *bravo* mutants have a phenotype of increased divisions at the QC compared to the Wild-type (WT) (Vilarrasa-Blasi et al., 2014) (Figure III-1A, B), which resembles the one described for *wox5* mutants (Bennett, van den Toorn, Willemsen, & Scheres, 2014; Forzani et al., 2014; Sarkar et al., 2007) (Figure III-1C). To address BRAVO and WOX5 interplay at repressing QC divisions, we generated the double *bravo wox5* mutant (III-7 Methods, Supplementary table III-1). The *bravo wox5* mutant also exhibited increased cell

division compared to the WT (Figure III-1A, D). Importantly, the frequency of divided QC was similar to that of *bravo* and *wox5* single mutants (Figure III-1E), suggesting that in the WT primary root apex, BRAVO and WOX5 interplay at repressing QC divisions.

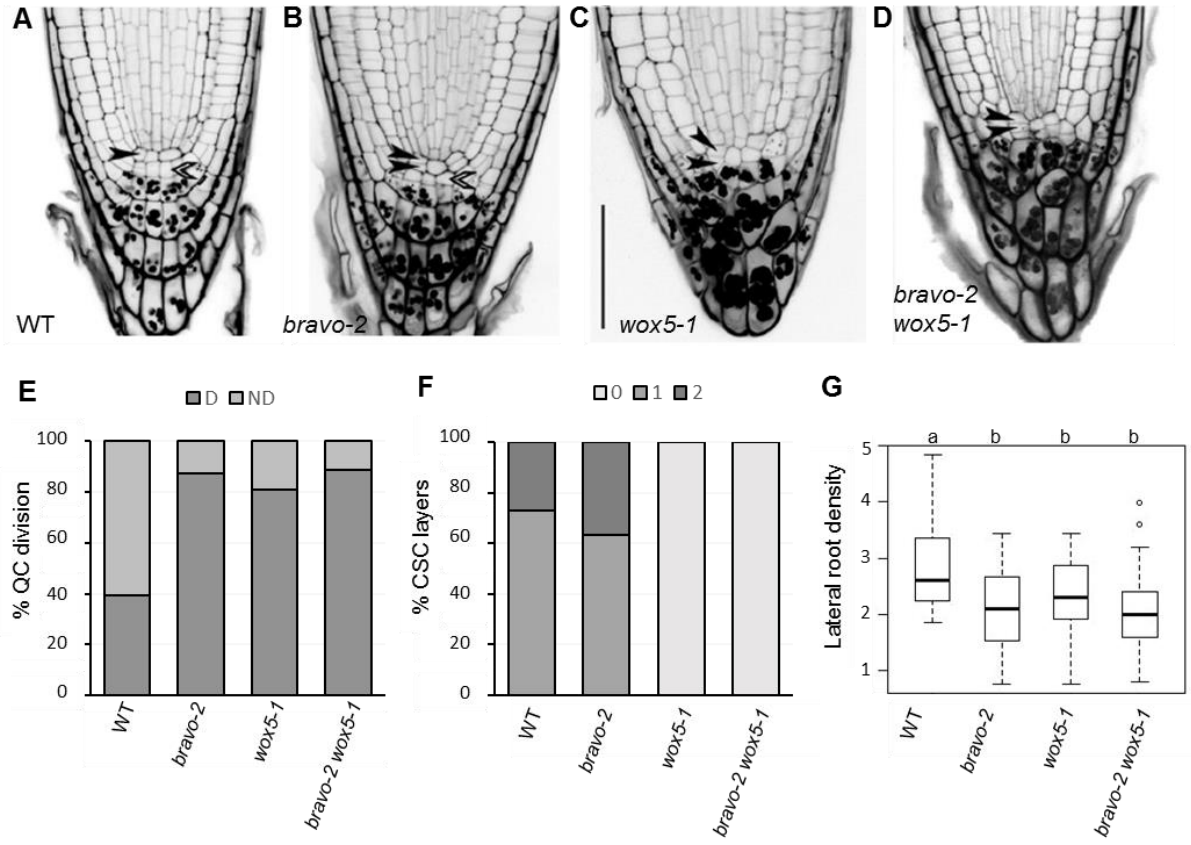

Figure III-1: BRAVO and WOX5 are required for the QC identity and stem cells maintenance

A-D) Confocal images of mPS-PI stained 6-day-old seedlings of *Col-0* (A), *bravo-2* (B), *wox5-1* (C) and *bravo-2 wox5-1* (D) mutants. Left black arrows indicate QC cells and right white arrows indicate CSC. Scale bar: 50 µm. **E)** Quantification of the QC divisions in 6–day-old roots expressed in percentage (n>50, 3 replicates). **F)** Quantification of CSC layers in 6-day-old roots expressed in percentage (n>50, 3 replicates). **G)** Lateral root density (number of lateral roots per mm of root length) of 7-day-old WT, *bravo-2*, *wox5-1* and *bravo-2 wox5-1* mutants (n>40, 2 replicates). Different letters indicate statistically significant differences (p-value < 0.05 Student´s t-test).

Previous studies proposed that WOX5 represses CSC differentiation in a non-cell autonomous manner (Bennett et al., 2014; Sarkar et al., 2007), whereas no link was reported between this process and BRAVO, since the *bravo* mutant are not defective in CSC differentiation (Figure III-1A, B, F). Genetic analysis indicates that *bravo wox5* mutant shows the same CSC differentiation as *wox5* single mutant (Figure III-1A, C, D, F), corroborating that BRAVO does not control CSC differentiation (Vilarrasa-Blasi et al., 2014).

To address whether these stem cell-specific defects account for overall root growth and development, root architecture was analysed. The *bravo wox5* double mutant shows slightly but significantly shorter roots than the WT (Supplementary figure III-2A) and fewer lateral root density (Figure III-1G). In the case of the lateral root density at 7-day-old seedlings the *bravo wox5* double mutant show the same phenotype as the single mutants (Figure III-1G), in agreement with previously reported findings for the *wox5* mutant (Tian, Jia, Niu, Yu, & Ding, 2014). However, this phenotype is more exaggerated in the *bravo wox5* double mutant at 10-day-old seedlings (Supplementary figure III-2B), all unveiling the joint contributions of these two transcription factors to overall root growth and architecture.

4.2 *BRAVO* and *WOX5* reinforce each other at the root stem cell niche

The QC division phenotype of the double *bravo wox5* mutant suggests an interplay between BRAVO and WOX5 at regulating QC divisions. Such interplay could take place through cross-regulation of their expressions. Indeed, we have previously shown that *WOX5* expression is reduced in *bravo* mutant (Vilarrasa-Blasi et al., 2014), indicating that BRAVO can regulate *WOX5* expression. To further understand mutual regulations between these two transcription factors, we investigated thoroughly *BRAVO* and *WOX5* expressions at the SCN in the single mutant backgrounds as well as in the double *bravo wox5* mutant background.

In the WT primary root, *BRAVO* expression, reported by the *pBRAVO:GFP* line, is specifically located in the QC and the vascular initials (Vilarrasa-Blasi et al., 2014) (Figure III-2A). *BRAVO* expression was increased in the *bravo* mutant (Figure III-2B, H), suggesting that BRAVO negatively regulates its own expression. In contrast, in the *wox5* mutant, *BRAVO* expression was strongly reduced, suggesting that WOX5 promotes *BRAVO* expression (Figures 2C, H). Overexpression of inducible WOX5 under a 35S promoter (35S:WOX5-GR) resulted in an increased *BRAVO* expression, as measured by RT-qPCR of the root tips (Supplementary figure III-3F). The fact that the increase is not as strong as the fold-induction of WOX5 suggests that BRAVO is only induced by WOX5 within the BRAVO native domain. Together, these results support that WOX5 induces *BRAVO* expression. Moreover, *BRAVO* expression was reduced in the double *bravo wox5* mutant (Supplementary figure III-4), like in the *wox5* mutant (Figure III-2C, H). Altogether, these results suggest that BRAVO regulates its own expression upstream of WOX5.

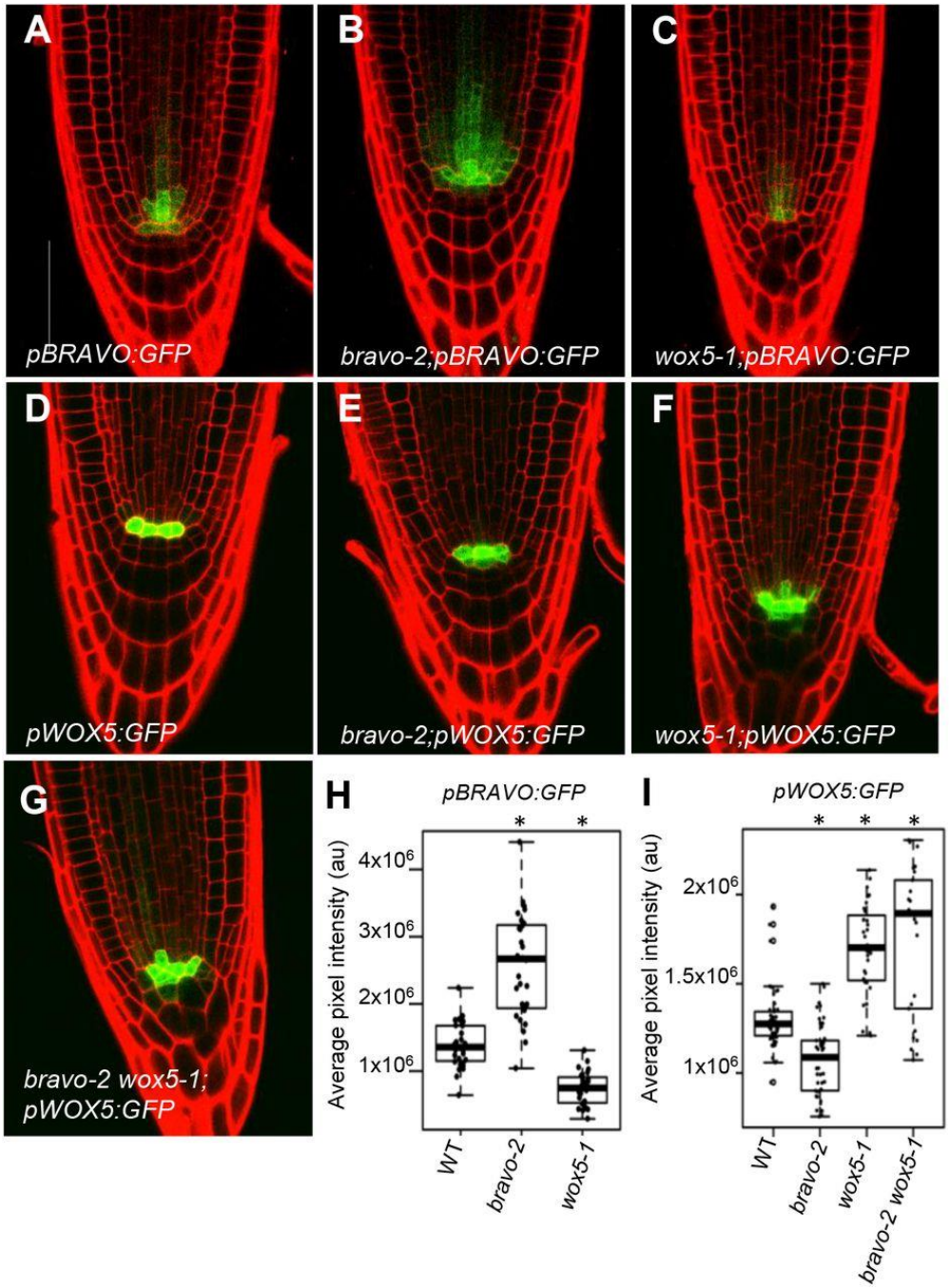

Figure III-2: BRAVO and WOX5 reinforce each other at the root stem cell niche

A-G) Confocal images of PI-stained 6-day-old roots. GFP-tagged expression is shown in green. A-C) *pBRAVO:GFP* in WT (A), *bravo-2* (B) and *wox5-1* (C) knockout backgrounds. D-G) *pWOX5:GFP* in the WT (D), *bravo-2* (E), *wox5-1* (F) and *bravo-2 wox5-1* (G) knockout backgrounds. Scale bar: 50 µm. **H, I)** Quantification of the GFP fluorescent signal of the roots in A-C (H) and D-G (I). Boxplot indicating the average pixel intensity of the GFP in the stem cell niche. (n>25, 3 biological replicates, *p-value < 0.05 Student´s *t*-test for each genotype versus the WT in the same condition).

WOX5 expression, as reported by the *pWOX5:GFP* line in the primary root, is known to be mainly restricted to the QC, yet there is some in the vascular initials (Pi et al., 2015) (Figure

III-2D). We found that *bravo* mutant displayed a significant reduction of *WOX5* expression (Figure III-2E, I), supporting that BRAVO induces *WOX5* expression. Further analysis of *WOX5* expression when overexpressing *BRAVO* under an inducible 35S promoter (35S:BRAVO-Ei) show that when induced, BRAVO levels were increased, whereas WOX5 levels were similar to the WT, indicating that BRAVO is not able to induce *WOX5* (Supplementary figure III-3A-E, S3G).

Together, these results support that BRAVO is necessary to maintain proper *WOX5* levels in the QC but not to induce them. Subsequently, an increased expression towards the provascular cells was found in *pWOX5:GFP* in the *bravo wox5* double mutant (Figure III-2G), similar to *wox5* mutant (Figure III-2F, I). These results suggest that *WOX5* restricts its own expression to the QC, and that BRAVO regulation on *WOX5* is upstream of *WOX5* autoregulation.

Brassinolide (BL) is the most active BR hormone compound. BL treatment is known to modify *BRAVO* and *WOX5* expressions, being the first reduced and the second increased (Gonzalez-Garcia et al., 2011; Vilarrasa-Blasi et al., 2014) (Supplementary figure III-4 and Supplementary figure III-5). We found that when roots were grown with BL, the changes in *BRAVO* and *WOX5* expressions in *bravo* mutant, *wox5* mutant and *bravo wox5* double mutant compared to the WT exhibited the same trends as when plants were grown in control media without BL (Supplementary figure III-4 and Supplementary figure III-5). These results suggest that the regulations between BRAVO and WOX5 and with themselves are not significantly altered by BL treatment.

4.3 *WOX5* induces *BRAVO*, which alleviates *WOX5* self-inhibition

To provide a global scheme of *BRAVO* and *WOX5* cross-regulations in the SCN that can account for all the changes in the mutants, we turned into mathematical modelling (III-7 Methods). Because *BRAVO* is induced in the WOX5 overexpression line (Supplementary figure III-3F) and *BRAVO* expression decreases in the *wox5* mutant (Figure III-2C), the model considered that WOX5 induces (directly and/or through intermediate molecules) the expression of *BRAVO* (Figure III-3A). To account for the increase in *BRAVO* expression in the *bravo* background (Figure III-2B), the model assumed that BRAVO drives an effective inhibition on its own expression (Figure III-3A), probably in an indirect manner. The model indicates that these two regulations can drive a decrease in *BRAVO* expression in the *bravo wox5* double mutant (Figure III-3B), as found in GFP expression data (Supplementary figure III-4).

Therefore, the model indicates that these two effective regulations on *BRAVO* are sufficient to account for its change of expression in the single and double mutants (Figure III-3B).

Because *WOX5* expression in the SCN increases in the *wox5* mutant (Figure III-2F), the model considered that WOX5 represses (directly or indirectly) its own promoter activity (Figure III-3A). In addition, the model assumed that BRAVO inhibits partially this repression (Figure III-3A). With these regulations, the model accounts for the increase of *WOX5* expression in the *bravo* mutant, and for the *WOX5* decreased expression in the *wox5* mutant and in the *bravo wox5* mutant (Figure III-3B), as we found in GFP expression data (Figure III-2F,G). Therefore, the model proposes that BRAVO promotes *WOX5* expression by alleviating *WOX5* self-inhibition.

With these interactions, the model can drive all the trends of changes found for *BRAVO* and *WOX5* expressions in whole SCN in the *bravo*, *wox5* and *bravo wox5* mutants (Figure III-3B, C). In the model, parameter values were chosen such that the fold-changes between promoter activities in the single mutants compared to the WT matched the fold-changes in GFP expressions of our empirical data (Figure III-3C, III-7 Methods). In addition, parameter values were restricted such that *BRAVO* promoter expression is lower than *WOX5* promoter expression in the WT for control conditions (Figure III-3B), as GFP expression (III-7 Methods) and RNAseq at the root tip suggest (Clark et al., 2019).

The model indicated that the trends of the expression changes between each mutant and the WT are maintained when the characteristic rate of BRAVO promoter activity decreases and/or the characteristic rate of WOX5 promoter activity increases (Figure III-3C). This is in agreement with the results we found upon BL treatment (Supplementary figure III-4 and Supplementary figure III-5), which reduces *BRAVO* expression and increases *WOX5* expression.

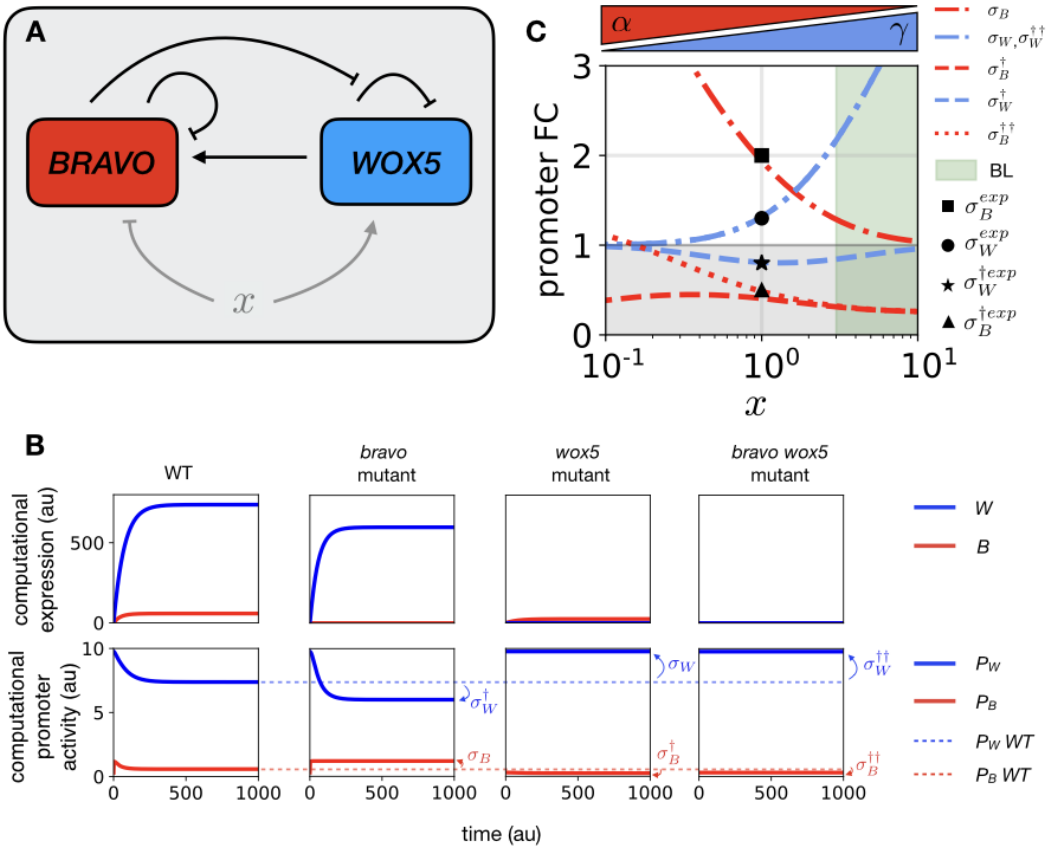

Figure III-3: WOX5 activates BRAVO which in turn alleviates WOX5 self-inhibition in the stem cell niche

A) Schematic representation of the effective regulations in the SCN between *BRAVO* and *WOX5*: *BRAVO* feeds back on its own activity by reducing it and is activated by *WOX5*. *WOX5* also feeds back on its own activity by reducing it, a regulation that becomes partially impaired by *BRAVO*. Additional factors x can be regulating both *BRAVO* and *WOX5* or either one. We exemplify one such a factor that regulates both, by downregulating *BRAVO* and upregulating WOX5. x can be understood as BR signalling. Arrows denote activation and bar-ended lines denote inhibition. **B)** Model solutions for the temporal evolution of expression and promoter activities for the WT and mutants using as initial condition all activities set to zero (B(t=0)=0,W(t=0)=0) and parameter values as in Supplementary table III-1. This time-evolution does not intend to mimic any data but is only shown to depict the changes in the stationary levels between WT and each mutant. Manifest in the panels are the fold-changes in promoter activities in the mutant compared to the WT (σ) as defined in III-7 Methods. **C)** Fold-changes in promoter activity (σ) in the mutant compared to the WT predicted by the mathematical model as a function of the control parameter x. This control parameter increases WOX5 and reduces BRAVO promoter activities (blue and red triangles; according to $\alpha=0.3/x$, $\gamma=250x/(x+9)$). x=1 corresponds to the CTL condition, while x>1 can mimic BL conditions (green shaded area). The experimentally observed values in CTL conditions (computed as ratios of the median GFP) are drawn as black markers (see legend). The experimental fold-changes corresponding to the double mutants are not shown, as are assumed to be equal to the single mutants within the confidence interval of the experiments ($\sigma_B^{\dagger\dagger exp} = \sigma_B^{\dagger exp}$ and $\sigma_W^{\dagger\dagger exp} = \sigma_W^{\dagger exp}$). Error bars of these data (which can span ranges $\pm\sigma$) are not depicted for clarity. In the plot, the region of fold change FC<1 (i.e. the promoter activity is reduced in the mutant) is shaded in gray to visually distinguish it from the region where FC>1 (i.e. the promoter activity is increased in the mutant).

4.4 BRAVO and WOX5 directly interact forming a transcriptional complex

Our results so far support that BRAVO and WOX5 reinforce each other at the SCN. To further decipher BRAVO and WOX5 interplay, we next evaluated the possible physical interaction between BRAVO and WOX5 proteins. Using Förster resonance energy transfer measured by fluorescence lifetime microscopy (FRET-FLIM) (Figure III-4A-K) and yeast two-hybrid assays (Figure III-4L and Supplementary figure III-6A) we found that BRAVO can directly interact with WOX5 (Figure III-4B, G, K and L), which indicates that BRAVO and WOX5 form a transcriptional complex.

In addition, as we previously showed that the BR-regulated BES1/TPL complex acts as a transcriptional repressor of BRAVO transcription (Espinosa-Ruiz et al., 2017; Vilarrasa-Blasi et al., 2014), that active BES1 directly interacts with BRAVO (Vilarrasa-Blasi et al., 2014), and that TPL interacts with WOX5 (Pi et al., 2015), we further investigated the interactions between BRAVO and WOX5 with these transcription factors. Although we found that BRAVO and WOX5 can directly interact with BES1, we found a stronger interaction with the active form BES1-D (Yin et al., 2002) (Figure III-4C, D, H, I, K), in agreement with (Vilarrasa-Blasi et al., 2014), and that the EAR domain of BES1 is necessary for BES1/BRAVO interaction (Supplementary figure III-6A). Our analysis uncovers that BES1 interacts with WOX5 (Figure III-4H, I, K and Supplementary figure III-6C) at a similar level as BRAVO (Figure III-4K and Supplementary figure III-6B), and that this interaction is stronger with BES1-D (Figure III-4K). Moreover, both BRAVO and WOX5 also interact with the co-repressor TPL (Figure III-4E, J, K, L and Supplementary figure III-6). Collectively, our data indicates that BRAVO and WOX5 directly interact with each other and with the active BES1/TPL transcriptional machinery, being all essential components to preserve the QC status at the root stem cell niche.

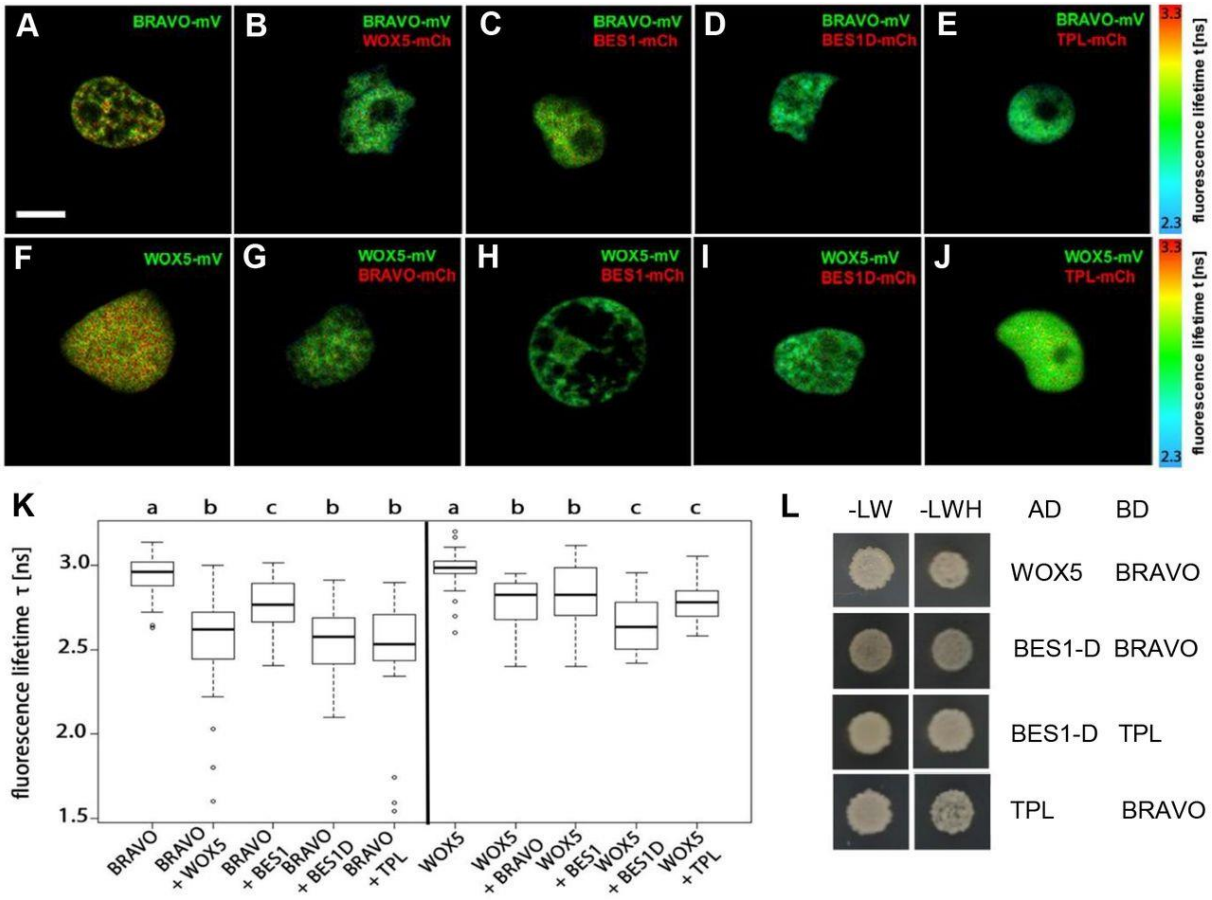

Figure III-4: BRAVO interacts with WOX5

A-J) Interaction of BRAVO with WOX5 (B), BES1 (C), BES1-D (D) and TPL (E); and interaction of WOX5 with BRAVO (G), BES1 (H), BES1-D (I) and TPL (J) measured by FRET-FLIM. mVenus fluorescence lifetime τ [ns] was measured in transiently expressing *Nicotiana benthamiana* leaf epidermal cells. mVenus fluorescence lifetime fitted pixel-wise with a mono-exponential model of BRAVO and WOX5 interactions. mV, mVenus; mCh, mCherry. Scale bar: 5 µm. **K**) Fluorescence-weighted average lifetimes of BRAVO and WOX5 interactions fitted with a double-exponential model of the indicated samples are summarized in box plots. Statistical significance was tested by one-way ANOVA with a Sidakholm post-hoc test. Different letters indicate statistically significant differences ($p<0.01$; $n>20$). **L)** Yeast two-hybrid assay showing BRAVO interacting with WOX5, BES1-D and TPL. In the left column yeast cells were grown on control media, and in the right column yeast cells were grown on control media lacking Leu, Trp and His, indicating an interaction between the proteins.

4.5 BRAVO-WOX5 complex is relevant for the control of QC divisions

The phenotype of divided QCs in the double *bravo wox5* mutant compared to that in the single mutants (Figure III-1A-E) suggests that BRAVO and WOX5 interplay at repressing QC divisions. We found two ways for this interplay to take place: through mutual regulation of their expressions (Figure III-2, Figure III-3A) and through the formation of a BRAVO-WOX5 protein complex (Figure III-4A-K). We turned into mathematical modelling to assess the contribution of each of these interplays to the phenotype of divided QCs (III-7 Methods). We

set a regulatory function for the frequency of divided QCs that explicitly incorporates the contributions individually mediated by BRAVO (T_B) and by WOX5 (T_W) and the jointly mediated contribution by both BRAVO and WOX5 together (hereafter named "joint contribution", T_{BW}) (III-7 Methods). In this regulatory function, the joint contribution (T_{BW}) takes into account the existence of the BRAVO-WOX5 complex, whereas the individual contributions (i.e. T_B and T_W) each include the mutual regulation of *BRAVO* and *WOX5* expressions. Specifically, since *WOX5* expression decreases in the *bravo* mutant (Figure III-2I), we reasoned that individual WOX5-mediated repression of QC divisions is attenuated in the *bravo* mutant compared to the WT, by a factor $q_W^{Bm}<1$ (III-7 Methods). Similarly, to take into account the regulation that WOX5 makes on *BRAVO* expression, we considered that the individual contribution mediated by BRAVO was attenuated by a factor q_B^{Wm} in the *wox5* mutant compared to that in the WT ($q_B^{Wm}<1$). Since the *wox5* mutant exhibits phenotypes that are absent in the *bravo* mutant, such as CSC differentiation, we reasoned that q_W^{Bm} may not be too small. Specifically, we used $q_W^{Bm}=0.8$, which is similar to the fold-change of *WOX5* expression in the *bravo* mutant compared to the WT (Figure III-2I, Figure III-3C). We evaluated the results for different values of q_B^{Wm}.

We used the data from the frequency of divided QCs in the WT, the single mutants and the double mutant (Figure III-1E), with an estimation of their confidence intervals (III-7 Methods), to extract which are the contributions of the BRAVO-mediated, the WOX5-mediated and the joint BRAVO-WOX5 contributions in the WT (Figure III-5, see III-7 Methods).

The results (Figure III-5A) show that in the WT the joint contribution of BRAVO-WOX5 is the most relevant when q_B^{Wm} is not very small, being $q_B^{Wm}|=0.5$ of the order of the attenuation of *BRAVO* expression in the *wox5* mutant. The individual contributions of WOX5 and BRAVO are much less relevant (Figure III-5A), and only the latter becomes relevant for small q_B^{Wm} values, i.e. if in the *wox5* mutant the repression of QC divisions mediated by BRAVO is very attenuated. Yet in this scenario, which would correspond to BRAVO acting downstream of WOX5 to repress QC divisions, the results indicate that the joint contribution of BRAVO and WOX5 in the WT to regulate QC divisions is also expected to be relevant (Figure III-5A).

Taken together, our analysis enlightens the significant contribution of BRAVO/WOX5 heteromeric complex to control QC divisions to preserve normal growth and development of primary and lateral root organs in the plant.

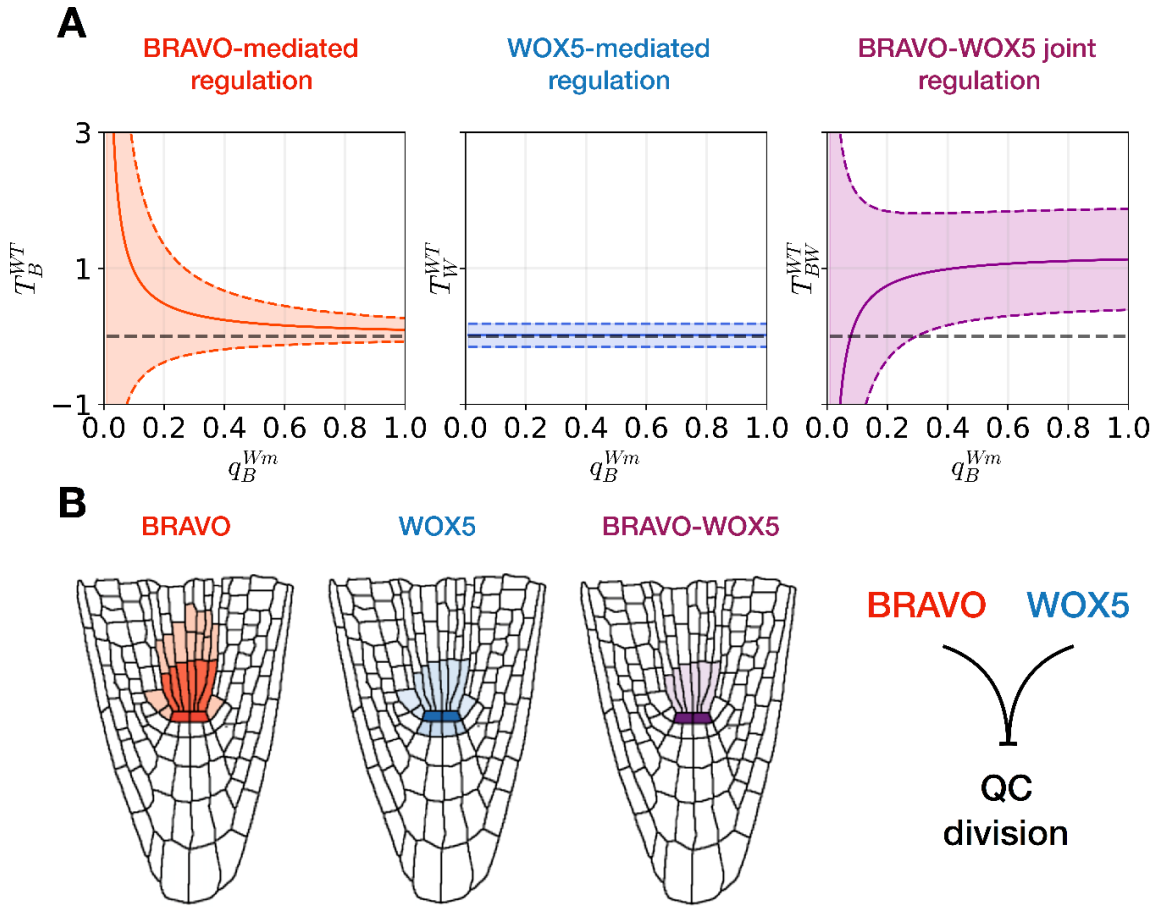

Figure III-5: BRAVO and WOX5 have a joint role in repressing QC divisions

A) Computational estimation of the contributions of BRAVO-mediated (T_B^{WT}), WOX5-mediated (T_W^{WT}) and BRAVO-WOX5 joint (T_{BW}^{WT}) regulations of QC divisions in the WT, as a function of the attenuating factor of BRAVO contribution in the *wox5* mutant, q_B^{Wm}. Continuous lines represent the best estimated values, while dashed lines are the enveloping confidence intervals (e.g. $T_B^{WT} \pm \delta T_B^{WT}$). The horizontal grey dashed lines mark the zero lines. For a wide range of q_B^{Wm} values, the joint contribution of BRAVO and WOX5 is important, while the individual contribution of BRAVO only increases for small values of q_B^{Wm}. In all three panels, we set q_W^{Bm}=0.8. Positive contributions correspond to repression of QC divisions, while negative contributions correspond to activation of QC divisions. **B)** Sketch representing the spatial distribution of BRAVO, WOX5 and their product BRAVO x WOX5, which can be interpreted as the protein complex. Their joint interaction peaks at the QC, where repression of cell division occurs.

5. Discussion

In the Arabidopsis primary root, BRAVO and WOX5 are two transcription factors that repress QC divisions and whose expressions co-localise mostly at the QC (Forzani et al., 2014; Vilarrasa-Blasi et al., 2014). Our results show that BRAVO and WOX5 interplay at different

levels to repress QC divisions. In addition, we show that the joint action of these cell-specific transcription factors promotes overall root growth and development.

Our data indicate that BRAVO and WOX5 interplay is by mutually promoting each other expressions. Hence, none of them is downstream the other. Yet these mutual regulations are very distinct. While WOX5 is able to induce *BRAVO*, BRAVO does not induce *WOX5* expression, but it drives partial inhibition of *WOX5* self-regulation. These differences, and the quantitative changes in expression they drive, suggest that the effect WOX5 has upon *BRAVO* and thereby upon BRAVO-mediated functions can be more relevant than the effect BRAVO has upon *WOX5* and WOX5-mediated functions. This is consistent with the known SCN phenotypes of *bravo* mutant and of *wox5* mutant (Bennett et al., 2014; Forzani et al., 2014; Pi et al., 2015; Sarkar et al., 2007; Vilarrasa-Blasi et al., 2014), since *wox5* mutant exhibits, besides the increased QC division phenotype similar to *bravo* mutant, an overall distorted and disorganized SCN morphology and CSC premature differentiation that is absent in the *bravo* mutant.

The mutual regulation between BRAVO and WOX5 involves that WOX5 represses its own expression and induces that of *BRAVO*, which in turn inhibits the repression that WOX5 makes on its own expression. Moreover, BRAVO is found to ultimately inhibit its own expression. This probably occurs through intermediate molecules, as BRAVO can activate its expression by direct binding to its own promoter (Vilarrasa-Blasi et al., 2014). By evaluating expression changes between the WT and the mutants we gained information from the overall regulation between BRAVO and WOX5. These result from direct binding of the proteins to the promoters and from all the processes these proteins drive, in which one or several molecules may participate to regulate the promoter expressions. Hence, the interactions described here are effective in the sense that they are the result of multiple specific regulations, direct and indirect, and mechanisms. For instance, *WOX5* self-repression could take place through a negative feedback in which WOX5 activates a repressor or represses an activator, among other possibilities. In this context, auxin-ARF and auxin-IAA (Tian, Wabnik, et al., 2014) as well PLETHORA genes (Burkart et al., 2019) all involve negative feedbacks with *WOX5*. The induction that WOX5 drives on *BRAVO* expression could be as well through a downstream target of WOX5.

Another interplay between BRAVO and WOX5 that our data reveal is their physical protein-protein interaction. The QC is where these two transcription factors co-localise mostly. Thus, it is compelling to identify WOX5 and BRAVO as partners that perform its repressing function only in the QC, where they converge. The consistent and overlapping role of BRAVO and

WOX5 at promoting lateral root development also appoints a relevant role of the BRAVO-WOX5 complex for this function.

Our analysis supports that BRAVO-WOX5 joint regulation of QC divisions is relevant, besides additional regulation that may be individually mediated by BRAVO. This joint regulation can be expected to be mediated by BRAVO-WOX5 physical interaction. This scenario provides an explanation of the phenotype of increased divisions at the QC upon BL treatment that takes into account the response of BRAVO and WOX5 to this treatment and their roles as repressors of QC divisions. The intensity and domain of expression of WOX5 increases in roots grown in BL medium, and yet the QC exhibits increased divisions (Gonzalez-Garcia et al., 2011). BL treatment, at the same time, strongly represses BRAVO (Vilarrasa-Blasi et al., 2014). Hence, if WOX5 needs its partner BRAVO, absent in the presence of BL, to perform its repression of QC divisions, then QC divisions are no longer repressed by WOX5 nor BRAVO in roots grown with BL. At a mechanistic level, the BRAVO-WOX5 protein complex may bind CYCLIN-D3:3, as shown for WOX5 to happen (Forzani et al., 2014) , and thereby repress QC divisions.

Interestingly, we also found that BRAVO and WOX5 promote root growth and lateral root development. In LR development, the formation of the organizing centre and the stem cell niche occurs after LR initiation (Banda et al., 2019). A high number of genes are commonly expressed at the SCN of primary and lateral roots, such as PLT, SHR, SCR or TCP (Goh et al., 2016; Shimotohno, Heidstra, Blilou, & Scheres, 2018). Mutation in these stem cell genes cause an increased number of aberrant lateral roots and reduced levels of *WOX5* (Shimotohno et al., 2018). Our study indicates that BRAVO WOX5 complex might be involved in stem cell niche maintenance not only in the primary root, but also in the lateral roots.

Finally, our study sheds light for future studies on the interplay between WOX5 and BR signalling to control CSC differentiation. WOX5 is known to repress CSC differentiation (Pi et al., 2015; Sarkar et al., 2007) . Upon BL treatment, and in *bes1-D* gain of function mutants, CSC differentiate prematurely (Gonzalez-Garcia et al., 2011) , in apparent contradiction with the inhibitory role associated with WOX5, since WOX5 is strongly expressed in these roots. One option could come from assuming that CSC differentiation induced by BR is independent from WOX5 and eclipses the repression mediated by WOX5. In this case, a tug-of-war between WOX5-mediated repression and BR-mediated activation of CSC differentiation would tip the balance in favour of BR-action. Another possibility would involve the action of BR downstream effectors such as BES1-D to inactivate WOX5 and/or impede its function. An increase of BES1-D by BL would boost the sequestration of WOX5 into WOX5-BES1-D complexes since we show WOX5 and BES1-D can physically interact. Assuming these complexes inactivate

WOX5 function, then CSC differentiation would no longer be repressed by WOX5 in the presence of BL. Moreover, the fact that BES1-D directly interacts and forms a complex with TOPLESS may further disturb some of the functions of WOX5. Indeed, it has been shown that WOX5 recruits TPL in order to repress CSC differentiation (Pi et al., 2015), an interaction that would become impaired in plants treated with high concentrations of BL, where most of TPL would be bound to BES1-D.

To conclude, understanding of signalling networks operating in stem cell development is becoming essential to decipher plant growth and adaptation to the environment. Systems biological approaches provide a closer picture to reality unveiling how complex and dynamic networks of cell-specific transcription factors act to preserve stem cell function in plants. Here, the example untapping the action of main regulators of quiescent cell division BRAVO and WOX5, not only discloses the role of transcription factor complex in preserving stem cell function, but also open up their joint roles in primary and lateral root development.

6. Acknowledgments

A.I.C-D. is a recipient of a BIO2016-78955 grant from the Spanish Ministry of Economy and Competitiveness and a European Research Council, ERC Consolidator Grant (ERC-2015-CoG – 683163).

N.B. is funded by the FI-DGR 2016FI_B 00472 grant from the AGAUR, Generalitat de Catalunya; I.B-P. by the FPU15/02822 grant from the Spanish Ministry of Education, Culture and Sport; and A.P-R. by the SEV-2015-0533 from the Severo Ochoa Programme for Centers of Excellence in R&D. M.I. and J.M. acknowledge support from the Spanish Ministry of Economy and Competitiveness and FEDER (EU) through grant FIS2015-66503-C3-3-P , from Ministerio de Ciencia, Innovación y Universidades / Agencia Estatal de Investigación / Fondo Europeo de Desarrollo Regional, Unión Europea through grant PGC2018-101896-B-I00 and from the Generalitat de Catalunya through Grup de Recerca Consolidat 2014 SGR 878 and 2017 SGR 1061. J.M. is funded by the Spanish Ministry of Education through BES-2016-078218. Y.S. and R.C.D. are funded by the Deutsche Forschungsgesellschaft (DFG) (grant STA12/12 1-1). CRAG is funded by “Severo Ochoa Programme” from Centers of Excellence in R&D 2016-2019 (SEV-2015-485 0533).

7. Methods

7.1 Plant Material and Root Measurement

All WT, mutants and transgenic lines are in the Arabidopsis ecotype Columbia (Col-0) background (Supplementary table III-2). The double mutant *bravo wox5* was generated by crossing the *bravo* and *wox5* single mutants. The double mutant homozygous lines were selected by genotyping. The primers used for *bravo* and *wox5* genotyping are listed in Supplementary table III-3.

Seeds were surface sterilized and stratified at 4°C for 48 hours before being plated onto 0.5X Murashige and Skoog (MS) salt mixture without sucrose and 0.8% plant agar, in the absence or presence of Brassinolide ($C_{28}H_{48}O_6$; Wako, Osaka, Japan). Beta-Estradiol (30 µM) from Sigma diluted in DMSO was used to induce BRAVO expression for 6 days. Dexamethasone (1 µM) from Sigma diluted in Ethanol was used to induce WOX5 expression for 6 days. For RT-qPCR experiments Beta-Estradiol and Dexamethasone treatments was applied for 24 hours.

Plates were incubated vertically at 22°C and 70% humidity in a 16 hours light/8 hours dark cycle. Primary root length was measured from plate images using ImageJ (https://imagej.nih.gov/ij/) and MyROOT (Betegon-Putze, Gonzalez, Sevillano, Blasco-Escamez, & Cano-Delgado, 2019) softwares. The lateral root density was calculated by dividing the total number of emerged lateral roots of individual seedlings by the mean of the root length of those seedlings.

7.2 Confocal Microscopy and Quantification of Fluorescence Signal

Confocal images were taken with a FV 1000 Olympus confocal microscopy after Propidium iodide (PI, 10 µg/ml) staining. PI and GFP were detected with a band-pass 570-670 nm filter and 500-545 nm filter, respectively. Images were taken in the middle plane of 6-day-old roots. The fluorescence intensity was quantified with ImageJ using the Integrated Density value obtained from individual plants. The quantified area was selected with a ROI that contained the SCN (Supplementary figure III-6). The laser settings for pBRAVO:GFP and pWOX5:GFP are different, as WOX5 has a stronger expression than BRAVO. The analysis of pBRAVO:GFP in *bravo wox5* double mutant background was done with different confocal settings. The analysis of QC cell division and CSC differentiation was carried out by imaging fixed roots through a modified pseudoSchiff (mPS-PI) staining method (Truernit et al., 2008). Images were processed with the Olympus FV (Olympus, Tokio, Japan) and ImageJ software.

7.3 RT-qPCR assay

RNA was extracted from root tip tissue with the Maxwell® RSC Plant RNA Kit (Promega) using the Maxwell® RSC instrument (Promega) according to the manufacturer's recommendations, quality and concentration were checked using NanoDrop 1000 Spectrophotometer (Thermo Fisher Scientific). cDNA was obtained from RNA samples by using the NZY First-Strand cDNA Synthesis Kit (NZYtech) according to the manufacturer's recommendations. RT-qPCR amplifications were performed from 10 ng of cDNA using LightCycler 480 SYBR Green I master mix (Roche) in 96-well plates according to the manufacturer's recommendations. The RT-qPCR was performed on a LightCycler 480 System (Roche). *ACTIN2* (AT3G18780) was used as housekeeping gene for relativizing expression. Primers used are described in Supplementary table III-3.

7.4 Yeast two-hybrid assay

Yeast two-hybrid assays were performed as the Matchmarker GAL4-based two-hybrid System (Clontech). Constructs were co-transformed into the yeast strain AH109 by the lithium acetate method (Gietz & Woods, 2002). The presence of the transgenes was confirmed by growth on SD-LW plates, and protein interaction was assessed by selection on SD-LWH plates. Interactions were observed after 4 days of incubation at 30ºC.

7.5 Transient expression in *Nicotiana benthamiana* for FLIM measurements

Preparation of transiently expressing *Nicotiana benthamiana* leaves and induction of fusion proteins tagged with either mVenus or mCherry by application of ß-Estradiol was carried out as described in (Bleckmann, Weidtkamp-Peters, Seidel, & Simon, 2010).

7.6 Acquisition of FLIM data

FLIM data acquisition was carried out using a confocal laser scanning microscope (LSM780 inverted microscope, Zeiss) equipped additionally with a time-correlated single-photon counting device with picosecond time resolution (Hydra Harp 400, PicoQuant). mVenus was excited at 485 nm with a pulsed (32 MHz) diode laser at 1.2 µW at the objective (40 x water immersion, C-Apochromat, NA 1.2, Zeiss). The emitted light was collected through the same objective and detected by SPAD detectors (PicoQuant) using a narrow range bandpass filter (534/35, AHF). Images were taken at 12.5 µs pixel time and a resolution of 138 nm/pixel in a 256x256 pixel image. A series of 40 frames was merged into one image and analysed using the Symphotime software package (PicoQuant).

7.7 Analyses and presentation of FLIM data

The fluorescent lifetime of the collected photons in each merged image was analysed using the Symphotime software (PicoQuant). For this, a ROI covering the whole nucleus was created to reduce background fluorescence. All photons in this ROI were used to build a histogram of the fluorescence decay. A double-exponential fit model was used to approximate the intensity-weighted average fluorescence lifetime τ [ns] of all photons of the ROI. The instrument response function was measured with KI-quenched erythrosine and used for reconvolution in the fitting process (Weidtkamp-Peters & Stahl, 2017). The data from replicate measurements was summarized in box plots created in R software (https://www.r-project.org/). Statistical significance was tested by one-way ANOVA with a Sidakholm post-hoc test. Different letters indicate statistically significant differences ($p < 0.01$).

For the creation of FLIM images, photons from individual pixels of a merged image were analysed for fluorescent lifetime using the Symphotime software (PicoQuant). A mono-exponential fit model was used, as the photon number in each pixel was too low for a double-exponential model (Stahl et al., 2013). The individual pixels are colour-coded according to their fluorescence lifetime.

7.8 Bimolecular fluorescence complementation assay (BiFC)

The *BRAVO* and *WOX5* coding sequences were inserted by LR-reaction (Invitrogen) into pBiFC binary vectors containing the N- and C- terminal YFP fragments (YFPN43 and YFPC43). Plasmids were transformed into the *Agrobacterium tumefaciens* GV3101 strain and appropriate combinations were infiltrated into *Nicotiana benthamiana* leaves (Occhialini, Gouzerh, Di Sansebastiano, & Neuhaus, 2016). The p19 protein was used to suppress gene silencing. Infiltrated leaves were imaged two days after infiltration using an Olympus FV1000 laser scanning confocal microscope.

7.9 Mathematical model of BRAVO and WOX5 effective regulations

We considered a model for the effective regulations that BRAVO and WOX5 perform on each other and on themselves in the SCN. In the model, *B* and *W* account for the total *BRAVO* and *WOX5* expressions in the whole SCN. These expressions are considered to be the product of the BRAVO and WOX5 promoter activities according to the following dynamics for the wild-type:

$$\frac{dB}{dt} = P_B(B,W) - d_B B,$$

$$\frac{dW}{dt} = P_W(B,W) - d_W W,$$

where $P_B(B,W)$ and $P_W(B,W)$ are the BRAVO and WOX5 promoter activities (production terms) respectively and $d_B B$ and $d_W W$ are the decay terms (assumed linear for simplicity, with decay rates d_B and d_W). To account for the regulation of the expression, each promoter activity depends on *BRAVO* and *WOX5* expressions. To compare with empirical data, we only considered the stationary state of the above dynamics (i.e. when time derivatives are equal to zero, $\frac{dB}{dt} = 0, \frac{dW}{dt} = 0$). In the stationary state, *BRAVO* expression is proportional to BRAVO promoter activity ($B = P_B(B,W)/d_B$) and *WOX5* expression is proportional to WOX5 promoter activity ($W = P_W(B,W)/d_W$). Therefore, we used the promoter activity in the stationary state as the computational model read-out to be compared with the empirical data on *pBRAVO:GFP* and *pWOX5:GFP*.

Promoter activity terms $P_B(B,W)$ and $P_W(B,W)$ correspond to functions that describe the effective regulations each expression ultimately performs on each promoter activity (see Figure III-3A for a cartoon of these regulations), These effective regulations involve several intermediate steps, including translational and post-translational processes, and additional molecules. These are not explicitly modelled but are all together absorbed in the functionalities of $P_B(B,W)$ and $P_W(B,W)$. We expect these functions to be non-linear and we used continuous Hill-like functions exhibiting saturation with exponents larger than 1 (see parameter values in Supplementary table III-1);

$$P_B(B,W) = \alpha \frac{1 + \varepsilon_B (K_B B)^2}{1 + (K_B B)^2} \frac{1 + \varepsilon_W (K_W W)^2}{1 + (K_W W)^2}$$

$$P_W(B,W) = \gamma \frac{1}{{W_0}^2 + W^2 \left(\frac{1}{B^2 + B_0^2} + W_1 \right)^2}$$

The BRAVO promoter activity $P_B(B,W)$ has: i) a basal production rate α, independent of *BRAVO* and *WOX5* expressions since our GFP data show that BRAVO promoter has activity in the double mutant *bravo wox5* (Supplementary figure III-2). ii) A term that sets the activation of *BRAVO* expression by *WOX5*, with *WOX5* expression threshold value $1/K_W$ and activation strength $\varepsilon_W > 1$. According to this term, the production of *BRAVO* increases to $\alpha\varepsilon_W > \alpha$ if *WOX5* expression is very high ($W >> 1/K_W$) and there is no *BRAVO*. iii) A term that accounts for the reduction of *BRAVO* expression by itself, with *BRAVO* expression threshold value $1/K_B$ and inhibition strength $\varepsilon_B < 1$. According to this term, the production of *BRAVO* decreases to $\alpha\varepsilon_B < \alpha$ when *BRAVO* is very high ($B >> 1/K_B$) and there is no *WOX5*. The WOX5 promoter activity P_W has: i) a basal production in the absence of *BRAVO* and *WOX5* expressions of value γ/W_0^2; ii) *WOX5* expression ultimately represses its own production. iii) Part of this self-repression is

dependent on *BRAVO*, which reduces the strength of *WOX5* self-repression. iv) The parameters W_0, B_0 and W_1 set a measure of the characteristic *WOX5* and *BRAVO* expressions for which these regulations can have an effect.

7.9.1 Modelling of the mutants

To model the mutants we used the same equations and parameter values as for the WT with the only changes being: in the *M* background (*M* can be either *bravo*, *wox5* or *bravo wox5*) the expression of the mutated gene is null at all times (*M*=0), despite its promoter activity P_M is nonzero, and is computed according to the promoter function P_M as defined for the WT but with *M*=0. No additional changes (e.g. no changes in parameter values) were considered to occur in the mutants. The model equations for all the mutants are detailed in III-9.3 Supplementary text. Herein we exemplify only the model for the *bravo* mutant (where the superscript *Bm* is used to denote this mutant):

$$B^{Bm} = 0, \quad P_B(0, W^{Bm}) = \alpha \frac{1+\varepsilon_W (K_W W^{Bm})^2}{1+(K_W W^{Bm})^2}$$

$$\frac{dW^{Bm}}{dt} = P_W(0, W^{Bm}) - d_W W^{Bm}, \quad P_W(0, W^{Bm}) = \gamma \frac{1}{{W_0}^2 + {W^{Bm}}^2 \left(\frac{1}{B_0^2}+W_1\right)^2}$$

To compare with empirical data on GFP expression in the mutants, we only considered the stationary state of the models of the mutants (see detail in III-9.3 Supplementary text).

7.9.2 Comparison of model outputs with empirical data on GFP expression

Model outputs of the promoter activities (production terms), P_B and P_W, obtained at the stationary state (i.e. when time-derivatives are equal to zero) were those used for comparison with the GFP data measured in the whole SCN. Superindex *WT*, *Bm, Wm* and *dm* were used to refer to the promoter in the stationary state for the WT, the *bravo* mutant, the *wox5* mutant and the double mutant, respectively (III-9.3 Supplementary text). Since GFP scale is arbitrary with respect to promoter activity, and arbitrary units can be set in the model, we used the ratios that set the fold-change between mutant and the WT as the relevant measure to be compared between model outputs and empirical data. For the empirical data we used the median GFP measured values and computed the ratio of the median GFP expression in the mutant over the median GFP expression data in the WT, for each mutant. For the model, we computed the ratios of the stationary production in each mutant over its stationary production value in the WT:

$$\sigma_B = \frac{P_B^{Bm}}{P_B^{WT}}, \quad \sigma_B^{\dagger} = \frac{P_B^{Wm}}{P_B^{WT}}, \quad \sigma_B^{\dagger\dagger} = \frac{P_B^{dm}}{P_B^{WT}}$$
$$\sigma_W = \frac{P_W^{Wm}}{P_W^{WT}}, \quad \sigma_W^{\dagger} = \frac{P_W^{Bm}}{P_W^{WT}}, \quad \sigma_W^{\dagger\dagger} = \frac{P_W^{dm}}{P_W^{WT}}$$

where the subscript in σ indicates the promoter that is analysed (whether it is that of BRAVO or WOX5) and the superscript is informative on the mutant: no superscript is used when the ratio is evaluated in the background of the gene whose promoter is studied; superscript † is used when the mutation is on a different gene than the one driven by the promoter; †† indicates the double mutant. Parameter values in Eq.1 (Supplementary table III-1) were chosen such that the values of these ratios obtained from the model fit the ratios computed from the median GFP expression values (Figure III-3C). Since the GFP data is a broad distribution, there is a broad range of parameters in which the model fits the experiments within the range of experimental deviations. In addition, the model reproduces for a wide range of parameter values whether these ratios are >1 (i.e. in the mutant, the promoter activity increases) or <1 (i.e. in the mutant, the promoter activity decreases).

Notice that based on the model equations, the following equality is found for the model outputs $\sigma_W^{\dagger} = \sigma_W^{\dagger\dagger}$ (since regulation of *WOX5* by *BRAVO* is set through *WOX5*). For *BRAVO*, $\sigma_B^{\dagger} \neq \sigma_B^{\dagger\dagger}$ since *BRAVO* is set to self-repress, although in the range of parameters chosen both ratios are rather similar.

Additionally, the model outputs were numerically computed for different values of α and γ (all the remaining parameter values being unchanged), to model different conditions of the growth medium. Specifically, we set α and γ as functions of an auxiliary control parameter x that indicates the medium condition (x=1 corresponds to CTL conditions, whereas higher x values correspond to a medium with BL). We used $\alpha=0.3/x$ and $\gamma=250x/(x+9)$, such that for x=1 α and γ take the values of the WT in CTL conditions (for x=1, α and γ take the values in Supplementary table III-1). Roughly, x controls the disparity between the basal production of *BRAVO* and *WOX5.* This allows us to interpret high values of x as the effect of BL.

7.9.3 Numerical methods to obtain model outputs

In the stationary state (i.e. when time-derivatives are equal to zero), the model for the WT reduces to a system of two coupled algebraic equations and for each mutant to a single algebraic equation (see III-9.3 Supplementary text). To find the stationary stable solutions we solved these algebraic equations numerically with custom-made software and using the fsolve routine embedded in Python (Python Software Foundation, https://www.python.org/), which uses a

modification of Powell's hybrid method for finding zeros of a system of nonlinear equations. The temporal evolution in Figure III-3B was computed using odeint function embedded in Python (Python Software Foundation, https://www.python.org/) for the WT and for each mutant.

7.9.4 Estimation of the error in the QC division data

We denote by *a,b,c* and *d* the values that we obtain empirically for the percentage of roots that exhibit a divided QC in the WT, the *bravo* mutant, the *wox5* mutant and the double *bravo wox5* mutant respectively (*a*=0.3939, *b*=0.8732, *c*=0.8070, *d*=0.8846). We can estimate the error in each of these measures, by assuming our measurement for each genotype corresponds to *N* independent equivalent roots where we observe whether the QC exhibits any division or not (i.e. we have *N* independent Bernouilli experiments). By assuming that the probability of observing a QC with at least one cell divided is *p* (*p=a,b,c,d* for each of the genotypes under study) we can estimate the error. Specifically, we assumed $p = N_k/N$, where N_k is the number of roots, from the total *N* of the specific genotype, that have a divided QC and set the error as the standard deviation of $p = \frac{N_k}{N}$: $\delta p \equiv std\left(p = \frac{N_k}{N}\right) = \sqrt{\frac{p(1-p)}{N}}$. For each genotype we took a conservative view and used *N*=15 for computing the errors, so as to avoid their underestimation.

7.9.5 A model to compute the contribution of BRAVO and WOX5 to regulate QC division

We aim at evaluating the contribution of BRAVO and WOX5 on regulating QC divisions. To this end we propose the following function:

$$F = \frac{F_0}{1 + T_B + T_W + T_{BW}}$$

which indicates the frequency at which we found a QC with at least one QC cell that is divided in the plane of observation, for roots of the same genotype. This function can be applied to the WT, to each single mutant and to the double mutant. T_B, T_W and T_{BW} are the contribution mediated by BRAVO, by WOX5 and by both BRAVO and WOX5 jointly respectively, on the regulation of QC division such that in the *wox5* mutant we have $T_W = 0$ and $T_{BW} = 0$, while in the *bravo* mutant we have $T_B = 0$ and $T_{BW} = 0$. Notice that for any of these contributions, it corresponds to repression of QC divisions when it takes positive values. In contrast, it corresponds to induction of QC divisions for negative values. This function takes the following expressions in the WT and in the mutants:

$$F^{WT} = \frac{F_0}{1 + T_B^{WT} + T_W^{WT} + T_{BW}^{WT}}$$

$$F^{Bm} = \frac{F_0}{1 + T_W^{Bm}} = \frac{F_0}{1 + T_W^{WT} q_W^{Bm}}$$

$$F^{Wm} = \frac{F_0}{1 + T_B^{Wm}} = \frac{F_0}{1 + T_B^{WT} q_B^{Wm}}$$

$$F^{dm} = F_0$$

where super-indexes WT, Bm, Wm account for WT, *bravo* mutant and *wox5* mutant respectively.

q_B^{Wm} parameter measures the change in the strength of the contribution BRAVO-mediates on QC division in the *wox5* mutant compared to the strength it does on the WT (i.e. the strength with which BRAVO inhibits QC division in the *wox5* mutant is $T_B^{Wm} = T_B^{WT} q_B^{Wm}$) . Analogously, q_W^{Bm} parameter measures the change in the strength of the repression that WOX5 does on QC division in the *bravo* mutant compared to the strength it does on the WT. Notice that we assume no additional changes happen in the function *F* in these mutants.

From these equations and using the empirical data ($F^{WT} = a, F^{Bm} = b, F^{Wm} = c, F^{dm} = d$, we can extract the values of T_B^{WT} , T_W^{WT} i T_{BW}^{WT}. First, we can write down ratios between these quantities:

$$\frac{F^{Bm}}{F^{WT}} = \frac{1 + T_B^{WT} + T_W^{WT} + T_{BW}^{WT}}{1 + T_W^{WT} q_W^{Bm}} = \frac{b}{a}$$

$$\frac{F^{Wm}}{F^{WT}} = \frac{1 + T_B^{WT} + T_W^{WT} + T_{BW}^{WT}}{1 + T_B^{WT} q_B^{Wm}} = \frac{c}{a}$$

$$\frac{F^{dm}}{F^{WT}} = 1 + T_B^{WT} + T_W^{WT} + T_{BW}^{WT} = \frac{d}{a}$$

and then isolate each term, such that the following is found:

$$T_B^{WT} \pm \delta T_B^{WT} = \frac{1}{q_B^{Wm}}\left(\frac{d}{c} - 1\right) \pm \frac{1}{q_B^{Wm}} \sqrt{\left(\frac{\delta d}{c}\right)^2 + \left(\frac{d}{c^2}\delta c\right)^2}$$

$$T_W^{WT} \pm \delta T_W^{WT} = \frac{1}{q_W^{Bm}}\left(\frac{d}{b} - 1\right) \pm \frac{1}{q_W^{Bm}} \sqrt{\left(\frac{\delta d}{b}\right)^2 + \left(\frac{d}{b^2}\delta b\right)^2}$$

$$T_{BW}^{WT} \pm \delta T_{BW}^{WT}$$
$$= \frac{d}{a} - 1 - \frac{1}{q_B^{Wm}}\left(\frac{d}{c} - 1\right) - \frac{1}{q_W^{Bm}}\left(\frac{d}{b} - 1\right)$$
$$\pm \sqrt{\left(\delta d\left(\frac{1}{a} - \frac{1}{q_B^{Wm}c} - \frac{1}{q_W^{Bm}b}\right)\right)^2 + \left(\frac{d}{a^2}\delta a\right)^2 + \left(\frac{d}{q_W^{Bm}b^2}\delta b\right)^2 + \left(\frac{d}{q_B^{Wm}c^2}\delta c\right)^2}$$

where the errors have been estimated using error propagation of the errors *in a,b,c* and *d* and assuming their independency. In Figure III-5, continuous lines correspond to the best estimated values (e.g. $T_B^{WT} = \frac{1}{q_B^{Wm}}\left(\frac{d}{c} - 1\right)$), and the shaded area represents the range within the errors (e.g. $T_B^{WT} \pm \delta T_B^{WT}$).

8. References

Aida, M., Beis, D., Heidstra, R., Willemsen, V., Blilou, I., Galinha, C., . . . Scheres, B. (2004). The PLETHORA genes mediate patterning of the Arabidopsis root stem cell niche. *Cell, 119*(1), 109-120. doi: 10.1016/j.cell.2004.09.018

Banda, J., Bellande, K., von Wangenheim, D., Goh, T., Guyomarc'h, S., Laplaze, L., & Bennett, M. J. (2019). Lateral Root Formation in Arabidopsis: A Well-Ordered LRexit. *Trends Plant Sci, 24*(9), 826-839. doi: 10.1016/j.tplants.2019.06.015

Bennett, T., van den Toorn, A., Willemsen, V., & Scheres, B. (2014). Precise control of plant stem cell activity through parallel regulatory inputs. *Development, 141*(21), 4055-4064. doi: 10.1242/dev.110148

Betegon-Putze, I., Gonzalez, A., Sevillano, X., Blasco-Escamez, D., & Cano-Delgado, A. I. (2019). MyROOT: a method and software for the semiautomatic measurement of primary root length in Arabidopsis seedlings. *Plant J, 98*(6), 1145-1156. doi: 10.1111/tpj.14297

Bleckmann, A., Weidtkamp-Peters, S., Seidel, C. A., & Simon, R. (2010). Stem cell signaling in Arabidopsis requires CRN to localise CLV2 to the plasma membrane. *Plant Physiol, 152*(1), 166-176. doi: 10.1104/pp.109.149930

Burkart, R. C., Strotmann, V. I., Kirschner, G. K., Akinci, A., Czempik, L., Maizel, A., . . . Stahl, Y. (2019). PLETHORA and WOX5 interaction and subnuclear localisation regulates Arabidopsis root stem cell maintenance. *bioRxiv*. doi: 10.1101/818187

Clark, N. M., Buckner, E., Fisher, A. P., Nelson, E. C., Nguyen, T. T., Simmons, A. R., . . . Sozzani, R. (2019). Stem-cell-ubiquitous genes spatiotemporally coordinate division through regulation of stem-cell-specific gene networks. *Nat Commun, 10*(1), 5574. doi: 10.1038/s41467-019-13132-2

De Rybel, B., Mahonen, A. P., Helariutta, Y., & Weijers, D. (2016). Plant vascular development: from early specification to differentiation. *Nat Rev Mol Cell Biol, 17*(1), 30-40. doi: 10.1038/nrm.2015.6

Dolan, L., Janmaat, K., Willemsen, V., Linstead, P., Poethig, S., Roberts, K., & Scheres, B. (1993). Cellular organisation of the Arabidopsis thaliana root. *Development, 119*(1), 71-84.

Espinosa-Ruiz, A., Martinez, C., de Lucas, M., Fabregas, N., Bosch, N., Cano-Delgado, A. I., & Prat, S. (2017). TOPLESS mediates brassinosteroid control of shoot boundaries and root meristem development in Arabidopsis thaliana. *Development, 144*(9), 1619-1628. doi: 10.1242/dev.143214

Forzani, C., Aichinger, E., Sornay, E., Willemsen, V., Laux, T., Dewitte, W., & Murray, J. A. (2014). WOX5 suppresses CYCLIN D activity to establish quiescence at the center of the root stem cell niche. *Curr Biol, 24*(16), 1939-1944. doi: 10.1016/j.cub.2014.07.019

Fulcher, N., & Sablowski, R. (2009). Hypersensitivity to DNA damage in plant stem cell niches. *Proc Natl Acad Sci U S A, 106*(49), 20984-20988. doi: 10.1073/pnas.0909218106

Gietz, R. D., & Woods, R. A. (2002). Transformation of yeast by lithium acetate/single-stranded carrier DNA/polyethylene glycol method. *Methods Enzymol, 350*, 87-96. doi: 10.1016/s0076-6879(02)50957-5

Goh, T., Toyokura, K., Wells, D. M., Swarup, K., Yamamoto, M., Mimura, T., . . . Guyomarc'h, S. (2016). Quiescent center initiation in the Arabidopsis lateral root primordia is dependent on the SCARECROW transcription factor. *Development, 143*(18), 3363-3371. doi: 10.1242/dev.135319

Gonzalez-Garcia, M. P., Vilarrasa-Blasi, J., Zhiponova, M., Divol, F., Mora-Garcia, S., Russinova, E., & Cano-Delgado, A. I. (2011). Brassinosteroids control meristem size by promoting cell cycle progression in Arabidopsis roots. *Development, 138*(5), 849-859. doi: 10.1242/dev.057331

Lozano-Elena, F., Planas-Riverola, A., Vilarrasa-Blasi, J., Schwab, R., & Cano-Delgado, A. I. (2018). Paracrine brassinosteroid signaling at the stem cell niche controls cellular regeneration. *J Cell Sci, 131*(2). doi: 10.1242/jcs.204065

Occhialini, A., Gouzerh, G., Di Sansebastiano, G. P., & Neuhaus, J. M. (2016). Dimerization of the Vacuolar Receptors AtRMR1 and -2 from Arabidopsis thaliana Contributes to Their Localisation in the trans-Golgi Network. *Int J Mol Sci, 17*(10), 1661. doi: 10.3390/ijms17101661

Pi, L., Aichinger, E., van der Graaff, E., Llavata-Peris, C. I., Weijers, D., Hennig, L., . . . Laux, T. (2015). Organizer-Derived WOX5 Signal Maintains Root Columella Stem Cells through Chromatin-Mediated Repression of CDF4 Expression. *Dev Cell, 33*(5), 576-588. doi: 10.1016/j.devcel.2015.04.024

Sarkar, A. K., Luijten, M., Miyashima, S., Lenhard, M., Hashimoto, T., Nakajima, K., . . . Laux, T. (2007). Conserved factors regulate signalling in Arabidopsis thaliana shoot and root stem cell organizers. *Nature, 446*(7137), 811-814. doi: 10.1038/nature05703

Scheres, B. (2007). Stem-cell niches: nursery rhymes across kingdoms. *Nat Rev Mol Cell Biol, 8*(5), 345-354. doi: 10.1038/nrm2164

Shimotohno, A., Heidstra, R., Blilou, I., & Scheres, B. (2018). Root stem cell niche organizer specification by molecular convergence of PLETHORA and SCARECROW transcription factor modules. *Genes Dev, 32*(15-16), 1085-1100. doi: 10.1101/gad.314096.118

Stahl, Y., Grabowski, S., Bleckmann, A., Kuhnemuth, R., Weidtkamp-Peters, S., Pinto, K. G., . . . Simon, R. (2013). Moderation of Arabidopsis root stemness by CLAVATA1 and ARABIDOPSIS CRINKLY4 receptor kinase complexes. *Curr Biol, 23*(5), 362-371. doi: 10.1016/j.cub.2013.01.045

Stahl, Y., Wink, R. H., Ingram, G. C., & Simon, R. (2009). A signaling module controlling the stem cell niche in Arabidopsis root meristems. *Curr Biol, 19*(11), 909-914. doi: 10.1016/j.cub.2009.03.060

Tian, H., Jia, Y., Niu, T., Yu, Q., & Ding, Z. (2014). The key players of the primary root growth and development also function in lateral roots in Arabidopsis. *Plant Cell Rep, 33*(5), 745-753. doi: 10.1007/s00299-014-1575-x

Tian, H., Wabnik, K., Niu, T., Li, H., Yu, Q., Pollmann, S., . . . Ding, Z. (2014). WOX5-IAA17 feedback circuit-mediated cellular auxin response is crucial for the patterning of root stem cell niches in Arabidopsis. *Mol Plant, 7*(2), 277-289. doi: 10.1093/mp/sst118

Truernit, E., Bauby, H., Dubreucq, B., Grandjean, O., Runions, J., Barthelemy, J., & Palauqui, J. C. (2008). High-resolution whole-mount imaging of three-dimensional tissue organization and gene expression enables the study of Phloem development and structure in Arabidopsis. *Plant Cell, 20*(6), 1494-1503. doi: 10.1105/tpc.107.056069

van den Berg, C., Willemsen, V., Hage, W., Weisbeek, P., & Scheres, B. (1995). Cell fate in the Arabidopsis root meristem determined by directional signalling. *Nature, 378*(6552), 62-65. doi: 10.1038/378062a0

van den Berg, C., Willemsen, V., Hendriks, G., Weisbeek, P., & Scheres, B. (1997). Short-range control of cell differentiation in the Arabidopsis root meristem. *Nature, 390*(6657), 287-289. doi: 10.1038/36856

Vilarrasa-Blasi, J., Gonzalez-Garcia, M. P., Frigola, D., Fabregas, N., Alexiou, K. G., Lopez-Bigas, N., . . . Cano-Delgado, A. I. (2014). Regulation of plant stem cell quiescence by a brassinosteroid signaling module. *Dev Cell, 30*(1), 36-47. doi: 10.1016/j.devcel.2014.05.020

Weidtkamp-Peters, S., & Stahl, Y. (2017). The Use of FRET/FLIM to Study Proteins Interacting with Plant Receptor Kinases. *Methods Mol Biol, 1621*, 163-175. doi: 10.1007/978-1-4939-7063-6_16

Yin, Y., Wang, Z. Y., Mora-Garcia, S., Li, J., Yoshida, S., Asami, T., & Chory, J. (2002). BES1 accumulates in the nucleus in response to brassinosteroids to regulate gene expression and promote stem elongation. *Cell, 109*(2), 181-191. doi: 10.1016/s0092-8674(02)00721-3

9. Supplementary information

9.1 Supplementary figures

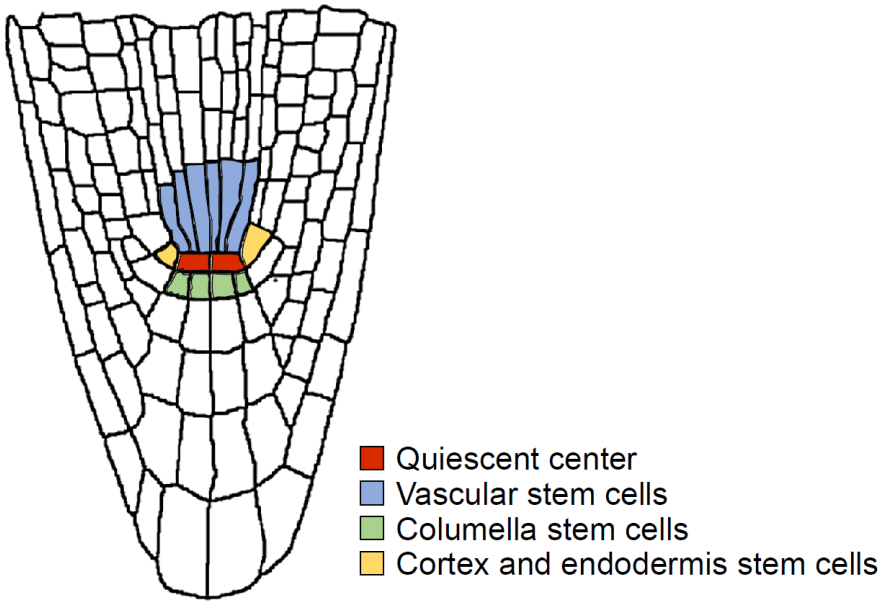

Supplementary figure III-1: Medial longitudinal view of the *Arabidopsis thaliana* primary root apex
Schematic representation of a 6-day-old primary root. At the root apex the stem cell niche is formed by the quiescent centre (QC) and the surrounding stem cells, which are highlighted in different colours.

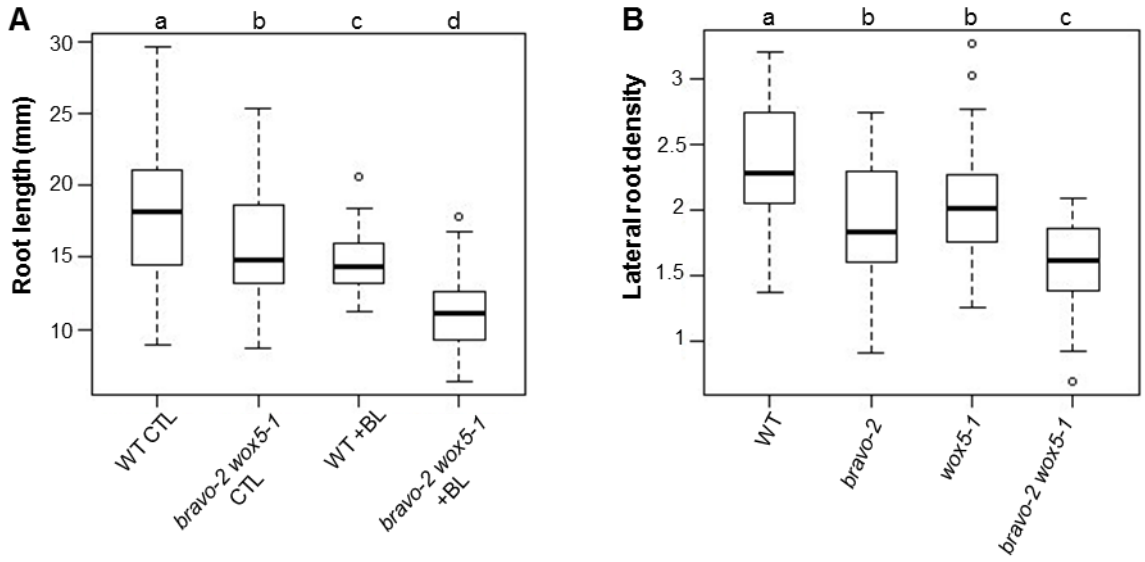

Supplementary figure III-2: BRAVO and WOX5 promote primary root growth and lateral root development

A) Root length of 6-day-old WT and *bravo-2 wox5-1* mutants in control and after BL treatment (n>30, 3 replicates). Different letters indicate statistically significant differences (p-value < 0.05 Student´s t-test). **B)** Lateral root density (number of lateral roots per mm of root length) of 10-day-olf WT, *bravo-2*, *wox5-1* and *bravo-2 wox5-1* mutants (n>52, 3 replicates). Different letters indicate statistically significant differences (p-value < 0.05 Student´s t-test).

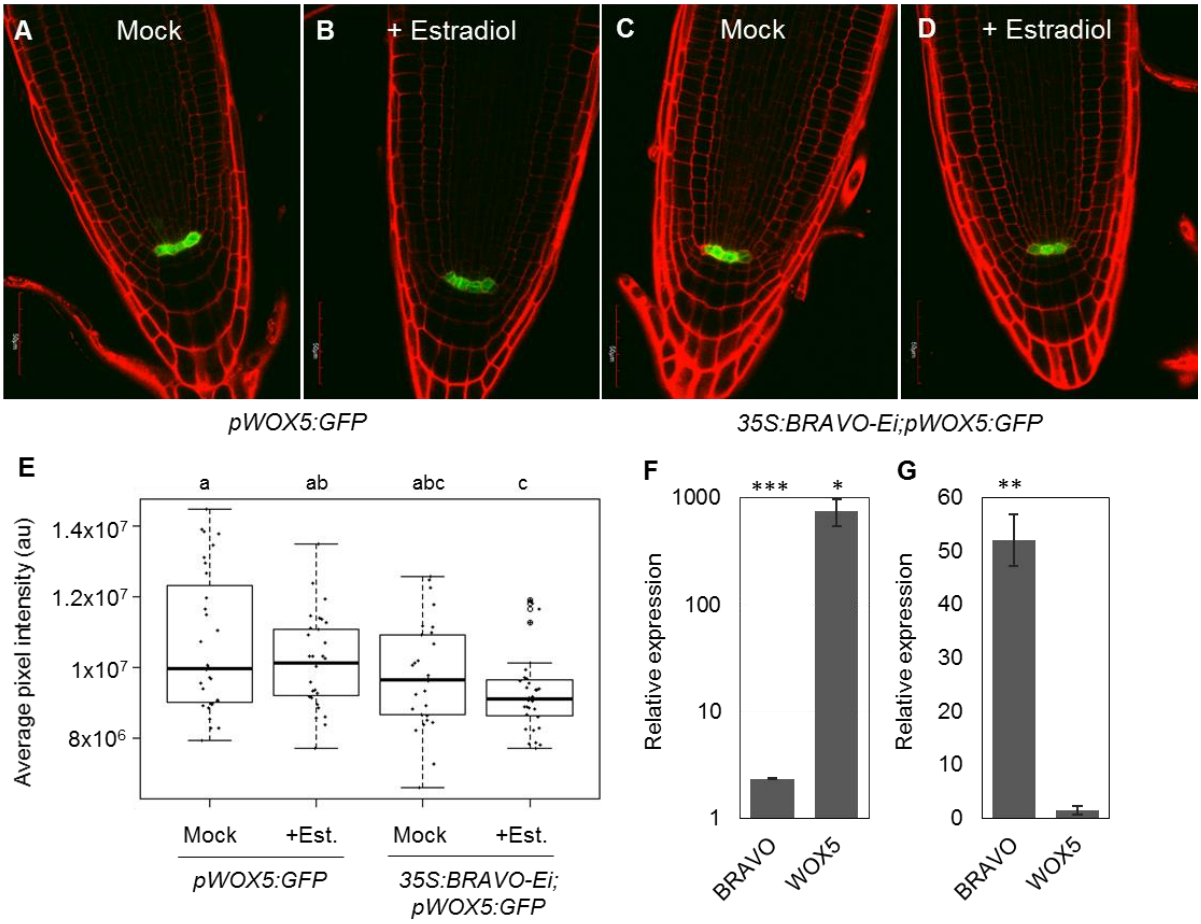

Supplementary figure III-3: BRAVO and WOX5 expression patterns in overexpressor lines

A-D) Confocal images of PI-stained 6-day-old roots. GFP expression is shown in green. *pWOX5:GFP* in WT and 35S:BRAVO-Ei background in control (A, C) and after 6 days 30 µM β-estradiol induction (B, D). Scale bar: 50 µm. **E)** Quantification of the GFP fluorescent signal of the roots in A-D. Boxplot indicating the average pixel intensity of the GFP in the stem cell niche (n>29, 3 biological replicates). Different letters indicate statistically significant differences (p-value < 0.05 Student´s *t*-test). **F)** Bars show the relative expression of BRAVO and WOX5 in 35S:WOX5-GR lines when induced with 1µM Dexamethasone for 24 hours. Values in control conditions are not represented as they are 1. Data obtained from two independent biological replicates. Asterisks indicate significant differences (* p-value < 0.05, *** p-value < 0.001 Student´s *t*-test). **G)** Bars show the relative expression of BRAVO and WOX5 in 35S:BRAVO-Ei lines when induced with 30 µM β-estradiol for 24 hours. Values in control conditions are not represented as they are 1. Data obtained from three independent biological replicates. Asterisks indicate significant differences (** p-value < 0.01 Student´s *t*-test).

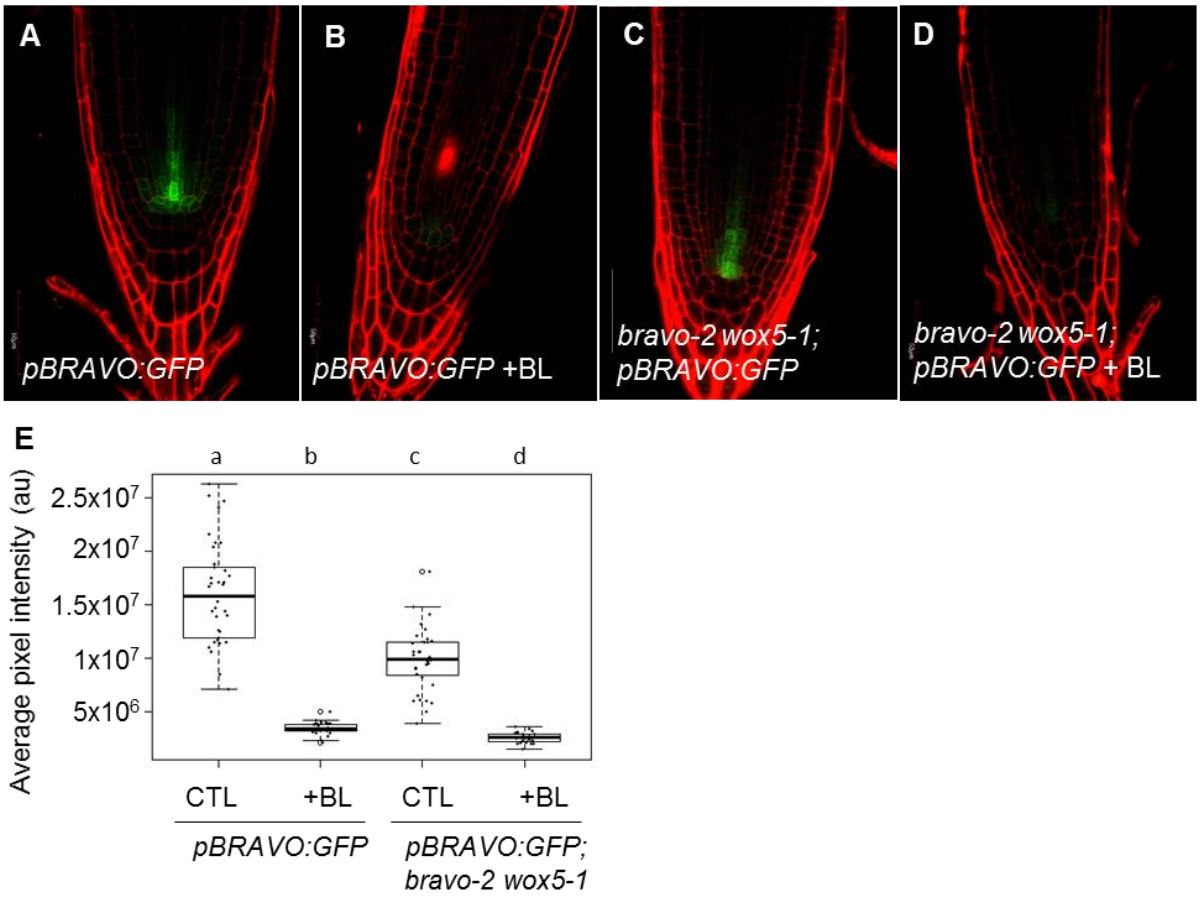

Supplementary figure III-4: BRAVO expression in the *bravo wox5* mutant background

A-D) Confocal images of PI-stained 6-day-old roots. GFP expression is shown in green. *pBRAVO:GFP* in WT and *bravo-2 wox5-1* background in control (A, C) and after BL treatment (B, D). Scale bar: 50 µm. **E)** Quantification of the GFP fluorescent signal of the roots in A-D in the stem cell niche. Different letters indicate statistically significant differences (p-value < 0.05 Student´s t-test).

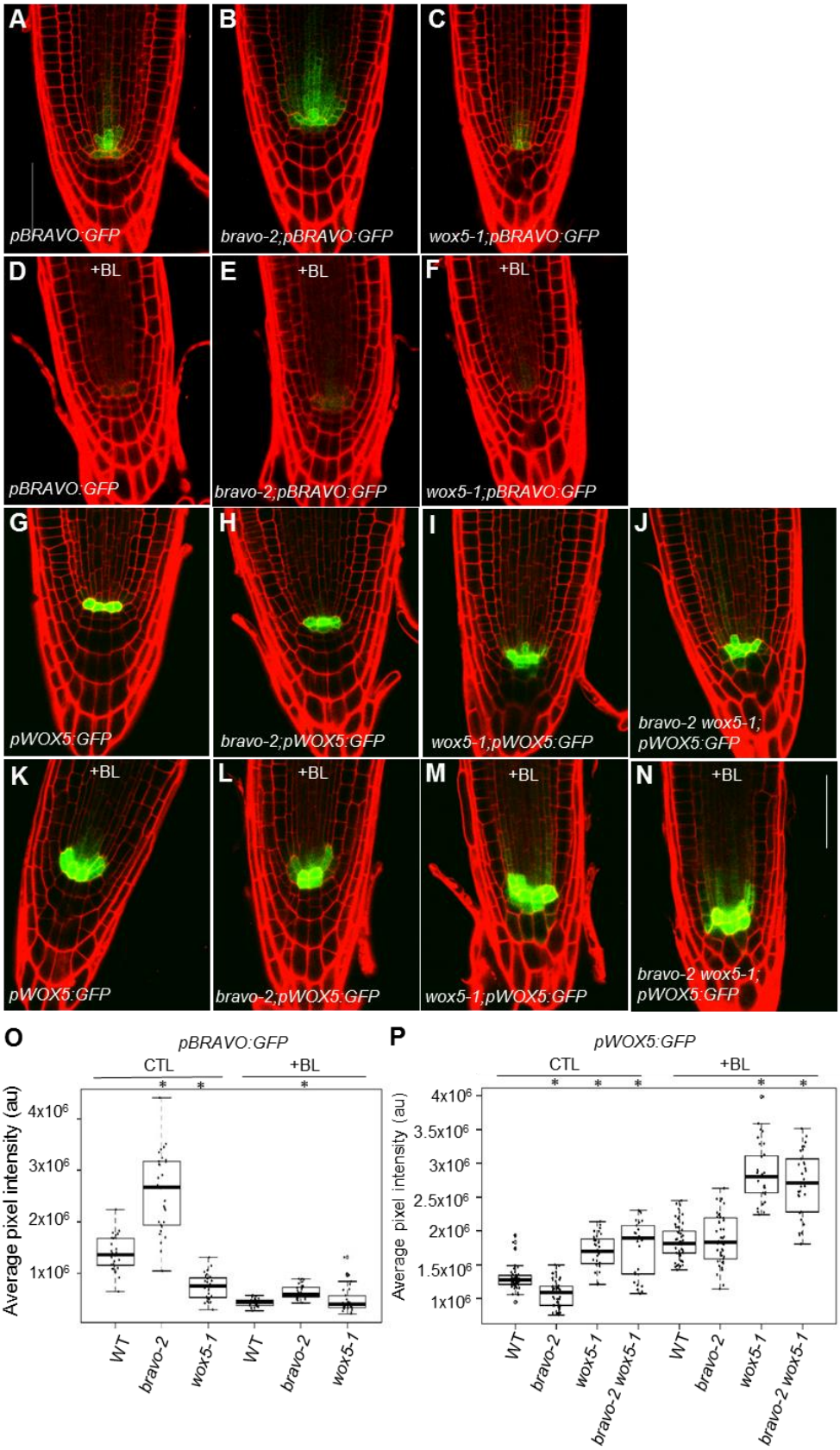

Supplementary figure III-5: BRAVO and WOX5 expression is BL regulated

A-N) Confocal images of PI-stained 6-day-old roots. GFP expression is shown in green. **A-C)** *pBRAVO:GFP* in WT, *bravo-2* and *wox5-1* knockout backgrounds in CTL (A-C) and after 48h 4nM BL treatment (D-F). **G-N)**

pWOX5:GFP in WT, *bravo-2*, *wox5-1* and *bravo-2 wox5-1* knockout backgrounds in CTL (G-J) and after 48h 4 nM BL treatment (K-N). Images in control conditions are the same that are shown in Figure III-2. Scale bar: 50 µm. **O, P)** Quantification of the GFP fluorescent signal of the roots in A-F (O) and G-N (P). Boxplot indicating the average pixel intensity of the GFP in the stem cell niche. (n>25, 3 biological replicates, *p-value < 0.05 Student´s *t*-test for each genotype versus the WT in the same condition). Quantification of lines in control conditions are the same that are shown in Figure III-2.

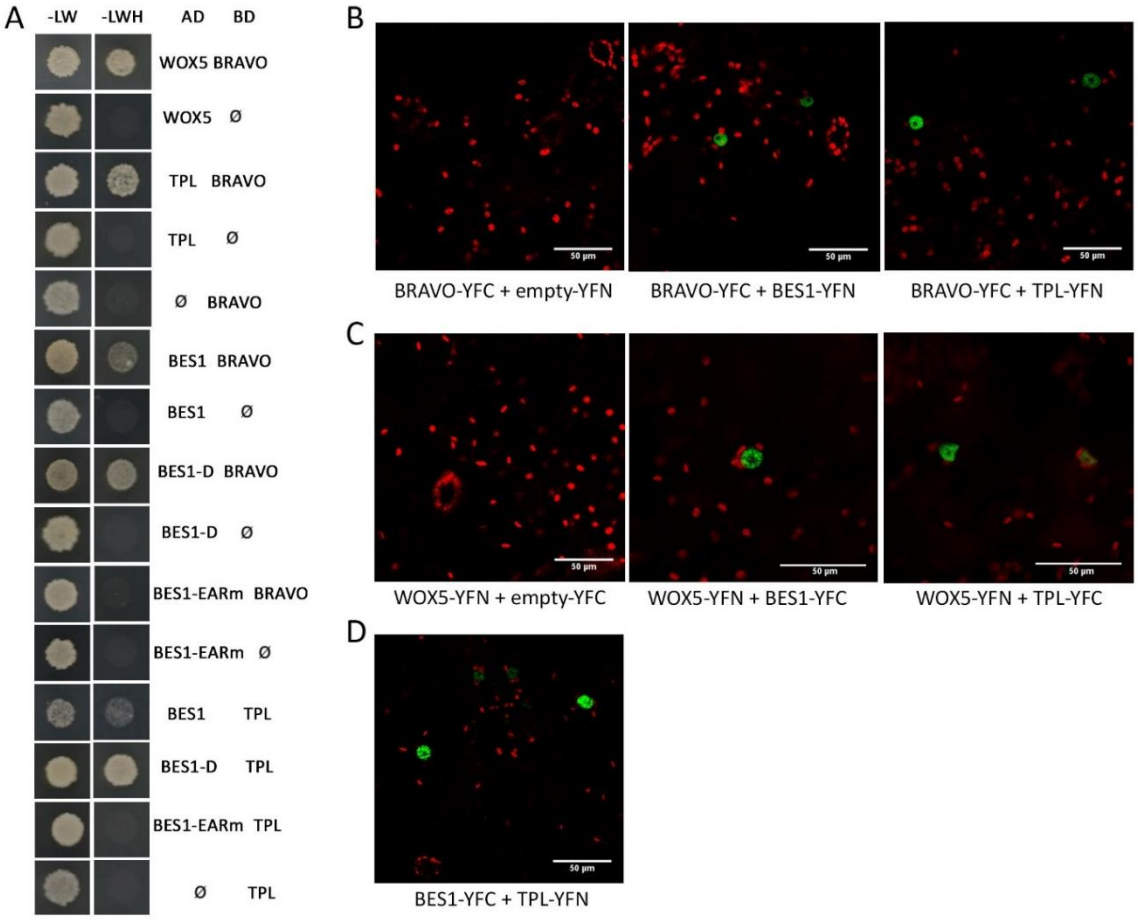

Supplementary figure III-6: Biochemical interactions of BRAVO and WOX5 with BES1 and TPL

A) Yeast two-hybrid assay showing BRAVO interactions with WOX5, BES1 and TPL *in vitro*. In the left column yeast cells were grown on control media, and in the right column yeast cells were grown on control media lacking Leu, Trp and His, indicating an interaction between the proteins. **B-D)** *In planta* interaction by Bimolecular Fluorescence Complementation assay (BiFC). Confocal images were merged with red fluorescence images corresponding to chlorophyll. Fluorescence was detected 48 h post agroinfiltration. Scale bar: 50 µm. B) BiFC showing BRAVO interaction with BES1 and TPL. Nuclear YFP fluorescence is observed in *N. benthamiana* leaves infiltrated with the BRAVO-eYFPC and both BES1 and TPL-eYFPN constructs. BRAVO-eYFPC and empty-eYFPN are included as a negative control. C) BiFC showing WOX5 interaction with BES1 and TPL. Nuclear YFP fluorescence is observed in *N. benthamiana* leaves infiltrated with the WOX5-eYFPN and both BES1 and TPL-eYFPC constructs. WOX5-eYFPN and empty-eYFPC are included as a negative control. D) BES1-eYFPC and TPL-eYFPN was included as a positive control of interaction. Scale bar: 50 µm.

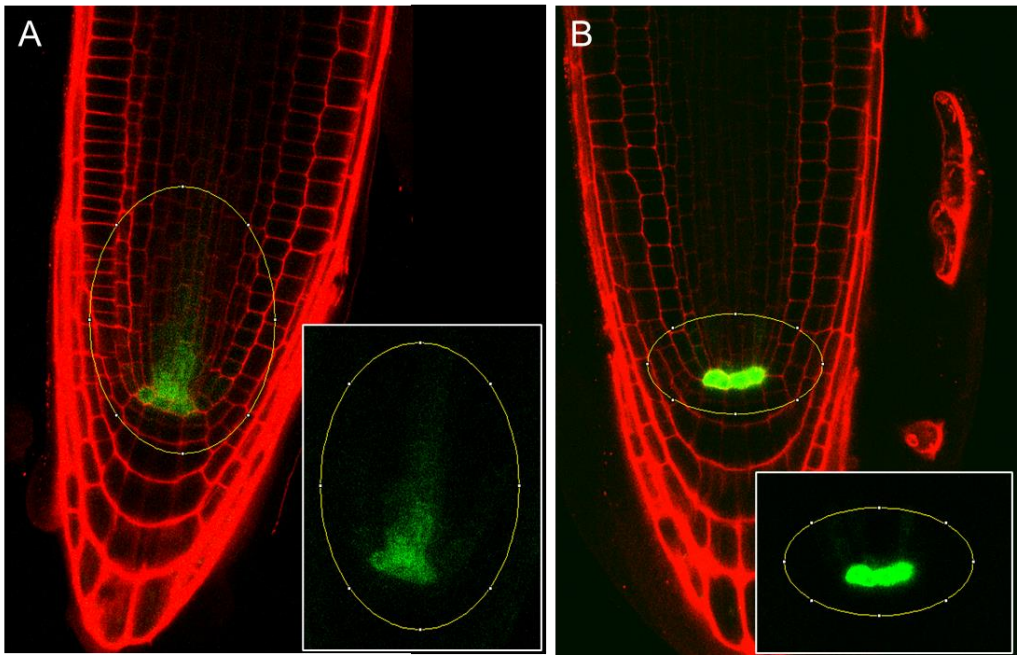

Supplementary figure III-7: ROIs used for the quantification of the GFP

A-B) Confocal images of *pBRAVO:GFP* (A) *and pWOX5:GFP* (B) PI-stained 6-day-old roots. GFP expression is shown in green. Insets show the GFP channels that were used for the quantification. Only the area inside the yellow circle was used for the GFP quantification.

9.2 Supplementary tables

Supplementary table III-1: Parameter values for the model of BRAVO and WOX5, used to generate the data in Figure III-3

Parameter values used to perform the numerical simulations. All are in arbitrary units. The right-most column indicates the concentration and time scales in which these values could be meaningful in a biological context.

Parameter	Value	Units
α	0,3	nM/min
γ	25	nM/min
K_M	0,02	nM^{-1}
K_W	0,01	nM^{-1}
ε_M	0,2	-
ε_W	4	-
W_0	1,6	-
M_0	30	nM/min
W_1	0,001	nM^{-1}
d_M	0,01	min^{-1}
d_W	0,01	min^{-1}

Supplementary table III-2: List of plant material lines used in this study

Name	Description	Reference
bravo-2	Knock out mutant	Vilarrasa-Blasi *et al.,* 2014
wox5-1	Knock out mutant	Sarkar *et al.*, 2007
35S:WOX5-GR	Overexpressor mutant	Sarkar *et al.*, 2007
35S:BRAVO-Ei	Overexpressor mutant	Vilarrasa-Blasi *et al.,* 2014
pBRAVO:GFP	Promoter reporter line	Lee *et al.*, 2006
pWOX5:GFP	Promoter reporter line	Sarkar *et al.*, 2007

Supplementary table III-3: List of primers used in this study

Name	Sequence (5'-3')	Description
bravo-2 F	TCCCTTAATCCCTAAACCCAGC	Genotype bravo mutation Forward primer
bravo-2 R	CCTGATGCAAGGGTACTATCG	Genotype bravo mutation Reverse primer
wox5-1 F	ATCTCATAAACCATGCATCGG	Genotype wox5 mutation Forward primer
wox5-1 R	TCGCTGGTTCCGATATACAAC	Genotype wox5 mutation Reverse primer
LBb1.3	ATTTTGCCGATTTCGGAAC	T-DNA border primer
RT-ACTIN2 F	CTGGATCGGTGGTTCCATTC	ACTIN2 RT-qPCR Forward primer
RT-ACTIN2 R	CCTGGACCTGCCTCATCATAC	ACTIN2 RT-qPCR Reverse primer
RT-BRAVO F	TGTTAGCAGCTCATCGAGCCT	BRAVO RT-qPCR Forward primer
RT-BRAVO R	GATGACGTGCCAATGGTTCTT	BRAVO RT-qPCR Reverse primer
RT-WOX5 F	TGATCTGTTTCGAGCCGGTC	WOX5 RT-qPCR Forward primer
RT-WOX5 R	AAACATTCTTGCTCTCTATCTTGCC	WOX5 RT-qPCR Reverse primer

9.3 Supplementary text

9.3.1 Model

For the WT genotype, the model reads (see III-7 Methods):

$$\frac{dB}{dt} = P_B(B,W) - d_B B$$

$$P_B(B,W) = \alpha \frac{1+\varepsilon_B(K_B B)^2}{1+(K_B B)^2} \frac{1+\varepsilon_W(K_W W)^2}{1+(K_W W)^2}$$

$$\frac{dW}{dt} = P_W(B,W) - d_W W$$

$$P_W(B,W) = \gamma \frac{1}{{W_0}^2 + W^2\left(\frac{1}{B^2+B_0^2}+W_1\right)^2}$$

For the *wox5* mutant (where superscript *Wm* denotes this mutant) the model reads (it has $W^{Wm} = 0$):

$$\frac{dB^{Wm}}{dt} = P_W(B^{Wm},0) - d_B B^{Wm}$$

$$P_B(B^{Wm},0) = \alpha \frac{1+\varepsilon_B\left(K_B B^{Wm}\right)^2}{1+(K_B B^{Wm})^2},$$

$$W^{Wm} = 0,$$

$$P_W(B^{Wm},0) = \gamma \frac{1}{{W_0}^2}$$

The model for *bravo* mutant (where superscript *Bm* denotes this mutant) has $B^{Bm} = 0$ and reads:

$$B^{Bm} = 0,$$

$$P_B(0,W^{Bm}) = \alpha \frac{1+\varepsilon_W\left(K_W W^{Bm}\right)^2}{1+(K_W W^{Bm})^2},$$

$$\frac{dW^{Bm}}{dt} = P_W(0,W^{Bm}) - d_W W^{Bm},$$

$$P_W(0, W^{Bm}) = \gamma \frac{1}{{W_0}^2 + {W^{Bm}}^2\left(\frac{1}{B_0^2} + W_1\right)^2}$$

Finally, for the double *bravo wox5* mutant (superscript *dm*) the model reads:

$B^{dm} = 0, W^{dm} = 0$

$P_B(0,0) = \alpha, \quad P_W(0,0) = \gamma \frac{1}{{W_0}^2} = P_W(0, W^{Bm})$

9.3.2 Stationary solutions

For each genotype, the stationary solutions are found by imposing the stationarity condition: $\frac{dB}{dt} = 0$ and $\frac{dW}{dt} = 0$, of the equations that describe each genotype.

For the WT, when we impose the stationary conditions the following set of two coupled algebraic equations is obtained in the stationary state:

$$d_B B^{WT} = \alpha \left(\frac{1 + \varepsilon_B (K_B B^{WT})^2}{1 + (K_B B^{WT})^2}\right)\left(\frac{1 + \varepsilon_W (K_W W^{WT})^2}{1 + (K_W W^{WT})^2}\right)$$

$$d_W W^{WT} = \gamma \left(\frac{1}{W_0^2 + (W^{WT})^2 \left(\frac{1}{B_0^2 + (B^{WT})^2} + W_1\right)^2}\right)$$

which is solved numerically (see III-7 Methods). We denote by B^{WT}, W^{WT} the stationary solutions for the expression of *BRAVO* and *WOX5* in the WT. The stationary *BRAVO* and *WOX5* promoter activities in the WT are:

$$P_B^{WT} \equiv P_B(B^{WT}, W^{WT}) = \alpha \left(\frac{1 + \varepsilon_B (K_B B^{WT})^2}{1 + (K_B B^{WT})^2}\right)\left(\frac{1 + \varepsilon_W (K_W W^{WT})^2}{1 + (K_W W^{WT})^2}\right)$$

$$P_W^{WT} \equiv P_W(B^{WT}, W^{WT}) = \gamma \left(\frac{1}{W_0^2 + (W^{WT})^2 \left(\frac{1}{B_0^2 + (B^{WT})^2} + W_1\right)^2}\right)$$

where, once we have the stationary values B^{WT}, W^{WT} we can obtain their values by substitution on the above expressions.

We proceed in the same way with each mutant with their corresponding equations set to the stationary state.

For the *wox5* mutant, we have $W^{Wm} = 0$, and the stationary expression of *BRAVO* satisfies

$$B^{Wm} = \frac{\alpha}{d_B}\frac{1+\varepsilon_B\left(K_B B^{Wm}\right)^2}{1+\left(K_B B^{Wm}\right)^2}$$

which is solved numerically. The stationary *BRAVO* and *WOX5* promoter activities (productions) in this mutant are:

$$P_B^{Wm} = \alpha\frac{1+\varepsilon_B\left(K_B B^{Wm}\right)^2}{1+\left(K_B B^{Wm}\right)^2},$$

$$P_W^{Wm} = \gamma\frac{1}{{W_0}^2}.$$

For the *bravo* mutant in the stationary state we have $B^{Bm} = 0$, and

$$W^{Bm} = \frac{\gamma}{d_W}\frac{1}{{W_0}^2 + {W^{Bm}}^2\left(\frac{1}{B_0^2} + W_1\right)^2}$$

which is solved numerically. Once solved, the stationary promoter activities in this mutant are found as:

$$P_B^{Bm} = \alpha\frac{1+\varepsilon_W\left(K_W W^{Bm}\right)^2}{1+\left(K_W W^{Bm}\right)^2},$$

$$P_W^{Bm} = \gamma\frac{1}{{W_0}^2 + {W^{Bm}}^2\left(\frac{1}{B_0^2}+W_1\right)^2}$$

Finally, the model of the double *bravo wox5* mutant already indicates the stationary state values:

$B^{dm} = 0, W^{dm} = 0$

$P_B^{dm} = \alpha,\ \ P_W^{dm} = \gamma\frac{1}{{W_0}^2} = P_W^{Wm}.$

IV. PLETHORA and WOX5 interaction and subnuclear localisation regulates *Arabidopsis* root stem cell maintenance

This chapter is a manuscript in preparation for submission and was uploaded on bioRxiv (doi: https://doi.org/10.1101/818187).

Authors:

Rebecca C. Burkart[1], Vivien I. Strotmann[1], Gwendolyn K. Kirschner[1,2], Abdullah Akinci[1], Laura Czempik[1,3], Alexis Maizel[4], Stefanie Weidtkamp-Peters[5], Yvonne Stahl[1]

Affiliations:

[1]Institute for Developmental Genetics, Heinrich-Heine University, Universitätsstr. 1, 40225 Düsseldorf, Germany

[2]present affiliation: King Abdullah University of Science and Technology (KAUST), Biological and Environmental Sciences and Engineering (BESE), Thuwal, 23955-6900, Saudi Arabia

[3]present affiliation: Molecular Plant Science/Plant Biochemistry, University of Wuppertal, Gaußstraße 20, 42119 Wuppertal, Germany

[4]Center for Organismal Studies (COS), University of Heidelberg, Im Neuenheimer Feld 230, 69120 Heidelberg, Germany

[5]Center for Advanced Imaging, Heinrich-Heine University, Universitätsstr. 1, 40225 Düsseldorf, Germany

Contributions:

Rebecca C. Burkart, Vivien I. Strotmann, Abdullah Akinci, Laura Czempik, and Gwendolyn K. Kirschner carried out the experiments. Yvonne Stahl and Rebecca C. Burkart designed the experiments, analysed and interpreted the data. Stefanie Weidtkamp-Peters contributed to FLIM data analyses. Alexis Maizel carried out light sheet imaging. Yvonne Stahl and Rebecca C. Burkart wrote the manuscript. All authors commented on the manuscript.

1. Abstract

Maintenance and homeostasis of the stem cell niche (SCN) in the *Arabidopsis* root is essential for growth and development of all root cell types. The SCN is organized around a quiescent centre (QC) that maintains the stemness of the cells in direct contact. The transcription factors WUSCHEL-RELATED HOMEOBOX 5 (WOX5) and the PLETHORAs (PLTs) are both expressed in the SCN where they maintain the QC and regulate the fate of the distal columella stem cells (CSCs). Although WOX5 and PLTs are known as important players in SCN maintenance, much of the necessary regulation of quiescence and division in the *Arabidopsis* root is not understood on a molecular level. Here, we describe the concerted mutual regulation of the key transcription factors WOX5 and PLTs on a transcriptional and protein interaction level, leading to a confinement of the WOX5 expression domain to the QC cells by negative feedback regulation. Additionally, by applying a novel SCN staining method, we demonstrate that both WOX5 and PLTs are necessary for root meristem maintenance as they regulate QC quiescence and CSC fate and show that QC divisions and CSC differentiation correlate. Moreover, we uncover that PLTs, especially PLT3, contains intrinsically disordered prion-like domains (PrDs) that are necessary for complex formation with WOX5 and its recruitment to subnuclear microdomains/nuclear bodies (NBs) in the CSCs. We propose that the partitioning of the PLT-WOX5 complexes to NBs, possibly by liquid-liquid phase separation, plays an important role during determination of CSC fate.

2. Introduction

The root system of higher plants is essential for plant life, as it provides anchorage in the soil and access to nutrients and water. It arises from a population of long-lasting stem cells residing in a structure called root apical meristem (RAM) at the tip of the root. Within the *Arabidopsis thaliana* RAM, the stem cell niche (SCN) consists of on average four slowly dividing cells, the QC cells, which act as a long-term reservoir and signalling centre by maintaining the surrounding shorter-lived, proliferating stem cells (also called initials) in a non-cell autonomous manner[1]. These stem cells continuously divide asymmetrically, thereby generating new stem cells that are still in contact with the QC. The hereby-produced daughter cells frequently undergo cell divisions and are shifted further away from the QC to finally differentiate. By this mechanism, the position of the stem cells in the root remains the same throughout development and their precise orientation of division leads to the formation of concentrically organized

clonal cell lineages representing a spatio-temporal developmental gradient[1–3]. From the inside to the outside the following root cell tissues develop: vasculature, pericycle, endodermis, cortex and epidermis plus columella and lateral root cap at the distal root tip (Figure IV-1a).

The necessary longevity and continuous activity of the RAM can only be achieved if its stem cell pool is constantly replenished, since cells are frequently leaving the meristematic region due to continuous cell divisions. Therefore, complex regulatory mechanisms involving phytohormones and key transcription factors (TFs) regulate stem cell maintenance and the necessary supply of differentiating descendants[4]. Here, the APETALA2-type PLT TF family and the homeodomain TF WOX5 play important roles[5,6]. WOX5 is expressed mainly in the QC, but maintains the surrounding stem cells non-cell-autonomously by repressing their differentiation[6,7]. Loss of WOX5 causes the differentiation of the distal CSCs into starch-accumulating columella cells (CCs), while increased WOX5 expression causes CSC over-proliferation. Hence, WOX5 abundance is critical and necessary to suppress premature CSC differentiation[6,7]. WOX5 also represses QC divisions, maintaining the quiescence of the QC by repressing CYCLIN D (CYCD) activity within the QC[8]. The auxin-induced PLTs form a clade of six TFs, and act as master regulators of root development, as multiple *plt* mutants fail to develop functional RAMs[5,9,10]. PLT1, 2, 3 and 4 are expressed mainly in and around the QC and form an instructive gradient, which is required for maintaining the balance of stem cell fate and differentiation. This PLT gradient is also necessary for separating auxin responses in the SCN and for the correct positioning of the QC and the expression of QC markers[5,9,10]. Genetically, WOX5 and PLT1 were shown to play an interconnected role in auxin-regulated CSC fate, whereas PLT1 and PLT3 were found to positively regulate WOX5 expression[11,12].

Although the implication of PLTs and WOX5 in controlling stem cell regulation and maintenance in the *Arabidopsis* RAM is well established and genetic evidence for cross regulation exists, the underlying molecular mechanisms remain largely elusive. Here, we show that the mutual regulation of expression, but also the ability of PLTs, especially PLT3, to recruit WOX5 to NBs in CSCs controls stem cell homeostasis in the *Arabidopsis* RAM. We propose a model in which the differential PLT/WOX5 complexes depending on subnuclear localisation regulate stem cell fate in the RAM, possibly by phase separation of PLT3 to NBs.

3. Results

WOX5 and PLTs are essential players in distal stem cell maintenance[5–7,9]. This, as well as their overlapping expression and protein localisation domains in the root SCN raised the question if

they could act together in distal stem cell regulation, where, in comparison to all the other PLTs, particularly PLT3 is highly expressed (Figure IV-1b)[9]. First, we tested if WOX5 influences *PLT3*-expression. Both a transcriptional and translational PLT3 fluorescent reporter line showed a reduced expression in the QC and CSC of a *wox5* mutant to around 60 % compared to the *Col-0* (*Col*) wild type roots (Figure IV-1b-g, Supplementary table IV-5). This extends the previously reported regulation of *PLT1* expression by WOX5[11] and shows that WOX5 positively regulates expression of several *PLTs*.

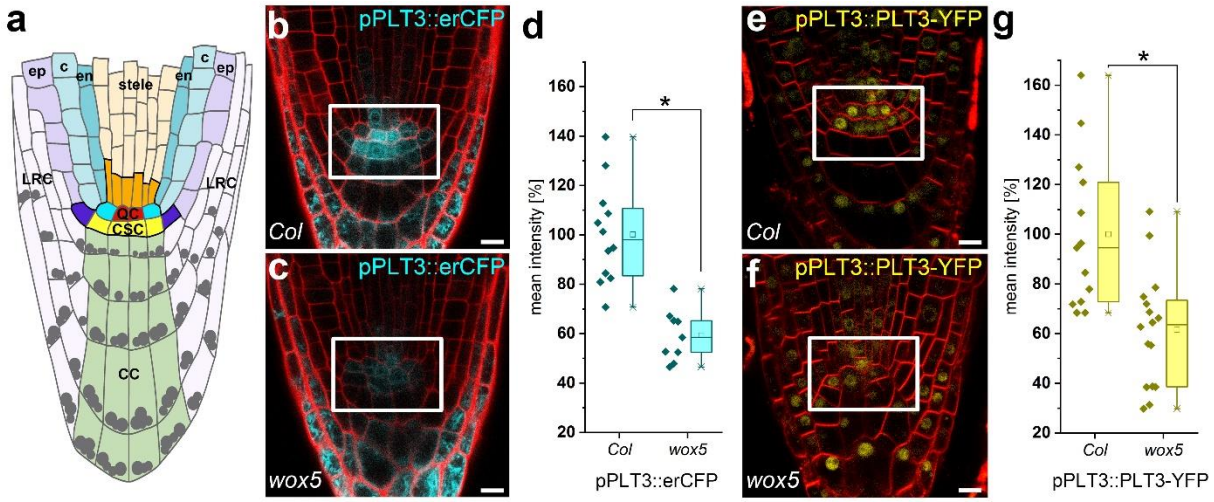

Figure IV-1: WOX5 positively regulates *PLT3* expression

a, Schematic representation of the *Arabidopsis* root meristem. The QC cells (red) maintain the surrounding stem cells (initials) outlined in black together building the root stem cell niche (SCN). The different cell types are colour-coded. QC = quiescent centre (red); CSC = columella stem cells (yellow); CC = columella cells (green); LRC = lateral root cap (light purple); ep = epidermis (dark purple); c = cortex (light blue); en = endodermis (dark blue); grey dots = starch granules. **b**,**c**, Representative images of pPLT3::erCFP (cyan) expressing and PI-stained (red) *Arabidopsis* roots in *Col* or *wox5* background, respectively. **d**, Mean fluorescence intensities of the pPLT3::erCFP roots summarized in box and scatter plots. The mean fluorescence intensity of the CFP signal in *Col* roots was set to 100 %. **e**,**f**, Representative images of pPLT3::PLT3-YFP (yellow) expressing and FM4-64-stained (red) *Arabidopsis* roots in *Col* or *wox5* background, respectively. **g**, Mean fluorescence intensities of the pPLT3::PLT3-YFP expressing roots summarized in box and scatter plots. The mean fluorescence intensity of the YFP signal in *Col* roots was set to 100 %. **d**,**g**, Box = 25-75 % of percentile, whisker = 1.5 interquartile range, – = median, □ = mean value, × = minimum/maximum. Asterisks indicate statistically significant differences as analysed by one-way ANOVA and post-hoc multiple comparisons using the Holm-Sidak test ($\alpha = 0.01$), number of analysed roots n = 9-16. **b**,**c**,**e**,**f**, Scale bars represent 10 µm. SCN = stem cell niche; PI = propidium iodide; YFP = yellow fluorescent protein; CFP = cyan fluorescent protein.

To test if *WOX5* expression also depends on PLTs, we used a transcriptional reporter, which expresses a nuclear-localised mVenus from the *WOX5* promoter. In agreement with previous reports, expression of *WOX5* in our transcriptional reporter line is confined to the QC and is only weakly expressed in the stele initials[6,7] (Figure IV-2a).

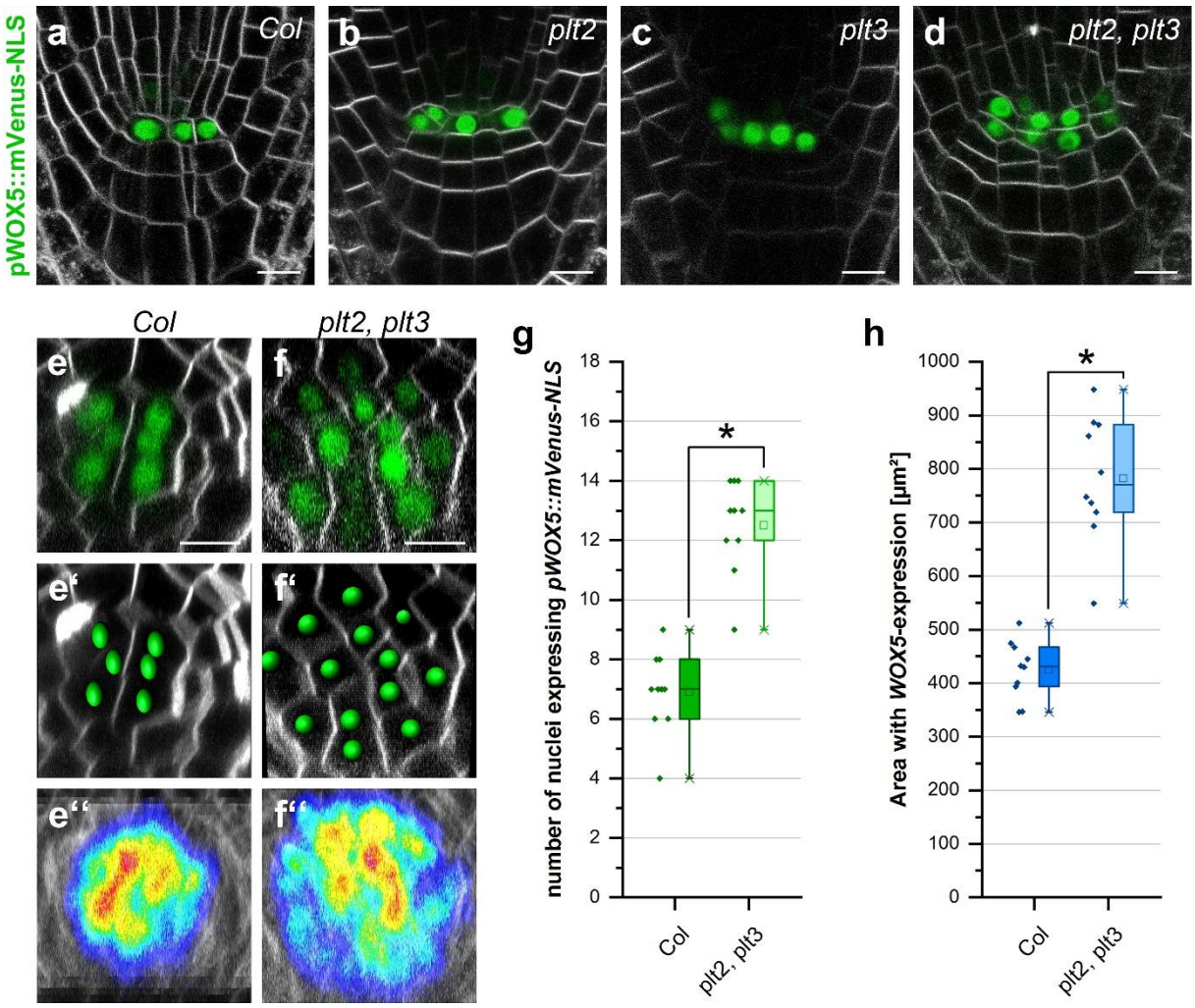

Figure IV-2: PLTs constrain the WOX5 expression domain

a-f, Representative FM4-64-stained *Arabidopsis* roots (grey) expressing pWOX5::mVenus-NLS (green) in *Col*, *plt2* and *plt3* single and *plt2, plt3* double mutant backgrounds in longitudinal (**a-d**), or transversal (**e-f**) optical sections. **e'**,**f'**, Analysis of (**e**) and (**f**) in Imaris in order to detect and count individual expressing nuclei. **e''**,**f''**, Overlay of 10 roots showing the area of detected fluorescence (high levels in red, low levels in blue) in *Col* and *plt2, plt3* double mutant roots. **g**, Number of nuclei expressing pWOX5::mVenus-NLS in *Col* and *plt2, plt3* double mutant roots summarized in box and scatter plots. **h**, Area of WOX5 expression in µm² in *Col* and *plt2, plt3* double mutant roots summarized in box and scatter plots. **g,h** Box = 25-75 % of percentile, whisker = 1.5 interquartile range, – = median, □ = mean value, × = minimum/maximum. Asterisks indicate statistically significant differences as analysed by one-way ANOVA and post-hoc multiple comparisons using the Holm-Sidak test ($\alpha = 0.01$, n = 10). Scale bars represent 10 µm; NLS = nuclear localisation signal.

In *plt2* and *plt3* single mutants, we observed additional mVenus-expressing cells in the QC region, which may derive from aberrant periclinal cell divisions in the QC (Figure IV-2b,c, Supplementary table IV-6). This effect is even stronger in the *plt2, plt3* double mutant roots, where extra cells are found in all observed roots and often even form an additional cell layer of *WOX5* expressing cells (Figure IV-2d). Previously, it was reported that the *Arabidopsis* wild type QC is composed of three to five cells with a low division rate[2,13–15]. We quantified the number of *WOX5* expressing cells and the area of *WOX5* expression per root by acquiring transverse optical sections through the roots. We observed four to nine *WOX5* expressing cells in the *Col* wild type (Figure IV-2e,g, Supplementary table IV-6), whereas we found nine to 14 *WOX5* expressing cells and a laterally expanded *WOX5* expression domain in the *plt2, plt3* double mutant (Figure IV-2f,g,h, Supplementary table IV-6). Taken together, our data show that WOX5 positively regulates *PLT3* expression, whereas PLT2 and PLT3 synergistically restrict *WOX5* to its defined expression domain in the QC, possibly by negative feedback regulation.

QC cells rarely divide as they provide a long-term reservoir to maintain the surrounding stem cells[13,16]. As WOX5 and PLTs control QC cell divisions and CSC maintenance[5–10], we asked if these two aspects are interdependent. Therefore, we analysed the cell division rates in the QC and the CSC phenotypes in wild type and mutant roots. To assess these two phenotypes and to probe for their interdependency, we had to measure the number of dividing QC cells and CSC layers within the same root simultaneously. Therefore, we established a novel staining method, named SCN staining, by combining the 5-ethynyl-2'-deoxyuridine (EdU) and modified pseudo Schiff base propidium iodide (mPS-PI) stainings to simultaneously visualise cell divisions, starch granule distribution and cell walls within the same root[13,17]. Applying this new staining combination, potential correlations between QC-divisions and CSC cell fates can be uncovered. The EdU-staining provides a useful method to analyse QC-divisions by staining nuclei that have gone through the S-phase, detecting cells directly before, during and after cell division[13]. However, cell layers and different cell types are hard to distinguish using only EdU staining due to the lack of cell wall staining. Therefore, we used the mPS-PI-method to stain cell walls and starch which is commonly used for CC and CSC cell fate characterisation[17–19]. CCs are differentiated, starch granule-containing cells in the distal part of the root and mediate gravity perception. They derive from the CSCs that form one or, directly after cell division, two cell layers distal to the QC. The CSCs lack big starch granules and can thereby easily be distinguished from the differentiated CCs by mPS-PI staining[17–19] (see Figure IV-3a,b,i).

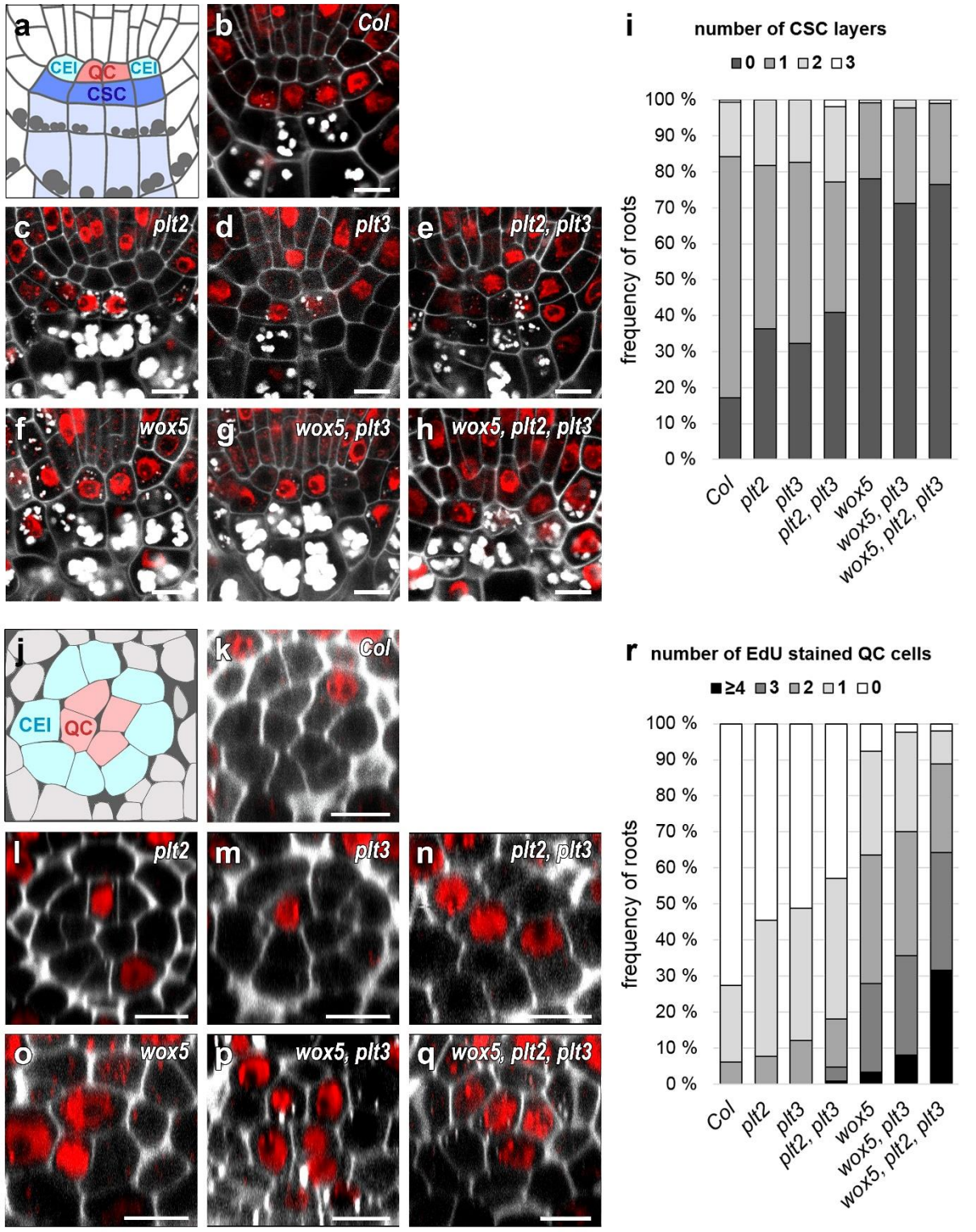

Figure IV-3: ***plt*** **and** ***wox5*** **mutants show more CSC differentiation and QC divisions**

a, Schematic representation of a longitudinal section of an *Arabidopsis* root SCN. QC cells are marked in red, CSCs are marked in dark blue, CCs in light blue and CEIs in turquoise. Combined mPS-PI (grey) and EdU (red) staining for 24 hours (SCN staining) in order to analyse the CSC (**a**-**i**) and QC division phenotype (**j**-**r**) within the same roots. **b**-**h**, Representative images of the SCN staining in *Col*, and the indicated single, double and triple mutant roots. **i**, Analyses of the SCN staining for CSC phenotypes. Frequencies of roots showing 0, 1, 2, or 3 CSC

layers are plotted as bar graphs. **j**, Schematic representation of a transversal section of an *Arabidopsis* root SCN. QC cells are marked in red, CEI initials are marked in turquoise. **r**, Analyses of the SCN staining for QC division phenotypes. Frequencies of roots showing 0, 1, 2, 3 or ≥4 dividing QC cells are plotted as bar graphs. Number of roots n = 77-146 from 2-5 independent experiments. QC = quiescent centre; CSC = columella stem cell; CEI = cortex endodermis initial; SCN = stem cell niche; mPS-PI = modified pseudo-Schiff propidium iodide; EdU = 5-ethynyl-2'-deoxyuridine; scale bars represent 5 µm (**b-h**) and 10 µm (**k-q**).

WOX5 is necessary for CSC maintenance as loss of WOX5 causes their differentiation[6]. In agreement with this, we found that the *wox5* mutants lack a starch-free cell layer in 78 % of analysed roots, indicating differentiation of the CSCs, compared to 17 % in *Col* (Figure IV-3a,b,f,i, Supplementary table IV-7). In the *plt2* and *plt3* single mutants, the frequency of roots lacking a CSC layer increases to above 30 % (36 % and 32 %, respectively), and in the *plt2, plt3* double mutant to 41 % (see Figure IV-3c,d,e,i, Supplementary table IV-7). Interestingly, the *wox5, plt3* double mutant as well as the *wox5, plt2, plt3* triple mutant show a frequency of differentiated CSCs comparable to the *wox5* single mutant (71 % and 77 %, respectively, Figure IV-3g,h,i, Supplementary table IV-7). This data suggests that PLTs and WOX5 may act together in the same pathway to maintain CSC homeostasis, as there is no additive effect observable in the multiple mutant roots. To analyse QC division phenotypes in detail, we quantified the number of EdU-stained cells in QC position in transversal optical sections. In *Col*, 27 % of the analysed roots show at least one cell division in the QC within 24 hours (Figure IV-3j,k,r, Supplementary table IV-7), which is consistent with already published frequencies[13]. This frequency almost doubles to 45-50 % in the *plt2* and *plt3* single mutants and is even higher in the *plt2, plt3* double mutant (57 %) (Figure IV-3l-n,r, Supplementary table IV-7). Additionally, the *plt*-double mutant roots often show disordered QC regions with a disruption of the circular arrangement of cells surrounding the QC (Figure IV-3n) which could be a result of uncontrolled divisions. In general, *wox5* mutants show a disordered SCN accompanied by a high overall QC cell division frequency of at least one dividing QC cell in 92 % of roots (Figure IV-3o,r) and on average more dividing QC cells per root (Supplementary table IV-7). The number of dividing QC cells per root increases further in the *wox5*, *plt3* double mutant and is even higher in the *wox5*, *plt2*, *plt3* triple mutant; here, in one third of the roots all QC cells undergo cell division (Figure IV-3p-r, Supplementary table IV-7). Taken together, this data suggests an additive effect of PLT2, PLT3 and WOX5 regarding the QC-division phenotype, in line with our hypothesis that WOX5 and PLTs act in parallel pathways to maintain the quiescence of the QC.

Additionally, we quantified roots showing at least one aberrant periclinal cell division in the QC in longitudinal optical sections (Supplementary figure IV-1). Whereas the occurrence of these aberrant periclinal divisions in *Col* wild type roots is very rare (3 %), it increases in the *plt*-single mutants to 21 % and in *wox5* and *wox5, plt3* mutants to around 40 %. We found the most severe phenotypes in the *plt2, plt3* double and *wox5, plt2, plt3* triple mutants with an occurrence of periclinal QC-cell divisions in 53 % of the observed roots, indicating a predominant regulatory role of PLTs in periclinal QC cell divisions (Supplementary figure IV-1b, Supplementary table IV-8).

To visualise correlations between QC division and CSC differentiation, we combined the acquired data in 2D-plots in which the frequencies of the two phenotypes are color-coded (Figure IV-4). This visualisation reveals a regular pattern for *Col* wild type roots, which peaks at one CSC-layer and no QC-divisions (Figure IV-4a). The pattern of the *plt* single mutants is more irregular with a shift to less CSC-layers (indicating more differentiation) and more EdU-stained QC cells (indicating more QC divisions) compared to the wild type *Col* roots (Figure IV-4b,c). The *plt2, plt3* double mutants have an additional maximum at a position showing no CSC layer and one divided QC cell, resulting in two phenotypic populations, one at a wild type-like position, the other showing a strong mutant phenotype (Figure IV-4d). The 2D-pattern for the *wox5* mutant shifts to less CSC-layers and more QC-divisions with a maximum at no CSC-layers and two QC-divisions (Figure IV-4e). The QC phenotype is more severe in the *wox5, plt3* double mutant towards more cell divisions and is even stronger in the *wox5, plt2, plt3* triple mutant which peaks at zero CSC layers and three QC-divisions (Figure IV-4f,g). In summary, our data suggests that higher CSC differentiation correlates with a higher division rate in the QC, possibly in order to replenish missing stem cells by increased QC divisions.

WOX5 and PLT3 are expressed and localise to overlapping domains in the SCN of the *Arabidopsis* root and based on our results regulate SCN maintenance together. To test for functionality of our reporter lines, we used the mVenus (mV) tagged WOX5 and PLT3 versions driven by their endogenous promoters for rescue experiments in the respective mutant phenotypes in *Arabidopsis.* We observed a full rescue of the *wox5* mutant expressing *pWOX5::WOX5-mV* and a partial rescue of the *plt3* mutant expressing *pPLT3::PLT3-mV* indicating that the labelling with mVenus did not or only very little influence WOX5 or PLT3 functionality (Supplementary figure IV-2, Supplementary table IV-9).

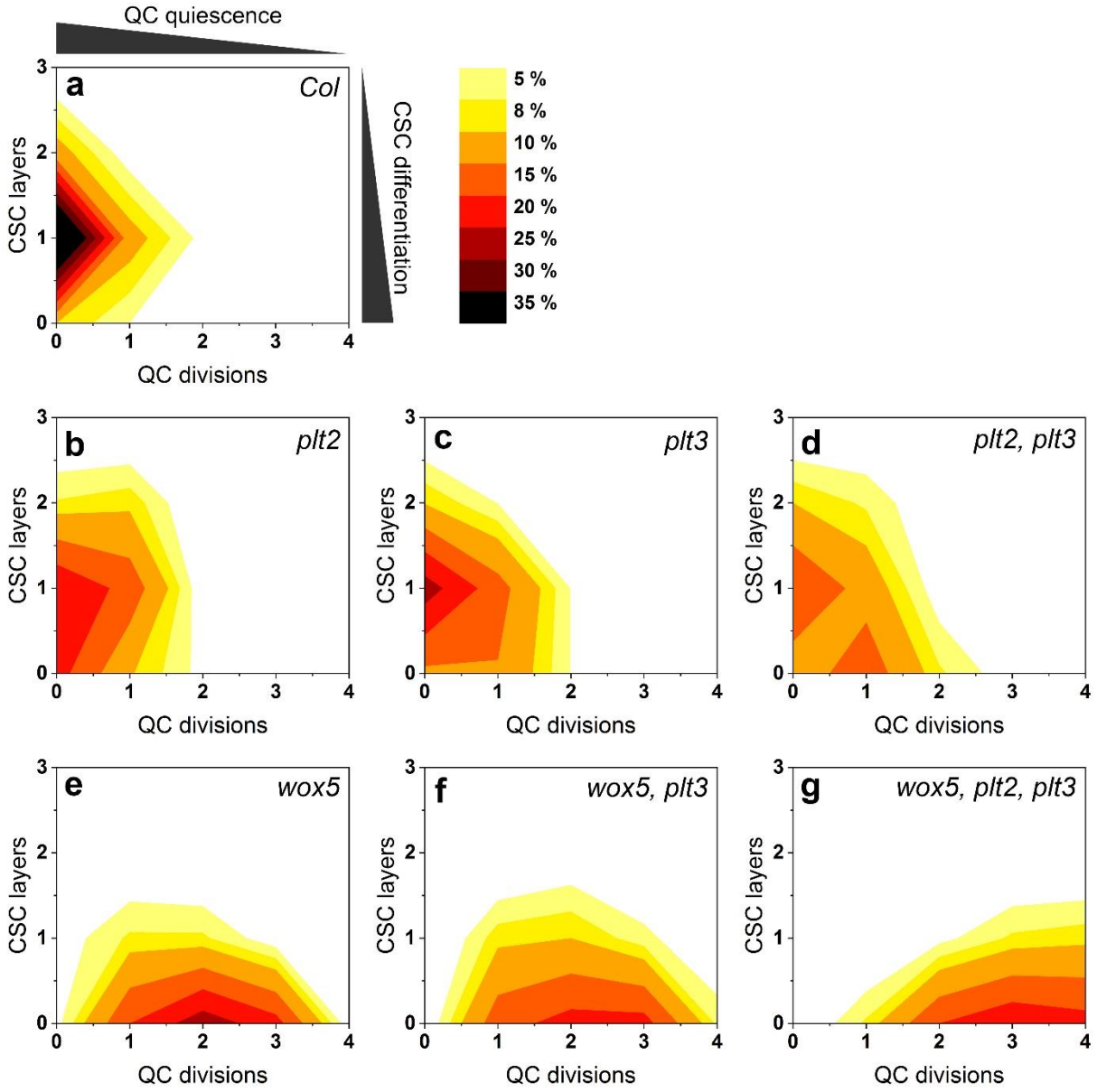

Figure IV-4: QC divisions correlate negatively with the number of CSC layers

The combined results of the SCN staining in Figure IV-3 are shown as 2D plots to visualise the correlation of the CSC layer number and QC divisions. Number of CSC layers are shown on the y axis and the QC divisions phenotype is shown on the x axis. The darker the colour, the more roots show the respective phenotype (see colour gradient top right indicating the frequencies). *Col* wild type roots mostly show one layer of CSCs and no EdU stained cells (no QC division) after 24 h EdU staining.

In the PLT3-mV reporter line, we observed PLT3 localisation in bright subnuclear structures, hereafter called nuclear bodies (NBs). Most frequently, we found PLT3 NBs in young, developing lateral root primordia (LRP) (Figure IV-5a, Supplementary movie IV-1) already at stages where PLT1 and PLT2 are not yet expressed[20]. Importantly, we occasionally observed PLT3 NBs in CSCs of established primary roots, but never in QC cells (Figure IV-5b-c').

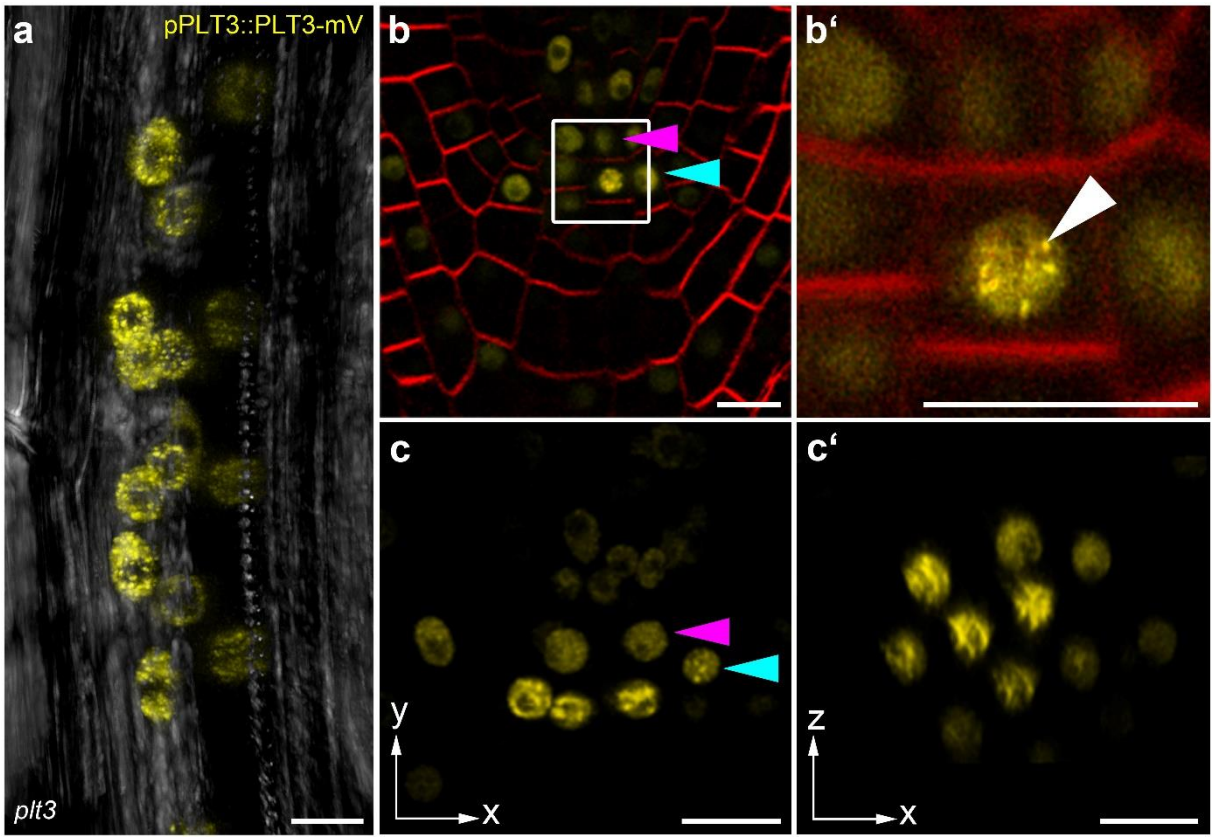

Figure IV-5: PLT3 localises to NBs in *Arabidopsis thaliana* LRPs and CSCs

a-c’, PLT3-mV expression driven by the PLT3 endogenous promoter in LRP (**a**) and primary root SCN (**b-c’**) in *plt3* mutant *Arabidopsis* roots. **a**, Representative image of PLT3-mV expression (yellow) in an LRP showing the subnuclear localisation to NBs. Transmitted light image in grey. **b,b’**, SCN of an PLT3-mV expressing FM4-64-stained (red) *Arabidopsis* primary root. The magnification of the CSC layer (**b’**) shows the subnuclear localisation of PLT3 to NBs in a CSC. White arrowhead points at a NB. **c,c’**, SCN of an PLT3-mV expressing *Arabidopsis* primary root. NBs are visible in the CSC layer in **c**, also in the transversal view of the CSC layer (**c’**). Arrowheads in **b** and **c** point at the QC (magenta) and CSC (cyan) positions. mV = mVenus; LRP = lateral root primordium; SCN = stem cell niche; NBs = nuclear bodies; CSC = columella stem cell. Scale bars represent 10 µm.

To further examine the PLT3 NBs in a context where no other PLTs are expressed, we used an β-estradiol-inducible system to control expression of PLT3 and WOX5 transiently in *Nicotiana benthamiana*[18]. Similar to our observations in *Arabidopsis*, we found that PLT3 mainly localises to NBs and to a lesser extend to the nucleoplasm (Figure IV-6b). In co-expression experiments in *N. benthamiana*, we found that PLT3 recruits WOX5 to the same NBs, whereas on its own WOX5 remains homogenously localised within the nucleoplasm (Figure IV-6g-g’’, Supplementary figure IV-4a).

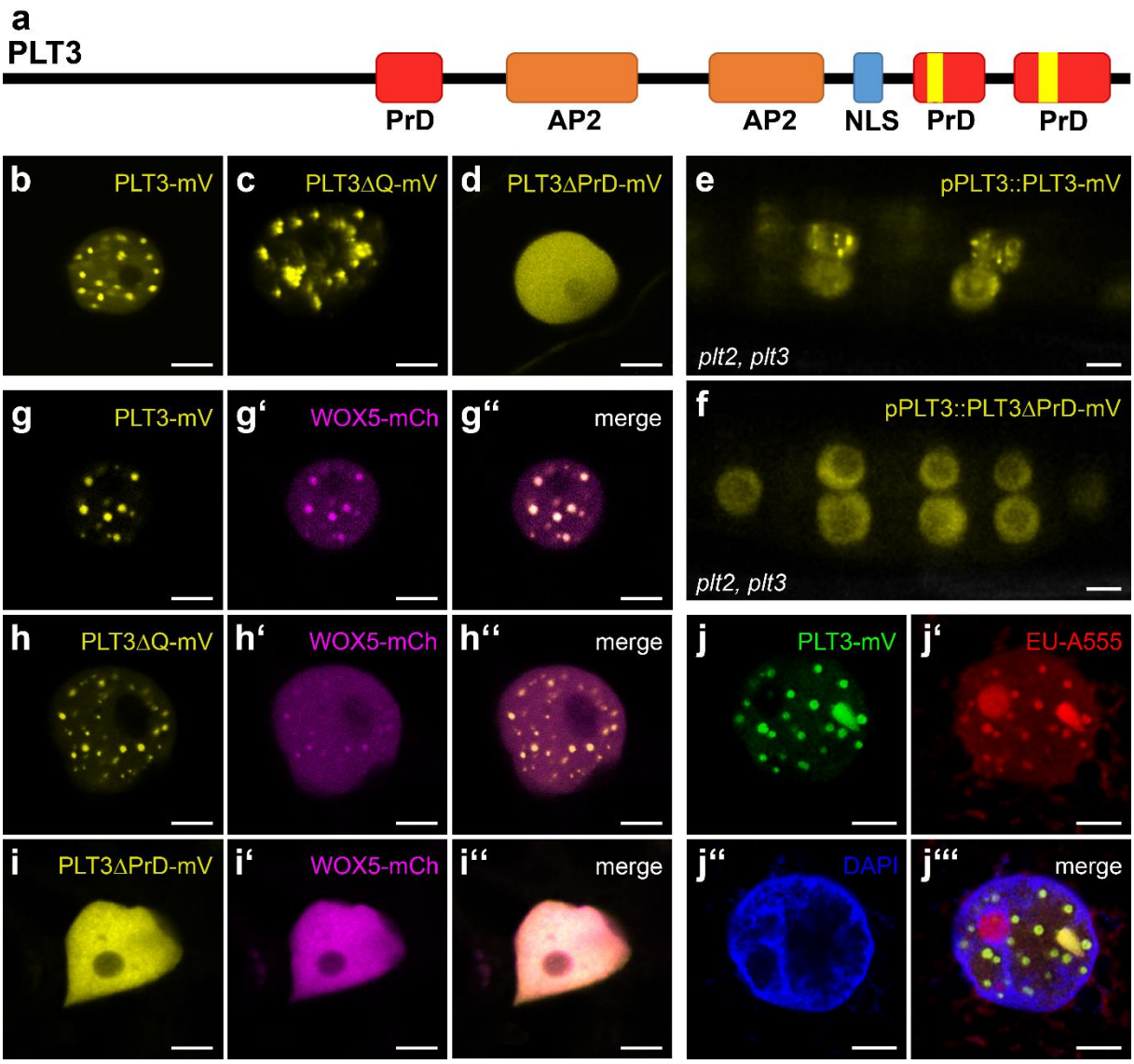

Figure IV-6: PLT3 PrDs influence its subnuclear localisation

a, Schematic representation of PLT3 protein domains. The areas in red are predicted prion-like domains (PrDs) and were deleted in PLT3ΔPrD-mV. The areas highlighted in yellow contain polyQ-stretches and were deleted in PLT3ΔQ-mV. **b-d**, Representative images of PLT3-mV (**b**), PLT3ΔQ-mV (**c**) and PLT3ΔPrD-mV (**d**) in transiently expressing *N. benthamiana* leaf epidermal cells. **e**,**f**, PLT3-mV (**e**) and PLT3ΔPrD-mV (**f**) expression driven by the PLT3 endogenous promoter in lateral root primordia of *plt2, plt3* double mutant *Arabidopsis* roots. **g-i’’**, Co-expression of PLT3-mV (**g**), PLT3ΔQ-mV (**h**) and PLT3ΔPrD-mV (**i**) with WOX5-mCh (**g’**,**h’**,**i’**) in transiently expressing *N. benthamiana* leaf epidermal cells. **j-j’’’**, Expression of PLT3-mV (**j**) in transiently expressing *N. benthamiana* leaf epidermal cells in combination with RNA staining with EU (18 h), visualised by click-reaction with Alexa Fluor® 555 (**j’**) and a DNA staining with DAPI (**j’’**). mV = mVenus; PrD = prion-like domain; AP2 = APETALA2 domain; NLS = nuclear localisation signal; EU = 5-ethynyl-2’-uridine. Scale bars represent 5 µm.

Next, we examined the domains possibly responsible for the localisation of PLT3 to NBs and found that the PLT3 amino acid (aa) sequence contains two glutamine (Q)-rich regions in the

C-terminal part of the protein (see Figure IV-6a). Proteins containing poly-Q stretches form aggregates or inclusions, a process often linked to pathological conditions in humans, such as Huntington's disease [21]. However, polyQ proteins also convey diverse cellular functions such as the promotion of nuclear assemblies (e.g. the transcription initiation complex), the formation of protein-protein complexes and the recruitment of other polyQ-containing proteins[22,23] as well as an enhancement in the transcriptional activation potential of TFs[22,24,25]. Interestingly, polyQs were also found to be enriched in TFs in plants[26]. Besides that, polyQ-containing proteins are proposed to act as key factors for the formation of RNA granules, which are ribonucleoprotein particles that mediate mRNA compartmentalisation[27]. Generally, the dynamic formation of subcellular structures could be necessary for a changing composition of the assemblies in dependence of their functional status[23]. The transition of these proteins between condensed and soluble forms requires high flexibility in their protein structure, which is provided by the flexible polyQ-stretches. Poly-Q domains are predominantly positioned at the surface of a protein supporting the idea of their involvement in protein-protein interactions[28].

Next, we tested, if the polyQ-stretches in PLT3 are responsible for the subnuclear localisation and the recruitment of WOX5 to NBs. To this end, we deleted the polyQ domains of PLT3 and expressed the resulting PLT3ΔQ fused to mVenus transiently in *N. benthamiana*. We found that the subnuclear localisation and the recruitment of WOX5 did not change compared to the full-length PLT3 (Figure IV-6b,c,h-h''). Therefore, we conclude that the polyQ domain in PLT3 is not, or at least not alone, responsible for the subnuclear localisation and translocation to NBs.

Apart from proteins with polyQ domains, many proteins that form concentration-dependent aggregates contain larger, intrinsically disordered regions (IDRs) with a low complexity similar to yeast prions[29]. Recently, the existence of more than 500 proteins with prion-like behaviour in *Arabidopsis* was reported[30] and the presence of prion-like domains (PrDs) in protein sequences are predictable with web-based tools[31]. Therefore, we analysed the PLT and WOX5 sequences using the PLAAC PrD prediction tool and found that PLT3 has three predicted PrDs in its aa sequence, two of them located at the C-terminus, containing the two polyQ-stretches (see Figure IV-6a, Supplementary figure IV-4). PLT1 and PLT2 also show two predicted PrDs, each, but no polyQ stretches within them. WOX5 does not show any predicted PrDs, nor any polyQ stretches (Supplementary figure IV-4). Just like polyQ-proteins, prions are responsible for some neurodegenerative diseases in mammals[32,33], but also their functional nature is becoming more eminent. The beneficial function of prions as a protein-based memory is highly discussed as their self-replicating conformations could act as molecular memories to transmit

heritable information[34,35]. Prion-like proteins in *Arabidopsis* were first discovered by analysing protein sequences of 31 different organisms, identifying Q- and N-rich regions in the proteins to be sufficient to cause protein aggregation[36]. In order to test the importance of the PrDs in PLT3, we replaced the first PrD by a 27 aa linker (AAGAAGGAGGGAAAAAGGAGAA AAAGA) and deleted the C-terminally located PrDs. The resulting PLT3-version (PLT3ΔPrD) was fused to the mVenus FP and expressed in *N. benthamiana* epidermal cells. We did not observe a localisation of PLT3ΔPrD-mVenus to NBs, but in contrast a homogenous distribution within the nucleus (Figure IV-6d). In addition, upon co-expression of PLT3ΔPrD-mVenus with WOX5-mCherry, we observed that WOX5 was no longer recruited to NBs (Figure IV-6i-i''). In line with this, we observed PLT3 NBs in developing *Arabidopsis* LRP expressing pPLT3::PLT3-mVenus, but no more NBs were found in a pPLT3::PLT3ΔPrD-mVenus expressing line (Figure IV-6e,f). Based on these observations, we conclude that the PrDs of PLT3 are responsible for the localisation to NBs and the recruitment of WOX5 to NBs.

Proteins containing polyQ-stretches or PrDs are often involved in RNA binding, RNA processing and/or RNA compartmentalisation[27,37–41]. To test if PLT3 is involved in these processes, we performed an RNA-staining in *N. benthamiana* epidermal cells transiently expressing PLT3-mVenus with 5-ethynyl-2'-uridine (EU) (see Figure IV-6j-j'''). EU is incorporated into RNA during transcription and we found that most of the stained RNA co-localises with the PLT3-mVenus NBs except for the EU-stained nucleolus (see Figure IV-6j-j'''). Based on these observations, we conclude that the PLT NBs act as important sites for the recruitment of RNA and other factors, including WOX5.

Because the WOX5 and PLT protein expression domains overlap in the SCN and PLT1, PLT2 and PLT3 contain PrDs, we asked whether PLTs and WOX5 interact *in vivo*, especially in light of the observed PrD-dependent recruitment of WOX5 to PLT3 NBs. Therefore, we used fluorescence lifetime imaging microscopy (FLIM) to measure Förster resonance energy transfer (FRET) to analyse the potential protein-protein interaction of WOX5 and PLTs *in vivo*. To perform FLIM, we inducibly co-expressed WOX5-mVenus as donor together with individual PLTs-mCherry as acceptors for FRET in *N. benthamiana* leaf epidermal cells. The fluorescence lifetime of the donor fluorophore mVenus fused to WOX5 alone is 3.03 ± 0.03 ns. A reduction of fluorescence lifetime is due to Förster resonance energy transfer (FRET) of the two fluorophores in very close proximity (≤ 10 nm) mediated by the interaction of the two observed proteins. When free mCherry is co-expressed as a negative control the WOX5-mVenus mean fluorescence lifetime is not significantly decreased (2.97 ± 0.07 ns) (Figure IV-7a,b,h, Supplementary table IV-10). When WOX5-mVenus is co-expressed with PLT1-mCherry the

fluorescence lifetime significantly decreases to 2.8 ± 0.12 ns, with PLT2-mCherry to 2.7 ± 0.13 ns and with PLT3-mCherry to 2.7 ± 0.17 ns, indicating FRET and hence protein-protein interactions (Figure IV-7c-e,h, Supplementary table IV-10).

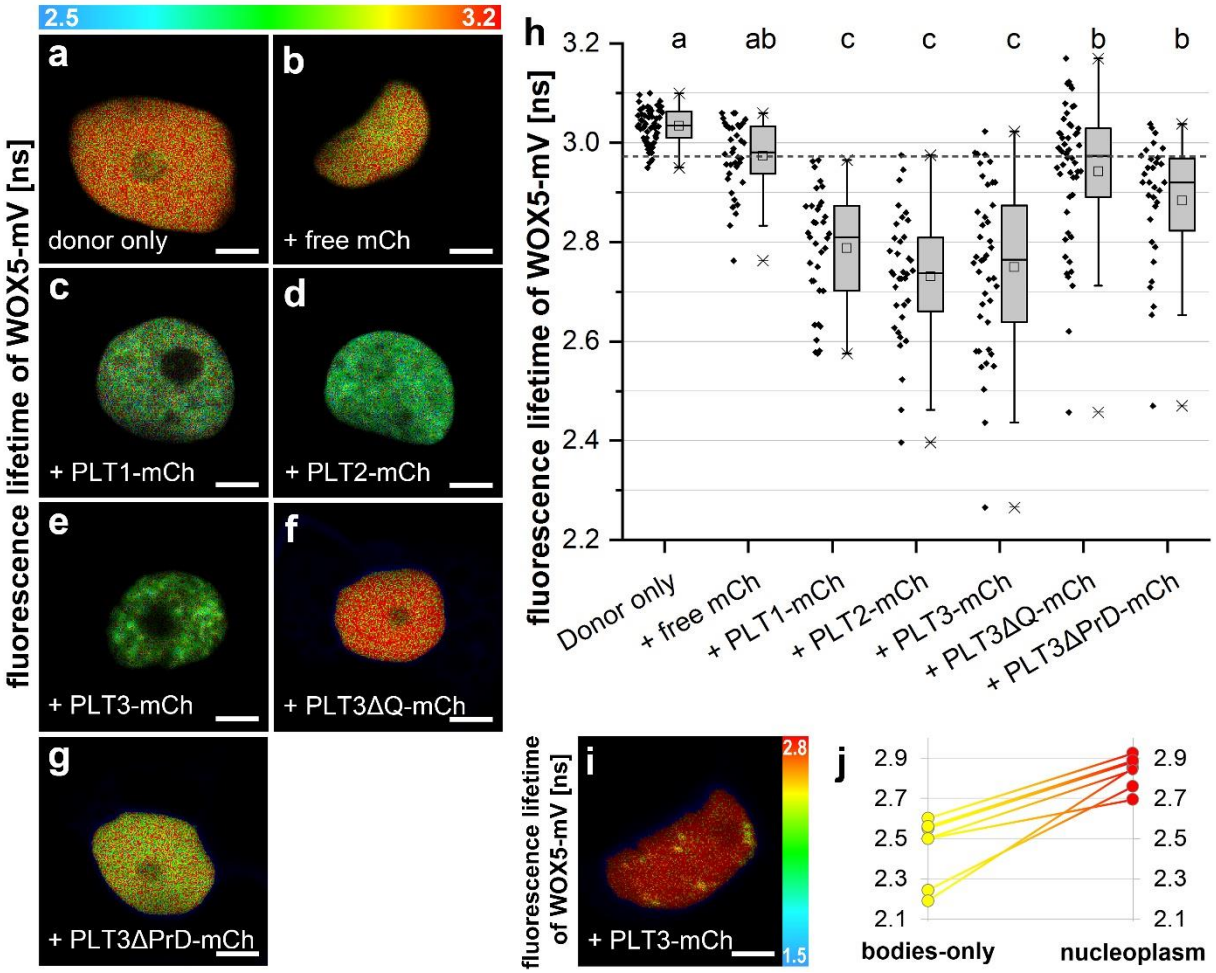

Figure IV-7: WOX5 can interact with PLTs

a-j, Fluorescence Lifetime Imaging (FLIM) results of transiently expressing *N. benthamiana* leaf epidermal cells. **a-g,i** FLIM images of WOX5-mVenus (donor only) plus the indicated acceptors after a pixel-wise mono-exponential fit of the mVenus fluorescence signal. The fluorescence lifetime of WOX5-mVenus in ns is color-coded. Low lifetimes (blue) due to FRET indicate strong interaction of the two proteins and high lifetimes (red) indicate weaker or no interaction. Scale bars represent 5 µm. **h**, Fluorescence lifetimes in ns are summarized in combined scatter and box plots. Statistical analysis of samples was carried out by one-way ANOVA and post-hoc multiple comparisons using the Holm-Sidak test. Samples with identical letters do not show significant differences ($\alpha = 0.01$; $n \geq 32$). Box = 25-75 % of percentile, whisker = 1.5 interquartile range, – = median, □ = mean value, × = minimum/maximum. **j**, Seven individual nuclei showing nuclear bodies during co-expression of WOX5-mV and PLT3-mCh were analysed for WOX5-mV lifetime in the nuclear bodies or nucleoplasm separately. mCh = mCherry; mV = mVenus.

The observed interaction of WOX5 with PLT1, PLT2 or PLT3 lead us to assume that they regulate SCN maintenance by the formation of complexes, either all together or in diverse compositions depending on the cell identity or their function. Interestingly, we observed a stronger lifetime decrease of WOX5-mVenus in the PLT3 NBs than in the nucleoplasm, indicating that the NBs function as main interaction sites of WOX5 with PLT3 (Figure IV-7i,j, Supplementary table IV-11).

To address this, we measured the interaction between WOX5 and PLT3 in *Arabidopsis* roots via FLIM experiments in a translational line expressing WOX5-mVenus and PLT3-mCherry under control of their respective endogenous promoters. This results in very low protein concentration in comparison to the inducible system used in *N. benthamiana*. Probably due to this, we could not observe NBs in established root meristems of our *Arabidopsis* FLIM line and we could not measure a relevant decrease in fluorescence lifetime in contrast to the above-described experiments in *N. benthamiana* (Supplementary figure IV-3, Supplementary table IV-12). In *Arabidopsis* seedlings, we only sometimes observed PLT3 NBs in the CSC layer of the root tip, but more frequently in young, developing LRP (Figure IV-5), whereas in *N. benthamiana* we observed NBs in almost all cells. Therefore, we argue that the formation of the NBs is concentration dependent. Indeed, in a transient *N. benthamiana* experiment, we could observe a correlation between the fluorescence intensity of nuclear PLT3-mVenus and the size and number of the NBs (Supplementary figure IV-5). NBs start to form after a certain intensity-threshold (Supplementary figure IV-5f) and get lower in number and bigger in volume with increasing intensity (Supplementary figure IV-5a-g). A similar concentration-dependency has been described previously for proteins that undergo phase separation, in particular liquid-liquid phase separation (LLPS)[42]. This mechanism separates membrane-free microdomains from the surrounding liquid and could represent the underlying NB-forming process of PLT3. In case of PLT3, this is possibly PrD-dependent as we observed a deficiency in NB formation of the PrD-deletion variant (Figure IV-6d).

Moreover, we asked if the PrDs and poly-Q domains in PLT3 are necessary for protein-protein interaction with WOX5. To test this, we performed FLIM experiments with mCherry-tagged full-length PLT3, PLT3ΔQ and PLT3ΔPrD as acceptors and WOX5-mVenus as donor in *N. benthamiana*. Here, we observed that co-expression of the PLT3 deletion variants did not lead to a significantly reduced fluorescence lifetime and therefore no protein-protein interaction takes place in comparison to the full-length version (Figure IV-7e-h). This implies that PrDs

containing the polyQ domains in PLT3 are necessary for the NB localisation, but also, notably, for protein complex-formation with WOX5.

In summary, our findings show that QC quiescence and CSC maintenance are mediated by mutual transcriptional regulation of PLTs and WOX5 as well as their direct protein-protein interaction and subnuclear partitioning to NBs due to PrDs.

4. Discussion

Based on our results we propose that the regulation of QC quiescence and CSC maintenance is mediated by mutual transcriptional regulation of PLTs and WOX5 by a negative feedback loop. Here, a high *PLT* expression in the QC-region is promoted by WOX5, which again confines WOX5 to a defined and restricted number of QC cells. In line with this, loss of PLTs lead to an expanded expression domain of *WOX5* and a decreased QC quiescence as more QC divisions occur. These observations are in agreement with previous findings, although just a minor role for PLT1 and PLT2 in confining *WOX5* expression was previously reported, as 17 % of *plt1, plt2* double mutant roots showed *WOX5* expression expanding into endodermal and columella stem cells[6]. As *WOX5* expression is normally limited to the QC, the question arises if, in absence of PLTs, either the *WOX5* expression domain expands to regions surrounding the QC or the QC region itself expands and therefore also the expression domain of *WOX5*. Interestingly, previous analyses show that the expression of several QC markers is missing or highly reduced in *plt* mutants, suggesting that they fail to maintain an intact QC[5]. The higher frequency of cell divisions in the QC region of *wox5* mutants can be explained by the reduced expression of *PLTs,* which consequently negatively impacts QC quiescence but also by a PLT-independent pathway where WOX5 itself may have a positive function on the QC quiescence. Previous findings suggest that WOX5 maintains QC quiescence through the repression of CYCD activity[8]. In light of our observation that PLT2, PLT3 and WOX5 show additive effects regarding the QC division phenotype, we propose a model in which WOX5 and PLTs could act in parallel pathways to maintain QC quiescence. The observed correlation between reduced QC quiescence and higher CSC differentiation could be a measure to replenish missing stem cells by QC divisions. This possible explanation is in agreement with the proposed function of the QC to serve as long-term stem cell reservoir, especially in case of stress or damage[16]. Supporting this, previous studies showed, even though uncorrelated, that loss of PLTs lead to CSC differentiation and also an increase in ectopic cell divisions in the QC[5,11]. For CSC

homeostasis, PLTs and WOX5 may act together in the same pathway, possibly by complex formation, as there is no observable additive effect in the multiple mutant roots which is in agreement with previous findings[11]. The ability of WOX5 to directly interact with PLT1, PLT2 and PLT3 implies that they control CSC maintenance by complex-formation, either all together or in varying homo- or heteromeric compositions depending on cell identity or function. In transient *N. benthamiana* experiments, PLT3 forms NBs and recruits WOX5 into them. The stronger lifetime decrease in NBs compared to the nucleoplasm measured by FLIM implies that the NBs function as sites for protein-protein interaction of WOX5 with PLT3. We could observe PLT3 NBs in cells of the CSC layer of some *Arabidopsis* primary root tips, but never in the QC region. On the other hand, PLT3 NBs were found more frequently in several cells of developing LRPs. LRPs are in a younger and less-determined stage than the primary root and the observed subnuclear localisation to NBs could represent a marker for the occurring determination and future cell differentiation. This goes along with the observed localisation of PLT3 to NBs in the CSCs in some of the primary roots. The PLT3 NBs could represent compartments for the recruitment of and interaction with WOX5 and possibly other factors involved in CSC fate determination and maintenance. Furthermore, we found that PLT3, in contrast to PLT1 and PLT2, has polyQ containing PrDs in its aa sequence that are necessary for the localisation to NBs and for complex-formation with WOX5. Proteins containing polyQ-stretches or PrDs are often involved in RNA binding, RNA processing and/or RNA compartmentalisation[27,37–41] and indeed, the PLT3 NBs co-localise with RNA. Just as PLT3, FLOWERING CONTROL LOCUS A (FCA) is a PrD-containing protein[30] that localises to subnuclear structures[41]. The FCA bodies separate from the cytosol by LLPS to provide compartments for RNA 3'-end processing factors[41]. Similarly, PLT3 NBs could represent compartments for the recruitment of interacting factors and RNA for further processing, sequestration or transportation. As PLT3 is a TF, the co-localising RNA could also represent newly transcribed RNA at the transcription sites where PLT3 binds to DNA, e.g. the WOX5 promoter region[12]. The possible liquid-like nature of the PLT3 NBs will be an interesting subject for further studies investigating its putative phase separation properties.

To summarize our results in a model, we propose that the regulation of QC quiescence and CSC maintenance are not only mediated by the mutual transcriptional regulation of PLT and WOX5, but also, importantly, by building protein complexes that are differentially localised within distinct nuclei in the SCN (see Figure IV-8). The observed subnuclear localisation of PLT3 to NBs could represent a marker for the determination to future cell differentiation in the CSC layer.

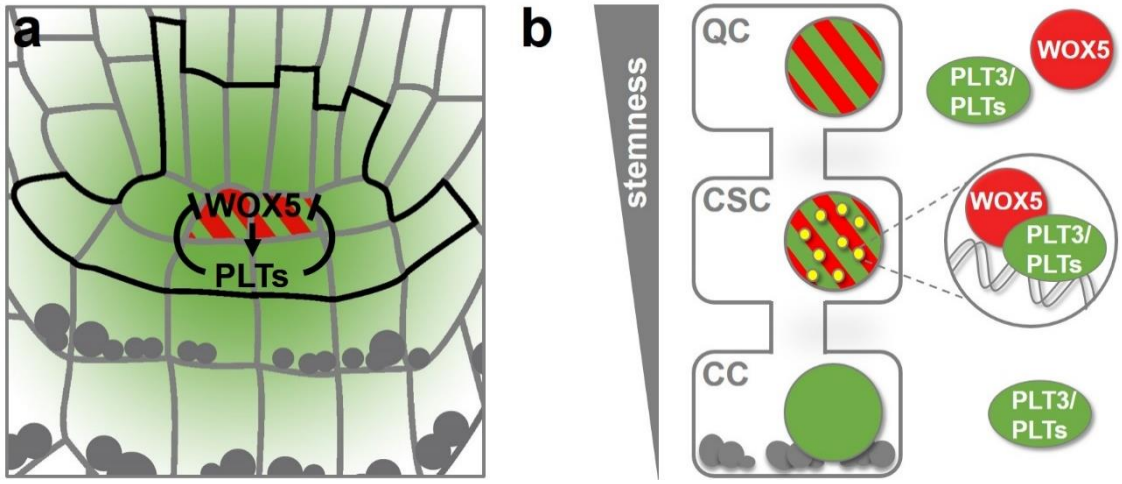

Figure IV-8: Model of PLT and WOX5 transcriptional regulation, interaction and subnuclear localisation during distal root stem cell maintenance

a, Transcriptional regulation of *WOX5* (red) and *PLT* (green) expression by negative feedback regulation in the *Arabidopsis* RAM. *WOX5* is expressed in the QC and promotes *PLT* expression, whereas *PLT* expression is restricting the *WOX5* expression domain to the QC position. **b**, Both WOX5 (red) and PLT3 (green) are present homogenously within the nuclei of the QC cells. WOX5 can move to the CSCs and is recruited there by PLT3 to NBs (yellow), where interaction takes place. This maintains the stem cell character of the CSCs but already leads to a determination to subsequent CC fate. Grey dots represent starch granules.

Furthermore, the PrD and polyQ domains in PLT3 may act as an initial starting point to compartmentalise and partition WOX5 that has moved from the QC towards the CSC layer into RNA-containing NBs, possibly by concentration-dependent LLPS process. The observed sites could represent transcriptionally active sites for the regulation of target genes involved in CSC fate determination. The dynamic compartmentalisation to subcellular or subnuclear microdomains of proteins with intrinsically disordered, PrD and/or polyQ domains was shown to have severe effects, e.g. in human pathological disorders (e.g. Huntington's disease). In *Arabidopsis,* it could present a fast and reversible concentration-dependent regulatory mechanism[29], e.g. in case of PLT3 and WOX5 to determine CSC cell fate. It remains to be determined if LLPS is the underlying mechanism of the observed subnuclear compartmentalisation and if also other processes in determination of cell fates and stemness in *Arabidopsis* are regulated by this mechanism.

5. Methods

5.1 Cloning

pWOX5::mVenus-NLS, pWOX5::WOX5-mVenus, pPLT3::PLT3-mVenus, pPLT3::PLT3-mCherry, pPLT3::PLT3ΔPrD-mVenus and β-estradiol inducible PLT3ΔPrD-mVenus were created by using the GreenGate cloning method [43]. The internal *BsaI* restriction sites in the WOX5 promoter and WOX5 CDS were removed by PCR amplification of the sequences upstream and downstream of the *BsaI* sites with primer pairs whereof one primer has an altered nucleotide sequence at this site (Supplementary table IV-1), followed by an overlap extension PCR to reconnect the gene fragments. The sequences upstream of the ATG start codon of WOX5 (4654 bp) and PLT3 (4494 bp) were used as promoter regions and were amplified by PCR and primers to add flanking *BsaI* restriction sites and matching overlaps for the GreenGate cloning system. Afterwards they were cloned into the GreenGate entry vector pGGA000 via *BsaI* restriction and ligation. The GreenGate promoter module carrying the β-estradiol inducible cassette was provided by [44]. The CDS of WOX5, PLT3 and PLT3ΔPrD as well as the FPs mVenus and mCherry were amplified by PCR using adequate primer pairs to add flanking *BsaI* restriction sites and matching overlaps for cloning into the GreenGate entry vectors pGGC000 (for CDS) and pGGD000 (for FPs) via *BsaI* restriction and ligation. The C-tag module carrying the FP Cerulean (pBLAD002) was a kind gift from Dr. Andrea Bleckmann, University of Regensburg. All created entry vectors were confirmed by sequencing. The expression cassettes were created with a GreenGate reaction using pGGZ001 as destination vector. The correct assembly of the modules was controlled by sequencing. All module combinations used to construct the expression vectors can be found in Supplementary table IV-3.

All other inducible constructs for *N. benthamiana* expression (free mCherry, WOX5-mVenus, PLT1-mVenus, PLT2-mVenus, PLT3-mVenus, PLT3ΔQ-mVenus) were created by Gateway cloning (Invitrogen™, Thermo Fisher Scientific Inc.). The CDS of WOX5, PLT1, PLT2, PLT3 and PLT3ΔQ were amplified and cloned into pENTR/D-TOPO®. The Entry-vectors were confirmed by sequencing. The destination vector carrying the mVenus (pRD04) is based on pMDC7[45] which contains a β-estradiol inducible system for expression *in planta*. The mVenus was introduced via restriction/ligation C-terminally to the Gateway cloning site. The destination vector carrying the mCherry (pABindmCherry) was described before [46]. The expression vectors

were created by LR-reaction of destination and entry vectors. Gateway expression vectors were verified by test digestion.

For the creation of the domain-deletion variants of PLT3 (PLT3ΔQ and PLT3ΔPrD), the CDS parts upstream and downstream of the desired sequence deletions were amplified with PCR and afterwards reconnected with overlap-PCR. The 27 aa linker (AAGAAGGAGGGAAAAAG GAGAAAAAGA) to replace the first PrD in PLT3ΔPrD was also introduced by overlap-PCR. All primer used for cloning can be found in Supplementary table IV-1.

5.2 plant work

All *Arabidopsis* lines used in this study were in the Columbia (*Col-0*) background. The single mutants *wox5-1* and *plt3-1* have been described before[9] (Supplementary table IV-4). The *plt2* (SALK_128164) and *wox5-1* (SALK038262) single mutants were provided by the *Arabidopsis* Biological Resource Center (ABRC, USA). The homozygous double and triple mutants were created by crossings (Supplementary table IV-4) and homozygous F3 genotypes were confirmed by PCR with appropriate primer pairs (Supplementary table IV-2). The transgenic lines were created by floral dip as described before[47] except for the published, transgenic *Col-0* lines with pPLT3::erCFP and pPLT3::PLT3-YFP[9] constructs. They were crossed into the *wox5-1* mutant background. Homozygous lines were confirmed by genotyping and hygromycin selection. All plants for crossing, floral dips, genotyping and seed amplification were grown on soil in phytochambers under long day (16 h light/ 8 h dark) conditions at 21 °C. For microscopy *Arabidopsis* seeds were fume-sterilised (50 ml 13 % sodiumhypochlorite (v/v) + 1 ml hydrochloric acid), imbedded in 0.2 % (w/v) agarose, stratified at 4 °C for 2 days and plated on GM agar plates (1/2 strength Murashige Skoog medium including Gamborg B5 vitamins, 1.2 % (w/v) plant agar, 1 % (w/v) sucrose, supplemented with 0.05 % (w/v) MES hydrate). *Arabidopsis* seedlings were grown for 5 days under continuous light at 21 °C and directly imaged afterwards.

5.3 Cell wall and plasma membrane staining

For root imaging, the cell walls in *Arabidopsis* seedlings were stained by incubation in aqueous solutions of either 10 µM propidium iodide (PI) or 2.5 µM FM4-64 dye (Invitrogen™, Thermo Fisher Scientific Inc.). The staining solution was used as mounting medium for microscopy.

5.4 *N. benthamiana* infiltration

For transient gene expression in *N. benthamiana*, the *Agrobacterium* strain GV3101::pMP50 was used as vector, carrying plasmids with the desired constructs and additionally either the

helper plasmid p19 as silencing suppressor or the helper plasmid pSOUP that harbours a replicase needed for GreenGate vectors. Cultures were grown over night in 5 ml dYT-medium at 28 °C on a shaker. The cultures were centrifuged for 10 min at 3345 g, the pellet was resuspended in infiltration medium (5 % (w/v) sucrose, 0.01 % (v/v) Silwet, 0.01 % (w/v) MgSO4, 0.01 % (w/v) glucose, 450 µM acetosyringone) to an optical density OD_{600} of 0.4 and cultures were incubated for one hour at 4 °C. The infiltration was done either with one single or with a combination of two different *Agrobacteria* cultures for co-expression of two constructs. A syringe without needle was used for the infiltration on the adaxial side of the leaves of well-watered *N. benthamiana* plants. For the expression of GreenGate constructs, an *Agrobacterium* strain carrying the p19 plasmid was co-infiltrated. The expression was induced 2-5 days after infiltration by applying an aqueous β-estradiol solution (20 µM β-estradiol, 0.1 % (v/v) Tween®-20) to the adaxial leaf surface. Imaging or FLIM experiments were done 3 to 16 hours after induction, depending on the expression level.

5.5 SCN staining

Arabidopsis seedlings were grown under continuous light for 5 days on GM agar plates without sucrose and then transferred on fresh plates containing additionally 10 µM EdU to continue growing for 24 hours. Afterwards we performed an mPS-PI staining like described before[17]. Preliminary to the clearing step, the EdU-staining was performed. The permeabilization of the cells and the subsequent staining of EdU-containing DNA with Alexa Fluor® 488 was done as described in the Click-it® EdU Imaging Kits from Invitrogen™ (Thermo Fisher Scientific Inc.) with adapted incubation times for *Arabidopsis* seedlings (permeabilization for 1-2 h and click-reaction for 1 h). The click-reaction cocktail was prepared freshly with self-made solutions (Tris buffer with 50 mM Tris and 150 mM NaCl at pH 7.2-7.5; 4 mM CuSO4; 1.5 µM Alexa Fluor® 488 picolyl azide; 50 mM ascorbic acid). The Alexa Fluor® 488 picolyl azide (Thermo Fisher Scientific Inc.) was added from a 500 µM stock in DMSO. The ascorbic acid was added last from a freshly prepared aqueous 500 mM stock solution. After staining was done, the clearing step with chloralhydrate was performed like described before[17].

Images were acquired with a ZEISS LSM880 confocal microscope. z-stacks through the QC-region were recorded to obtain transversal views. In order to calculate the CSC phenotype, the number of CSC layers was counted in xy-images of each root. The QC-division phenotype is the number of EdU-Alexa Fluor® 488-stained cells in the QC, which was counted in the cross-sectional images up to a maximal number of 4 stained QC cells. The phenotype frequencies of CSC differentiation and QC divisions (Figure IV-3) where visualised in bar graphs with Excel

(Microsoft Office 365 ProPlus, Microsoft Corporation). In order to correlate the two investigated phenotypes, we combined the CSC data and the QC-division data in 2D-plots. The combined QC/CSC-phenotype of every root was entered in a matrix with QC-divisions on the x- and CSC layers on the y-axis. 2D plots were created with Origin 2018b (OriginLab Corporation).

5.6 RNA staining

The RNA-staining in *N. benthamiana* epidermal cells was done on *N. benthamiana* leaves harbouring a construct for a β-estradiol inducible *PLT3-mVenus* expression. 5-ethynyl-2'-uridine (EU) was infiltrated in *N. benthamiana* leaves the day before staining. The expression of *PLT3-mVenus* was induced the next morning, 3 hours before fixation of the plant tissue. For fixation and permeabilization of cells, pieces of the leaves were cut and treated with 4 % (w/v) paraformaldehyde and 0.5 % (v/v) TritonX-100 in PBS under vacuum for 1 h. The click-reaction of EU with Alexa Fluor® 555 picolyl azide was performed similarly to the EdU-Alexa Fluor® 488-staining described for the SCN staining in this article. A DAPI- counterstaining was carried out afterwards by incubating the leaf pieces in 0.1 µg/ml DAPI for 30 min. PBS was used as mounting medium for imaging.

5.7 Microscopy

Imaging of *Arabidopsis* roots and *Nicotiana* leaves was carried out with a ZEISS LSM780 or LSM880. Excitation and detection of fluorescent emission of fluorescent dyes was done as follows: DAPI was exited at 405 nm and emission was detected at 408-486 nm, Cerulean was excited at 458 nm and emission was detected at 460-510 nm; CFP was excited at 458 nm and emission was detected at 463-547 nm. mVenus was excited at 514 nm and emission was detected at 517-560 nm, or for co-expression with red dyes excited at 488 nm and detected at 500-560 nm. YFP was excited at 514 nm and emission was detected at 518-548 nm. Alexa Fluor® 488 was excited at 488 nm and emission was detected at 490-560 nm. Alexa Fluor® 555 was excited at 561 nm and emission was detected at 565-640 nm. PI was excited at 561 nm and emission was detected at 590-710 nm. FM4-64 was excited at 514 nm or 561 nm and emission was detected at 670-760 nm. mCherry was excited at 561 nm and emission was detected at 590-640 nm. Imaging of more than one fluorophore was done in sequential mode to avoid cross talk. The movie of pPLT3::PLT3-mVenus in a lateral root primordium was acquired with a MuViSPIM (Luxendo, Bruker) light sheet microscope and a 40x/0.8 Nikon objective with a 1.5x tube lens on the detection axis to provide a 60x magnification.

5.8 Image deconvolution

The microscope images in Figure IV-5a, c-c' and Supplementary figure IV-5a-c were deconvolved with Huygens 16.10.0p3 64b (Scientific Volume Imaging B.V.).

5.9 Analyses of expression patterns and levels in *Arabidopsis*

For the comparison of relative fluorescence levels in the SCN of 5 day old *Arabidopsis* seedlings expressing either transcriptionally FP tagged *PLT3* (*pPLT3::erCFP*) or translationally FP tagged *PLT3* (*pPLT3::PLT3-YFP*) driven by the endogenous PLT3 promoter in either the *Col* wild type or the *wox5-1* mutant, images of 9-16 roots per genotype were acquired with constant settings per FP. A ZEISS LSM880 confocal microscope was used. The mean fluorescence levels were measured with Fiji[48] in equally sized rectangular ROIs including the QC and CSC positions in the SCN. The thereby generated values were normalised to the *Col* mean fluorescence intensity and visualised in box and scatter plots created with Origin 2018b (OriginLab Corporation).

Images of the root tips of 5 day old *Arabidopsis* seedlings expressing *mVenus-NLS* driven by the endogenous WOX5 promoter in *Col* and *plt2* or *plt3-1* single mutants and the *plt2, plt3* double mutant were acquired. Additionally, z-stacks through the QC region of the roots were recorded to get a transversal view of the QC. The visualisation and counting of nuclei with *WOX5* expression (Figure IV-2) was done with Imaris (version 9.1.2, Bitplane, Oxford Instruments plc). Box and scatter plots showing the number of expressing nuclei were created with Origin 2018b (OriginLab Corporation). For the heat-map images, 10 acquired images were overlaid with Fiji[48] and the resulting fluorescence distribution was displayed with a 16-colors lookup table. To calculate the area of lateral *WOX5* expression in the QC region, a freehand-ROI surrounding the expressing cells was created in every image with Fiji[48]. The ROI-areas were visualised in box and scatter plots created with Origin 2018b (OriginLab Corporation).

5.10 FLIM measurements

FLIM was performed either in *N. benthamiana* leaf epidermal cells expressing the desired gene combinations or in roots of 6-10 dag old *Arabidopsis* seedlings expressing *WOX5-mVenus* and *PLT3-mCherry* with their endogenous promoters. The FLIM measurements in *Arabidopsis* were performed in LRPs due to higher fluorescence levels and less movement during measurements compared to the RAM. mVenus-tagged proteins were always used as donor and mCherry-tagged proteins as acceptor for FRET. A ZEISS LSM 780 was used for the experiments equipped with a single-photon counting device (Hydra Harp 400, PicoQuant GmbH). The mVenus donor was excited with a linearly polarized diode laser (LDH-D-C-485)

at 485 nm and a pulse frequency of 32 MHz. The excitation power was adjusted to 0.1-0.5 µW at the objective (C-Apochromat 40x/1.2 W Corr M27, ZEISS) for experiments in *N. benthamiana* and 1.5-2 µW for experiments in *Arabidopsis*. The higher laser power in *Arabidopsis* was needed due to lower fluorescence levels. τ-SPAD single photon counting modules with 2 channel detection units (PicoQuant GmbH) and a bandpass filter (534/30) were used to detect parallel and perpendicular polarized emission of the mVenus fluorescence. Images were acquired with a frame size of 256x256 pixel, a pixel dwell time of 12.6 µs and a zoom factor of 8. 40 to 60 frames were recorded in the *N. benthamiana* experiments, 80 frames in the experiments performed in *Arabidopsis*.

Fluorescent lifetimes were obtained by further analyses of the acquired data with SymPhoTime64 (PicoQuant GmbH). The instrument response function (IRF) of the microscope hardware is needed for fluorescence lifetime calculation to correct the system-specific internal time lag between laser pulse and data acquisition. The IRF was recorded preliminary to each experiment by time-correlated single photon counting (TCSPC) of an aqueous solution of erythrosine B in saturated potassium iodide. For data analysis of *N. benthamiana* experiments, an intensity threshold of 100-200 photons per pixel was applied to remove background fluorescence and a mono-exponential fit was used. Due to low fluorescence intensities in *Arabidopsis* experiments, no threshold was applied to obtain the maximal possible photon number. In this case, a two-exponential fit was used to separate the mVenus fluorescence signal from the background fluorescence created by the plant tissue. This results in two lifetimes whereof one matches with the mVenus fluorescence lifetime of about 3 ns and the other representing the very short background lifetime of less than 0.4 ns. All data was obtained in at least two independent experiments. For visualisation of the lifetimes, box and scatter plots were created with Origin 2018b (OriginLab Corporation). Lifetime images of representative measurements were created with a pixel wise FLIM-fit in SymPhoTime64 (PicoQuant GmbH). The line graph showing the lifetime difference between the bodies and the nucleoplasm of WOX5-mVenus co-expressed with PLT3-mCherry was created using Excel (Microsoft Office 365 ProPlus, Microsoft Corporation).

5.11 Correlation of PLT3-NBs and PLT3-mVenus fluorescence intensity

Z-stacks of nuclei in *N. benthamiana* epidermal cells that transiently express *PLT3-mVenus* were acquired with constant settings on the ZEISS LSM880. The obtained 3D-images were deconvolved with Huygens 16.10.0p3 64b (Scientific Volume Imaging B.V.) and subsequently

analysed with Imaris (version 9.1.2, Bitplane, Oxford Instruments plc). Scatter plots were created with Origin 2018b (OriginLab Corporation).

5.12 Prediction of protein domains

The PrDs in the WOX5, PLT1, PLT2 and PLT3 aa sequences were predicted with the PLAAC application[31]. The nuclear localisation signals (NLSs) of WOX5 and the studied PLT proteins were predicted with cNLS Mapper[49] for WOX5 and PLT3 and SeqNLS[50] for PLT1 and PLT2.

5.13 Figure assembly

All figures in this study were assembled using Adobe Photoshop CS5 (Adobe Inc.).

6. References

1. van den Berg, C., Willemsen, V., Henriks, G., Weisbeek, P. & Scheres, B. Short-range control of cell differentiation in the Arabidopsis root meristem. *Nature* **390,** 287–289; 10.1038/36856 (1997).
2. Dolan, L. *et al.* Cellular organisation of the Arabidopsis thaliana root. *Development* **119,** 71–84 (1993).
3. Benfey, P. N. & Scheres, B. Root development. *Curr Biol* **10,** PR813-R815; 10.1016/s0960-9822(00)00814-9 (2000).
4. Drisch, R. C. & Stahl, Y. Function and regulation of transcription factors involved in root apical meristem and stem cell maintenance. *Front Plant Sci* **6,** 505; 10.3389/fpls.2015.00505 (2015).
5. Aida, M. *et al.* The PLETHORA genes mediate patterning of the Arabidopsis root stem cell niche. *Cell* **119,** 109–120; 10.1016/j.cell.2004.09.018 (2004).
6. Sarkar, A. K. *et al.* Conserved factors regulate signalling in Arabidopsis thaliana shoot and root stem cell organizers. *Nature* **446,** 811–814; 10.1038/nature05703 (2007).
7. Pi, L. *et al.* Organizer-Derived WOX5 Signal Maintains Root Columella Stem Cells through Chromatin-Mediated Repression of CDF4 Expression. *Dev Cell* **33,** 576–588; 10.1016/j.devcel.2015.04.024 (2015).
8. Forzani, C. *et al.* WOX5 suppresses CYCLIN D activity to establish quiescence at the center of the root stem cell niche. *Curr Biol* **24,** 1939–1944; 10.1016/j.cub.2014.07.019 (2014).
9. Galinha, C. *et al.* PLETHORA proteins as dose-dependent master regulators of Arabidopsis root development. *Nature* **449,** 1053–1057; 10.1038/nature06206 (2007).
10. Mähönen, A. P. *et al.* PLETHORA gradient formation mechanism separates auxin responses. *Nature* **515,** 125–129; 10.1038/nature13663 (2014).
11. Ding, Z. & Friml, J. Auxin regulates distal stem cell differentiation in Arabidopsis roots. *PNAS* **107,** 12046–12051; 10.1073/pnas.1000672107 (2010).
12. Shimotohno, A., Heidstra, R., Blilou, I. & Scheres, B. Root stem cell niche organizer specification by molecular convergence of PLETHORA and SCARECROW transcription factor modules. *Genes Dev* **32,** 1085–1100; 10.1101/gad.314096.118 (2018).
13. Cruz-Ramírez, A. *et al.* A SCARECROW-RETINOBLASTOMA protein network controls protective quiescence in the Arabidopsis root stem cell organizer. *PLoS Biol* **11,** e1001724; 10.1371/journal.pbio.1001724 (2013).
14. Kidner, C., Sundaresan, V., Roberts, K. & Dolan, L. Clonal analysis of the Arabidopsis root confirms that position, not lineage, determines cell fate. *Planta* **211,** 191–199; 10.1007/s004250000284 (2000).
15. González-García, M.-P. *et al.* Brassinosteroids control meristem size by promoting cell cycle progression in Arabidopsis roots. *Development* **138,** 849–859; 10.1242/dev.057331 (2011).
16. Vilarrasa-Blasi, J. *et al.* Regulation of plant stem cell quiescence by a brassinosteroid signaling module. *Dev Cell* **30,** 36–47; 10.1016/j.devcel.2014.05.020 (2014).

17. Truernit, E. *et al.* High-resolution whole-mount imaging of three-dimensional tissue organization and gene expression enables the study of Phloem development and structure in Arabidopsis. *Plant Cell* **20,** 1494–1503; 10.1105/tpc.107.056069 (2008).

18. Stahl, Y. *et al.* Moderation of Arabidopsis root stemness by CLAVATA1 and ARABIDOPSIS CRINKLY4 receptor kinase complexes. *Current Biology* **23,** 362–371; 10.1016/j.cub.2013.01.045 (2013).

19. Stahl, Y., Wink, R. H., Ingram, G. C. & Simon, R. A Signaling Module Controlling the Stem Cell Niche in Arabidopsis Root Meristems. *Current Biology* **19,** 909–914; 10.1016/j.cub.2009.03.060 (2009).

20. Du, Y. & Scheres, B. PLETHORA transcription factors orchestrate de novo organ patterning during Arabidopsis lateral root outgrowth. *PNAS* **114,** 11709–11714; 10.1073/pnas.1714410114 (2017).

21. Scarafone, N. *et al.* Amyloid-like fibril formation by polyQ proteins: a critical balance between the polyQ length and the constraints imposed by the host protein. *PloS one* **7,** e31253; 10.1371/journal.pone.0031253 (2012).

22. Atanesyan, L., Günther, V., Dichtl, B., Georgiev, O. & Schaffner, W. Polyglutamine tracts as modulators of transcriptional activation from yeast to mammals. *Biol Chem* **393,** 63–70; 10.1515/BC-2011-252 (2012).

23. Mikecz, A. von. PolyQ fibrillation in the cell nucleus: who's bad? *Trends Cell Biol* **19,** 685–691; 10.1016/j.tcb.2009.09.001 (2009).

24. Schwechheimer, C., Smith, C. & Bevan, M. W. The activities of acidic and glutamine-rich transcriptional activation domains in plant cells: design of modular transcription factors for high-level expression. *Plant Mol Biol* **36,** 195–204; 10.1023/a:1005990321918 (1998).

25. Gerber, H. *et al.* Transcriptional activation modulated by homopolymeric glutamine and proline stretches. *Science* **263,** 808–811; 10.1126/science.8303297 (1994).

26. Kottenhagen, N., Gramzow, L., Horn, F., Pohl, M. & Theißen, G. Polyglutamine and Polyalanine Tracts Are Enriched in Transcription Factors of Plants. *German conference on Bioinformatics*; 10.4230/OASICS.GCB.2012.93 (2012).

27. Castilla-Llorente, V. & Ramos, A. PolyQ-mediated regulation of mRNA granules assembly. *Biochem Soc Trans* **42,** 1246–1250; 10.1042/BST20140099 (2014).

28. Totzeck, F., Andrade-Navarro, M. A. & Mier, P. The Protein Structure Context of PolyQ Regions. *PloS one* **12,** e0170801; 10.1371/journal.pone.0170801 (2017).

29. Cuevas-Velazquez, C. L. & Dinneny, J. R. Organization out of disorder: liquid-liquid phase separation in plants. *Curr Opin Plant Biol* **45,** 68–74; 10.1016/j.pbi.2018.05.005 (2018).

30. Chakrabortee, S. *et al.* Luminidependens (LD) is an Arabidopsis protein with prion behavior. *PNAS* **113,** 6065–6070; 10.1073/pnas.1604478113 (2016).

31. Lancaster, A. K., Nutter-Upham, A., Lindquist, S. & King, O. D. PLAAC: a web and command-line application to identify proteins with prion-like amino acid composition. *Bioinformatics* **30,** 2501–2502; 10.1093/bioinformatics/btu310 (2014).

32. Aguzzi, A., Nuvolone, M. & Zhu, C. The immunobiology of prion diseases. *Nat. Rev. Immunol.* **13,** 888–902; 10.1038/nri3553 (2013).

33. Kim, H. J. *et al.* Mutations in prion-like domains in hnRNPA2B1 and hnRNPA1 cause multisystem proteinopathy and ALS. *Nature* **495,** 467–473; 10.1038/nature11922 (2013).

34. Shorter, J. & Lindquist, S. Prions as adaptive conduits of memory and inheritance. *Nature Reviews Genetics* **6,** 435–450; 10.1038/nrg1616 (2005).

35. Bailey, C. H., Kandel, E. R. & Si, K. The persistence of long-term memory: a molecular approach to self-sustaining changes in learning-induced synaptic growth. *Neuron* **44,** 49–57; 10.1016/j.neuron.2004.09.017 (2004).

36. Michelitsch, M. D. & Weissman, J. S. A census of glutamine/asparagine-rich regions: implications for their conserved function and the prediction of novel prions. *PNAS* **97,** 11910–11915; 10.1073/pnas.97.22.11910 (2000).

37. Alberti, S., Halfmann, R., King, O., Kapila, A. & Lindquist, S. A systematic survey identifies prions and illuminates sequence features of prionogenic proteins. *Cell* **137,** 146–158; 10.1016/j.cell.2009.02.044 (2009).

38. Schomburg, F. M., Patton, D. A., Meinke, D. W. & Amasino, R. M. FPA, a gene involved in floral induction in Arabidopsis, encodes a protein containing RNA-recognition motifs. *Plant Cell* **13,** 1427–1436; 10.1105/TPC.010017 (2001).

39. Macknight, R. *et al.* FCA, a Gene Controlling Flowering Time in Arabidopsis, Encodes a Protein Containing RNA-Binding Domains. *Cell* **89,** 737–745; 10.1016/S0092-8674(00)80256-1 (1997).

40. Sonmez, C. *et al.* RNA 3' processing functions of Arabidopsis FCA and FPA limit intergenic transcription. *PNAS* **108,** 8508–8513; 10.1073/pnas.1105334108 (2011).

41. Fang, X. *et al.* Arabidopsis FLL2 promotes liquid-liquid phase separation of polyadenylation complexes. *Nature* **569,** 265–269; 10.1038/s41586-019-1165-8 (2019).

42. McSwiggen, D. T., Mir, M., Darzacq, X. & Tjian, R. Evaluating phase separation in live cells: diagnosis, caveats, and functional consequences. *Genes Dev* **33,** 1619–1634; 10.1101/gad.331520.119 (2019).

43. Lampropoulos, A. *et al.* GreenGate - A Novel, Versatile, and Efficient Cloning System for Plant Transgenesis. *PloS one* **8,** e83043; 10.1371/journal.pone.0083043 (2013).

44. Denninger, P. *et al.* Distinct RopGEFs Successively Drive Polarization and Outgrowth of Root Hairs. *Curr. Biol.* **29,** 1854-1865.e5; 10.1016/j.cub.2019.04.059 (2019).

45. Curtis, M. D. & Grossniklaus, U. A gateway cloning vector set for high-throughput functional analysis of genes in planta. *Plant Physiol.* **133,** 462–469; 10.1104/pp.103.027979 (2003).

46. Bleckmann, A., Weidtkamp-Peters, S., Seidel, C. A. M. & Simon, R. Stem cell signaling in Arabidopsis requires CRN to localize CLV2 to the plasma membrane. *Plant Physiol.* **152,** 166–176; 10.1104/pp.109.149930 (2010).

47. Zhang, X., Henriques, R., Lin, S.-S., Niu, Q.-W. & Chua, N.-H. Agrobacterium-mediated transformation of Arabidopsis thaliana using the floral dip method. *Nat. Protoc.* **1,** 641–646; 10.1038/nprot.2006.97 (2006).

48. Schindelin, J. *et al.* Fiji: an open-source platform for biological-image analysis. *Nat. Methods* **9,** 676–682; 10.1038/nmeth.2019 (2012).

49. Kosugi, S., Hasebe, M., Tomita, M. & Yanagawa, H. Systematic identification of cell cycle-dependent yeast nucleocytoplasmic shuttling proteins by prediction of composite motifs. *PNAS* **106,** 10171–10176; 10.1073/pnas.0900604106 (2009).

50. Lin, J.-R. & Hu, J. SeqNLS: nuclear localization signal prediction based on frequent pattern mining and linear motif scoring. *PloS one* **8,** e76864; 10.1371/journal.pone.0076864 (2013).

7. Supplementary information

7.1 Supplementary figures

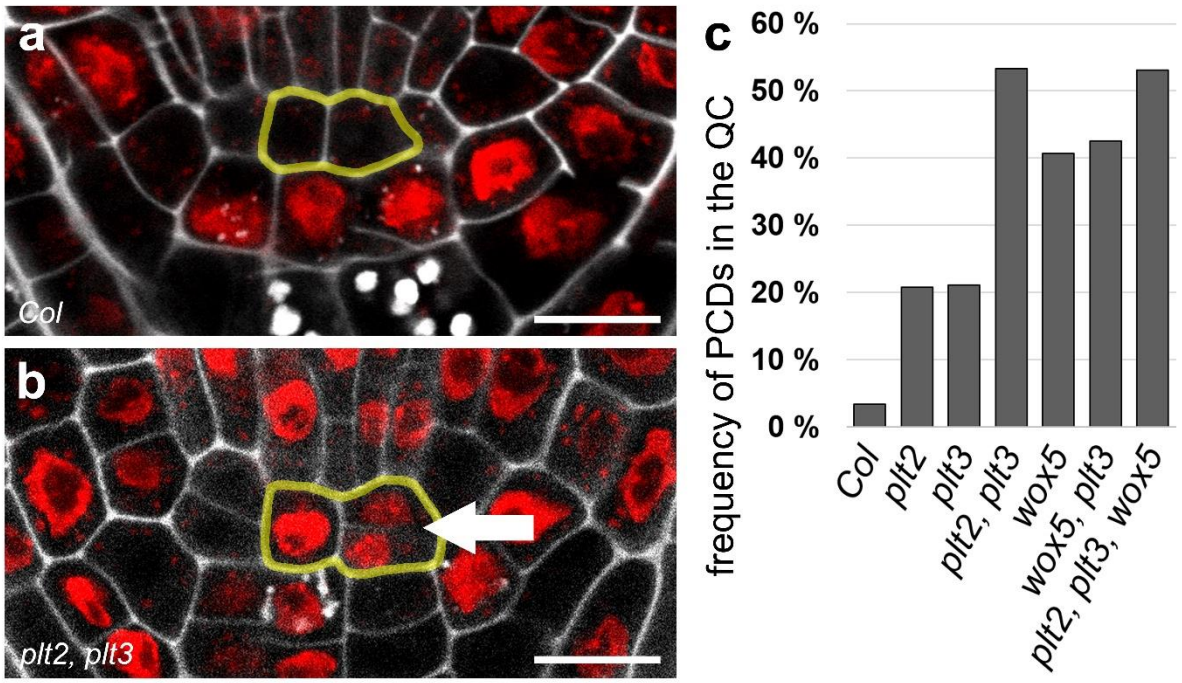

Supplementary figure IV-1: *plt* and *wox5* mutants show more periclinal cell divisions in the QC

a, Representative figure of an *Arabidopsis* wildtype (*Col*) root SCN staining. **b**, Representative figure of an *Arabidopsis plt2, plt3* double mutant root SCN staining showing a periclinal cell division (PCD) in the QC (arrow). QC cells in (**a**) and (**b**) are outlined in yellow. Scale bars represent 10 µm. **c**, Analysis of the PCD phenotype. The frequency of roots (in percent) showing at least one PCD in the QC is plotted as a bar graph. Number of analysed roots n = 77-146. PCD = periclinal cell division.

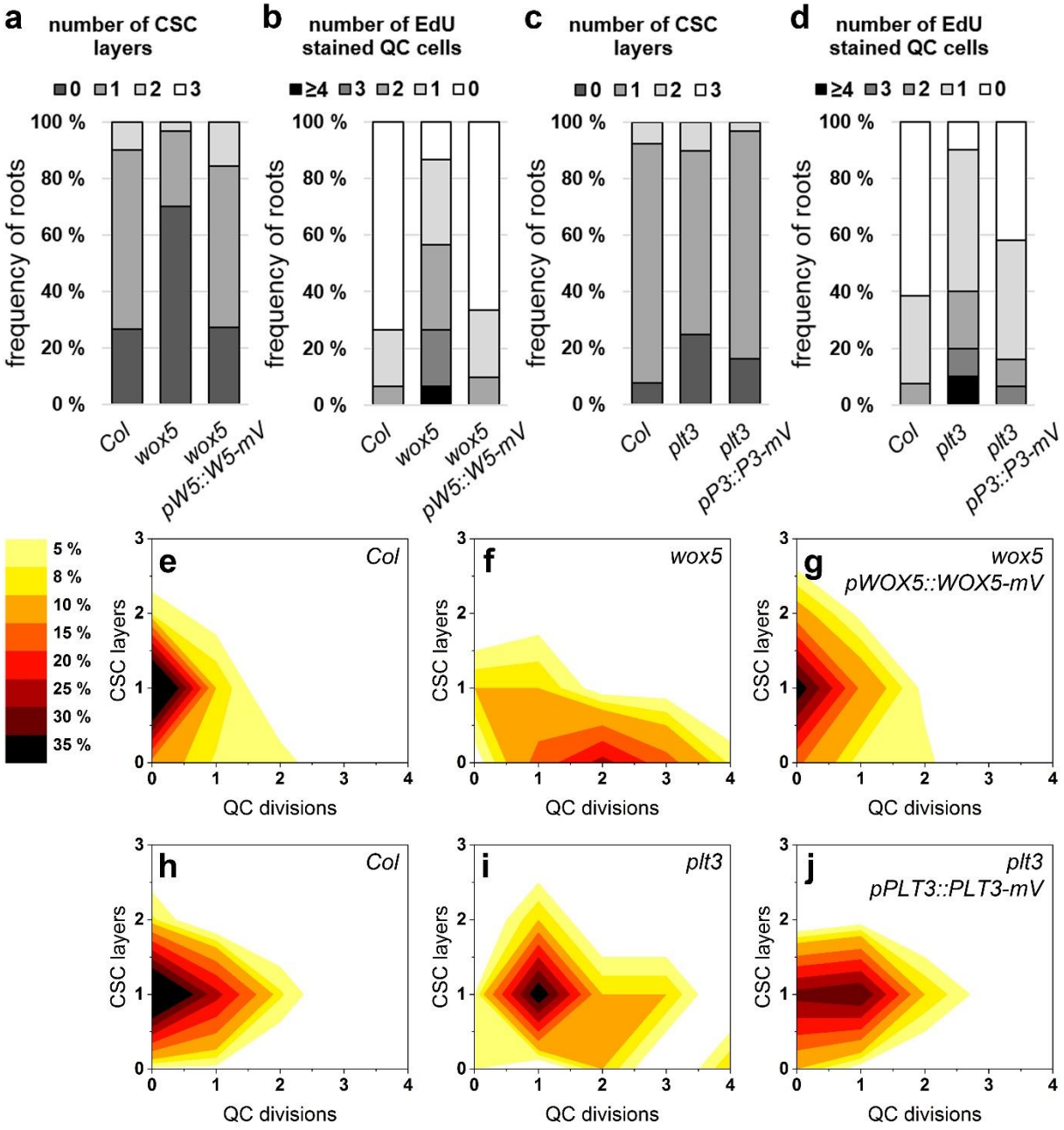

Supplementary figure IV-2: Expression of *WOX5-mVenus* and *PLT3-mVenus* rescues the respective mutant phenotypes

SCN staining was performed for two separate rescue experiments in *Arabidopsis thaliana* seedlings with *Col* background, *wox5* or *plt3* mutant background and in seedlings expressing *WOX5-mV* or *PLT3-mV* driven by their endogenous promoters in the respective mutant backgrounds. **a-d**, Analyses of the SCN staining for CSC (**a,c**) or QC division (**b,d**) phenotypes. The frequencies of roots showing 0-3 CSC layers or 0-4 dividing QC cells are plotted as bar graphs. **e-j**, The combined results of the SCN staining are shown as 2D plots. Number of CSC layers are shown on the y axis and the QC division phenotype is shown on the x axis. The darker the colour, the more roots show the respective phenotype (see colour gradient on the left indicating the frequencies). Number of analysed roots n = 26-51. EdU = 5-ethynyl-2´-deoxyuridine; CSC = columella stem cell; QC = quiescent centre; W5 = WOX5; P3 = PLT3.

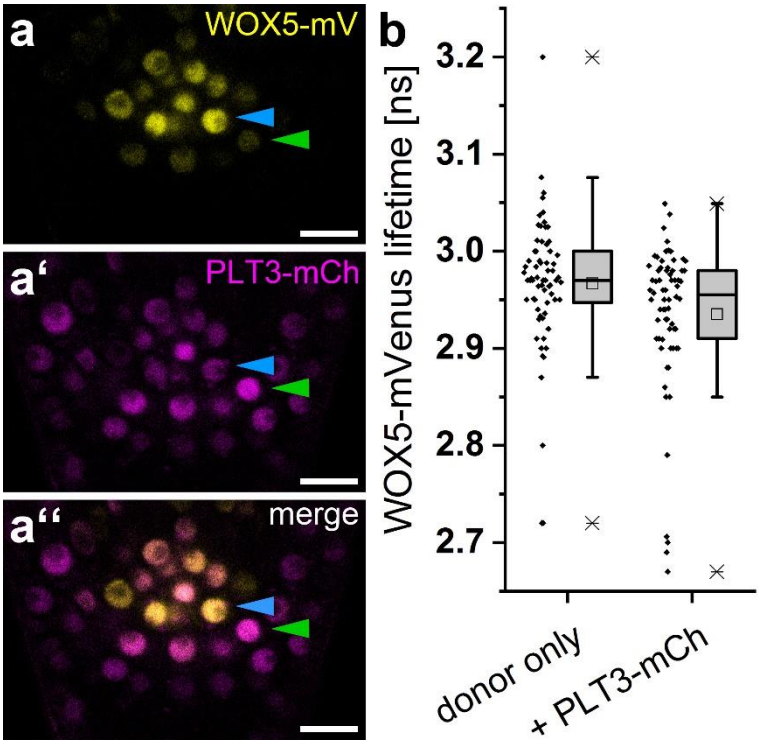

Supplementary figure IV-3: WOX5 does not interact with PLT3 in established *Arabidopsis* root meristems
a-a', Representative image of the SCN in a lateral root of an *Arabidopsis* reporter line expressing *WOX5-mV* (**a**) and *PLT3-mCh* (**a'**) driven by their respective endogenous promoters. The TFs localise to overlapping domains (**a''**). Blue arrowheads mark QC cells, green arrowheads mark CSCs. **b**, Fluorescence Lifetime Imaging (FLIM) results of experiments performed in *Arabidopsis thaliana* expressing either only *WOX5-mV* (donor-only) or both *WOX5-mV* and *PLT3-mCh* driven by their respective endogenous promoters. Donor fluorescence lifetimes in ns are summarized in combined scatter and box plots. Number of measurements n = 67-68. Box = 25-75 % of percentile, whisker = 1.5 interquartile range, – = median, □ = mean value, × = minimum/maximum. mV = mVenus; mCh = mCherry; SCN = stem cell niche.

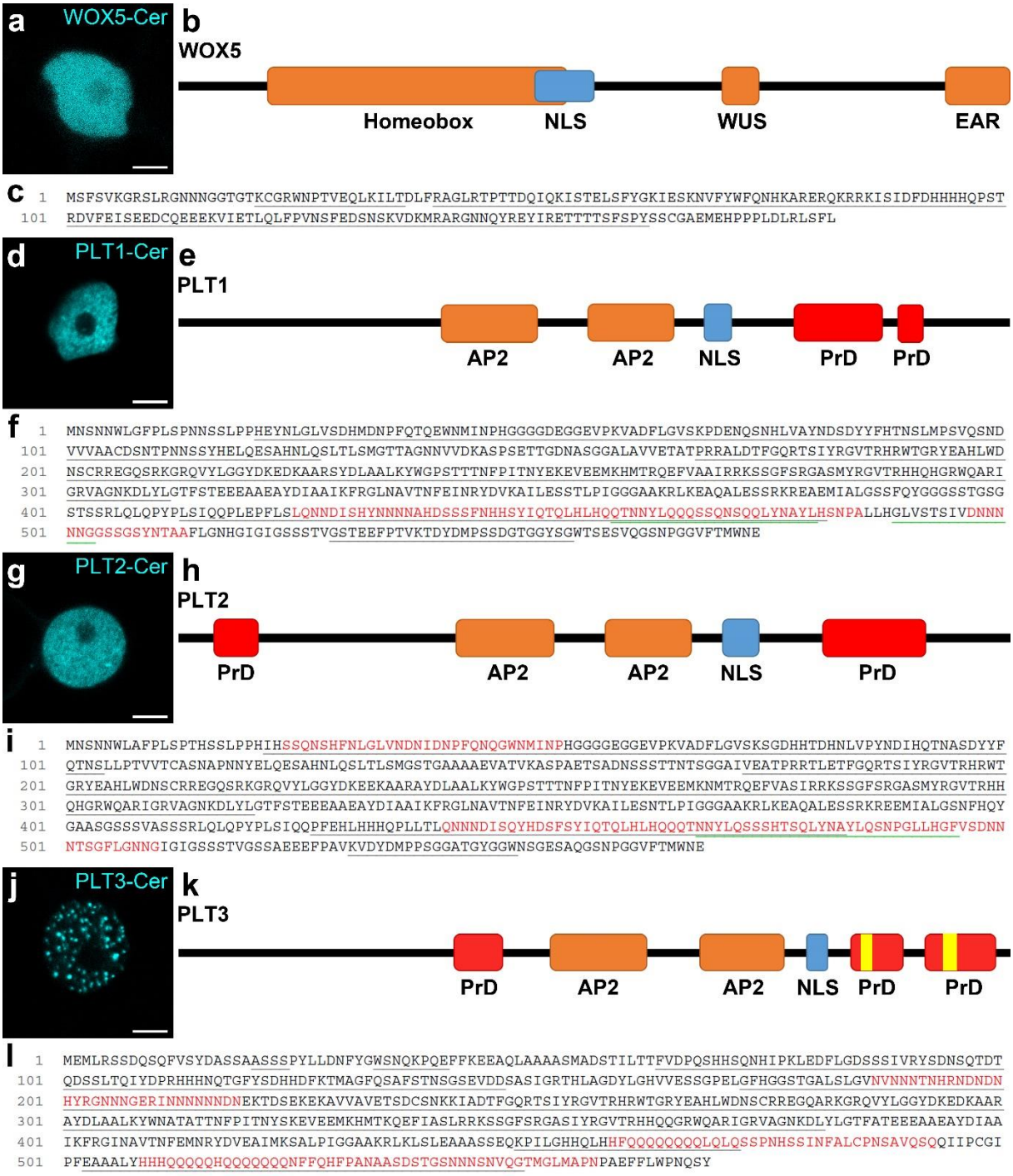

Supplementary figure IV-4: Subnuclear localisation and PrD prediction of WOX5, PLT1, PLT2 and PLT3

a,d,g,j, (Sub-)nuclear localisation of WOX5-Cer (**a**), PLT1-Cer (**d**), PLT2-Cer (**g**) and PLT3-Cer (**j**) in transiently expressing *N. benthamina* epidermal cells. Scale bars represent 5 µm. **b,e,h,k**, Schematic representation of WOX5 (**b**), PLT1 (**e**) PLT2 (**h**) and PLT3 (**k**) protein domains. The areas in red are predicted prion-like domains (PrDs), analysed using the PLAAC prediction tool. Yellow areas are polyQ stretches in the PLT3 amino acid sequence. **c,f,i,l**, Protein sequences of WOX5 (**c**) PLT1 (**f**), PLT2 (**i**) and PLT3 (**l**). The red highlighted sequences are the predicted PrDs. Cer = Cerulean fluorescent protein; PrD = prion-like domain; EAR = Ethylene-responsive binding factor-associated repression domain; WUS = WUSCHEL box; AP2 = APETALA2 domain; NLS = nuclear localisation signal.

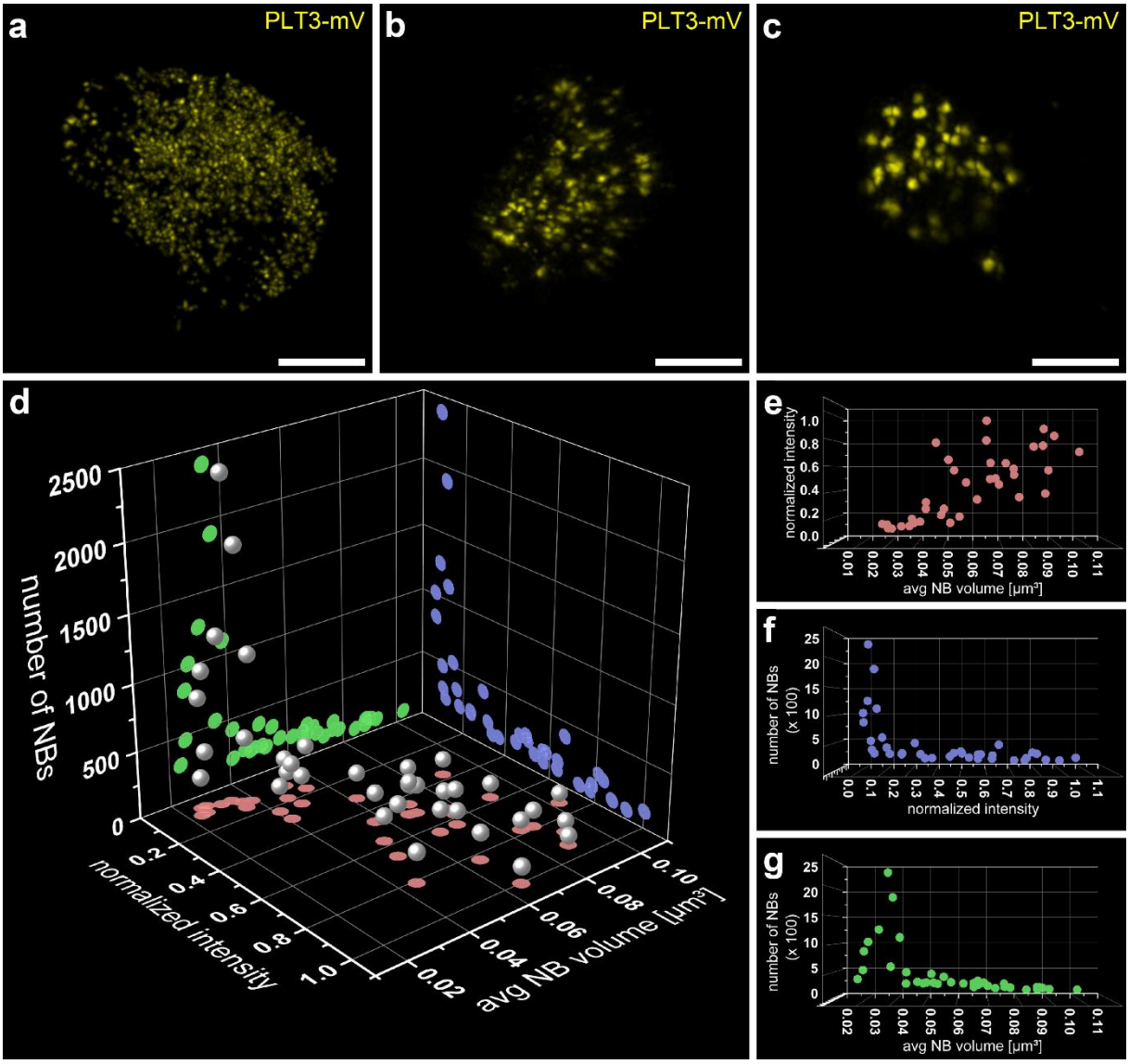

Supplementary figure IV-5: PLT3-NB formation is concentration-dependent

a-c, Nuclear-localised PLT3-mV expressed in *N. benthamiana* leaf epidermal cells with low (**a**) medium (**b**) and high (**c**) concentration. **d,** Average volume, intensity and number of PLT3-mV NBs per nucleus are summarized in a 3D-scatter plot. The corresponding 2D-scatter plots are shown in **e** (average NB volume in µm² versus normalized NB intensity), **f** (normalized NB intensity versus number of NBs) and **g** (average NB volume in µm² versus number of NBs). Number of analysed nuclei n = 37. mV = mVenus; NB = nuclear body; avg = average.

7.2 Supplementary movie

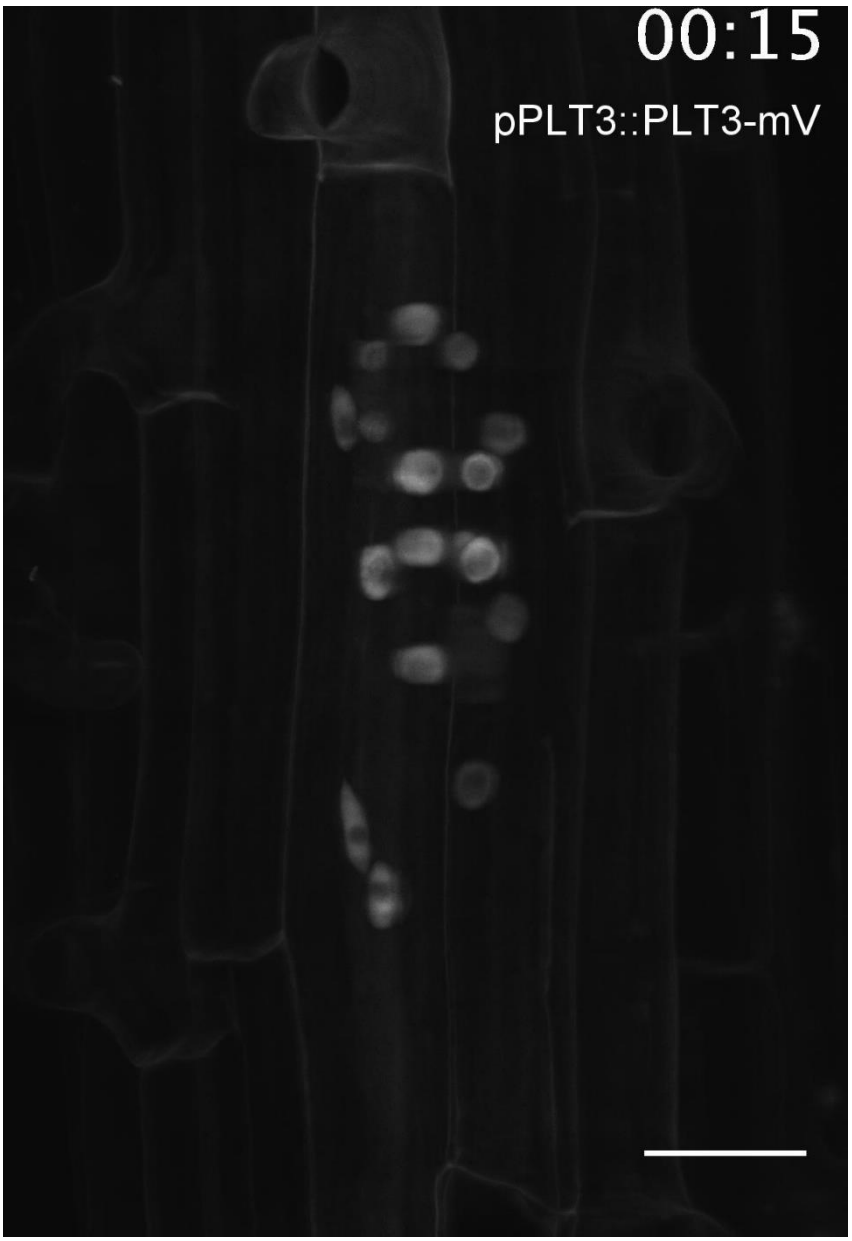

Supplementary movie IV-1: Dynamic formation of nuclear bodies in a *PLT3-mVenus* expressing LRP

The video shows a developing lateral root in an *Arabidopsis thaliana* plant expressing mVenus-tagged *PLT3* driven by the endogenous promoter (pPLT3::PLT3 mVenus) over 18 hours. Scale bar represents 25 µm. The movie can be found here: https://www.biorxiv.org/content/10.1101/818187v1.supplementary-material (doi: https://doi.org/10.1101/818187)

7.3 Supplementary tables

Supplementary table IV-1: List of cloning primers

cloning system	gene ID	alias	primer name	orientation	sequence
GreenGate	**Promoter modules**				
	AT3G11260	pWOX5	RD_GreenGate pWOX5 F	F	AAAGGTCTCAACCTAAAGACTTTTATCTACCAACTTCAAAAG
			RD_GreenGate pWOX5 R	R	AAAGGTCTCATGTTCGTTCAGATGTAAAG
			RD_GG pWOX5 BsaI a v2 F	F	AGAGACCAAATTATTTTGGTTATATGGTAG
			RD_GG pWOX5 BsaI a v2 R	R	CTACCATATAACCAAAATAATTTGGTCTCT
			RD_GreenGate pWOX5 BsaI b F	F	ATTACGATGTGAGAGCGCCTTCAACTTT
			RD_GreenGate pWOX5 BsaI b R	R	AAAGTTGAAGGCGCTCTCACATCGTAAT
	AT5G10510	pPLT3	RD_GG pPLT3 F V2	F	AAAGGTCTCAACCTAATTTTAACGTATTCTTTC
			RD_GG pPLT3 R V2	R	AAAGGTCTCATGTTAAACTTTCTTATAAAAACAATT
	CDS modules				
	AT3G11260	WOX5	RD_GreenGate WOX5 F	F	AAAGGTCTCAGGCTTAATGTCTTTCTCCGTG
			RD_GreenGate WOX5 Mitte R	R	GACGTCGTGGTGGTTTCTCGAATATATT
			RD_GreenGate WOX5 Mitte F	F	AATATATTCGAGAAACCACCACGACGTC
			RD_GreenGate WOX5 R	R	AAAGGTCTCACTGAAAGAAAGCTTAATCG
	AT5G10510	PLT3	RD_GreenGate PLT3 F	F	AAAGGTCTCAGGCTTAATGGAGATGTTGAG
			RD_GreenGate PLT3 R	R	AAAGGTCTCACTGAGTAAGACTGATTAGGC
		PLT3ΔPrD	RD_GreenGate PLT3 F	F	AAAGGTCTCAGGCTTAATGGAGATGTTGAG
			RD_PLT3ΔPrD1 CDS1 R	R	CCAGCTGCAACACCAAGTGACAAAG
			RD_PLT3ΔPrD1 linker F	F	CTTGGTGTTGCAGCTGGTGCTG
			RD_PLT3ΔPrD1 linker R	R	GTCTTCTCTGCTCCTGCGGCAG
			RD_PLT3ΔPrD1 CDS2 F	F	CGCAGGAGCAGAGAAGACAGATTCTG
			RD_GG PLT3ΔPrDs R	R	AAAGGTCTCACTGAGTGAAGTTGATGATGAC
	C-tag modules				
	-	mVenus	RD_GreenGate mVenus C-tag F	F	AAAGGTCTCATCAGCAATGGTGAGCAAGG
			RD_GreenGate mVenus C-tag R	R	AAAGGTCTCAGCAGTTACTTGTACAGCTC
	-	mCherry	RD_GG mCherry C-tag F	F	AAAGGTCTCATCAGCAATGGTGAGCAAGG
			RD_GG mCherry C-tag R	R	AAAGGTCTCAGCAGTTACTTGTACAGCTCGTC
Gateway	AT3G11260	WOX5	YS_WOX5 F CACC	F	CACCATGTCTTTCTCCGTGAAAGGTCGAAGCTTACG
			YS_WOX5 R -stop	R	AAGAAAGCTTAATCGAAGATCTAATGGC
	AT3G20840	PLT1	YS_PLT1 F CACC	F	CACCATGAATTCTAACAACTGGCTTGGCT
			YS_PLT1 r -stop	R	CTCATTCCACATAGTGAAAACACCACCAGGG
	AT1G51190	PLT2	YS_PLT2 F CACC	F	CACCATGAATTCTAACAACTGGCTCGCGTTCCCTCT
			YS_PLT2 R -stop	R	TTCATTCCACATCGTGAAAACACCTCCT
	AT5G10510	PLT3	YS_PLT3 F CACC	F	CACCATGGAGATGTTGAGGTCATCTGATCAGTCTCA
			YS_PLT3 R -stop	R	GTAAGACTGATTAGGCCAGAGGAAG
		PLT3ΔQ	YS_PLT3 F CACC	F	CACCATGGAGATGTTGAGGTCATCTGATCAGTCTCA
			RD_PLT3 Seg1 R	R	GAGATGAGAAATGGTGAAGTTGATGATGAC
			RD_PLT3 Seg2 F	F	CTTCACCATTTCTCATCTCCTAATCACAGTAGC
			RD_PLT3 Seg2 R	R	GAAGAAGTTGTGGTGGTGGTAAAGAGCAG
			RD_PLT3 Seg3 F	F	CACCACCACAACTTCTTCCAGCATTTTCC
			YS_PLT3 R -stop	R	GTAAGACTGATTAGGCCAGAGGAAG

Supplementary table IV-2: List of genotyping primers

gene ID	alias	primer name	orien-tation	sequence
AT3G11260	*wox5-1*	GK_WOX5 F	F	AAACAGTTGAGGACTTTACATCTGA
		WOX5 R	R	CGGATAATATGTCATAATTCAAAAT
AT5G10510	*plt3-1*	GK_PLT3L	F	TTGTGATTTGCCATTGACTAAAGGT
		GK_PLT3R	R	GAAAACAGTCCAATGGTCTCACATC
AT1G51190	*plt2*	RD_plt2 SALK128164 neu L	F	GCTTAAATAGATATATGGTCATGCTTATATTC
		RD_plt2 SALK128164 neu R	R	CAAGAAGACTCCAGCCGATC
		SALK LBB1V2		AAACCAGCGTGGACCGCTTGCTGCAACTCT

Supplementary table IV-3: List of expression vectors used in this study

cloning system	construct	promoter	N-tag	CDS	C-tag	terminator	plant sel. marker	destination vector	bacterial sel. marker	plasmid ID
		module A	module B	module C	module D	module E	module F	module Z		
GreenGate	**pWOX5:: mVenus-NLS**	WOX5 promoter	Ω-element (pGGB002)	mVenus	linker-NLS (pGGD007)	tUBQ10 (pGGE009)	BASTA (pGGF002)	pGGZ001	Spec	pVS10
	pWOX5:: WOX5-mV	WOX5 promoter	Ω-element (pGGB002)	WOX5	mVenus	tUBQ10 (pGGE009)	Hyg (pGGF005)	pGGZ001	Spec	pRD48
	pPLT3:: PLT3-mV	PLT3 promoter	Ω-element (pGGB002)	PLT3	mVenus	tUBQ10 (pGGE009)	Hyg (pGGF005)	pGGZ001	Spec	pRD73
	pPLT3:: PLT3-mCh	PLT3 promoter	Ω-element (pGGB002)	PLT3	mCherry	tUBQ10 (pGGE009)	-	pGGM 000	Kan	pRD83
	pWOX5:: WOX5-mV	WOX5 promoter	Ω-element (pGGB002)	WOX5	mVenus	tUBQ10 (pGGE009)	Hyg (pGGF005)	pGGN000	Kan	pRD84
	pPLT3::PLT3-mCh pWOX5::WOX5-mV	pRD83 + pRD84						pGGZ001	Spec	pRD89
	pPLT3:: PLT3ΔPrD-mV	PLT3 promoter	Ω-element (pGGB002)	PLT3 ΔPrD	mVenus	tUBQ10 (pGGE009)	Hyg (pGGF005)	pGGZ001	Spec	pRD125
	inducible PLT3ΔPrD-mV	Ubi-XVE oLexA-35S	Ω-element (pGGB002)	PLT3 ΔPrD	mVenus	tUBQ10 (pGGE009)	Hyg (pGGF005)	pGGZ001	Spec	pRD106
	inducible PLT3ΔPrD-mCh	Ubi-XVE oLexA-35S	Ω-element (pGGB002)	PLT3 ΔPrD	mCherry	tUBQ10 (pGGE009)	Hyg (pGGF005)	pGGZ001	Spec	pRD138
Gateway	**inducible WOX5-mV**	Ubi-XVE oLexA-35S	-	WOX5	mVenus	T3A	Hyg	pRD04	Spec	pRD26
	inducible WOX5-mCh	Ubi-XVE oLexA-35S	-	WOX5	mCherry	T3A	Hyg	pABind mCherry	Spec	pFB02
	inducible PLT1-mCh	Ubi-XVE oLexA-35S	-	PLT1	mCherry	T3A	Hyg	pABind mCherry	Spec	pRD144
	inducible PLT2-mCh	Ubi-XVE oLexA-35S	-	PLT2	mCherry	T3A	Hyg	pABind mCherry	Spec	pRD147
	inducible PLT3-mV	Ubi-XVE oLexA-35S	-	PLT3	mVenus	T3A	Hyg	pRD04	Spec	pRD25
	inducible PLT3-mCh	Ubi-XVE oLexA-35S	-	PLT3	mCherry	T3A	Hyg	pABind mCherry	Spec	pFB06
	inducible PLT3ΔQ-mV	Ubi-XVE oLexA-35S	-	PLT3 ΔQ	mVenus	T3A	Hyg	pRD04	Spec	pRD57
	inducible PLT3ΔQ-mCh	Ubi-XVE oLexA-35S	-	PLT3 ΔQ	mCherry	T3A	Hyg	pABind mCherry	Spec	pRD81
	inducible free mCherry	Ubi-XVE oLexA-35S	-	mCherry	-	T3A	Hyg	pMDC7	Spec	-

Supplementary table IV-4: *Arabidopsis* mutants and transgenic lines

gene ID	alias	reference
AT3G11260	*wox5-1*	SALK038262 (ABRC)
AT5G10510	*plt3-1*	Galinha *et al*. (2007)
AT1G51190	*plt2*	SALK_128164 (ABRC)
AT1G51190, AT5G10510	*plt2, plt3*	this study, crossing of *plt2* and *plt3-1*
AT3G11260, AT5G10510	*wox5, plt3*	this study, crossing of *wox5-1* and *plt3-1*
AT3G11260, AT1G51190, AT5G10510	*wox5, plt2, plt3*	this study, crossing of *plt2, plt3* and *wox5, plt3*
AT5G10510	pPLT3::erCFP (*Col-0*)	Galinha *et al*. (2007)
AT5G10510	pPLT3::erCFP (*wox5-1*)	this study, crossing of pPLT3::erCFP (*Col-0*) and *wox5-1*
AT5G10510	pPLT3::PLT3-YFP (*Col-0*)	Galinha *et al*. (2007)
AT5G10510	pPLT3:: PLT3-YFP (*wox5-1*)	this study, crossing of pPLT3::PLT3-YFP (*Col-0*) and *wox5-1*
AT5G10510	pPLT3::PLT3-mVenus (*plt2, plt3*)	this study
AT5G10510	pPLT3::PLT3ΔPrD-mVenus (*plt2, plt3*)	this study
AT3G11260	pWOX5::mVenus-NLS (*Col-0*)	this study
AT3G11260	pWOX5::mVenus-NLS (*plt2*)	this study
AT3G11260	pWOX5::mVenus-NLS (*plt3-1*)	this study
AT3G11260	pWOX5::mVenus-NLS (*plt2, plt3*)	this study

Supplementary table IV-5: Intensity values of transcriptional and translational FP tagged PLT3 expression experiments in *Col-0* and *wox5* related to Figure IV-1

root #	pPLT3::erCFP fluorescence intensity [%]		pPLT3::PLT3-YFP fluorescence intensity [%]	
	Col-0	***wox5***	***Col-0***	***wox5***
1	84	65	96	69
2	108	67	121	31
3	81	78	73	72
4	93	48	68	64
5	101	46	68	38
6	95	65	95	109
7	113	52	109	75
8	128	53	72	39
9	82	58	78	79
10	71		127	30
11	105		164	63
12	139		84	39
13			145	66
14				55
15				56
16				99
mean	**100**	**59**	**100**	**62**
st. dev.	**20.10**	**10.39**	**31.13**	**23.01**

Supplementary table IV-6: Quantification of transcriptional mVenus tagged WOX5 expression in the QC region of *Col* and *plt2*, *plt3* related to Figure IV-2

root #	number of cells with WOX5 expression		lateral area of WOX5 expression in the root tip [µm²]	
	Col	*plt2, plt3*	*Col*	*plt2, plt3*
1	7	14	432.03	719.28
2	4	9	345.88	886.24
3	7	13	393.67	861.28
4	7	13	400.62	882.48
5	8	12	346.86	548.73
6	6	11	430.11	736.44
7	8	14	467.05	793.77
8	6	12	512.33	693.18
9	7	13	444.99	948.22
10	9	14	474.60	747.27
mean	**6.90**	**12.50**	**424.81**	**781.69**
st. dev.	**1.30**	**1.50**	**51.26**	**111.59**

Supplementary table IV-7: Average QC and CSC phenotypes related to Figure IV-3

genotype	average QC cell-divisions per root (± st. dev.)	average CSC layers per root (± st. dev.)	number of analysed roots
Col	0.34 ± 0.59	0.99 ± 0.59	146
plt2	0.53 ± 0.64	0.82 ± 0.72	77
plt3	0.61 ± 0.64	0.85 ± 0.69	121
plt2, plt3	0.81 ± 0.88	0.84 ± 0.82	105
wox5	1.87 ± 0.98	0.23 ± 0.44	118
wox5, plt3	2.11 ± 0.98	0.31 ± 0.51	87
wox5, plt2, plt3	2.83 ± 1.05	0.24 ± 0.46	98

Supplementary table IV-8: Percentage of periclinal cell divisions in the QC shown in Supplementary figure IV-1

genotype	periclinal QC cell divisions [%]	number of analysed roots
Col	3	146
plt2	21	77
plt3	21	121
plt2, plt3	53	105
wox5	41	118
wox5, plt3	43	87
wox5, plt2, plt3	53	98

Supplementary table IV-9: Average QC and CSC phenotypes of rescue experiments, related to Supplementary figure IV-2

Genotype	average QC cell-divisions per root (± SD)	average CSC layers per root (± SD)	number of analysed roots
rescue experiment of *wox5* mutant			
Col	0.33 ± 0.61	0.83 ± 0.59	30
wox5	1.77 ± 1.14	0.33 ± 0.55	30
wox5 pWOX5::WOX5-mV	0.43 ± 0.67	0.88 ± 0.65	51
rescue experiment of *plt3* mutant			
Col	0.46 ± 0.65	1.00 ± 0.40	26
plt3	1.60 ± 1.14	0.85 ± 0.59	20
plt3 pPLT3::PLT3-mV	0.81 ± 0.87	0.87 ± 0.43	31

Supplementary table IV-10: Average fluorescence lifetimes (τ) and standard deviation (st. dev.) obtained in WOX5/PLT FLIM experiments related to Figure IV-7.

Donor	Acceptor	average τ [ns]	st. dev. [ns]	n
WOX5-mVenus	-	3.03	0.03	62
	+ free mCherry	2.97	0.07	37
	+ PLT1-mCherry	2.79	0.12	35
	+ PLT2-mCherry	2.73	0.13	36
	+ PLT3-mCherry	2.75	0.17	42
	+ PLT3ΔQ-mCherry	2.94	0.14	50
	+ PLT3ΔPrD-mCherry	2.88	0.13	32

Supplementary table IV-11: FLIM results of subnuclear data analysis in WOX5-mV and PLT3-mCh co-expressing *N. benthamiana* epidermal cells related to Figure IV-7

date	measurement #	WOX5-mVenus fluorescence lifetime [ns]	
		bodies-only	nucleoplasm
2019-06-11	WOX5-mV PLT3-mCh_7	2.24	2.76
	WOX5-mV PLT3-mCh_15	2.19	2.85
2019-06-10	WOX5-mV PLT3-mCh_23	2.60	2.92
	WOX5-mV PLT3-mCh_25	2.55	2.88
2018-06-29	WOX5-mV PLT3-mCh_4	2.56	2.89
2018-06-28	WOX5-mV PLT3-mCh_1	2.50	2.84
	WOX5-mV PLT3-mCh_9	2.50	2.69
mean		**2.45**	**2.83**
st. dev.		**0.15**	**0.07**

Supplementary table IV-12: Average fluorescence lifetimes (τ) and standard deviation (st. dev.) obtained in *Arabidopsis* FLIM experiments related to Supplementary figure IV-3.

Donor	Acceptor	average τ [ns]	st. dev. [ns]	n
WOX5-mVenus	-	2.97	0.07	67
	PLT3-mCherry	2.94	0.08	68

V. A novel role for EARLY FLOWERING 3 (ELF3) links circadian/light signalling and root stem cell maintenance by microdomain formation

This chapter is a manuscript in preparation for submission.

Authors:

Rebecca C. Burkart[1], Laura Czempik[2], Vivien I. Strotmann[1], Philipp Wuthenow[1], Yvonne Stahl[1]

Affiliations:

[1]Institute for Developmental Genetics, Heinrich-Heine University, Universitätsstr. 1, 40225 Düsseldorf, Germany

[2] Molecular Plant Science/Plant Biochemistry University of Wuppertal, 42119 Wuppertal, Germany

Contributions:

Rebecca C. Burkart, Laura Czempik, Vivien I. Strotmann and Philipp Wuthenow carried out the experiments. Yvonne Stahl and Rebecca C. Burkart designed the experiments, Rebecca C. Burkart analysed and interpreted the data. The manuscript was written by Rebecca C. Burkart and was revised and commented by Yvonne Stahl.

1. Abstract

Maintaining homeostasis of the stem cell niche (SCN) of the *Arabidopsis thaliana* root is essential for plant life as it influences not only root growth and development but also all aboveground organs by providing water and nutrients. A group of slowly dividing cells, the quiescent centre (QC) cells, are located in the centre of the SCN and maintain the surrounding stem cells, including the distally located columella stem cells (CSCs) that give rise to the differentiated columella cells which mediate gravity perception. Important players of the necessary balanced regulation of QC quiescence and CSC maintenance are the transcription factors (TFs) of the PLETHORA (PLT) family and WUSCHEL-RELATED HOMEOBOX5 (WOX5) that maintain QC quiescence and regulate CSC fate in an interdependent manner. However, little is known about the integration of external environmental stimuli in the regulation of root SCN homeostasis. Here, we report for the first time a function of the clock-related transcriptional regulator EARLY-FLOWERING3 (ELF3) in root SCN maintenance, where it positively influences QC quiescence and maintains CSCs together with PLT3. We show that ELF3 is expressed in the root SCN, where it localises to subcellular microdomains which show liquid-like behaviour in transient *N. benthamiana* experiments. We reveal that PHYTOCHROME INTERACTING FACTOR (PIF)-proteins may act as nuclear shuttles for ELF3, where it is recruited to PLT3-nuclear bodies (NBs). We propose a model, where the potentially reversible subcellular localisation of ELF3 to phase-separated microdomains and its interaction with PLT3 and co-localisation to NBs could represent a fast and flexible read out for cell fate determination, thereby creating a link to a potential involvement of environmental stimuli in root SCN homeostasis.

2. Introduction

Plant vigour strongly depends on the balanced growth of a root system that gives access to water and nutrients and anchors the plant in the soil. This is enabled by a group of pluripotent stem cells located in the stem cell niche (SCN) at the tip of the root within the so-called root apical meristem (RAM). In *Arabidopsis thaliana*, the root SCN is composed of on average four long-lasting cells, the quiescent centre (QC) cells and the surrounding layer of stem cells, including the distally located columella stem cells (CSCs)[1,2] (Figure V-1a). The maintenance of the stem cells is ensured by the QC cells that prevent their differentiation[3]. The delicate homeostasis of the root SCN with its very defined number of QC and stem cells as well as the differentiation

status of surrounding cells involves a tight regulation by phytohormones and transcription factors (TFs)[4]. Important players in this process are the TFs of the PLETHORA (PLT) family and WUSCHEL-RELATED-HOMEOBOX5 (WOX5). *WOX5* is expressed in the QC cells and encodes a homeobox TF that maintains the surrounding stem cells non-cell-autonomously[5,6]. PLTs are auxin-activated AP2 (APETALA2)-type TFs. Four of them are expressed in the RAM (*PLT1*, *PLT2*, *PLT3* and *PLT4*), forming a protein concentration gradient which peaks in the SCN and decreases with a higher differentiation status of the root cells. They are known as regulators of stem cell identity and QC specification[7,8]. Recently, we showed that WOX5 and PLTs control CSC maintenance and QC quiescence in an interdependent way[9] (see chapter IV). Still, many of the involved players are unknown and there is only limited knowledge about how external cues, e.g. light and day-length, influence root growth and the delicate organisation of the RAM. Timing is very important in a plants` life cycle, as it obviously depends on diurnal and annual rhythms. Therefore, plants need to set up a stable biological clock, called the circadian clock. The circadian clock is an endogenously generated rhythmic system for timing, set up by environmental time cues to about 24 h according to the period of earth rotation and allows organisms to adapt to environmental oscillations[10]. An important component of the *Arabidopsis* circadian clock is EARLY FLOWERING3 (ELF3), a player in light-regulated flowering time[11,12]. The ELF3 protein and transcript levels show rhythmic variations, peaking at dusk[13–15]. It is part of the evening complex (EC), where it interacts with ELF4 and LUX (LUX ARRHYTHMO) to control daily rhythms in gene expression through transcriptional regulation[16]. One example is the EC-dependent repression of *PHYTOCHROME INTERACTING FACTOR4 (PIF4)* and *PIF5* in the evening, both gene products promoting hypocotyl growth[16]. In general, PIFs regulate the expression of light-responsive genes as they are known to transduce light signals perceived by phytochromes or cryptochromes, thereby regulating plant-growth[17–24]. ELF3 itself is proposed to act as a hub that connects the EC to other processes, including circadian clock, light-signalling, photosynthesis, hormone signalling, thermomorphogenesis and growth, thereby coordinating endogenous and environmental signals[16,25–29]. This is in agreement with the hypothesis, that ELF3 functions as a link between shoot- and root-growth in response to environmental stimuli[30]. Supporting this, ELF3 was reported to regulate rhythmic root elongation[31], designating it an ideal candidate for the integration of circadian/light signalling in root growth and meristem organisation.

In this study, we elucidate a novel function of ELF3 in root SCN homeostasis. We show that it is involved in CSC maintenance where it acts together with PLT3. Additionally, ELF3 and PLT3 both act positively on QC quiescence. Their subcellular localisation to punctuate

structures and the existence of intrinsically disordered domains (IDRs) in their protein sequences suggests a formation of phase-separated droplets that co-localise upon co-expression. We show that the translocation of ELF3 to PLT3 nuclear bodies (NBs) and their complex formation is potentially mediated by PIF proteins. We find that PLT3 and ELF3 co-localisation and interaction depend on IDRs, hereafter called prion-like domains (PrDs), that are present in both proteins and are responsible for the formation of the PLT3 NBs.

We propose a model where the observed ELF3-bodies appear upon external stimuli and, through interaction with PLT3, serve as a fast read-out for cell fate determination which connects stem cell fate to the plants' response on environmental changes.

3. Results

3.1 *PLT3* and *ELF3* are both expressed in the RAM of *Arabidopsis thaliana*

In the main root of *Arabidopsis thaliana*, *PLT1*, *PLT2*, *PLT3* and *PLT4* are expressed within the RAM, forming a protein gradient that peaks in the QC and where decreasing concentration correlates with increasing cell differentiation[8]. In particular PLT3 shows high protein levels in the QC and CSC layer (Figure V-1b), giving a promising candidate for the regulation of distal stem cell maintenance and QC identity. Actually, we previously reported that PLT3 regulates CSC maintenance and QC quiescence together with WOX5 in an interdependent manner[9] (see chapter IV). Still, many players involved in the regulation of root SCN homeostasis remain elusive and there is little knowledge about how external cues, e.g. light, day-length and temperature, influence root growth and the delicate organisation of the root meristem. Concerning circadian rhythms, it is known that the root clock differs from the shoot clock regarding the expression of clock-related genes but it also responds to a photosynthesis-related signal[32]. Additionally, there is evidence that circadian rhythms influence root elongation in response to carbon supply and rhythmic starch degradation[31,33]. Furthermore, defects in lateral root growth of mutants of circadian-clock-related genes have been described[33–35]. Interestingly, a direct connection between the circadian clock and root meristem organisation was reported, as sugar-activated TOR (target of rapamycin)-signalling is influenced by actors of the circadian clock and regulates clock-dependent root meristem cell proliferation[35]. As ELF3 was shown to play an important role in rhythmic root growth[31] and has been proposed to act as connecting link between shoot and root growth in response to environmental stimuli[30], it is a promising candidate connecting light response to root SCN maintenance.

ELF3 is known as key component of the circadian clock[36,37] and its function in flowering time, clock regulation and thermomorphogenesis has been studied thoroughly[12–15,29,38–46]. Although a function of ELF3 during circadian root growth was previously indicated[31], there is only limited knowledge of *ELF3* expression in root tissues and, so far, it has not been shown to be present in the root SCN of *Arabidopsis thaliana*. Here, we show that ELF3 is present ubiquitously in all cells of the RAM, including the SCN (Figure V-1c).

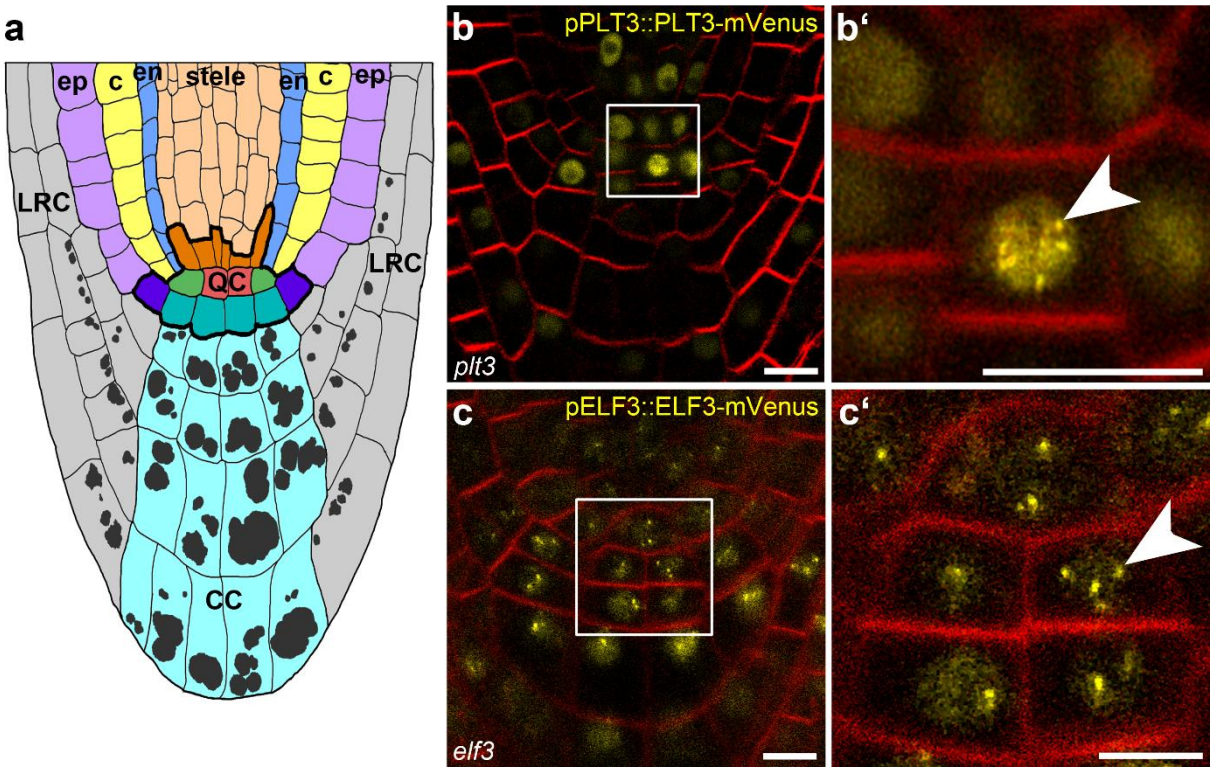

Figure V-1: Localisation of PLT3 and ELF3 in the SCN of *Arabidopsis thaliana*

a, Schematic representation of the *Arabidopsis* root meristem. The QC cells (red) maintain the surrounding stem cells (initials) outlined in black, together building the root stem cell niche (SCN). The different cell types are colour coded. QC = quiescent centre (red); CC = columella cells (light cyan); LRC = lateral root cap (grey); ep = epidermis (light purple); c = cortex (yellow); en = endodermis (dark blue); cortex/endodermis initials (green); grey dots = starch granules. **b**,**c**, Representative images of the SCN of pPLT3::PLT3-mVenus (**b**) and pELF3::ELF3-mVenus (**c**) (yellow) expressing and FM4-64-stained (red) *Arabidopsis* seedlings in *plt3* or *elf3* background, respectively. **b’,c’,** Magnification of b and c, arrowheads point at NBs. Scale bars represent 5 µm.

The overlapping expression domains of *ELF3* and *PLT3* in the root as well as the tendency of ELF3 and PLT3 proteins to form NBs[9,29,38] (Figure V-1b’ and c’) prompted us to investigate a potential interconnection regarding meristem maintenance in the *Arabidopsis* root. Therefore, we analysed the QC and CSC phenotypes of the respective single and double mutants.

3.2 *plt3* and *elf3* mutants show defects in the *Arabidopsis* root stem cell niche (SCN)

The QC cells are long-lasting cells with low division rates, serving as a long-term-reservoir for maintaining the surrounding stem cells[47,48]. PLTs are known regulators of QC quiescence and CSC maintenance[7,8,49], interconnecting QC divisions and CSC differentiation[9]. We questioned, whether ELF3 also acts on SCN homeostasis, potentially in a PLT3-dependent manner. To address this, we analysed the root meristem phenotypes of *Arabidopsis Col* wildtype and *elf3* and *plt3* single and double mutant seedlings, using a new staining method which we named SCN staining, that combines the 5-ethynyl-2'-deoxyuridine (EdU) and modified pseudoSchiff base propidium iodide (mPS-PI) stains to simultaneously visualise cell divisions, starch granule distribution and cell walls within the same root[9,47,50]. This method allows us to detect cell divisions in the QC as a marker of disturbed QC quiescence and starch granules as a marker of cell differentiation in the distal root meristem. The mPS-PI staining method is commonly used for CSC and columella cell (CC) characterisation, as starch granules are normally absent from the CSC-layer which is located distal to the QC and gives rise to the underlying differentiated CCs that accumulate starch in order to perceive gravity[50–52] (Figure V-2a).

Our results show that *Col* roots possess, on average, one layer of CSCs and only 20 % of the observed roots show a higher differentiation, indicated by the lack of a starch-free CSC layer (Figure V-2b,f). Regarding the CSC phenotype, both, the *elf3* and the *plt3* single mutant, show a tendency towards higher differentiation with a frequency of around 30 % of roots lacking an CSC layer (28 % and 31 %, respectively, Figure V-2c,d,f), which is about 1.5 fold higher than that of *Col*. *elf3* additionally has a higher number of less differentiated roots, showing two starch-free CSC layers (17 %) compared to *Col* (12 %). This value does not change much in the *elf3, plt3* double mutant (18 %), which also shows a frequency of starch-accumulating roots similar to the *elf3* and *plt3* single mutants of about 30 % (32 %, Figure V-2e,f). According to this data, ELF3 and PLT3 positively influence the maintenance of the CSC layer, potentially acting in the same pathway as no additive effect is observed in the double mutant.

Furthermore, we studied the QC division phenotypes by counting the number of EdU-stained QC cells. For this purpose, we recorded Z-stacks through the stem cell region of the root and analysed the transversal sections. According to previously published data the QC is composed of on average four cells with a low division frequency of about 20 % within 24 h[1,2,47]. Our data reveal a division frequency of 33 % of *Col* roots showing at least one cell division in the QC within 24 h (Figure V-2h,l). Unlike *Col*, the *elf3* single mutant shows a higher division frequency (43 %, Figure V-2i,l). We also observe an even higher division frequency in the *plt3* single mutant (48 %, Figure V-2j,l). Interestingly, the division frequency further increases in

the *elf3, plt3* double mutant (68 %), indicating an additive effect and individual roles for ELF3 and PLT3 in QC maintenance.

Altogether, our data reveals an ELF3-dependent regulation of the SCN homeostasis, potentially acting together with PLT3 during CSC maintenance.

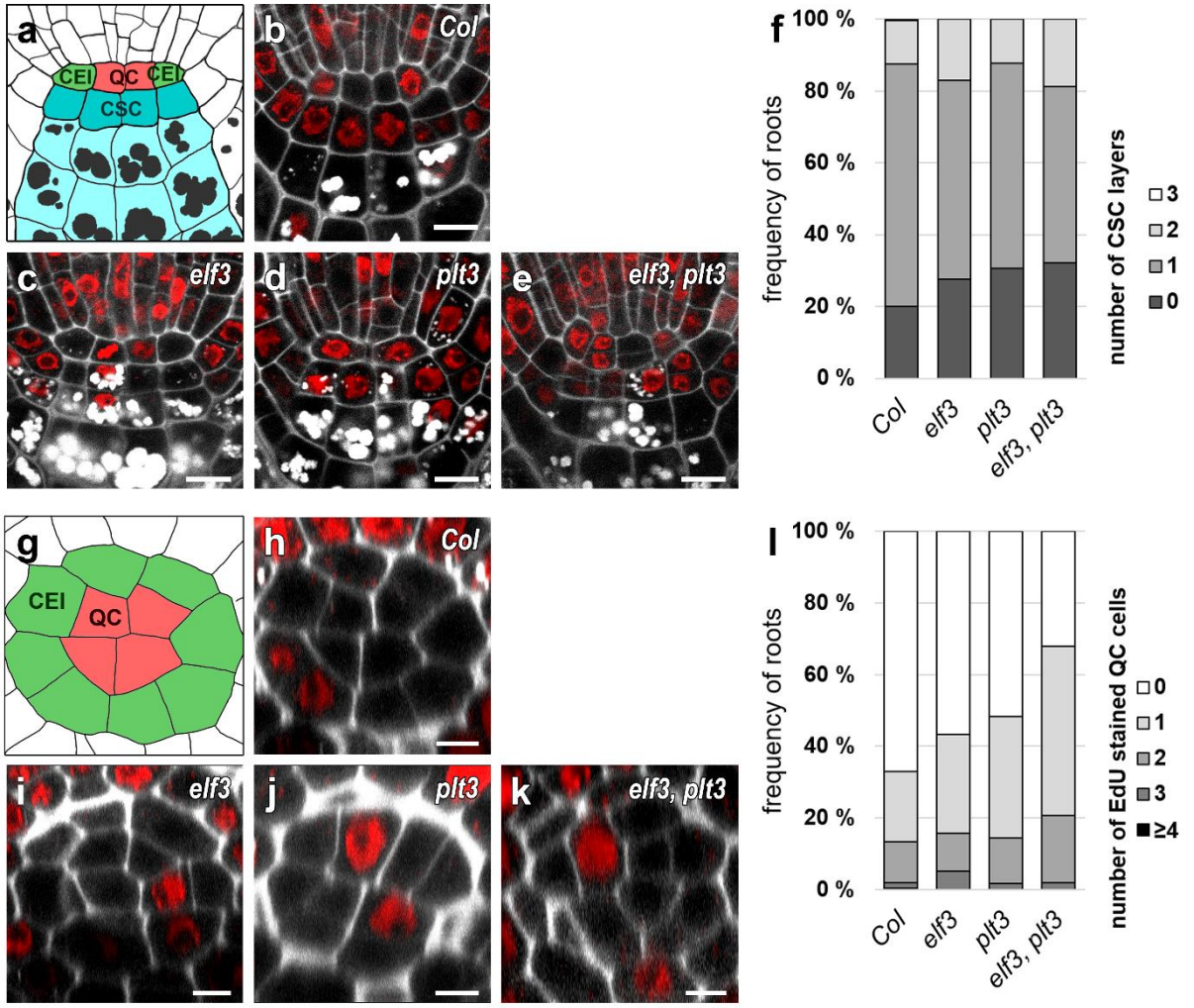

Figure V-2: CSC and QC phenotypes of *Col* wildtype and *elf3* and *plt3* single and double mutants

a,g, Schematic representation of a longitudinal (**a**) and transversal (**g**) section of a wild-typic SCN in the *Arabidopsis* root. QC = quiescent centre (red), CSC = columella stem cells (dark cyan), CEI = cortex endodermis initials (green). Starch (grey dots) accumulating columella cells are shown in light cyan. **b-e, h-k,** Combined mPS-PI (grey) and EdU (red) staining for 24 hours (SCN staining) in order to analyse the CSC (**b-f**) and QC division (**h-l**) phenotype within the same roots. **b-e,** Representative images of the SCN staining in *Col*, and the indicated single and double mutant roots. **f,** Analyses of the SCN staining for CSC phenotypes. Frequencies of roots showing 0, 1, 2, or 3 CSC layers are plotted as bar graphs. **l,** Analyses of the SCN staining for QC division phenotypes. Frequencies of roots showing 0, 1, 2, 3 or ≥4 dividing QC cells are plotted as bar graphs. The number of analysed roots can be found in Supplementary table V-7. SCN = stem cell niche; mPS-PI = modified pseudo-Schiff propidium iodide; EdU = 5-ethynyl-2'-deoxyuridine; scale bars represent 5 µm.

For a more detailed visualisation and to examine the correlation between CSC and QC phenotypes, we plotted the data in 2D-histograms where the y-axis represents the number of CSC-layers and the x-axis the number of QC-divisions per root. The frequencies of the analysed roots are shown in a color-coded manner in the 2D-plots (Figure V-3).

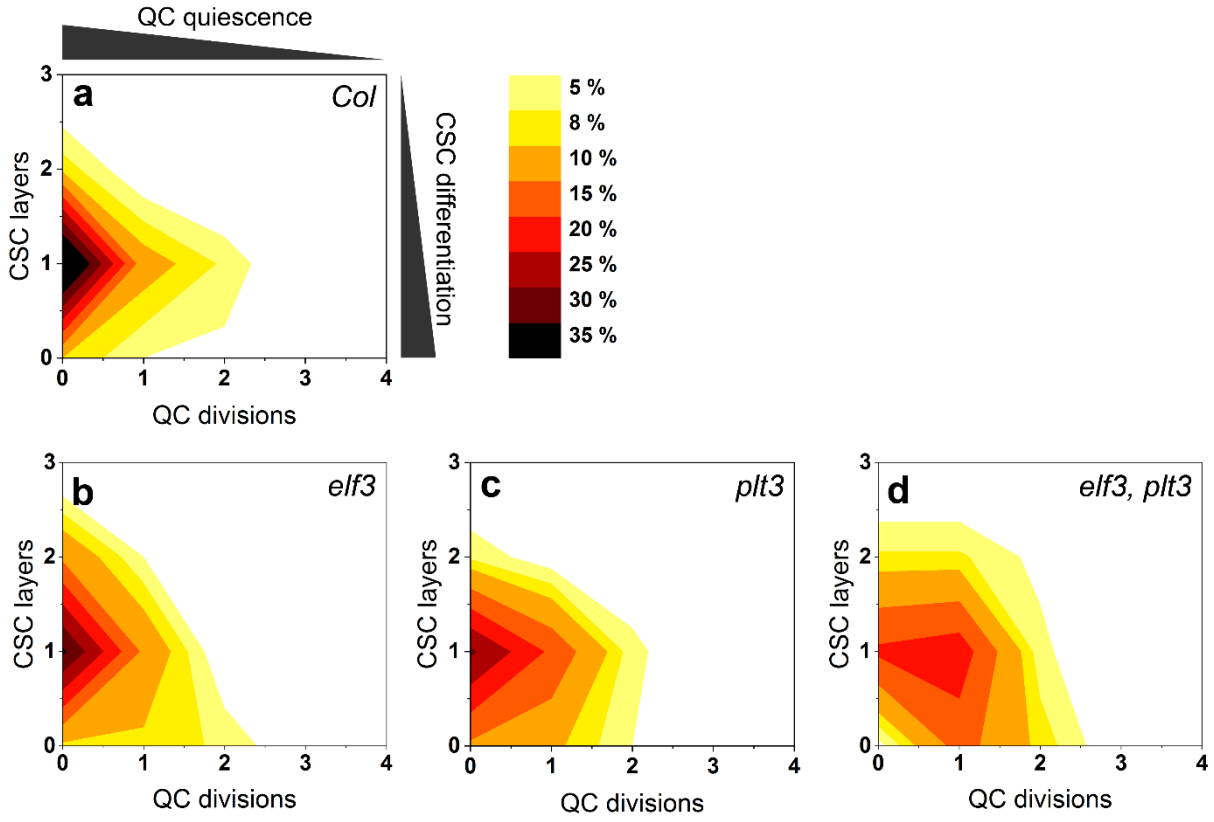

Figure V-3: QC divisions correlate with the number of CSC layers

The combined results of the SCN staining in Figure V-2 are shown as 2D plots to visualise the correlation of the disturbance in CSC maintenance and QC quiescence. Number of CSC layers are shown on the y axis and the QC division phenotype is shown on the x axis. The darker the colour, the more roots show the respective phenotype (see colour gradient top right indicating the frequencies of the observed phenotypes). *Col* wild type roots peak at one layer of CSCs and no EdU stained cells (no QC division) after 24 h EdU staining (**a**).

This results in a very regular pattern for *Col* with a peak at one CSC-layer and no QC-divisions (with a frequency of 47 % of roots, Figure V-3a). This peak stays the same in the *elf3* and *plt3* single mutants, but with lower frequencies (36 % for *elf3* and 31 % for *plt3*). However, the pattern of the 2D plots shifts towards a higher CSC-differentiation and a slightly higher QC division rate (Figure V-3b,c), indicating a correlation of higher root differentiation with less QC quiescence. Compared to this, the *elf3, plt3* double mutant shows a much broader 2D-pattern where the peak shifts to one CSC-layer and one QC-division (23 % of the roots, Figure V-3d). Additionally, the root frequencies shift to both less and more CSC-layers, each

accompanied by more QC divisions (Figure V-3d). As the bar plots (Figure V-2) already revealed, an additive effect in QC divisions can be observed in the *elf3, plt3* double mutant compared to the single mutants, but not for the CSC phenotype, indicating an interdependent role for ELF3 and PLT3 in CSC maintenance. The average QC and CSC phenotypes for all examined genotypes are summarized in Supplementary table V-7.

Altogether, the results suggest that a disturbance in QC quiescence leads to a loss of the defined number of CSC layers. Concerning PLT3 and ELF3, both TFs are involved in SCN homeostasis in a way where they positively influence QC-quiescence and together act positively in CSC-maintenance.

3.3 PLT3 and ELF3 proteins co-localise upon co-expression

As shown before, PLT3 and ELF3 both localise to small subcellular body-like structures in *Arabidopsis thaliana* as well as in transient *N. benthamiana* expression experiments[9,38]. To further assess their subcellular distribution, we analysed protein localisation, co-localisation and interaction of ELF3 and PLT3 fused to fluorescent proteins (FPs) in a transient *N. benthamiana* expression system.

Consistent with the previous findings[9,38], our mVenus-tagged ELF3 and PLT3 fusion proteins both localise to subcellular body-like structures in *Arabidopsis* (Figure V-1b',c') and transient *N. benthamiana* experiments. Although in *Arabidopsis* they are both nuclear-localised, we found a distinct localisation in the *N. benthamiana* experiments. While PLT3 still localises primarily to the nucleus and forms NBs (Figure V-4c), ELF3 localises with higher concentration to the cytoplasm, forming bright cytoplasmic bodies, but also shows a weaker nuclear localisation with less body-formation (Figure V-4f). Upon co-expression, ELF3-mVenus was recruited to the PLT3 NBs and co-localised with PLT3-mCherry (Figure V-4i-i'').

As we showed previously, the PLT3 localisation to NBs strongly depends on three intrinsically disordered prion-like domains (PrDs), one located in the N-terminal part of the protein, the other two at the C-terminus (Figure V-4a). A PrD-lacking PLT3 variant shows a homogenous nuclear protein localisation where no more NB formation can be observed[9] (Figure V-4e). Proteins containing PrDs are known to form concentration-dependent aggregates similar to yeast prions[53]. In *Arabidopsis* there are over 500 PrD-containing proteins with prion-like behaviour[54]. Prions are mainly known for their pathogenic role in mammalian neurodegenerative diseases[55,56], but recent data also focuses on their functional nature, mainly as protein-based memory due to their ability to form self-replicating conformations[57,58]. The analyses of protein sequences of 31 organisms, including *Arabidopsis*, revealed Glutamine (Q)-

and Asparagine (N)- rich regions in prion-like proteins to be sufficient for protein-aggregation[59]. The presence of poly-Q-stretches within the two C-terminal PrDs of PLT3 is striking (Figure V-4a). However, a deletion of these alone does not change protein localisation compared to the full-length protein (Figure V-4d). As ELF3 also shows a localisation to bodies we asked if this is due to PrDs in the protein sequence. Thus, we used the web-based PLAAC tool to predict PrDs in ELF3[60]. As a result, we found two PrDs located in the C-terminal part of the ELF3 protein, one of them containing poly-Q-stretches (Figure V-4b). As observed for PLT3, the localisation does not change when only the polyQ-stretches are deleted in an mVenus-tagged ELF3 variant (ELF3ΔQ-mVenus, Figure V-4g). In contrast to PLT3, ELF3 still forms bodies when the full PrDs are deleted (ELF3ΔPrD-mVenus, Figure V-4h). Supporting this, we made the same observation with the ELF3ΔPrD-mVenus deletion variant in *Arabidopsis*, where we could still observe body-formation of the ELF3ΔPrD-mVenus (Supplementary figure V-1). Recently, ELF3 has been described to aggregate PrD-dependently in response to temperature. The PrDs in ELF3 are proposed to mediate the ability to reversibly undergo phase transition in response to high temperatures and thereby shifting between an active and inactive state[29]. However, in our experiments the deletion of the PrDs in ELF3 is not sufficient to fully abolish body-formation, indicating that the PrDs alone are not responsible for its localisation to bodies.

Next, we asked if the co-localisation of PLT3 and ELF3 depends on the presence of the poly-Q-stretches and PrDs. Therefore, we co-expressed FP-tagged PLT3 and ELF3 full length proteins and deletion variants in several combinations. We observed that the co-localisation does not change when only one of both proteins has its poly-Q-stretch deleted (Figure V-4j and l). When the poly-Q-stretches in both proteins are deleted ELF3ΔQ-mVenus still colocalises with PLT3ΔQ-mCherry in the nucleus but also shows a high body-forming cytoplasmatic fraction (Figure V-4m-m''). In case of the PrD-deletion variants, the PLT3-dependent recruitment of ELF3-mVenus is impaired when co-expressed with the PLT3ΔPrD-mCherry compared to the co-expression with the full length PLT3. This observation is accompanied by an absence of NBs of both proteins and is independent of the presence of the ELF3 PrDs (Figure V-4k-k''; o-o''), showing that the PLT3-PrDs, but not the ELF3-PrDs, are important for the ELF3 recruitment and co-localisation to PLT3 NBs. In agreement with this we observed that, if only the ELF3 PrDs are removed and the ELF3ΔPrD-mVenus is co-expressed with the full length PLT3-mCherry, no change in protein localisation can be observed compared to the full-length variant (Figure V-4n-n'').

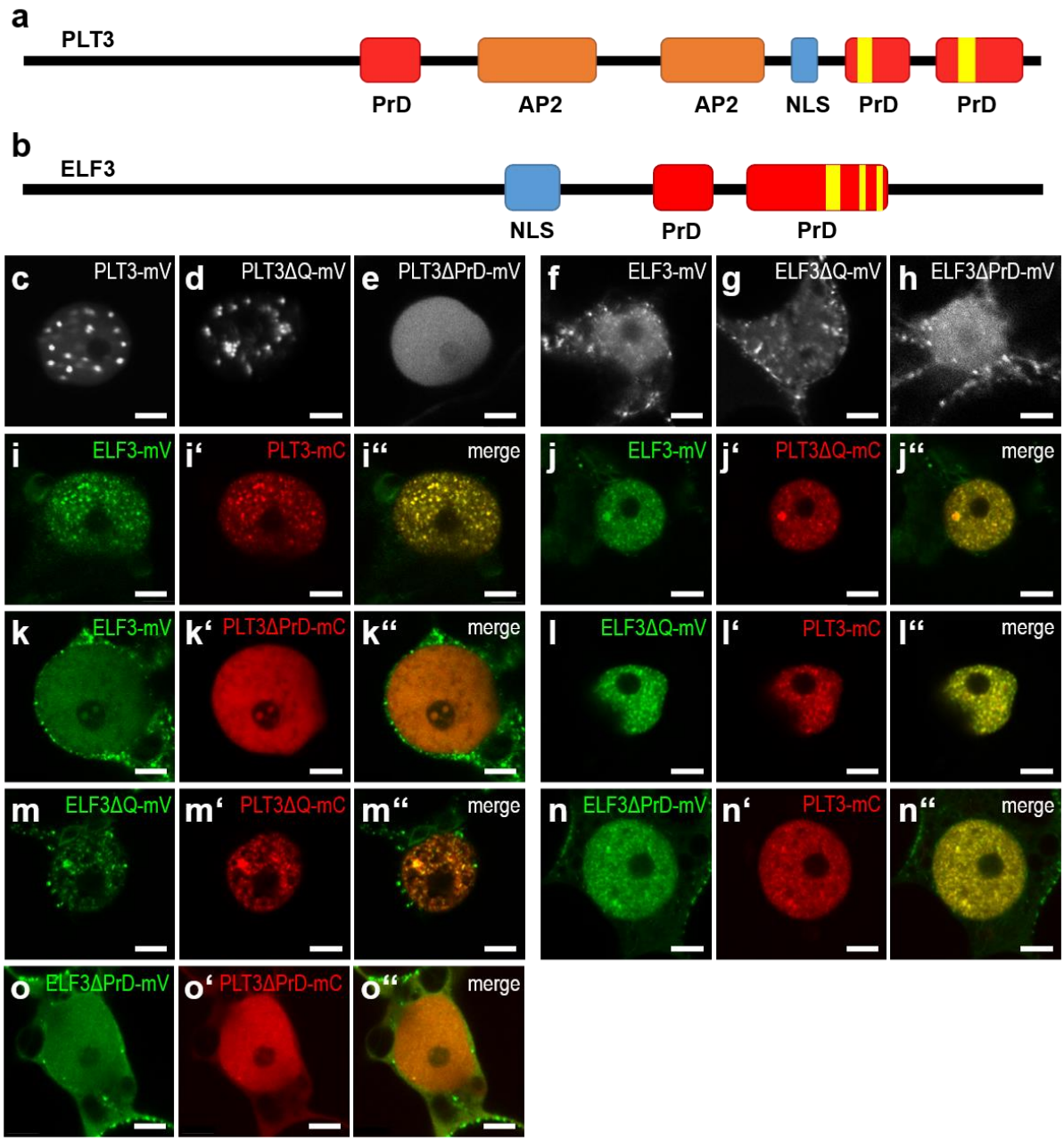

Figure V-4: Domain-dependent subcellular (co)-localisation of ELF3 and PLT3 in *N. benthamiana*

a,b, Schematic representation of the protein domains in PLT3 (**a**) and ELF3 (**b**). The prion-like domains (PrDs, red) were predicted with a web-based tool[60]. The poly-Q stretches are marked in yellow within the PrDs. AP2 domains are shown in orange, NLS in blue. **c-h,** Subcellular localisation of indicated transiently expressed mV-tagged PLT3- or ELF3-variants. **i-o'',** Subcellular localisation of indicated combinations of transiently expressed mV-tagged ELF3-variants (green) and mC-tagged PLT3-variants (red). Scale bars represent 5 µm. mV = mVenus; mC = mCherry; PrD = prion-like domain; AP2 = APETALA2 domain; NLS = nuclear localisation signal.

The localisation experiments reveal a PLT3-dependent recruitment of ELF3 to NBs. Additionally, we observed that this is accompanied by a nuclear import of ELF3 because upon co-expression of ELF3-mVenus and PLT3-mCherry, the cytoplasmic ELF3-fraction was smaller (Figure V-4i-i''). Furthermore, upon co-expression of PLT3ΔPrD-mCherry, the ELF3 variants still show a strongly visible, body-forming cytoplasmic localisation (Figure V-4k-k''; o-o''), indicating a disturbance of a potential PLT3-dependent nuclear import of ELF3.

To quantify the PLT3-dependent nuclear import of ELF3, we measured the mean fluorescence intensities of the mVenus-tagged ELF3 variants and ELF3-mVenus co-expressions with the mCherry-tagged PLT3 variants in the nucleus and cytoplasm (Figure V-5). In this experiment, a difference in the mVenus-intensity-ratio (nucleus/cytoplasm) means a translocation of the ELF3 fusion protein (values see Supplementary table V-8). No significant change is observed between the ELF3 variants (2.44 for ELF3-mVenus, 3.38 for ELF3ΔQ-mVenus and 3.17 for ELF3ΔPrD-mVenus, Figure V-5a-g). Interestingly, the intensity-ratio is about four times higher upon ELF3-mVenus/PLT3-mCherry co-expression (11.86, Figure V-5g,h-i'') than in absence of PLT3, indicating a PLT3-dependent nuclear import of ELF3. This increase is less strong when PLT3ΔQ-mCherry is co-expressed with ELF3-mVenus (7.91, Figure V-5g,j-k'') and gets totally lost upon PLT3ΔPrD-mCherry co-expression (2.59, Figure V-5g,l-m'').

Taken together, the data of the localisation and intensity studies show that ELF3 is imported to the nucleus and recruited to NBs in a PLT3-dependent manner, mediated by the PLT3 PrDs.

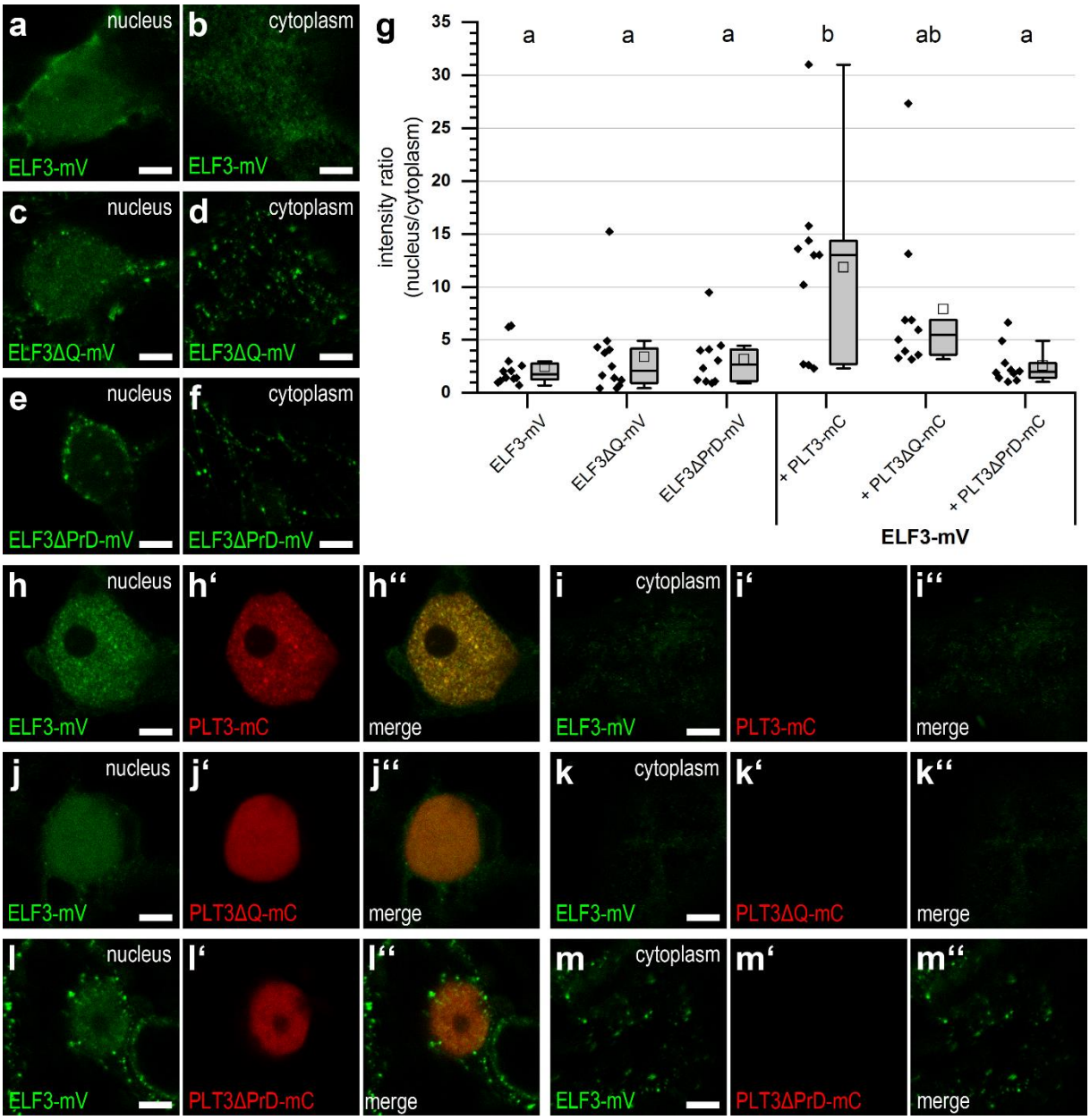

Figure V-5: PLT3-dependent nuclear recruitment of ELF3 is mediated by the PLT3 PrDs

a-f, Representative images of nuclear (left) and corresponding cytoplasmic (right) localisation of indicated mV-tagged ELF3-variants (green) in *N. benthamiana*. **g,** Nuclear/cytoplasmic mV intensity ratios are summarized in combined scatter and box plots. Statistical analysis of samples was carried out by one-way ANOVA and post-hoc multiple comparisons using the Holm-Sidak test. Samples with identical letters do not show significant differences ($\alpha = 0.01$; $n \geq 10$). Box = 25-75 % of percentile, whisker = 1.5 interquartile range, – = median, □ = mean value. **h-m'',** Representative images of nuclear (left) and corresponding cytoplasmic (right) localisation of ELF3-mV (green) with co-expression of indicated mC-tagged PLT3-variants (red) in *N. benthamiana*. Scale bars represent 5 µm. mV = mVenus; mC = mCherry.

To assess the functionality of our constructs, we performed rescue experiments in *Arabidopsis*. We already showed in previous experiments that stable *Arabidopsis* lines expressing *PLT3*-

mVenus driven by the endogenous promoter could rescue the *plt3* root phenotype[9] (see chapter IV). Furthermore, we were able to rescue the elongated hypocotyl, small leaf area and low leaf number phenotypes of the *elf3* mutant with our ELF3-mVenus construct expressed in *Arabidopsis*, driven by its endogenous promoter (Supplementary figure V-2). These morphologies are light-dependent and often defective in mutants of light-signalling pathway components[16,61–67]. Additionally, the PrD-deletion variant, ELF3ΔPrD-mVenus, also rescued these phenotypes of the *elf3* mutant (Supplementary figure V-2, Supplementary Table V-9, Supplementary table V-10, Supplementary table V-11). This indicates that the PrDs only play a minor role in the ELF3-dependent regulation of light-controlled hypocotyl-growth, leaf area and leaf number. In light of recent findings[29], the PrD-deletion variant could be defective in thermo-responsiveness, but this remains to be determined. Nevertheless, our results show that the constructs used in this study result in functional proteins.

3.4 ELF3 and PLT3 localise to bodies with different behaviour

As shown in the localisation studies (chapter V-3.3), the localisation of PLT3 to NBs strongly depends on PrDs. In contrast, our results show that the localisation of ELF3 to cytoplasmic bodies is mostly independent of its PrDs. This observation leads to the hypothesis that the nature of the PLT3 bodies and the ELF3 bodies differ from each other. To address this, we recorded 3D-time series of cytoplasmic ELF3-mVenus and nuclear PLT3-mVenus in transient *N. benthamiana* experiments and performed a tracking of the mobile bodies (Figure V-6).

The data obtained from the tracking revealed that the behaviours of the ELF3- and PLT3-bodies are indeed different. First, we observed fusion and fission events for the cytoplasmic ELF3-bodies (Figure V-6a-a'',b-b''), indicating a liquid-like behaviour that was not observed for the PLT3 NBs. Moreover, the PLT3 NBs do not cover a big distance but rather stay around their origin, indicated by the low displacement length of 0.50 ± 0.16 µm, while the cytoplasmic ELF3-bodies move much further, as indicated by the higher displacement length of 2.53 ± 4.33 µm (Figure V-6c,d,f). This is accompanied by a more than 10-times higher speed for ELF3 (0.74 ± 0.08 µm/s) compared to PLT3 (0.06 ± 0.001 µm/s) (Figure V-6e). Additionally, we observed that the speed of the ELF3-bodies strongly depends on their mean intensity, where dark bodies are faster than bright ones (Figure V-6g). A higher intensity means a higher number of fluorophores, hence a bigger accumulation of proteins. It is not surprising that bigger aggregates move slower, but in case of PLT3 this effect is much weaker (Figure V-6h), indicating a disturbance in mobility, probably due to its nuclear environment which could involve e.g. DNA-binding.

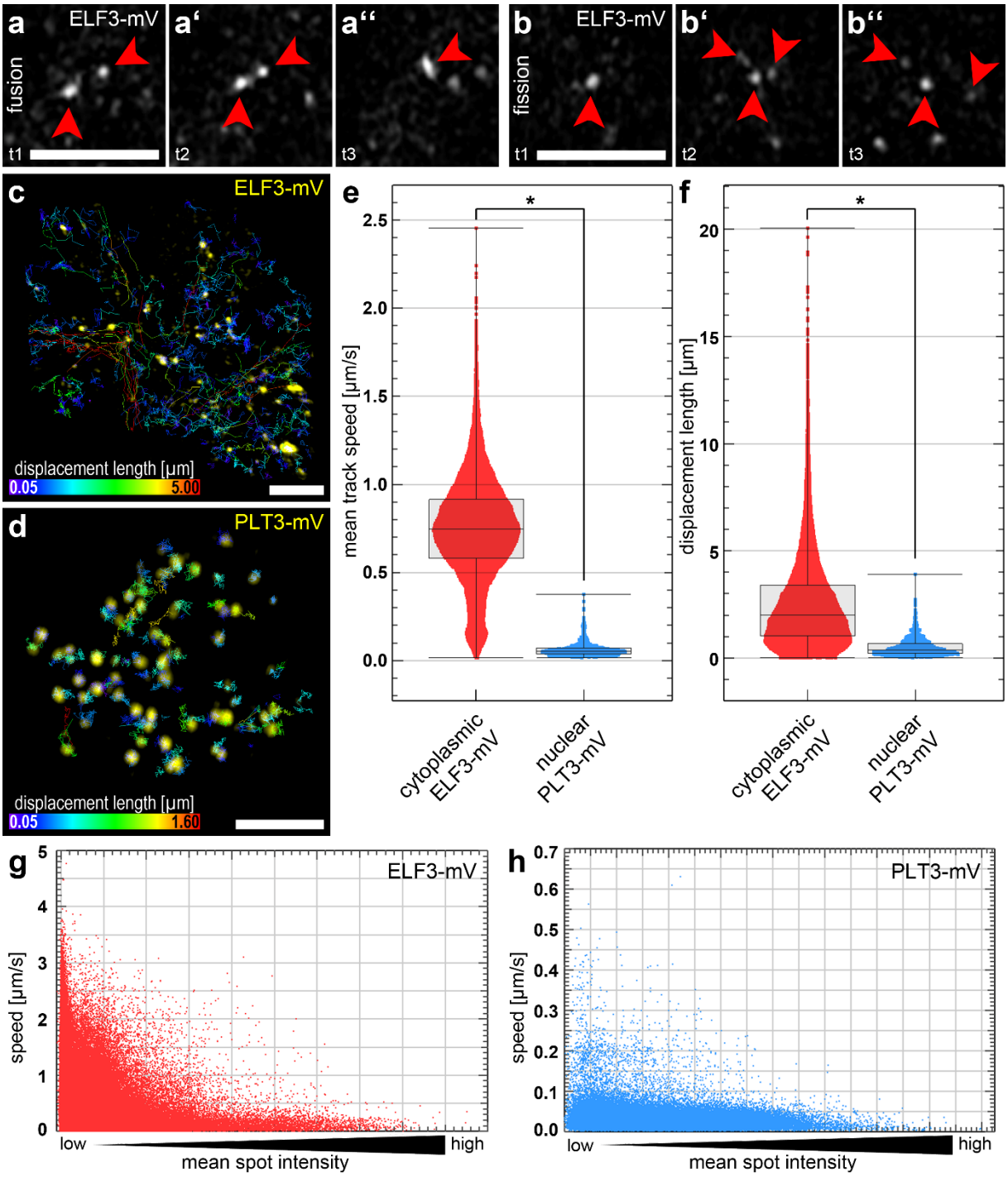

Figure V-6: Tracking reveals a higher mobility for ELF3 bodies than PLT3-bodies in *N. benthamiana*. **a-a'',** Example for a fusion event of two ELF3-mV bodies. Three time points (t1-t3) are shown. Red arrowheads point at the fusing bodies. **b-b'',** Example for a fission event of an ELF3-mV body. Three time points (t1-t3) are shown. Red arrowheads point at the body that fissions into three. **c,d,** Representative MIP-images of tracking experiments of cytoplasmic ELF3-mV (**c**, yellow) and nuclear PLT3-mV (**d**, yellow). Colour-coded lines represent tracks of the mobile bodies where the colour represents the displacement length in µm (colour-scale see regarding image). **e,f,** Box and scatter plots of the mean track speed (**e**) and the track displacement length (**f**) of cytoplasmic ELF3-bodies (red) and nuclear PLT3-bodies (blue). Asterisks mark statistically significant differences, analysed with the Kolmogorov-Smirnov-Test and a confidence level of 0.01. The data and number of data points is

summarized in Supplementary table V-12. Box = 25-75 % of percentile, whisker = minimum/maximum – = median. **g,h,** Scatter plots of the speed of the tracked ELF3-bodies (**g**, red) and PLT3-bodies (**h**, blue) in dependence of their mean mV intensity. Scale bars represent 5 µM. MIP = maximum intensity projection; mV = mVenus.

The tracking results reveal a potentially liquid-like nature of the ELF3-bodies, which has recently been proposed[29]. Additionally, the cytoplasmic ELF3-bodies differ strongly in mobility from the PLT3 NBs, which are much slower and more tied to their origin.

3.5 ELF3 and PLT3 interaction is mediated by the PrDs

The observed strong co-localisation in NBs prompted us to look for a potential interaction of ELF3 and PLT3 and whether this interaction depends on the PrDs or the polyQ-stretches of both proteins. Therefore, we performed Fluorescence Lifetime Imaging Microscopy (FLIM, Figure V-7) in transient *N. benthamiana* experiments. Interaction measurements with FLIM are based on Förster-Resonance-Energy-Transfer (FRET), taking place when two fluorophores are in very close proximity (< 10 nm), resulting in the reduction of the fluorescence lifetime of a donor fluorophore that transmits energy to the acceptor fluorophore[68].

We used mVenus-tagged ELF3 variants as donors (ELF3-mV, ELF3ΔQ-mV and ELF3ΔPrD-mV) and mCherry-tagged PLT3 variants as acceptors (PLT3-mC, PLT3ΔQ-mC and PLT3ΔPrD-mC) for FLIM. As negative controls, free mCherry was co-expressed with the respective donor. The negative controls did not show a significant decrease in mVenus fluorescence lifetime compared to the regarding donor-only samples ($\Delta\tau = 0.03 \pm 0.04$ ns for ELF3-mV and free mCherry co-expression, $\Delta\tau = 0.04 \pm 0.04$ ns for ELF3ΔQ-mV and free mCherry co-expression, $\Delta\tau = 0.02 \pm 0.04$ ns for ELF3ΔPrD-mV and free mCherry co-expression) (Figure V-7b,g,k,n). A strong lifetime reduction of 0.53 ± 0.26 ns was detected upon PLT3-mC co-expression, compared to the ELF3-mV donor-only (Figure V-7c,n), indicating an interaction of the full-length ELF3 and PLT3 proteins. This lifetime reduction is decreased to only 0.26 ± 0.17 ns when PLT3 is lacking the poly-Q-stretches (PLT3ΔQ-mC, Figure V-7d,n), probably due to a weaker interaction of both proteins. This is even more severe with the PrD-deletion variant of PLT3 (PLT3ΔPrD-mC), where no significant decrease in fluorescence lifetime can be detected anymore ($\Delta\tau = 0.10 \pm 0.15$ ns, Figure V-7e,n), indicating a loss of the interaction.

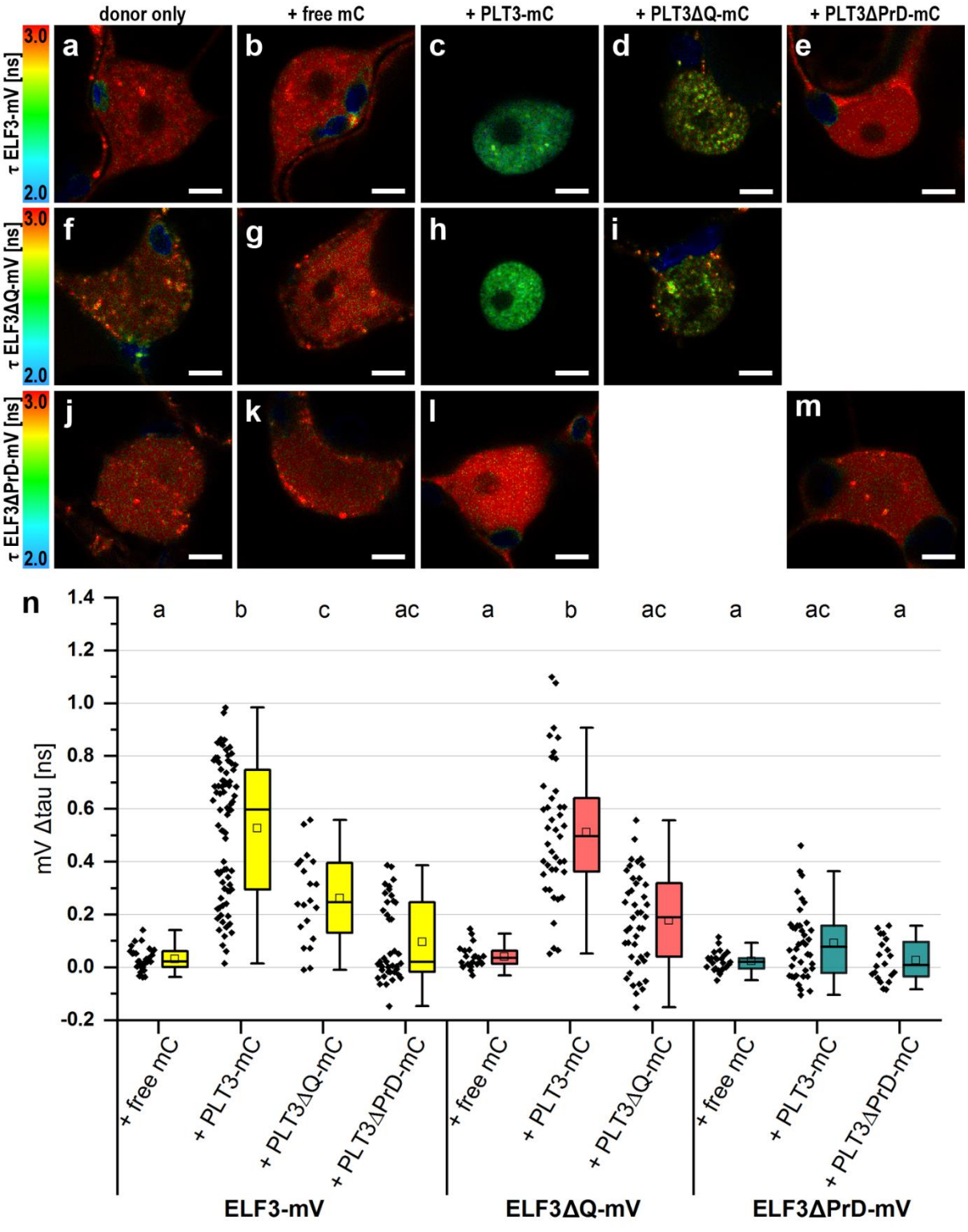

Figure V-7: ELF3 and PLT3 interaction is mediated by the PrDs in *N. benthamiana*

a-m, Representative mVenus (mV) fluorescence lifetime images of indicated mV-tagged ELF3-variants alone or in combination with free mCherry (mC) and mC-tagged PLT3-variants. The mV fluorescence lifetime is colour-coded from blue (short lifetimes) to red (long lifetimes). The regarding colour-scales in ns are shown on the left. Dark blue structures are chloroplasts and were not included in data analysis. Scale bars represent 5 µm. **n,** Reduction in fluorescence lifetime [ns] compared to the respective donor only samples are summarized in

combined scatter and box plots. Statistical analysis of samples was carried out by one-way ANOVA and post-hoc multiple comparisons using the Holm-Sidak test. Samples with identical letters do not show significant differences ($\alpha = 0.01$; $n \geq 20$). Box = 25-75 % of percentile, whisker = 1.5 interquartile range, – = median, □ = mean value.

The FLIM-results reveal that a lack of the PLT3 poly-Q-stretches located in the PrDs does not lead to a complete loss of interaction but the full deletion of the PrDs does. This indicates that the PLT3-PrDs are the domains responsible for PLT3/ELF3 interaction, supporting the data obtained in the localisation studies, revealing the PLT3-PrD dependent nuclear import and NB recruitment of ELF3. When the ELF3ΔQ-mV is used as donor for the FLIM measurements, a lifetime reduction of 0.51 ± 0.26 ns for PLT3-mC co-expression can be measured (Figure V-7h,n), which is not significantly different to the reduction measured with the full-length ELF3 protein, indicating that the polyQs in ELF3 do not, or not alone, mediate the interaction with PLT3. When PLT3ΔQ-mC is co-expressed with ELF3ΔQ-mV the lifetime reduction of 0.18 ± 0.18 ns is less strong but not significantly different to the regarding co-expression with full length ELF3 (Figure V-7i,n), showing that the ELF3-polyQs are not necessary for interaction. Concerning the ELF3 PrDs, none of the combinations using ELF3ΔPrD-mV as donor for FLIM do show a significant lifetime reduction, indicating that the PrDs in ELF3 are necessary for interaction with PLT3 (Figure V-7l,m,n). All mean lifetime values obtained in the FLIM experiments can be found in Supplementary table V-13.

Taken together, the data obtained by FLIM experiments reveals that the PrDs in PLT3 and ELF3 mediate the interaction of both proteins.

3.6 PIFs as mediators for ELF3 translocation and PLT3-ELF3 complex formation

The transient *N. benthamiana* expression system allows reliable subcellular localisation- and interaction studies *in planta* and is therefore a useful tool to examine plant proteins in a close-to-native environment. Yet, the presence of a variety of other plant proteins could affect the observed processes, including protein localisation and complex formation. For this reason, we used mammalian HEp-2 cells as an orthogonal system for transient protein expression. We asked, if we observe similar (co-) localisation of PLT3 and ELF3 in this environment free of other plant proteins. Supporting the transient *N. benthamiana* experiments, we observed comparable subcellular localisations of individually expressed mVenus-tagged PLT3 and ELF3 in transient HEp-2 cell experiments, assuming conserved mechanisms. PLT3-mVenus localises predominantly to the nucleus and forms NBs (Figure V-8a), whereas ELF3-mVenus is mostly cytoplasmic, forming cytoplasmic bodies, but also localises to a lower extend to the nucleus (Figure V-8b).

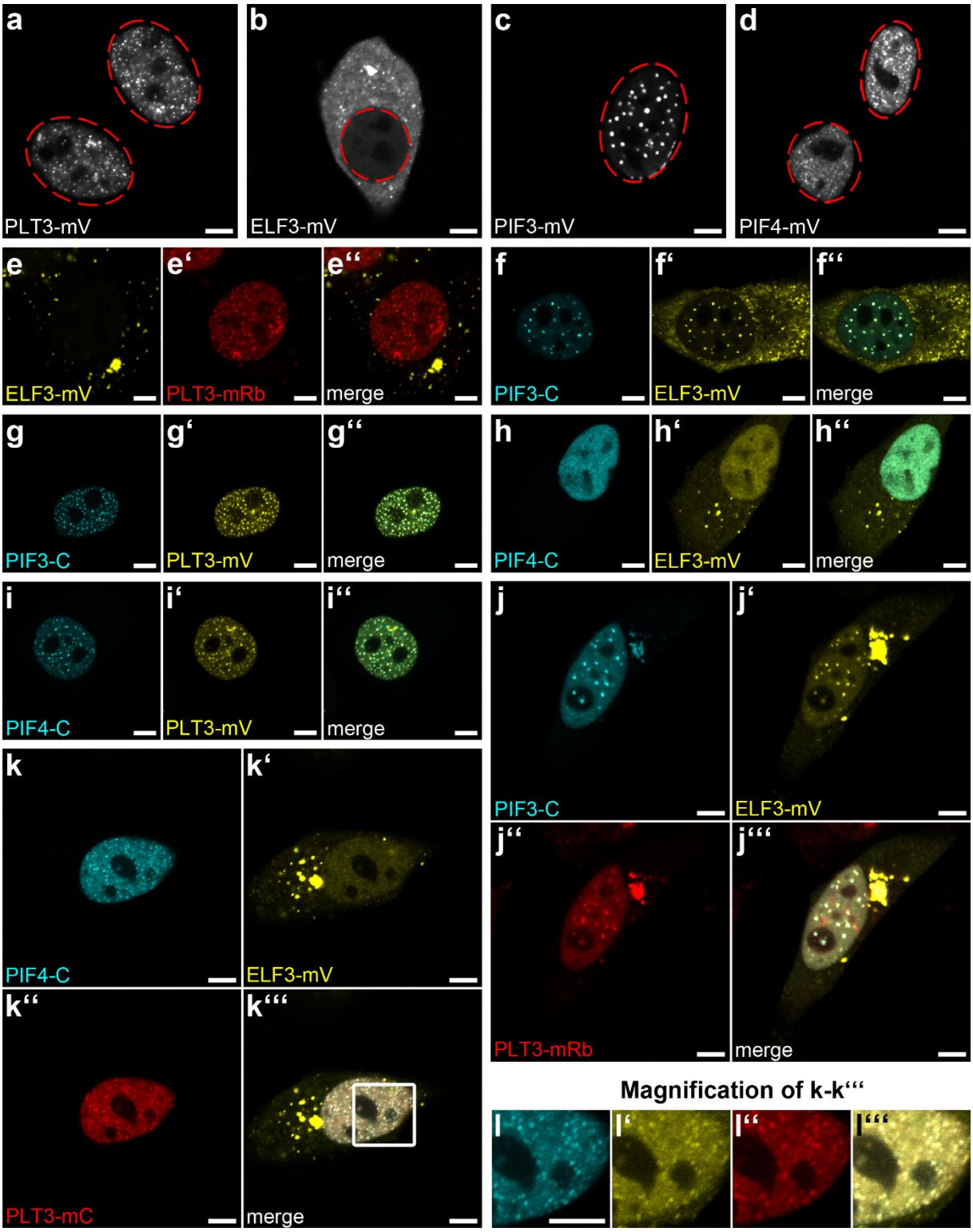

Figure V-8: PIF3 and PIF4 import ELF3 to the nucleus and co-localise with PLT3 in HEp-2 cells

a-d, Subcellular localisation of mV-tagged PLT3 (**a**), ELF3 (**b**), PIF3 (**c**), and PIF4 (**d**) in HEp-2 cells. Nuclei are outlined in red. **e-e’’,** ELF3-mV (yellow) localises to cytoplasmic bodies when co-expressed with PLT3-mRb (red), which forms NBs. **f-f’’,h-h’’,** ELF3-mV (yellow) co-localises with PIF3-C (**f**, cyan) and PIF4-C (**h**, cyan) in the nucleus. **g-g’’,i-i’’**, PLT3-mV co-localises with PIF3-C (**g**) and PIF4-C (**i**) in NBs. **j-k’’’**, FP-tagged ELF3 (yellow) and PLT3 (red) colocalise in the nucleus with PIF3-C (**j**, cyan) and PIF4-C (**k**, cyan). **l-l’’’,** Magnification

of k-k'''. Scale bars represent 5 µm. FP = fluorescent protein; mV = mVenus; mRb = mRuby2; C = Cerulean; mC = mCherry.

In contrast to the observations from *N. benthamiana* experiments, ELF3-mVenus still localises predominantly to the cytoplasm and no co-localisation with the PLT3-mRuby2 NBs can be observed during co-expression in HEp-2 cells (Figure V-8e-e''), indicating that PLT3 alone is not able to recruit ELF3 to NBs. Interestingly, published experiments in mammalian expression systems revealed that PIF3 is responsible for the nuclear import of another factor involved in light-response. In HeLa cells, PIF3 binds and shuttles the photo-activated PHYTOCHROME B (phyB) to the nucleus where it co-localises to the PIF3 NBs[69]. This prompted us to ask if PIFs could act as a mediator for nuclear shuttling and facilitate complex formation of ELF3 and PLT3. As part of the evening complex, ELF3 is known to regulate *PIF4/5* expression. PIF4/5 promote hypocotyl growth and are repressed by the evening complex in the evening[16]. Interestingly, a similar growth promoting role has been reported for PIF3[21] which additionally has been shown to play a role in root growth inhibition[70]. As ELF3 is also known to interact with several PIF proteins, including PIF4[42,46], the question arises if PIFs are involved in root meristem regulation, possibly through mediating ELF3-PLT3 interaction. In our HEp-2 experiments, both, PIF3-mVenus and PIF4-mVenus localise to the nucleus, forming NBs, where the PIF3-NBs are mostly bigger than the ones formed by PIF4 (Figure V-8c,d). Remarkably, when ELF3-mVenus is co-expressed with PIF3-Cerulean, a strong co-localisation of ELF3 and PIF3 to NBs can be observed, additionally to the cytoplasmic localisation of ELF3-mVenus (Figure V-8f-f''), indicating a PIF3-dependent recruitment of ELF3 to NBs. Also, PLT3-mVenus co-localises with PIF3-Cerulean to NBs upon co-expression (Figure V-8g-g''). The same observations can be made when PIF4-Cerulean is co-expressed with either ELF3-mVenus or PLT3-mVenus, where both co-localise with PIF4-Cerulean in the nucleus (Figure V-8h-h'', i-i'') suggesting that PIF4 is also able to recruit ELF3 to the nucleus. Furthermore, we co-expressed FP-tagged ELF3 and PLT3 together with either PIF3 (Figure V-8j-j''') or PIF4 (Figure V-8k-k''' and l-l''') and could observe in both cases a co-localisation of all three proteins to NBs. This data reveals that PIF3 and PIF4 can translocate ELF3 to the nucleus, possibly enabling its recruitment to NBs and interaction with PLT3.

3.7 PIF3 and PIF4 co-localise and interact with PLT3 *in planta*

We further aimed to investigate the localisation of PIF3 and PIF4 and their interaction with PLT3 *in planta*. Therefore, we performed transient *N. benthamiana* experiments with FP-tagged PIF3 and PIF4 (Figure V-9).

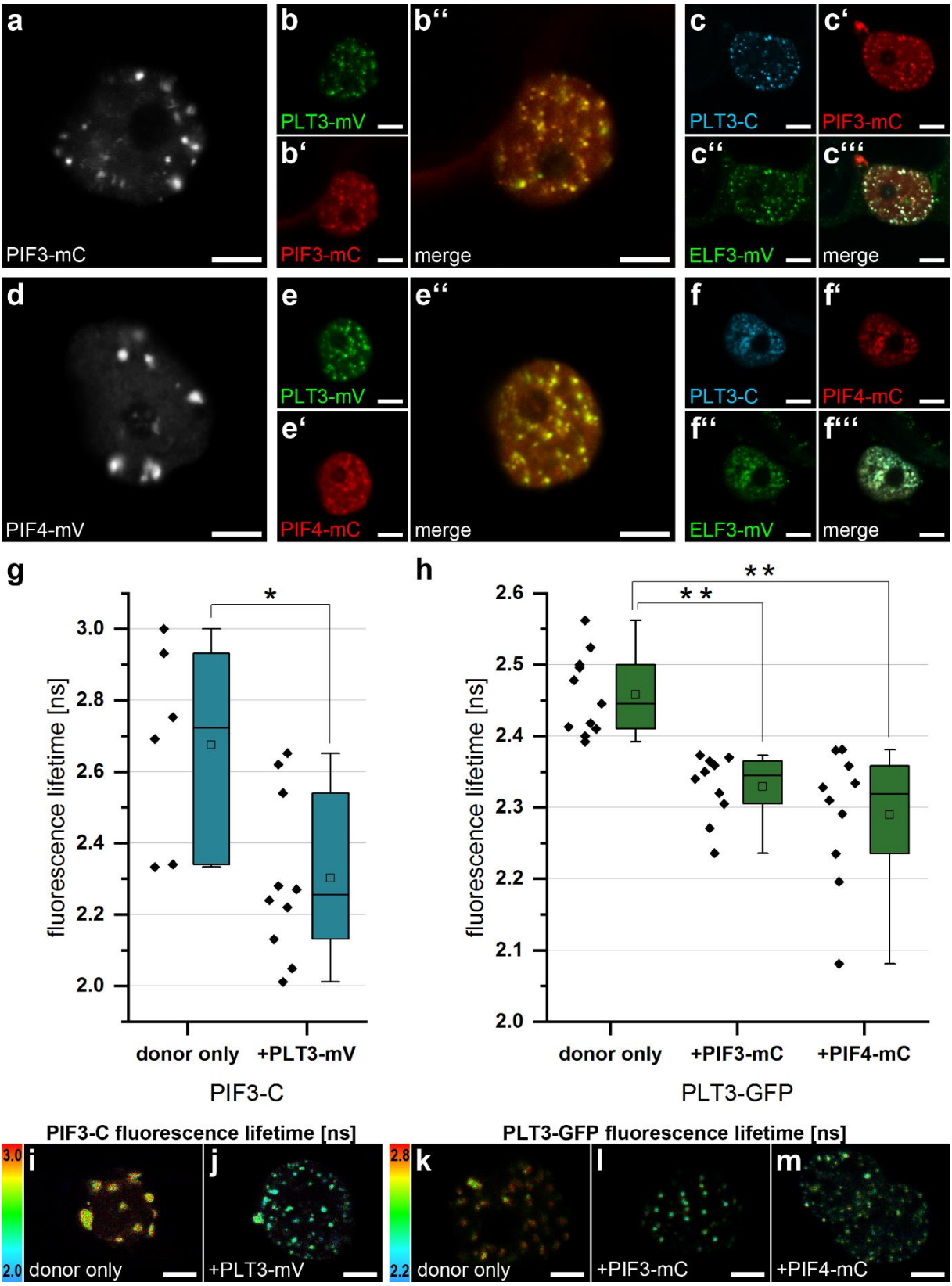

Figure V-9: PLT3 co-localises and interacts with PIF proteins in *N. benthamiana*

a, Subcellular localisation of PIF3-mC to NBs. **b-b'',** Co-localisation of PLT3-mV (green) and PIF3-mC (red) to NBs. **c-c''',** Co-localisation of PLT3-C (blue), PIF3-mC (red) and ELF3-mV (green) to NBs. **d,** Subcellular localisation of PIF4-mV to NBs. **e-e'',** Co-localisation of PLT3-mV (green) and PIF4-mC (red) to NBs.

f-f'', Nuclear co-localisation of PLT3-C (blue), PIF4-mC (red) and ELF3-mV (green). **g,h,** Fluorescence lifetimes in ns of PIF3-C (**g**) and PLT3-GFP (**h**) FLIM experiments are summarized in combined scatter and box plots. Statistical analysis of samples was carried out by one-way ANOVA and post-hoc multiple comparisons using the Holm-Sidak test. Asterisks indicate significant differences (*: $\alpha = 0.05$, $n \geq 6$; **: $\alpha = 0.01$, $n \geq 10$). Box = 25-75 % of percentile, whisker = 1.5 interquartile range, – = median, □ = mean value. **i,j,** Representative fluorescence lifetime images of PIF3-C FLIM experiments. The fluorescence lifetime in ns is colour-coded, the colour scale is shown on the left. **k-m,** Representative fluorescence lifetime images of PLT3-GFP FLIM experiments. The fluorescence lifetime in ns is colour-coded, the colour scale is shown on the left. Scale bars represent 5 µm. mV = mVenus; mC = mCherry; C = Cerulean; GFP = green fluorescent protein; NB = nuclear body; FLIM = fluorescence lifetime imaging microscopy.

Both, PIF3 and PIF4 localise in part homogenously in the nucleoplasm and additionally form bright subnuclear structures (Figure V-9a,d), as observed in the HEp-2 experiments before. When PIF3-mCherry or PIF4-mCherry are co-expressed with PLT3-mVenus, they co-localise to NBs (Figure V-9b-b'', e-e''). The co-expression of all three proteins (PLT3-Cerulean, ELF3-mVenus and PIF3- or PIF4-mCherry) leads to a co-localisation of all of them to NBs (Figure V-9c-c''', f-f''').

To investigate the interaction of PLT3 with PIF3 and PIF4 we performed FLIM in transient *N. benthamiana* experiments. We used two different combinations of FP-tags. In a first experiment, PIF3-Cerulean acted as donor and PLT3-mVenus as acceptor fluorophore. In a second experiment we used PLT3-GFP as donor and mCherry-tagged PIF3 or PIF4 as acceptor fluorophore. In the first described setup, the fluorescent lifetime drops significantly from 2.68 ± 0.29 ns of the donor only (PIF3-Cerulean, Figure V-9g,i) to 2.30 ± 0.23 ns with PLT3-mVenus co-expression (Figure V-9g,j), indicating a strong interaction of both proteins. The second fluorophore combination shows a lifetime decrease from 2.46 ± 0.06 ns of the donor only (PLT3-GFP, Figure V-9h,k) to 2.33 ± 0.05 ns for co-expression with PIF3-mCherry (Figure V-9h,l) and 2.29 ± 0.09 ns for co-expression with PIF4-mCherry (Figure V-9h,m), indicating an interaction of PLT3 with PIF3 and PIF4.

This data reveals a possible involvement of the PIF proteins PIF3 and PIF4 in root SCN homeostasis through complex formation with PLT3 and ELF3.

4. Discussion

We revealed for the first time that ELF3 is expressed in the root of *Arabidopsis thaliana*, where it localises to nuclear foci, herein called NBs. Hence, ELF3 shares an overlapping expression pattern with PLT3 in the root, including the meristematic zone, where PLT3 is strongly expressed. Both proteins have prion-like IDRs in their protein sequence and form body-like structures in transient *N. benthamiana* experiments and in their endogenous environment in *Arabidopsis*, where they are nuclear localised[9,38] (Figure V-1). These common traits of PLT3 and ELF3 prompted us to look at their subcellular localisation in more detail. We found that their subcellular localisation differs in transient *N. benthamiana* experiments. PLT3 localises in the nucleus to NBs whereas the majority of the ELF3 protein is cytoplasmic, forming bodies. Apart from their localisation, the nature of these bodies also seems to differ since we observed strong differences in mobility. The different behaviour of the ELF3- and PLT3-bodies could be in part due to their different environment, as the cytoplasmic ELF3 is much more mobile than the nuclear PLT3. Nevertheless, the discrepancies are very strong, which could additionally be explained by different underlying mechanisms for the formation of phase-separated droplets. As ELF3 is highly mobile and also shows fusion and fission events, indicating a liquid-like behaviour, the underlying body-forming mechanism could be liquid-liquid phase separation (LLPS), which is in line with recent findings, where it was additionally shown that ELF3-bodyformation is concentration-dependent[29]. The lower mobility and the missing fusion and fission events in case of the PLT3-bodies could be a hint for a higher viscosity and a different phase-forming state. This still remains to be determined, particularly because the lower mobility of the PLT3-bodies can at least partially be explained by their nuclear environment, e.g. through DNA-binding.

The cytoplasmic localisation of the ELF3-bodies in the *N. benthamiana* experiments indicates a missing factor for a nuclear import, as ELF3 is typically nuclear-localised in *Arabidopsis*. However, in the transient *N. benthamiana* experiments, ELF3 and PLT3 co-localise and interact in the nucleus upon co-expression, revealing that ELF3 can be translocated to the nucleus. The localisation of PLT3 to NBs depends on the PrDs in the protein sequence, indicating a PrD-dependent phase-separation. In contrast to this, our results show that the ELF3 body-formation is mostly independent of its PrDs, demonstrating that possibly another domain is important for the formation of phase-separated droplets. Additionally, the PrDs are not essential for the ELF3-dependent control of light-regulated hypocotyl-growth, leaf area and leaf number, implying that not the PrDs but rather the body-formation could be important for the light-dependent ELF3-

function, which remains to be examined. Remarkably, it has been found recently that the PrDs of ELF3 mediate reversible phase separation in response to temperature, thereby allowing ELF3 to switch between an active and inactive state[29]. This supports our hypothesis that the phase-separated bodies are important for proper functionality of the ELF3 protein. Interestingly, the ELF3 co-localisation with PLT3 is independent of the ELF3 PrDs, but both, ELF3 and PLT3 PrDs mediate protein interaction. Consequently, the recruitment of ELF3 to NBs does not depend on its PrDs and is hence independent of the interaction with PLT3. This could be a hint for a possible involvement of additional factors in the nuclear import of ELF3 and its recruitment to NBs. Therefore, we studied the localisation in a more neutral plant-protein-free environment, using mammalian HEp-2 cells for transient expression. Indeed, the subcellular localisation in HEp-2 cells is comparable to the one in *N. benthamiana*: Individually expressed, PLT3 localises to NBs and ELF3 forms cytoplasmic bodies. Interestingly, in co-expression experiments, no co-localisation is observed, indicating that PLT3 alone is not responsible for the nuclear import of ELF3. As expected, another factor is needed to mediate the recruitment of ELF3 to NBs. Here, we found that both, PIF3 and PIF4, are sufficient to import ELF3 to the nucleus. All analysed proteins, PIF3, PIF4, and ELF3, co-localise with PLT3. As PIF3 was already shown to import light-activated phyB to the nucleus[69], the question arises if PIFs act as general mediators for nuclear import of components in circadian/light-dependent pathways, but this needs to be determined. We additionally found that PIF3 and PIF4 co-localise with PLT3 and ELF3 in *N. benthamiana* and could determine an interaction of both PIFs with PLT3. As shown before, several PIFs, including PIF4, also interact with ELF3[42,46]. Possibly, they all reside in the same complex. PIF-containing NBs have been reported in conjunction with light signalling, where they are proposed to act as sites to trigger PIF degradation. PIF degradation is a major step in light signalling and has been described for several PIFs including PIF3 and PIF1[71–75]. The photoactivation of phytochromes induces PIF3 NB formation, phosphorylation, and subsequent degradation by direct interaction, followed by dissolution of the so-called photobodies[71,72,74]. Additionally, a similar mechanism has been reported for PIF1, that localises to phyB-photobodies and is phosphorylated after light-induction, followed by ubiquitination and subsequent degradation[75]. The localisation of phyB to photobodies and accompanied repression of PIF3 accumulation is necessary for the photoinhibition of hypocotyl elongation[73]. Similarly, the NBs formed with the PLT3-ELF3-PIF complex could represent sites either for degradation or for sequestration of PIFs and maybe also ELF3 or even PLT3.

To assess a possible role for ELF3 in root meristem organisation, possibly coinciding with PLT3, we explored the SCN phenotype and thereby uncovered a link between environmental

stimuli and SCN homeostasis, as ELF3 is an important player of light- and clock-signalling. We previously showed, that PLT3 and WOX5 positively influence CSC maintenance and QC quiescence[9] (see chapter IV). In the case of ELF3, we can report a similar effect in CSC maintenance, as the *elf3* mutant roots showed a higher frequency in differentiated roots, but it additionally had a slightly higher frequency of roots showing more than one CSC layer. The CSC deficiencies correlate with roots showing more QC divisions. This means that the maintenance of one defined CSC layer through ELF3 correlates with a positive influence on QC quiescence. However, the *plt3* single mutant also strongly shifted to a higher root differentiation and less QC quiescence. The QC phenotype is additive as the *elf3, plt3* double mutant showed even more QC divisions than the single mutants but the CSC phenotype stayed rather comparable to the single mutants, suggesting a potentially interdependent role of ELF3 and PLT3 in CSC maintenance. In total, a disturbance in QC quiescence seems to cause a loss of a defined number of CSC layers.

Recently, we proposed a model where PLT3 and WOX5 regulate CSC maintenance together by the formation of protein complexes, where NB formation functions as a marker for future cell fate determination[9] (see chapter IV). The dynamic and PrD-dependent compartmentalisation to microdomains could serve as a fast and reversible regulatory mechanism[53] e.g. for the determination of the CSC cell fate and future differentiation to CCs. In this study we add ELF3 and PIFs to the model, where ELF3 is also part of the NB-forming protein complex in the CSC layer to determine the cell fate that is necessary for the balanced production of differentiated CCs (Figure V-10). In this model, upon certain environmental stimuli, the ELF3-NBs are ubiquitously present in the cells of the RAM, potentially stabilized by PIF proteins that are responsible for the nuclear import of ELF3 (Figure V-10a). PIFs are present in tissues of the RAM, as shown previously[76,77]. The recruitment of ELF3 and interaction with PLT3 in the NBs occurs in CSCs as a marker for cell fate determination and could depend on the concentration of the available PLT3 protein. Supporting this, we previously reported that the formation of PLT3-NBs is concentration dependent (see chapter IV). PLT3 in turn recruits WOX5 to the NBs. The so-assembled foci could act as transcriptionally active sites for the gene-regulation involved in CSC fate determination (Figure V-10b). If one player is missing, this leads to a mis-determination in cell fate and hence to a loss of one defined CSC-layer.

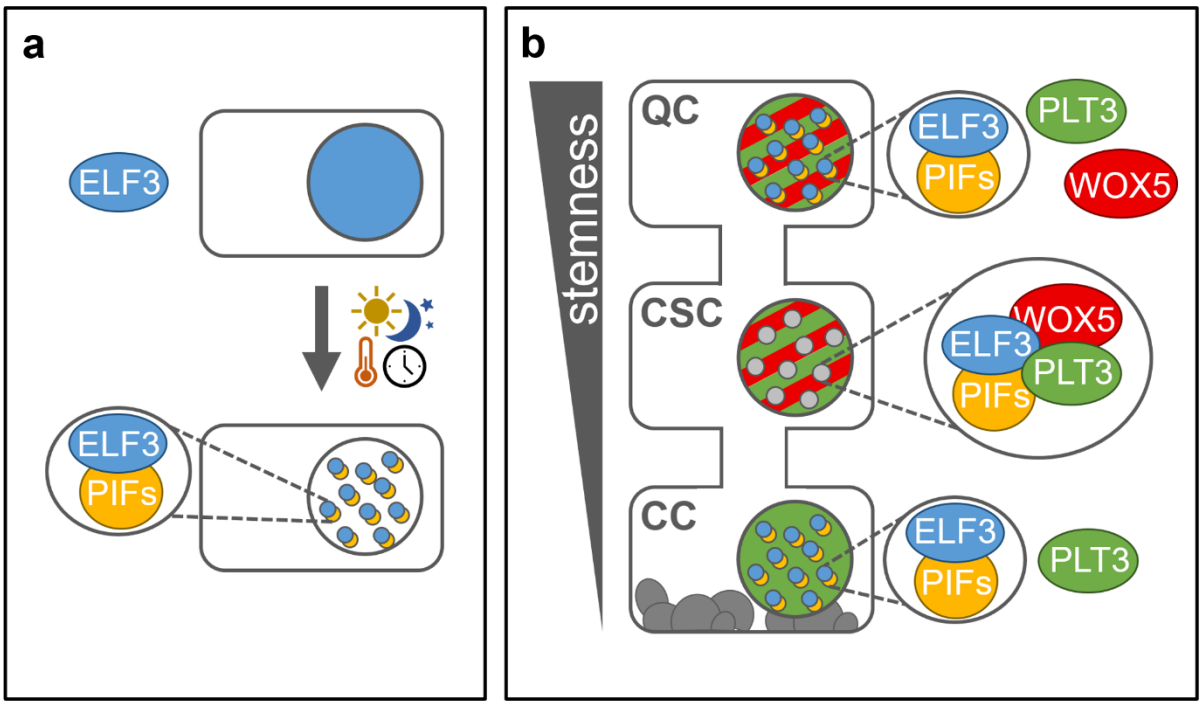

Figure V-10: Model of *A. thaliana* distal root stem cell fate regulation via dynamic differential subnuclear localisation of transcription factor complexes, integrating external cues through ELF3

a, First, ELF3 (blue) localises homogenously in the nucleus. After induction through light, day length or temperature, ELF3 translocates to NBs, stabilized by PIF proteins (yellow). **b,** During CSC fate determination, ELF3 (blue), PIFs (yellow), PLT3 (green) and WOX5 (red) form a complex that localises to NBs in the CSCs, which act as marker for future cell differentiation. PLT3 and WOX5 are additionally homogenously present in the nucleus. In response to the before occurred environmental stimulus, the CSC fate is directed towards maintenance or differentiation, resulting in one CSC-layer and the adjacent differentiated CCs. In the QC and the maintained CSC, WOX5 and PLT3 are homogenously present in the nucleus, whereas WOX5 is lacking in the differentiated CCs. The ELF3-NBs, stabilized by PIFs, are ubiquitously present. Grey structures in CCs represent starch granules. CSC = columella stem cell; CC = columella cell; QC = quiescent centre; NB = nuclear body.

With the addition of the circadian clock-related ELF3 to our model, a link to a potential involvement of environmental stimuli such as light, day-length and, importantly, temperature in the regulation of the SCN homeostasis is generated. These external cues could also have an influence on the NB-formation, as it has been shown for thermoresponsiveness[29], and thereby regulating the CSC-fate towards a higher or lower number of stem cells, depending on the need of the plant to adapt to the changing environment. ELF3 has been proposed to act as a hub that links a range of different processes which comprises not only clock-, light and temperature-dependent signalling but also photosynthesis, hormone signalling and growth, thereby responding on a variety of environmental signals[16,25–29]. Because of this, a subcellular translocation to flexible microdomains could be a mechanism for the spatial and temporal separation of the different cellular processes where ELF3 is involved. A similar mechanism has

already been discussed for plant-receptor complexes at the plasma-membrane, where a spatio-temporal separation of signal-transduction in response to different external and internal cues is achieved by microdomain-formation[78] (see chapter II).

5. Methods

5.1 Cloning

The GreenGate cloning method[79] was used to create the expression vectors in Supplementary table V-4. The sequences upstream of the ATG start codon of ELF3 (3542) and PLT3 (4494) were used as promoter regions. The promoters, as well as the Cytomegalovirus (CMV) promoter, a strong constitutive promoter for expression in mammalian cells, were cloned in the GreenGate entryvector pGGA000 via *BsaI* restriction and ligation. The GreenGate promoter module carrying the β-estradiol inducible cassette was provided by[80]. Internal *BsaI* restriction sites in the PIF4 sequence were removed by PCR amplification using primers with an altered nucleotide sequence at this site (Supplementary Table 1), resulting in two gene fragments that were subsequently reconnected by an overlap extension PCR. The CDS of ELF3, ELF3ΔPrD, PLT3, PLT3ΔPrD, PIF3 and PIF4 were cloned in entry vector pGGC000 and the FPs mVenus and mCherry in pGGD000 via *BsaI* restriction and ligation. The C-tag module carrying the FP Cerulean (pBLAD002) was a kind gift from Dr. Andrea Bleckmann, University of Regensburg. All entry vectors were confirmed by sequencing. The expression cassettes were created with a GreenGate reaction using pGGZ001 as destination vector. The correct assembly of the modules was confirmed by sequencing. All primer used for GreenGate cloning can be found in Supplementary Table 1.

The Gateway® cloning method (Invitrogen™, Thermo Fisher Scientific Inc.) was used to create the expression vectors in Supplementary table V-5. The CDS of ELF3, ELF3ΔQ, PLT3, PLT3ΔQ and mCherry were cloned into pENTR/D-TOPO®. The entry vectors were confirmed by sequencing. The Gateway destination vector carrying the mVenus (pRD04) originates from pMDC7[81] that contains the cassette for β-estradiol inducible expression *in planta*. The mVenus was introduced via restriction/ligation C-terminally to the Gateway cloning site. The destination vectors with C-terminally located GFP (pABindGFP) and mCherry (pABindmCherry) were described before[82]. The Gateway destination vectors for mammalian cell culture (pH-Ch-N and pH-mRuby2-N) were a kind gift from Christian Hoischen, Leibniz Institute on Aging - Fritz-Lipmann-Institute, Jena. The mammalian Gateway destination vector carrying the mVenus for C-terminal fusion (pRD10) is based on these vectors and the mVenus was introduced via restriction/ligation. A subsequent LR-reaction of entry and destination vectors was carried out to create the expression vectors. The Gateway expression vectors were verified by test digestion. All primer used for Gateway cloning can be found in Supplementary Table 2.

The domain deletion variants of ELF3 (ELF3ΔQ and ELF3ΔPrD) were created by amplifying the sequences upstream and downstream of the deletion. The PrDs were replaced by a 27 aa linker (aagaaggagggaaaaaggagaaaaaga). Fragments and linker were reconnected by overlap extension PCR. The PLT3 deletion variants (PLT3ΔQ and PLT3ΔPrD) have been described before[9] (see chapter IV-5.1).

5.2 Plant work

All *Arabidopsis* lines used in this study were in the *Columbia* (*Col-0*) background. The *elf3-1* and *plt3-1* single mutants have been described before[8,83]. The homozygous *elf3, plt3* double mutant was created by crossing (Supplementary table V-6). The homozygous *plt3* genotype was confirmed by PCR (primer pairs see Supplementary table V-3), to obtain the homozygous *elf3* genotype, a selection regarding the elongated hypocotyl phenotype was performed. All transgenic lines in this study were created by floral dip as described previously[84]. Homozygous lines were confirmed by hygromycin selection. The transgenic line expressing *pPLT3::PLT3-mV* in the *plt3* mutant background has been described previously[9]. Plants for crossing, floral dips, genotyping and seed amplification were grown on soil in phytochambers under constant light or long day (16 h light/ 8 h dark) conditions at 21 °C. For microscopy, a fume-sterilisation (50 ml 13 % sodiumhypochlorite (v/v) + 1 ml hydrochloric acid) of the *Arabidopsis* seeds was done beforehand. Sterile seeds were then imbedded in 0.2 % (w/v) agarose, stratified for 2 days at 4 °C and plated on GM agar plates (1/2 strength Murashige Skoog medium including Gamborg B5 vitamins, 1.2 % (w/v) plant agar, 1 % (w/v) sucrose, supplemented with 0.05 % (w/v) MES hydrate). Afterwards, seedlings were grown under continuous light at 21 °C for 5 days. For root imaging, cell walls were stained with either propidium iodide or FM4-64 dye (Invitrogen™, Thermo Fisher Scientific Inc.) as described previously[9] (see chapter IV-5.3).

5.3 Hypocotyl length measurements

Seeds were sterilized and plated on GM agar plates like described above (see V-5.2 Plant work). Afterwards, seedlings were grown in short day (8 h dark/ 16 h light) conditions at 21 °C for seven days. Photos were taken and hypocotyl length was measured with Fiji[85]. Box plots were created with Origin 2020 (OriginLab Corporation).

5.4 Quantification of leaf area and leaf number

Six seedlings of each genotype from 5.3 Hypocotyl length measurements were transferred on soil and continued growing in short day (8 h dark/ 16 h light) conditions at 21 °C. Pictures were taken from 23 days old plants. The leaves were counted and the leaf area was measured with

Fiji[85]. Afterwards the phytochamber was switched to long day (16 h light/ 8 h dark, 21 °C) conditions, pictures were taken again from 30, 36 and 40 days old plants and leaves were counted. Box plots were created with Origin 2020 (OriginLab Corporation).

5.5 *N. benthamiana* infiltration

For transient gene expression, leaves of *N. benthamiana* plants were infiltrated with an *Agrobacterium* strain as described previously[9] (see chapter IV-5.4).

5.6 SCN staining

The combined mPS-PI- and EdU-staining was performed like described before[9] (see chapter IV-5.5). The 2D plots were created with Origin 2020 (OriginLab Corporation).

5.7 Cell culture

All work was done under sterile conditions. Human epithelial cells, HEp-2 (epithelial larynx carcinoma, ATCC-CCL-23) were routinely cultured in Dulbecco´s modified Eagle´s medium (DMEM, Thermo Fisher Scientific Inc.) at 37 °C under 5 % CO2. Medium was supplemented with 10 % foetal calf serum (FCS), 100 U/ml penicillin and 100 µg/ml streptomycin. For splitting, cells were washed with 5 ml DPBS-Buffer (‚Dulbecco's Phosphate Buffered Saline‘) and subsequently incubated for 5 min in 2 ml Trypsin-solution (0.25 % Trypsin, 0.02 % EDTA in DPBS-Buffer) in an incubator (37 °C, 5 % CO_2). Trypsinisation was stopped by adding 2 ml medium and 1 ml of the cell-suspension was transferred in a new flask with 7 ml medium. For microscopy, cells were transfected in 2 ml-imaging dishes with the FuGENE® HD transfection reagent (Promega Corporation) according to the manufacturers protocol and a transfection reagent to DNA ratio of 2:1.

5.8 Microscopy

Imaging was carried out with a ZEISS LSM780 or LSM880. Fluorescent dyes were excited, and emission was detected as follows: Cerulean was excited at 458 nm and emission was detected at 460-510 nm. mVenus was excited at 514 nm and emission was detected at 517-560 nm, or for co-expression with red dyes excited at 488 nm and detected at 500-560 nm. Alexa Fluor® 488 was excited at 488 nm and emission was detected at 490-560 nm. PI was excited at 561 nm and emission was detected at 590-710 nm. FM4-64 was excited at 514 nm or 561 nm and emission was detected at 670-760 nm. mCherry and mRuby2 were excited at 561 nm and emission was detected at 590-640 nm. To avoid cross talk, imaging of more than one fluorophore was carried out in the sequential mode.

5.9 Intensity measurements

The intensity measurements were performed in a transient *N. benthamiana* experiment. To analyse the ratio of the nuclear and cytoplasmic fraction of the ELF3-mVenus variants and the ELF3-mVenus in dependence of co-expressed PLT3-mCherry variants, images of nuclei and cytoplasm of the same cell were acquired with constant settings for the mVenus channel at the ZEISS LSM880. Fiji[85] was used for data analysis and mean intensities of ROIs were measured in the nucleus and corresponding cytoplasm. The intensity ratio was plotted in a box plot created with Origin 2020 (OriginLab Corporation).

5.10 Body-tracking

3D time series of the nuclear PLT3-mVenus bodies and the cytoplasmic ELF3-mVenus bodies were acquired with the ZEISS LSM880 airyscan fast mode in transient *N. benthamiana* experiments. The tracking and data analysis were done with Imaris (version 9.1.2, Bitplane, Oxford Instruments plc). For the PLT3-mVenus nuclei, a shift correction was performed beforehand with Imaris (version 9.1.2, Bitplane, Oxford Instruments plc).

5.11 FLIM measurements

The FLIM measurements in *N. benthamiana* leaf epidermal cells were performed as described previously[9] (see chapter IV-5.10). Additional fluorophore-combinations to the therein described mVenus and mCherry donor-acceptor pair were used for the PIF-interaction experiments (Figure V-9). Here, Cerulean was used as donor fluorophore and mVenus as acceptor fluorophore (Figure V-9g) and in a second experiment, GFP was used as donor fluorophore and mCherry as acceptor fluorophore (Figure V-9h). All donor fluorophores were excited with a linearly polarized diode laser (LDH-D-C-485) at pulse frequency of 32 MHz. Cerulean was excited at 440 nm and GFP at 485 nm. The bandpass filters were chosen according to the excitation maxima of the donor fluorophores (482/35 for Cerulean and 520/30 for GFP). FLIM data analysis was done as described previously[9] (see chapter IV-5.10), except that the applied intensity threshold was in a range of 50-200 photons per pixel and data obtained with the donor fluorophore Cerulean was fitted bi-exponentially due to the two lifetimes of the fluorophore. Subsequently the intensity weighted lifetime has been taken for further analysis. Box and scatter plots were created with Origin 2020 (OriginLab Corporation).

5.12 Prediction of protein domains

The PrDs in ELF3 and PLT3 were predicted using the PLAAC application[60]. The nuclear localisation signals (NLS) in ELF3 and PLT3 were predicted with cNLS Mapper[86].

5.13 Figure assembly

All figures created in this study were assembled with Adobe Photoshop CS5 (Adobe Inc.), except for Figure V-4 and Figure V-10 that were assembled with PowerPoint (Microsoft Office 365 ProPlus, Microsoft Corporation).

6. References

1. Dolan, L. *et al.* Cellular organisation of the Arabidopsis thaliana root. *Development* **119,** 71–84 (1993).
2. Kidner, C., Sundaresan, V., Roberts, K. & Dolan, L. Clonal analysis of the Arabidopsis root confirms that position, not lineage, determines cell fate. *Planta* **211,** 191–199; 10.1007/s004250000284 (2000).
3. van den Berg, C., Willemsen, V., Henriks, G., Weisbeek, P. & Scheres, B. Short-range control of cell differentiation in the Arabidopsis root meristem. *Nature* **390,** 287–289; 10.1038/36856 (1997).
4. Drisch, R. C. & Stahl, Y. Function and regulation of transcription factors involved in root apical meristem and stem cell maintenance. *Front Plant Sci* **6,** 505; 10.3389/fpls.2015.00505 (2015).
5. Pi, L. *et al.* Organizer-Derived WOX5 Signal Maintains Root Columella Stem Cells through Chromatin-Mediated Repression of CDF4 Expression. *Dev Cell* **33,** 576–588; 10.1016/j.devcel.2015.04.024 (2015).
6. Sarkar, A. K. *et al.* Conserved factors regulate signalling in Arabidopsis thaliana shoot and root stem cell organizers. *Nature* **446,** 811–814; 10.1038/nature05703 (2007).
7. Aida, M. *et al.* The PLETHORA genes mediate patterning of the Arabidopsis root stem cell niche. *Cell* **119,** 109–120; 10.1016/j.cell.2004.09.018 (2004).
8. Galinha, C. *et al.* PLETHORA proteins as dose-dependent master regulators of Arabidopsis root development. *Nature* **449,** 1053–1057; 10.1038/nature06206 (2007).
9. Burkart, R. C. *et al.* PLETHORA and WOX5 interaction and subnuclear localisation regulates Arabidopsis root stem cell maintenance. *bioRxiv*; 10.1101/818187 (2019).
10. McClung, C. R. Plant circadian rhythms. *The Plant cell* **18,** 792–803; 10.1105/tpc.106.040980 (2006).
11. McWatters, H. G., Bastow, R. M., Hall, A. & Millar, A. J. The ELF3 zeitnehmer regulates light signalling to the circadian clock. *Nature* **408,** 716–720; 10.1038/35047079 (2000).
12. Zagotta, M. T. *et al.* The Arabidopsis ELF3 gene regulates vegetative photomorphogenesis and the photoperiodic induction of flowering. *The Plant journal : for cell and molecular biology* **10,** 691–702; 10.1046/j.1365-313x.1996.10040691.x (1996).
13. Liu, X. L., Covington, M. F., Fankhauser, C., Chory, J. & Wagner, D. R. ELF3 encodes a circadian clock-regulated nuclear protein that functions in an Arabidopsis PHYB signal transduction pathway. *The Plant cell* **13,** 1293–1304; 10.1105/tpc.13.6.1293 (2001).
14. Hicks, K. A., Albertson, T. M. & Wagner, D. R. EARLY FLOWERING3 encodes a novel protein that regulates circadian clock function and flowering in Arabidopsis. *The Plant cell* **13,** 1281–1292; 10.1105/tpc.13.6.1281 (2001).
15. Covington, M. F. *et al.* ELF3 modulates resetting of the circadian clock in Arabidopsis. *The Plant cell* **13,** 1305–1315; 10.1105/tpc.13.6.1305 (2001).
16. Nusinow, D. A. *et al.* The ELF4-ELF3-LUX complex links the circadian clock to diurnal control of hypocotyl growth. *Nature* **475,** 398–402; 10.1038/nature10182 (2011).

17. Martínez-García, J. F., Huq, E. & Quail, P. H. Direct targeting of light signals to a promoter element-bound transcription factor. *Science* **288,** 859–863; 10.1126/science.288.5467.859 (2000).

18. Leivar, P. *et al.* The Arabidopsis phytochrome-interacting factor PIF7, together with PIF3 and PIF4, regulates responses to prolonged red light by modulating phyB levels. *The Plant cell* **20,** 337–352; 10.1105/tpc.107.052142 (2008).

19. Leivar, P. *et al.* Multiple phytochrome-interacting bHLH transcription factors repress premature seedling photomorphogenesis in darkness. *Curr. Biol.* **18,** 1815–1823; 10.1016/j.cub.2008.10.058 (2008).

20. Ni, M., Tepperman, J. M. & Quail, P. H. Binding of phytochrome B to its nuclear signalling partner PIF3 is reversibly induced by light. *Nature* **400,** 781–784; 10.1038/23500 (1999).

21. Soy, J. *et al.* Phytochrome-imposed oscillations in PIF3 protein abundance regulate hypocotyl growth under diurnal light/dark conditions in Arabidopsis. *The Plant journal* **71,** 390–401; 10.1111/j.1365-313X.2012.04992.x (2012).

22. Soy, J., Leivar, P. & Monte, E. PIF1 promotes phytochrome-regulated growth under photoperiodic conditions in Arabidopsis together with PIF3, PIF4, and PIF5. *Journal of experimental botany* **65,** 2925–2936; 10.1093/jxb/ert465 (2014).

23. Pedmale, U. V. *et al.* Cryptochromes Interact Directly with PIFs to Control Plant Growth in Limiting Blue Light. *Cell* **164,** 233–245; 10.1016/j.cell.2015.12.018 (2016).

24. Ma, D. *et al.* Cryptochrome 1 interacts with PIF4 to regulate high temperature-mediated hypocotyl elongation in response to blue light. *PNAS* **113,** 224–229; 10.1073/pnas.1511437113 (2016).

25. Huang, H. *et al.* Identification of Evening Complex Associated Proteins in Arabidopsis by Affinity Purification and Mass Spectrometry. *Molecular & cellular proteomics* **15,** 201–217; 10.1074/mcp.M115.054064 (2016).

26. Chow, B. Y., Helfer, A., Nusinow, D. A. & Kay, S. A. ELF3 recruitment to the PRR9 promoter requires other Evening Complex members in the Arabidopsis circadian clock. *Plant signaling & behavior* **7,** 170–173; 10.4161/psb.18766 (2012).

27. Ezer, D. *et al.* The evening complex coordinates environmental and endogenous signals in Arabidopsis. *Nature plants* **3,** 17087; 10.1038/nplants.2017.87 (2017).

28. Silva, C. S. *et al.* Molecular mechanisms of Evening Complex activity in Arabidopsis. *PNAS* **117,** 6901–6909; 10.1073/pnas.1920972117 (2020).

29. Jung, J.-H. *et al.* A prion-like domain in ELF3 functions as a thermosensor in Arabidopsis. *Nature* **585,** 256–260; 10.1038/s41586-020-2644-7 (2020).

30. Joseph, B., Lau, L. & Kliebenstein, D. J. Quantitative Variation in Responses to Root Spatial Constraint within Arabidopsis thaliana. *The Plant cell* **27,** 2227–2243; 10.1105/tpc.15.00335 (2015).

31. Yazdanbakhsh, N., Sulpice, R., Graf, A., Stitt, M. & Fisahn, J. Circadian control of root elongation and C partitioning in Arabidopsis thaliana. *Plant, cell & environment* **34,** 877–894; 10.1111/j.1365-3040.2011.02286.x (2011).

32. James, A. B. *et al.* The circadian clock in Arabidopsis roots is a simplified slave version of the clock in shoots. *Science* **322,** 1832–1835; 10.1126/science.1161403 (2008).

33. Ruts, T., Matsubara, S., Wiese-Klinkenberg, A. & Walter, A. Aberrant temporal growth pattern and morphology of root and shoot caused by a defective circadian clock in Arabidopsis thaliana. *The Plant journal* **72,** 154–161; 10.1111/j.1365-313X.2012.05073.x (2012).

34. Voß, U. *et al.* The circadian clock rephases during lateral root organ initiation in Arabidopsis thaliana. *Nat Commun* **6,** 7641; 10.1038/ncomms8641 (2015).

35. Li, B. *et al.* PRR5, 7 and 9 positively modulate TOR signaling-mediated root cell proliferation by repressing TANDEM ZINC FINGER 1 in Arabidopsis. *Nucleic acids research* **47,** 5001–5015; 10.1093/nar/gkz191 (2019).

36. Oakenfull, R. J. & Davis, S. J. Shining a light on the Arabidopsis circadian clock. *Plant, cell & environment* **40,** 2571–2585; 10.1111/pce.13033 (2017).

37. McClung, C. R. The Plant Circadian Oscillator. *Biology* **8,** 14; 10.3390/biology8010014 (2019).

38. Herrero, E. *et al.* EARLY FLOWERING4 recruitment of EARLY FLOWERING3 in the nucleus sustains the Arabidopsis circadian clock. *The Plant cell* **24,** 428–443; 10.1105/tpc.111.093807 (2012).

39. Hicks, K. A. *et al.* Conditional circadian dysfunction of the Arabidopsis early-flowering 3 mutant. *Science (New York, N.Y.)* **274,** 790–792; 10.1126/science.274.5288.790 (1996).

40. Ding, L. *et al.* Two B-Box Domain Proteins, BBX18 and BBX23, Interact with ELF3 and Regulate Thermomorphogenesis in Arabidopsis. *Cell reports* **25,** 1718-1728.e4; 10.1016/j.celrep.2018.10.060 (2018).

41. Tong, M. *et al.* The Evening Complex establishes repressive chromatin domains via H2A.Z deposition. *Plant physiology* **182,** 612–625; 10.1104/pp.19.00881 (2020).

42. Jiang, Y. *et al.* The ELF3-PIF7 Interaction Mediates the Circadian Gating of the Shade Response in Arabidopsis. *iScience* **22,** 288–298; 10.1016/j.isci.2019.11.029 (2019).

43. Anwer, M. U. *et al.* Natural variation reveals that intracellular distribution of ELF3 protein is associated with function in the circadian clock. *eLife* **3**; 10.7554/eLife.02206 (2014).

44. Press, M. O., Lanctot, A. & Queitsch, C. PIF4 and ELF3 Act Independently in Arabidopsis thaliana Thermoresponsive Flowering. *PloS one* **11,** e0161791; 10.1371/journal.pone.0161791 (2016).

45. Box, M. S. *et al.* ELF3 controls thermoresponsive growth in Arabidopsis. *Current Biology* **25,** 194–199; 10.1016/j.cub.2014.10.076 (2015).

46. Nieto, C., López-Salmerón, V., Davière, J.-M. & Prat, S. ELF3-PIF4 interaction regulates plant growth independently of the Evening Complex. *Current Biology* **25,** 187–193; 10.1016/j.cub.2014.10.070 (2015).

47. Cruz-Ramírez, A. *et al.* A SCARECROW-RETINOBLASTOMA protein network controls protective quiescence in the Arabidopsis root stem cell organizer. *PLoS Biol* **11,** e1001724; 10.1371/journal.pbio.1001724 (2013).

48. Vilarrasa-Blasi, J. *et al.* Regulation of plant stem cell quiescence by a brassinosteroid signaling module. *Dev Cell* **30,** 36–47; 10.1016/j.devcel.2014.05.020 (2014).

49. Mähönen, A. P. *et al.* PLETHORA gradient formation mechanism separates auxin responses. *Nature* **515,** 125–129; 10.1038/nature13663 (2014).

50. Truernit, E. *et al.* High-resolution whole-mount imaging of three-dimensional tissue organization and gene expression enables the study of Phloem development and structure in Arabidopsis. *Plant Cell* **20,** 1494–1503; 10.1105/tpc.107.056069 (2008).

51. Stahl, Y., Wink, R. H., Ingram, G. C. & Simon, R. A Signaling Module Controlling the Stem Cell Niche in Arabidopsis Root Meristems. *Current Biology* **19,** 909–914; 10.1016/j.cub.2009.03.060 (2009).

52. Stahl, Y. *et al.* Moderation of Arabidopsis root stemness by CLAVATA1 and ARABIDOPSIS CRINKLY4 receptor kinase complexes. *Current Biology* **23,** 362–371; 10.1016/j.cub.2013.01.045 (2013).

53. Cuevas-Velazquez, C. L. & Dinneny, J. R. Organization out of disorder: liquid-liquid phase separation in plants. *Curr Opin Plant Biol* **45,** 68–74; 10.1016/j.pbi.2018.05.005 (2018).

54. Chakrabortee, S. *et al.* Luminidependens (LD) is an Arabidopsis protein with prion behavior. *PNAS* **113,** 6065–6070; 10.1073/pnas.1604478113 (2016).

55. Aguzzi, A., Nuvolone, M. & Zhu, C. The immunobiology of prion diseases. *Nat. Rev. Immunol.* **13,** 888–902; 10.1038/nri3553 (2013).

56. Kim, H. J. *et al.* Mutations in prion-like domains in hnRNPA2B1 and hnRNPA1 cause multisystem proteinopathy and ALS. *Nature* **495,** 467–473; 10.1038/nature11922 (2013).

57. Bailey, C. H., Kandel, E. R. & Si, K. The persistence of long-term memory: a molecular approach to self-sustaining changes in learning-induced synaptic growth. *Neuron* **44,** 49–57; 10.1016/j.neuron.2004.09.017 (2004).

58. Shorter, J. & Lindquist, S. Prions as adaptive conduits of memory and inheritance. *Nature Reviews Genetics* **6,** 435–450; 10.1038/nrg1616 (2005).

59. Michelitsch, M. D. & Weissman, J. S. A census of glutamine/asparagine-rich regions: implications for their conserved function and the prediction of novel prions. *PNAS* **97,** 11910–11915; 10.1073/pnas.97.22.11910 (2000).

60. Lancaster, A. K., Nutter-Upham, A., Lindquist, S. & King, O. D. PLAAC: a web and command-line application to identify proteins with prion-like amino acid composition. *Bioinformatics* **30,** 2501–2502; 10.1093/bioinformatics/btu310 (2014).

61. Reed, J. W. *et al.* Independent action of ELF3 and phyB to control hypocotyl elongation and flowering time. *Plant physiology* **122,** 1149–1160; 10.1104/pp.122.4.1149 (2000).

62. Lucas, M. de *et al.* A molecular framework for light and gibberellin control of cell elongation. *Nature* **451,** 480–484; 10.1038/nature06520 (2008).

63. Yang, S. W., Jang, I.-C., Henriques, R. & Chua, N.-H. FAR-RED ELONGATED HYPOCOTYL1 and FHY1-LIKE associate with the Arabidopsis transcription factors LAF1 and HFR1 to transmit phytochrome A signals for inhibition of hypocotyl elongation. *The Plant cell* **21,** 1341–1359; 10.1105/tpc.109.067215 (2009).

64. Liu, X. *et al.* Light-regulated hypocotyl elongation involves proteasome-dependent degradation of the microtubule regulatory protein WDL3 in Arabidopsis. *The Plant cell* **25,** 1740–1755; 10.1105/tpc.113.112789 (2013).

65. Kim, W.-Y., Hicks, K. A. & Somers, D. E. Independent roles for EARLY FLOWERING 3 and ZEITLUPE in the control of circadian timing, hypocotyl length, and flowering time. *Plant physiology* **139,** 1557–1569; 10.1104/pp.105.067173 (2005).

66. Lu, S. X. *et al.* CCA1 and ELF3 Interact in the control of hypocotyl length and flowering time in Arabidopsis. *Plant physiology* **158,** 1079–1088; 10.1104/pp.111.189670 (2012).

67. Wang, C.-Q., Sarmast, M. K., Jiang, J. & Dehesh, K. The Transcriptional Regulator BBX19 Promotes Hypocotyl Growth by Facilitating COP1-Mediated EARLY FLOWERING3 Degradation in Arabidopsis. *The Plant cell* **27,** 1128–1139; 10.1105/tpc.15.00044 (2015).

68. Förster, T. Zwischenmolekulare Energiewanderung und Fluoreszenz. *Ann. Phys.* **437,** 55–75; 10.1002/andp.19484370105 (1948).

69. Beyer, H. M. *et al.* Red Light-Regulated Reversible Nuclear Localization of Proteins in Mammalian Cells and Zebrafish. *ACS synthetic biology* **4,** 951–958; 10.1021/acssynbio.5b00004 (2015).

70. Bai, S. *et al.* PIF3 is involved in the primary root growth inhibition of Arabidopsis induced by nitric oxide in the light. *Molecular plant* **7,** 616–625; 10.1093/mp/sst142 (2014).

71. Bauer, D. *et al.* Constitutive photomorphogenesis 1 and multiple photoreceptors control degradation of phytochrome interacting factor 3, a transcription factor required for light signaling in Arabidopsis. *The Plant cell* **16,** 1433–1445; 10.1105/tpc.021568 (2004).

72. Al-Sady, B., Ni, W., Kircher, S., Schäfer, E. & Quail, P. H. Photoactivated phytochrome induces rapid PIF3 phosphorylation prior to proteasome-mediated degradation. *Molecular cell* **23,** 439–446; 10.1016/j.molcel.2006.06.011 (2006).

73. van Buskirk, E. K., Reddy, A. K., Nagatani, A. & Chen, M. Photobody Localization of Phytochrome B Is Tightly Correlated with Prolonged and Light-Dependent Inhibition of Hypocotyl Elongation in the Dark. *Plant Physiol* **165,** 595–607; 10.1104/pp.114.236661 (2014).

74. Qiu, Y. *et al.* Mechanism of early light signaling by the carboxy-terminal output module of Arabidopsis phytochrome B. *Nature communications* **8,** 1905; 10.1038/s41467-017-02062-6 (2017).

75. Paik, I. *et al.* A phyB-PIF1-SPA1 kinase regulatory complex promotes photomorphogenesis in Arabidopsis. *Nature communications* **10,** 4216; 10.1038/s41467-019-12110-y (2019).

76. Birnbaum, K. *et al.* A gene expression map of the Arabidopsis root. *Science* **302,** 1956–1960; 10.1126/science.1090022 (2003).

77. Nawy, T. *et al.* Transcriptional profile of the Arabidopsis root quiescent center. *Plant Cell* **17,** 1908–1925; 10.1105/tpc.105.031724 (2005).

78. Burkart, R. C. & Stahl, Y. Dynamic complexity: plant receptor complexes at the plasma membrane. *Curr Opin Plant Biol* **40,** 15–21; 10.1016/j.pbi.2017.06.016 (2017).

79. Lampropoulos, A. *et al.* GreenGate - A Novel, Versatile, and Efficient Cloning System for Plant Transgenesis. *PloS one* **8,** e83043; 10.1371/journal.pone.0083043 (2013).

80. Denninger, P. *et al.* Distinct RopGEFs Successively Drive Polarization and Outgrowth of Root Hairs. *Curr. Biol.* **29,** 1854-1865.e5; 10.1016/j.cub.2019.04.059 (2019).

81. Curtis, M. D. & Grossniklaus, U. A gateway cloning vector set for high-throughput functional analysis of genes in planta. *Plant Physiol.* **133,** 462–469; 10.1104/pp.103.027979 (2003).

82. Bleckmann, A., Weidtkamp-Peters, S., Seidel, C. A. M. & Simon, R. Stem cell signaling in Arabidopsis requires CRN to localize CLV2 to the plasma membrane. *Plant Physiol.* **152,** 166–176; 10.1104/pp.109.149930 (2010).

83. Zagotta, M. T., Shannon, S., Jacobs, C. & Meeks-Wagner. Early-Flowering Mutants of Arabidopsis thaliana. *Functional Plant Biol.* **19,** 411; 10.1071/PP9920411 (1992).

84. Zhang, X., Henriques, R., Lin, S.-S., Niu, Q.-W. & Chua, N.-H. Agrobacterium-mediated transformation of Arabidopsis thaliana using the floral dip method. *Nat. Protoc.* **1,** 641–646; 10.1038/nprot.2006.97 (2006).

85. Schindelin, J. *et al.* Fiji: an open-source platform for biological-image analysis. *Nat. Methods* **9,** 676–682; 10.1038/nmeth.2019 (2012).

86. Kosugi, S., Hasebe, M., Tomita, M. & Yanagawa, H. Systematic identification of cell cycle-dependent yeast nucleocytoplasmic shuttling proteins by prediction of composite motifs. *PNAS* **106,** 10171–10176; 10.1073/pnas.0900604106 (2009).

7. Supplementary information

7.1 Supplementary figures

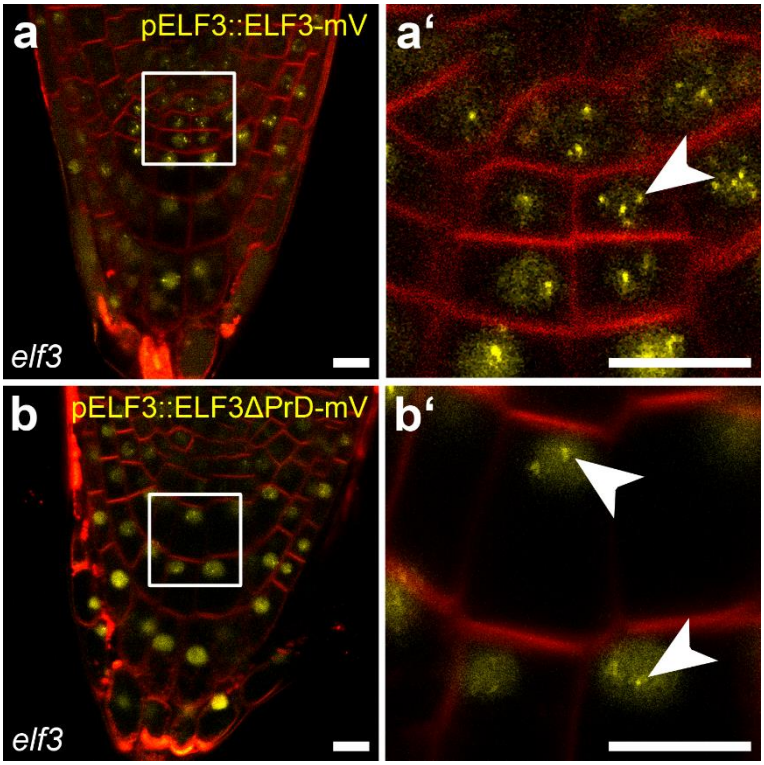

Supplementary figure V-1: Localisation of ELF3-mV and ELF3ΔPrD-mV in the RAM of *A. thaliana*

a-a’, Localisation of endogenously expressed ELF3-mV (yellow) in the *elf3* mutant root. Cell walls are stained with FM4-64 (red). **a’** is a magnification of **a**, indicated by the white square in **a**. **b-b’,** Localisation of an endogenously expressed ELF3-PrD deletion variant (ELF3ΔPrD-mV) in the *elf3* mutant root. Cell walls are stained with FM4-64 (red). **b’** is a magnification of **b**, indicated by the white square in **b**. White arrowheads point at NBs. Scale bars represent 5 µm. mV = mVenus; PrD = prion-like domain.

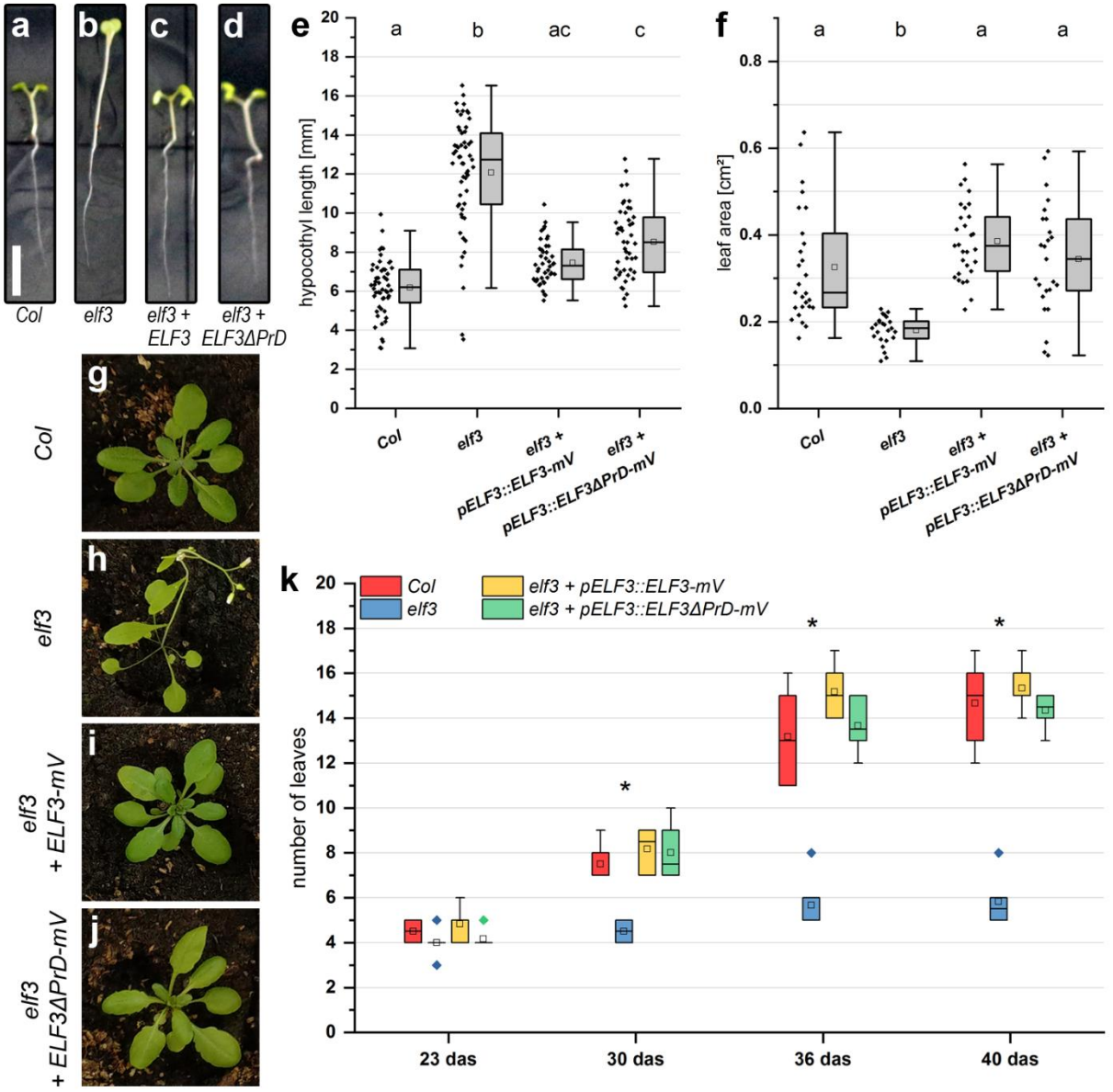

Supplementary figure V-2: Phenotypes of *Col* wild type, *elf3* mutant and transgenic rescue lines

a-d, Representative images of 7-day old seedlings of Col wild type (**a**), *elf3* mutant (**b**), transgenic *elf3* + pELF3::ELF3-mV line (**c**) and *elf3* + pELF3::ELF3ΔPrD-mV line, expressing the PrD deletion variant (**d**), grown in short day conditions. The *elf3* mutant shows an elongated hypocotyl phenotype. **e,** Hypocotyl lengths in mm are summarized in combined box and scatter plots. **f,** Leaf area in cm² of 23 days old plants grown in short day conditions are summarized in combined box and scatter plots. Statistical analysis of samples in **e** and **f** was carried out by one-way ANOVA and post-hoc multiple comparisons using the Holm-Sidak test. Samples with identical letters do not show significant differences ($\alpha = 0.01$). Sample numbers are indicated in Supplementary Table V-9 and Supplementary table V-10, respectively. **g-j,** Representative images of 30 days old plants with indicated genotype. **k,** Number of leaves of 23, 30, 36 and 40 days old plants are summarized in box plots. Statistical analysis was carried out by one-way ANOVA and post-hoc multiple comparisons using the Holm-Sidak test. Asterisks indicate significant differences ($\alpha = 0.01$, n = 6). Box = 25-75 % of percentile, whisker = 1.5 interquartile range, – = median, □ = mean value. mV = mVenus; das = days after sawing.

7.2 Supplementary tables

Supplementary table V-1: List of primers for GreenGate cloning

gene ID	alias	primer name	orientation	sequence
Promoter modules				
AT2G25930	pELF3	PW_GG_p-ELF3 F	F	TTTGGTCTCAACCTTTTCGATCAAAGCAGCAGATTC
		PW_GG_p-ELF3 R	R	AAAGGTCTCATGTTCACTCACAATTCACAACC
AT5G10510	pPLT3	RD_GG pPLT3 F V2	F	AAAGGTCTCAACCTAATTTTAACGTATTCTTTC
		RD_GG pPLT3 R V2	R	AAAGGTCTCATGTTAAACTTTCTTATAAAAACAATT
-	pCMV for *HEp-2*	PW_GG_P-CMV F	F	AAAGGTCTCAACCTCCGCCATGCATTAGTTATTAATAG
		PW_GG_P-CMV R	R	AAAGGTCTCATGTTGATCTGACGGTTCACTAAACC
CDS modules				
AT2G25930	ELF3	RD_GG ELF3 F	F	AAAGGTCTCAGGCTTAATGAAGAGAGGGAAAG
		RD_GG ELF3 R	R	AAAGGTCTCACTGAAGGCTTAGAGGAGTCATAG
	ELF3ΔPrD	PW_GG_p-ELF3 F	F	TTTGGTCTCAACCTTTTCGATCAAAGCAGCAGATTC
		RD_ELF3deltaPrD1 R	R	CCAGCTGCCAACCTCCCAACTAC
		RD_ELF3 linker F	F	GAGGTTGGCAGCTGGTGCTGC
		RD_ELF3 linker R	R	CGCGGTGCTCCTGCGG
		RD_ELF3deltaPrD2 F	F	AGGAGCACCGCGAGCAAGAAAG
		PW_GG_p-ELF3 R	R	AAAGGTCTCATGTTCACTCACAATTCACAACC
AT5G10510	PLT3	RD_GreenGate PLT3 F	F	AAAGGTCTCAGGCTTAATGGAGATGTTGAG
		RD_GreenGate PLT3 R	R	AAAGGTCTCACTGAGTAAGACTGATTAGGC
	PLT3ΔPrD	RD_GreenGate PLT3 F	F	AAAGGTCTCAGGCTTAATGGAGATGTTGAG
		RD_PLT3ΔPrD1 CDS1 R	R	CCAGCTGCAACACCAAGTGACAAAG
		RD_PLT3ΔPrD1 linker F	F	CTTGGTGTTGCAGCTGGTGCTG
		RD_PLT3ΔPrD1 linker R	R	GTCTTCTCTGCTCCTGCGGCAG
		RD_PLT3ΔPrD1 CDS2 F	F	CGCAGGAGCAGAGAAGACAGATTCTG
		RD_GG PLT3ΔPrDs R	R	AAAGGTCTCACTGAGTGAAGTTGATGATGAC
AT1G09530	PIF3	RD_GG PIF3 CDS F	F	AAAGGTCTCAGGCTTAATGCCTCTGTTTGAG
		RD_GG PIF3 CDS R	R	AAAGGTCTCACTGACGACGATCCACAAA
AT2G43010	PIF4	RD_GG PIF4 CDS F	F	AAAGGTCTCAGGCTTAATGGAACACCAAG
		RD_GG PIF4 CDS R	R	AAAGGTCTCACTGAGTGGTCCAAACGAG
		RD_GG PIF4 Mitte F	F	GATCCCCTCCAAAGACCAACCTC
		RD_GG PIF4 Mitte R	R	GAGGTTGGTCTTTGGAGGGGATC
C-tag modules				
-	mVenus	RD_GreenGate mVenus C-tag F	F	AAAGGTCTCATCAGCAATGGTGAGCAAGG
		RD_GreenGate mVenus C-tag R	R	AAAGGTCTCAGCAGTTACTTGTACAGCTC
-	mCherry	RD_GG mCherry C-tag F	F	AAAGGTCTCATCAGCAATGGTGAGCAAGG
		RD_GG mCherry C-tag R	R	AAAGGTCTCAGCAGTTACTTGTACAGCTCGTC
Terminator modules				
-	SV40-polyA for *HEp-2*	PW_GG_SV40pA F	F	AAAGGTCTCACTGCGCCATACCACATTTGTAGAG
		PW_GG_SV40pA R	R	AAAGGTCTCATAGTCGCCTTAAGATACATTGATGAG
Plant resistance modules				
-	SV40 ori for *HEp-2*	PW_GG_SV40o F	F	AAAGGTCTCAACTAGGTGTGGAAAGTCCCC
		PW_GG_SV40o R	R	AAAGGTCTCAATACGGCCTCCAAAAAAGCC

Supplementary table V-2: List of primers for Gateway Cloning

gene ID	alias	primer name	orientation	sequence
AT2G25930	ELF3	PW ELF3 CACC F	F	CACCATGAAGAGAGGGAAAGATGA
		ELF3 ohne Stopp R	R	AGGCTTAGAGGAGTCATAGC
	ELF3 for *HEp-2*	PW ELF3 CACC F	F	CACCATGAAGAGAGGGAAAGATGA
		ELF3 R-stop +2BP	R	CCAGGCTTAGAGGAGTCATAGC
AT5G10510	PLT3	YS_PLT3 F CACC	F	CACCATGGAGATGTTGAGGTCATCTGATCAGTCTCA
		YS_PLT3 R -stop	R	GTAAGACTGATTAGGCCAGAGGAAG
	PLT3ΔQ	YS_PLT3 F CACC	F	CACCATGGAGATGTTGAGGTCATCTGATCAGTCTCA
		RD_PLT3 Seg1 R	R	GAGATGAGAAATGGTGAAGTTGATGATGAC
		RD_PLT3 Seg2 F	F	CTTCACCATTTCTCATCTCCTAATCACAGTAGC
		RD_PLT3 Seg2 R	R	GAAGAAGTTGTGGTGGTGGTAAAGAGCAG
		RD_PLT3 Seg3 F	F	CACCACCACAACTTCTTCCAGCATTTTCC
		YS_PLT3 R -stop	R	GTAAGACTGATTAGGCCAGAGGAAG
	PLT3 for *Hep-2*	YS_PLT3 F CACC	F	CACCATGGAGATGTTGAGGTCATCTGATCAGTCTCA
		RD_PLT3 R -stop +2bp	R	AAGTAAGACTGATTAGGCCAGAGGAAG
-	mVenus	RD_mVenus PacI F	F	CCCTTAATTAAAATGGTGAGCAAGGGCGAGG
		MAS-Turquoise-SpeI-R	R	TTTACTAGTTACTTGTACAGCTCGTCCATGC
-	mVenus for *Hep-2*	YS_mVenus AgeI F	F	AAACCGGTATGGTGAGCAAGGGCGAGGA
		YS_mVenus MfeI R	R	AAACAATTGTTACTTGTACAGCTCGTCCATGCCG

Supplementary table V-3: List of genotyping primers

gene ID	alias	primer name	orien-tation	sequence
AT5G10510	*plt3-1*	GK_PLT3L	F	TTGTGATTTGCCATTGACTAAAGGT
		GK_PLT3R	R	GAAAACAGTCCAATGGTCTCACATC
		SALK LBB1V2		AAACCAGCGTGGACCGCTTGCTGCAACTCT

Supplementary table V-4: List of GreenGate expression vectors used in this study

construct	promoter	N-tag	CDS	C-tag	term-inator	plant sel. marker	destinatio n vector	bacterial sel. marker	plasmid ID
	module A	module B	module C	module D	module E	module F	module Z		
pELF3::ELF3-mV	ELF3 promoter	Ω-element (pGGB002)	ELF3	mVenus	tUBQ10 (pGGE009)	Hyg (pGGF005)	pGGZ001	Spec	pRD99
pELF3::ELF3ΔPrD-mV	ELF3 promoter	Ω-element (pGGB002)	ELF3 ΔPrD	mVenus	tUBQ10 (pGGE009)	Hyg (pGGF005)	pGGZ001	Spec	pRD124
35S::ELF3-mV	35S (pGGA004)	Ω-element (pGGB002)	ELF3	mVenus	tUBQ10 (pGGE009)	Hyg (pGGF005)	pGGZ001	Spec	pRD98
inducible ELF3ΔPrD-mV	Ubi-XVE oLexA-35S	Ω-element (pGGB002)	ELF3 ΔPrD	mVenus	tUBQ10 (pGGE009)	Hyg (pGGF005)	pGGZ001	Spec	pRD119
pPLT3:: PLT3-mV	PLT3 promoter	Ω-element (pGGB002)	PLT3	mVenus	tUBQ10 (pGGE009)	Hyg (pGGF005)	pGGZ001	Spec	pRD73
pPLT3:: PLT3ΔPrD-mV	PLT3 promoter	Ω-element (pGGB002)	PLT3 ΔPrD	mVenus	tUBQ10 (pGGE009)	Hyg (pGGF005)	pGGZ001	Spec	pRD125
inducible PLT3-C	Ubi-XVE oLexA-35S	Ω-element (pGGB002)	PLT3	Cerulean	tUBQ10 (pGGE009)	Hyg (pGGF005)	pGGZ001	Spec	pRD80
inducible PLT3ΔPrD-mV	Ubi-XVE oLexA-35S	Ω-element (pGGB002)	PLT3 ΔPrD	mVenus	tUBQ10 (pGGE009)	Hyg (pGGF005)	pGGZ001	Spec	pRD106
inducible PLT3ΔPrD-mC	Ubi-XVE oLexA-35S	Ω-element (pGGB002)	PLT3 ΔPrD	mCherry	tUBQ10 (pGGE009)	Hyg (pGGF005)	pGGZ001	Spec	pRD138
inducible PIF3-mC	Ubi-XVE oLexA-35S	Ω-element (pGGB002)	PIF3	mCherry	tUBQ10 (pGGE009)	Hyg (pGGF005)	pGGZ001	Spec	pLC08
inducible PIF3-mV for HEp-2	pCMV	Ω-element (pGGB002)	PIF3	mVenus	SV40-polyA	SV40 ori	pGGZ001	Spec	pRD93
inducible PIF3-C for HEp-2	pCMV	Ω-element (pGGB002)	PIF3	Cerulean	SV40-polyA	SV40 ori	pGGZ001	Spec	pRD94
inducible PIF4-mV	Ubi-XVE oLexA-35S	Ω-element (pGGB002)	PIF4	mVenus	tUBQ10 (pGGE009)	Hyg (pGGF005)	pGGZ001	Spec	pLC10
inducible PIF4-mC	Ubi-XVE oLexA-35S	Ω-element (pGGB002)	PIF4	mCherry	tUBQ10 (pGGE009)	Hyg (pGGF005)	pGGZ001	Spec	pLC11
inducible PIF4-mV for HEp-2	pCMV	Ω-element (pGGB002)	PIF4	mVenus	SV40-polyA	SV40 ori	pGGZ001	Spec	pRD95
inducible PIF4-C for HEp-2	pCMV	Ω-element (pGGB002)	PIF4	Cerulean	SV40-polyA	SV40 ori	pGGZ001	Spec	pRD96

Supplementary table V-5: List of Gateway expression vectors used in this study

construct	promoter	CDS	C-tag	termi-nator	plant sel. marker	destination vector	bacterial sel. marker	plasmid ID
inducible ELF3-mV	Ubi-XVE oLexA-35S	ELF3	mVenus	T3A	Hyg	pRD04	Spec	pPW06
inducible ELF3ΔQ-mV	Ubi-XVE oLexA-35S	ELF3ΔQ	mVenus	T3A	Hyg	pRD04	Spec	pPW47
inducible ELF3-mV for HEp-2	Ubi-XVE oLexA-35S	ELF3 (+2bp)	mVenus	T3A	Hyg	pRD10	Amp	pRD49
inducible PLT3-mV	Ubi-XVE oLexA-35S	PLT3	mVenus	T3A	Hyg	pRD04	Spec	pRD25
inducible PLT3-GFP	Ubi-XVE oLexA-35S	PLT3	GFP	T3A	Hyg	pABind GFP	Spec	pFB05
inducible PLT3-mC	Ubi-XVE oLexA-35S	PLT3	mCherry	T3A	Hyg	pABind mCherry	Spec	pFB06
inducible PLT3ΔQ-mV	Ubi-XVE oLexA-35S	PLT3ΔQ	mVenus	T3A	Hyg	pRD04	Spec	pRD57
inducible PLT3ΔQ-mC	Ubi-XVE oLexA-35S	PLT3ΔQ	mCherry	T3A	Hyg	pABind mCherry	Spec	pRD81
inducible PLT3-mV for HEp-2	Ubi-XVE oLexA-35S	PLT3 (+2bp)	mVenus	T3A	Hyg	pRD10	Amp	pRD11
inducible PLT3-mRb2 for HEp-2	Ubi-XVE oLexA-35S	PLT3 (+2bp)	mRuby2	T3A	Hyg	pH-mRuby2-N	Amp	pRD13
inducible PLT3-mC for HEp-2	Ubi-XVE oLexA-35S	PLT3 (+2bp)	mCherry	T3A	Hyg	pH-Ch-N	Amp	pRD36
inducible free mCherry	Ubi-XVE oLexA-35S	mCherry	-	T3A	Hyg	pMDC7	Spec	-

Supplementary table V-6: *Arabidopsis* mutants and transgenic lines

gene ID	alias	reference
AT2G25930	*elf3-1*	Zagotta *et al*. (1992)
AT5G10510	*plt3-1*	Galinha *et al*. (2007)
AT2G25930, AT5G10510	*elf3 plt3*	this study, crossing of *elf3-1* and *plt3-1*
AT2G25930	*pELF3::ELF3-mV (elf3-1)*	this study
AT2G25930	*pELF3::ELF3ΔPrD-mV (elf3-1)*	this study
AT5G10510	*pPLT3::PLT3-mV (plt3-1)*	Burkart *et al.* (2019), see chapter IV

Supplementary table V-7: Average QC and CSC phenotypes related to Figure V-3

genotype	average QC cell-divisions per root (± st. dev.)	average CSC layers per root (± st. dev.)	number of analysed roots
Col	0.49 ± 0.79	0.93 ± 0.58	209
elf3	0.65 ± 0.87	0.89 ± 0.66	76
plt3	0.65 ± 0.77	0.82 ± 0.63	172
elf3, plt3	0.91 ± 0.77	0.87 ± 0.71	53

Supplementary table V-8: Average nuclear/cytoplasmic intensity ratio of ELF3-mVenus variant expressing *N. benthamiana* leaf epidermal cells with and without PLT3-mCherry variant co-expression (related to Figure V-5)

construct	intensity ratio (nucleus/cytoplasm)	standard deviation	number of analysed cells
ELF3-mVenus	2.44	1.91	12
ELF3ΔQ-mVenus	3.38	4.06	12
ELF3ΔPrD-mVenus	3.17	2.62	10
ELF3-mVenus + PLT3-mCherry	11.86	8.54	10
ELF3-mVenus + PLT3ΔQ-mCherry	7.91	7.43	10
ELF3-mVenus + PLT3ΔPrD-mCherry	2.59	1.80	10

Supplementary Table V-9: Average hypocotyl length in *elf3* rescue experiment (related to Supplementary figure V-2e)

genotype	average hypocotyl length	standard deviation	number of analysed seedlings
Col	6.18	1.45	52
elf3	12.08	2.86	57
***elf3* + pELF3:ELF3-mV**	7.44	1.10	44
***elf3* + pELF3:ELF3ΔPrD-mV**	8.52	1.80	47

Supplementary table V-10: Average leaf area in *elf3* rescue experiments (related to Supplementary figure V-2f)

genotype	average leaf area	standard deviation	number of analysed leaves	number of plants
Col	2.95	0.58	27	6
elf3	2.26	0.25	24	6
***elf3* + pELF3:ELF3-mV**	3.26	0.42	29	6
***elf3* + pELF3:ELF3ΔPrD-mV**	3.04	0.64	25	6

Supplementary table V-11: Average number of leaves in *elf3* rescue experiments (related to Supplementary figure V-2k)

genotype	age of plants	average number of leaves	standard deviation	number of plants
Col	23 days	4.50	0.55	6
	30 days	7.50	0.84	
	36 days	13.17	2.04	
	40 days	14.67	1.97	
elf3	23 days	4.00	0.63	6
	30 days	4.50	0.55	
	36 days	5.67	1.21	
	40 days	5.83	1.17	
***elf3* + pELF3:ELF3-mV**	23 days	4.83	0.75	6
	30 days	8.17	0.98	
	36 days	15.17	1.17	
	40 days	15.33	1.03	
***elf3* + pELF3:ELF3ΔPrD-mV**	23 days	4.17	0.41	6
	30 days	8.00	1.26	
	36 days	13.67	1.21	
	40 days	14.33	0.82	

Supplementary table V-12: Average speed and displacement length of the body-tracking in ELF3-mVenus and PLT3-mVenus expressing *N. benthamiana* epidermal leaf cells (related to Figure V-6)

construct	mean track speed [µm/s]	variance	track displace-ment length [µm]	variance	number of analysed bodies	number of analysed cells
ELF3-mVenus	0.74	0.08	2.53	4.33	28493	10
PLT3-mVenus	0.06	0.001	0.50	0.16	1334	9

Supplementary table V-13: Average fluorescence lifetimes (τ) and standard deviation (st. dev.) obtained in FLIM experiments and corresponding lifetime changes (Δτ) in comparison to the donor only. The Δτ were calculated from each experiment separately.

donor	acceptor	average τ [ns]	st. dev. [ns]	average Δτ [ns]	st. dev. [ns]
ELF3-mVenus	-	2.98	0.08	-	-
	+ free mCherry	2.99	0.05	0.03	0.04
	+ PLT3-mCherry	2.42	0.32	0.53	0.26
	+ PLT3ΔQ-mCherry	2.70	0.17	0.26	0.17
	+ PLT3ΔPrD-mCherry	2.92	0.15	0.10	0.15
ELF3ΔQ-mVenus	-	2.88	0.15	-	-
	+ free mCherry	3.03	0.04	0.04	0.04
	+ PLT3-mCherry	2.35	0.35	0.51	0.26
	+ PLT3ΔQ-mCherry	2.69	0.21	0.18	0.18
ELF3ΔPrD-mVenus	-	3.02	0.03	-	-
	+ free mCherry	3.00	0.04	0.02	0.04
	+ PLT3-mCherry	2.93	0.12	0.09	0.13
	+ PLT3ΔPrD-mCherry	2.99	0.07	0.03	0.08

Supplementary table V-14: Average fluorescence lifetimes (τ) and standard deviation (st. dev.) obtained in FLIM experiments with PIF-proteins and corresponding lifetime changes (Δτ) in comparison to the donor only.

donor	acceptor	average τ [ns]	st. dev. [ns]	average Δτ [ns]	st. dev. [ns]
PIF3-Cerulean	-	2.68	0.29	-	-
	+ PLT3-mVenus	2.30	0.23	0.37	0.23
PLT3-GFP	-	2.46	0.06	-	-
	+ PIF3-mCherry	2.33	0.05	0.13	0.05
	+ PIF3-mCherry	2.29	0.09	0.17	0.09

Summary

This study elucidates the function of complex formation and subcellular microdomain localisation of specific transcription factors (TFs) involved in the control of root stem cell niche (SCN) homeostasis in *Arabidopsis thaliana*. Additionally, it reveals the integration of external cues in the regulation of SCN maintenance.

Starting with an overview about known TFs involved in root apical meristem (RAM) maintenance (chapter I), a basis for further investigations is built, showing that WUSCHEL-RELATED HOMEOBOX5 (WOX5) is one of the most important players in root stem cell maintenance and in the control of cell divisions in the quiescent centre (QC). Furthermore, a first link to regulations via TF-complex formation and potential subcellular translocation is drawn. In chapter II an example of a known function of microdomain formation in cellular signalling processes is discussed. Herein, the fast and reversible formation of microdomains through plant receptor complexes at the plasma membrane leads to the ability of a spatio-temporal separation of signalling processes. This could represent a general mechanism to precisely separate the required cellular processes spatially and temporally in response to momentary signals.

In chapter III, investigations on the control of QC quiescence, using protein interaction experiments and mathematical modelling, uncover a new interconnected regulation through complex formation of the TFs BRAVO (BRASSINOSTEROIDS AT VASCULAR AND ORGANIZING CENTER) and WOX5, where they positively influence QC quiescence. Furthermore, in chapter IV it is revealed that PLETHORAs (PLTs) and WOX5 both control QC quiescence and interdependently regulate columella stem cell (CSC) maintenance through transcriptional regulation but also direct protein-protein interaction. Prion-like domains (PrDs) were identified in the PLTs that mediate protein interaction with WOX5 and are responsible for the localisation of PLT3 to nuclear microdomains, where WOX5 gets recruited. These microdomains appear mostly in cells of young developing lateral root primordia but occasionally also in CSCs of the RAM. Because of their occurrence in tissues that must undergo cell fate determination, they may represent a marker for future cell differentiation.

Finally, by applying a new staining method for SCN phenotyping, this study uncovers a new link between SCN homeostasis and environmental stimuli, as the transcriptional regulator EARLY FLOWERING3 (ELF3) is involved in the control of QC quiescence and CSC maintenance in a PLT3-dependent manner (chapter V). The clock-related ELF3 is proposed to

act as a hub that connects a variety of processes including clock- and light-signalling, photosynthesis, hormone signalling, thermomorphogenesis and growth, thereby coordinating the responses on diverse environmental signals. Like PLT3, the ELF3 protein has PrDs and localises to microdomains. This localisation seems to be reversible and depends on external stimuli, as shown previously. Therefore, the flexible subcellular localisation could represent a mechanism to spatially and temporally separate the different cellular processes where ELF3 is involved, similar to the above-described signalling through plant receptor-complexes. Regarding SCN maintenance, ELF3 and PLT3 directly interact and locate together to nuclear microdomains as shown with fluorescence-lifetime imaging microscopy and localisation studies. These ELF3- and PLT3-containing microdomains, potentially also recruiting WOX5 as described above, might act as markers for cell-fate determination in response to environmental stimuli.

In summary, the results of this study add knowledge to the not yet fully understood intricate regulation of the SCN homeostasis in the root of *Arabidopsis thaliana*, that strongly depends on the formation of TF-complexes and their flexible subcellular localisation to microdomains. By understanding root stem cell fate regulation, a basis for research on more efficient root growth is created, that could aim at increasing the yield of crop plants in order to feed a growing world population and provide better resilience to the challenges of climate change.

Zusammenfassung

In dieser Arbeit wird die Funktion von Transkriptionsfaktor (TF)-Komplexen und deren subzellulären Lokalisation in Mikrodomänen in Bezug auf die Stammzellnischen (SZN)-Homöostase in der Wurzel von *Arabidopsis thaliana* untersucht. Zusätzlich wird eine Verbindung zwischen SZN-Erhaltung und dem Einfluss von externen Umweltreizen geschaffen.

In Kapitel I wird ein Überblick über bekannte TFs in der Regulation des Wurzelapikalmeristems gegeben. Dieser dient als Grundlage für weitere Untersuchungen und zeigt außerdem, dass WUSCHEL-RELATED-HOMEOBOX5 (WOX5) eines der wichtigsten Akteure in der Kontrolle des Wurzelstammzellschicksals sowie der Zellteilung im ruhenden Zentrum ist. Zudem wird eine Beteiligung von TF-Komplexen und deren flexible subzelluläre Lokalisation in der Regulation des Wurzelapikalmeristems anhand bekannter Beispiele diskutiert. Das zweite Kapitel über die Komplexbildung von Pflanzenrezeptoren diente als Beispiel für eine bekannte Funktion von Mikrodomänen in zellulären Signalwegen. Hierin vermittelt die schnelle und reversible Bildung von Mikrodomänen an der Plasmamembran die Fähigkeit einer zeitlichen und örtlichen Trennung der verschiedenen Signalantworten. Dies könnte ein allgemeiner Mechanismus sein, um die benötigten zellulären Prozesse räumlich und zeitlich präzise zu trennen, die als Antwort auf verschiedene temporäre Signale stattfinden.
In Kapitel III wird mithilfe von Experimenten zur Proteininteraktion und mathematischer Modellierung gezeigt, dass die Zellteilung im ruhenden Zentrum durch Interaktion der TFs BRAVO (BRASSINOSTEROIDS AT VASCULAR AND ORGANIZING CENTER) und WOX5 reguliert wird, und dies zum Erhalt des Ruhezustands des ruhenden Zentrums führt. Zudem wird in dieser Arbeit gezeigt, dass PLETHORAs (PLTs) und WOX5 beide den Ruhezustand des ruhenden Zentrums kontrollieren (Kapitel IV). Außerdem regulieren sie in Abhängigkeit voneinander den Erhalt der Columellastammzellen (CSZs), sowohl auf transkriptioneller Ebene als auch durch Protein-Protein-Interaktion. Prionen-ähnliche Domänen (PrDs) wurden in den PLTs gefunden, die die Proteininteraktion mit WOX5 vermitteln und die für die Lokalisation von PLT3 in nukleären Mikrodomänen verantwortlich sind, in die WOX5 rekrutiert wird. Diese Mikrodomänen kommen meistens in jungen, sich entwickelnden Organanlagen von Lateralwurzeln vor, sind aber gelegentlich auch in CSZs des Wurzelapikalmeristems zu finden. Aufgrund ihres Vorkommens in Geweben, deren

Zellschicksal noch nicht determiniert ist, könnten die Mikrodomänen als Marker für die zukünftige Zelldifferenzierung dienen.
Schließlich wird in Kapitel V dieser Arbeit durch die Anwendung einer neuen Färbemethode zur SZN-Phänotypisierung herausgefunden, dass eine Verbindung zwischen SZN-Homöostase und Umweltreizen besteht, da der Transkriptionsregulator EARLY FLOWERING3 (ELF3) zusammen mit PLT3 am Erhalt des Ruhezustands des ruhenden Zentrums und des CSZ-Schicksals beteiligt ist. ELF3 wirkt als Knotenpunkt, welcher eine Vielfalt an Prozessen verbindet. Hierzu gehören Signalprozesse hinsichtlich circadianer Uhr, Licht und Pflanzenhormonen, Photosynthese, Thermomorphogenese und Wachstum. Somit koordiniert ELF3 die Signalantworten verschiedener Umwelteinflüsse. Wie auch PLT3 enthält das ELF3 Protein PrDs und es lokalisiert in Mikrodomänen. Diese Lokalisation scheint reversibel zu sein und hängt von externen Reizen ab, wie bereits gezeigt wurde. Deshalb könnte die flexible subzelluläre Lokalisation ein Mechanismus zur räumlichen und zeitlichen Trennung der unterschiedlichen zellulären Prozesse sein, in die ELF3 involviert ist, ähnlich wie bei den zuvor beschriebenen Pflanzenrezeptoren. Hinsichtlich der SZN-Erhaltung wirken ELF3 und PLT3 durch direkte Proteininteraktion und lokalisieren zusammen in nukleären Mikrodomänen, wie mit bildgebender Fluoreszenzlebenszeit-Mikroskopie und Lokalisations-Experimenten gezeigt wurde. In diese Mikrodomänen wird, wie oben beschrieben, möglicherweise auch WOX5 rekrutiert und sie wirken vermutlich als Marker für die Determinierung des Zellschicksals in Antwort auf Umweltreize.

Zusammenfassend zeigen die Ergebnisse dieser Arbeit, dass die komplexe Regulation der SZN-Homöostase in der Wurzel von *Arabidopsis thaliana* von der Bildung bestimmter TF-Komplexe und ihrer flexiblen subzellulären Lokalisation in Mikrodomänen abhängt. Mit dem Verständnis über die Kontrolle des Wurzelstammzellschicksals kann eine Basis für die Forschung nach effizienterem Wurzelwachstum geschaffen werden, deren weiterführende Zielsetzung sowohl die Bewältigung der Ernährung einer wachsenden Weltbevölkerung durch ergiebigere Nutzpflanzen sein könnte, als auch eine stärkere Resilienz bei schwierigen Umweltbedingungen hinsichtlich des fortschreitenden Klimawandels.

Appendix

1. Abbreviations

%	percent
&	and
°C	degrees Celsius
µg	microgram
µM	micromolar
µm	micrometre
µs	microsecond
µW	microwatt
2D	two-dimensional
35S	promoter taken from CaMV for constitutive expression in plants
3D	three-dimensional
A. thaliana	*Arabidopsis thaliana*
A. tumefaciens	*Agrobacterium tumefaciens*
A555	Alexa Fluor® 555
aa	amino acid
ABCR	*Arabidopsis* Biological Resource Center
ACR4	ARABIDOPSIS CRINKLY4
AD	activation domain
AIL	AINTEGUMENTA-LIKE
AP2	APETALA2
ARF	AUXIN RESPONSE FACTOR
ARR1	ARABIDOPSIS RESPONSE REGULATOR1
AtFlot1	FLOTILLIN1
au	arbitrary unit
AUX	auxin
BAK1	BRI1 ASSOCIATED KINASE1
BBM	BABYBOOM
BD	DNA-binding domain
BES1	BRI1-EMS SUPRESSOR1
BES1-D	active form of BES1

BIB	BALD IBIS
BiFC	bimolecular fluorescence complementation
BIK1	BOTRYTIS-INDUCED KINASE1
BIR1, 2, 3	BAK1-INTERACTING RLK1, 2, 3
BKI1	BRI1 KINASE INHIBITOR1
BL	brassinolide
bp	base pairs
BR	brassinosteroid
BRAVO	BRASSINOSTEROID AT VASCULAR AND ORGANIZING CENTER
BRI1	BRASSINOSTEROID INSENSITIVE1
BRL	BRI1-LIKE
BRN1,2	BEARSKIN1,2
BRX	BREVIS RADIX
BSK1	BR-SIGNALLING KINASE1
c	cortex
C	Cerulean
CaMV	cauliflower mosaic virus
CC	columella cell
CDF4	CYCLIN DOF FACTOR4
cDNA	coding DNA
CDS	coding sequence
CEI	cortex endodermis initials
CFP	cyan fluorescent protein
CLC	CLATHRIN-LIGHT-CHAIN
CLE	CLAVATA3/EMBRYO SURROUNDING REGION
CLEL	CLE-like
CLV1, 2, 3	CLAVATA1, 2, 3
cm	centimetre
CMV	cytomegalovirus
Col	*Arabidopsis* ecotype Columbia
Col-0	*Arabidopsis* ecotype Columbia
CRN	CORYNE
CSC	columella stem cell

CSZ	Columellastammzellen
CuSO4	copper(II)-sulphate
CYCD	CYCLIN D
dag	days after germination
DAPI	4′,6-diamidin-2-phenylindol
das	days after sawing
DMSO	dimethyl sulfoxide
DNA	deoxy-ribonucleic acid
DPBS	Dulbecco's Phosphate Buffered Saline
e.g.	example given
EC	evening complex
ED	extracellular domain
EDTA	ethylenediaminetetraacetic acid
EdU	5-ethynyl-2’-deoxyuridine
EFR	EF-Tu RECEPTOR
EF-Tu	ELONGATION FACTOR-TU
EGF	epidermal growth factor
Ei	beta-estradiol inducible
ELF3	EARLY FLOWERING3
ELF3ΔPrD	prion-domain deletion variant of ELF3
ELF3ΔQ	poly-glutamine deletion variant of ELF3
en	endodermis
ep	epidermis
erCFP	endoplasmic reticulum localised CFP
ERF	ETHYLENE RESPONSE FACTOR
Est.	beta-estradiol
EtOH	ethanol
EU	5-ethynyl-2’-uridine
ext	extracellular
eYFP	enhanced YFP
eYFPC	C-terminal part of eYFP
eYFPN	N-terminal part of eYFP
F	forward
FBS	foetal bovine serum

FC	fold change
FCA	FLOWERING CONTROL LOCUS A
FCCS	fluorescence cross-correlation spectroscopy
FER	FERONIA
FLIM	fluorescence lifetime imaging microscopy
FLS2	FLAGELLIN SENSITIVE2
FP	fluorescent protein
FRET	Förster Resonance Energy Transfer
g	gram
GFP	green fluorescent protein
GLV	GOLVEN
GR	glucocorticoid receptor
H	histidine
h	hours
H3K4me3	tri-methylated histone H3 lysine 4
HD-ZIP	homeodomain leucine zipper
HeLa	human cell line, cells taken from cervical cancer from Henrietta Lacks
HEp-2	human epithelial cell line from a human cervix carcinoma, HeLa derivative
His	histidine
i.	inducible
i.e.	id est
IAA	indole-3-acetic acid
IDR	intrinsically disordered region
int	intracellular
IRF	instrument response function
JA	jasmonic acid
JKD	JACKDAW
KD	kinase domain
KI	potassium-iodide
L	leucine
Leu	leucine
LLPS	liquid-liquid phase separation
LRC	lateral root cap

LRP	lateral root primordium
LRR	leucine rich repeat
LSM	laser scanning microscope
LUX	LUX ARRHYTHMO
LysM	lysin motif
mC	mCherry
mCh	mCherry
MES	2-(N-morpholino)-ethane sulfonic acid hydrate
MFIS	multiparameter fluorescence imaging spectroscopy
MGP	MAGPIE
MHz	mega hertz
min	minute
MIP	maximum intensity projection
miRNA	micro RNA
ml	millilitre
mm	millimetre
mM	millimolar
mPS-PI	modified pseudo Schiff base propidium iodide
mRb	mRuby2
MS	Murashige and Skoog
mV	mVenus
MYC2	MYC2/JASMONATE INSENSITIVE1
n	number
N	asparagine
N. benthamiana	*Nicotiana benthamiana*
NA	numeric aperture
NaCl	sodium chloride
NB	nuclear body
ng	nanogram
NLS	nuclear localisation signal
nm	nanometre
nM	nanomolar
ns	nanosecond
NTT	NO TRANSMITTING TRACT

NUT	NUTCRACKER
OD	optical density
ori	origin of replication
P3	PLT3
PAMP	pathogen associated molecular pattern
pBRAVO	promoter of *BRAVO*
PBS	phosphate-buffered saline
PCD	periclinal cell division
pCMV	constitutive promoter for human cell lines, taken from CMV
PCR	polymerase chain reaction
pELF3	promoter of *ELF3*
PHB	PHABULOSA
phyB	PHYTOCHROME B
PI	propidium iodide
PIF	PHYTOCHROME INTERACTING FACTOR
PIN	PINFORMED
PLT	PLETHORA
PLT3ΔPrD	prion-domain deletion variant of PLT3
PLT3ΔQ	poly-glutamine deletion variant of PLT3
PM	plasma membrane
polyA	poly-adenylation site
polyQ	poly glutamine
pPLT3	promoter of *PLT3*
PrD	prion-like domain
PRR	pattern recognition receptor
PTI	PRR-triggered immunity
pWOX5	promoter of *WOX5*
Q	glutamine
QC	quiescent centre
R	reverse
RALF	RAPID ALKALINIZATION FACTOR
RAM	root apical meristem
RBR	RETINOBLASTOMA-RELATED
RGF	ROOT MERISTEM GROWTH FACTOR

RLK	receptor-like kinase
RLP	receptor-like protein
RM	root meristem
RNA	ribonucleic acid
RNAseq	RNA sequencing
ROI	region of interest
ROS	reactive oxygen species
ROW1	REPRESSOR OF WUSCHEL1
RT-qPCR	real-time quantitative polymerase chain reaction
s	second
SAM	shoot apical meristem
SCN	stem cell niche
SCR	SCARECROW
SD medium	synthetic defined medium
SERK3	SOMATIC EMBRYOGENESIS RECEPTOR KINASE3
SHR	SHORTROOT
SHY2	SHORT HYPOCOTYL2
SIEL	SHORT ROOT INTERACTING EMBRYONIC LETHAL
SMB	SOMBRERO
SPAD	single-photon avalanche diode
SPT	SPATULA
SPT	single particle tracking
SSO-FLIM	Selected Surface Observation-FLIM
st. dev.	standard deviation
SV40	simian virus 40
SZN	Stammzellnische
T3A	ribulose-1,5-bisphosphate carboxylase 3A subunit terminator
TCP	TF family, named after the first four characterized members (TEOSINTE BRANCHED1, CYCLOIDEA, PROLIFERATING CELL NUCLEAR ANTIGEN FACTOR1 & 2)
TCSPC	time correlated single photon counting
TF	transcription factor
TMD	transmembrane domain
TMO7	TARGET OF MONOPTEROS7

TOR	target of rapamycin
TPL	TOPLESS
Tris	tris(hydroxymethyl)aminomethane
Trp	tryptophane
tUBQ10	UBQ10 terminator
U	enzyme unit for one 1 µmol substrate per minute
UBQ10	POLYUBIQUITIN 10
UPB1	UPBEAT1
USA	United States of America
v/v	volume by volume
VAEM	variable angle epifluorescence microscopy
VA-TIRFM	variable angle total internal reflection microscopy
VSC	vascular stem cells
W	tryptophane
w/v	weight by volume
W5	WOX5
WOX5	WUSCHEL RELATED HOMEOBOX5
WT	wild type
WUS	WUSCHEL
Y2H	yeast-two-hybrid
YFC	C-terminal part of eYFP
YFN	N-terminal part of eYFP
YFP	yellow fluorescent protein
β-Est.	beta-estradiol
Δτ	fluorescence lifetime decrease
τ	fluorescence lifetime

2. Exemplary plasmid maps

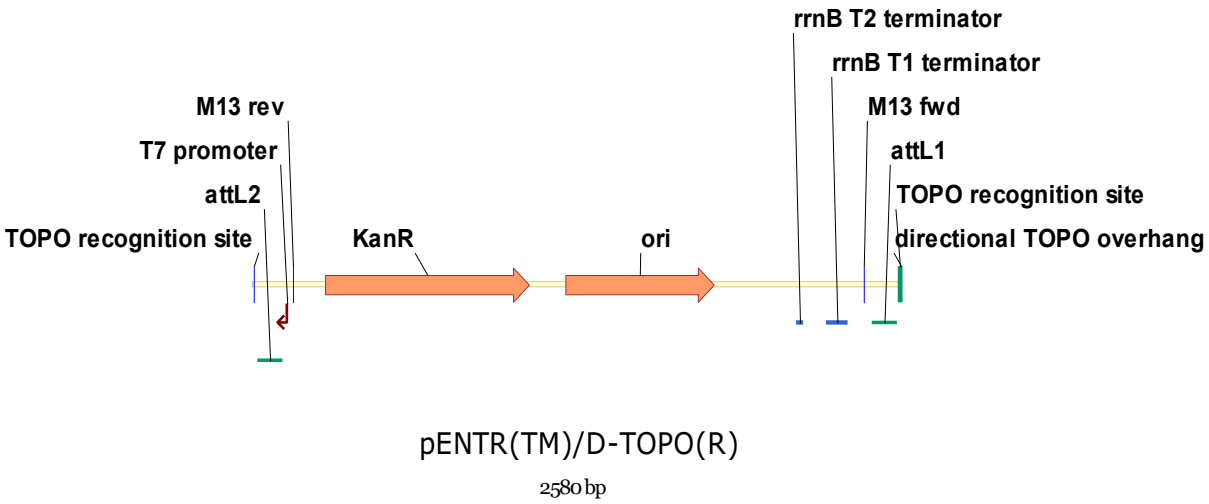

Plasmid map 1: Empty Gateway™ entry vector pENTR™/D-TOPO® (Invitrogen™, Thermo Fisher Scientific Inc.)

Empty entry vector for the introduction of PCR products by TOPO-cloning (Gateway™ pENTR™/D-TOPO™ cloning kit, Invitrogen™, Thermo Fisher Scientific Inc.). KmR = Kanamycin resistance; ori = origin of replication; M13 rev/fwd are reverse and forward primer binding sites for sequencing. attL: Gateway recombination sites for LR-reaction. rrnB T1 and T2 transcription terminators are termination regions of the rrnB gene in *Escherichia coli*. T7 promoter is a promoter for expression in *Escherichia coli*.

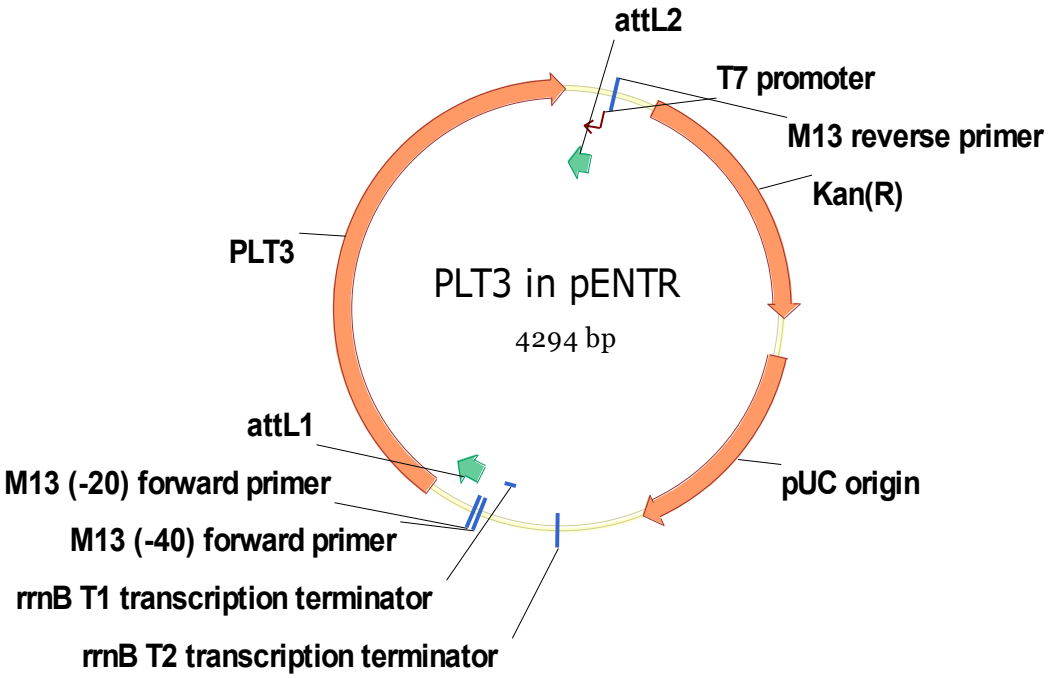

Plasmid map 2: Exemplary Gateway™ entry vector with PLT3

This entry vector was used for LR-reactions with the Gateway™ LR Clonase™ II Enzyme Mix (Invitrogen™, Thermo Fisher Scientific Inc.) to create expression plasmids. PLT3 = PLETHORA3; Kan(R) = Kanamycin resistance; pUC origin: origin of replication. M13 primer: reverse and forward primer binding sites for sequencing. attL: Gateway™ recombination sites for LR-reaction. rrnB T1 and T2 transcription terminators are termination regions of the rrnB gene in *Escherichia coli*. T7 promoter is a promoter for expression in *Escherichia coli*.

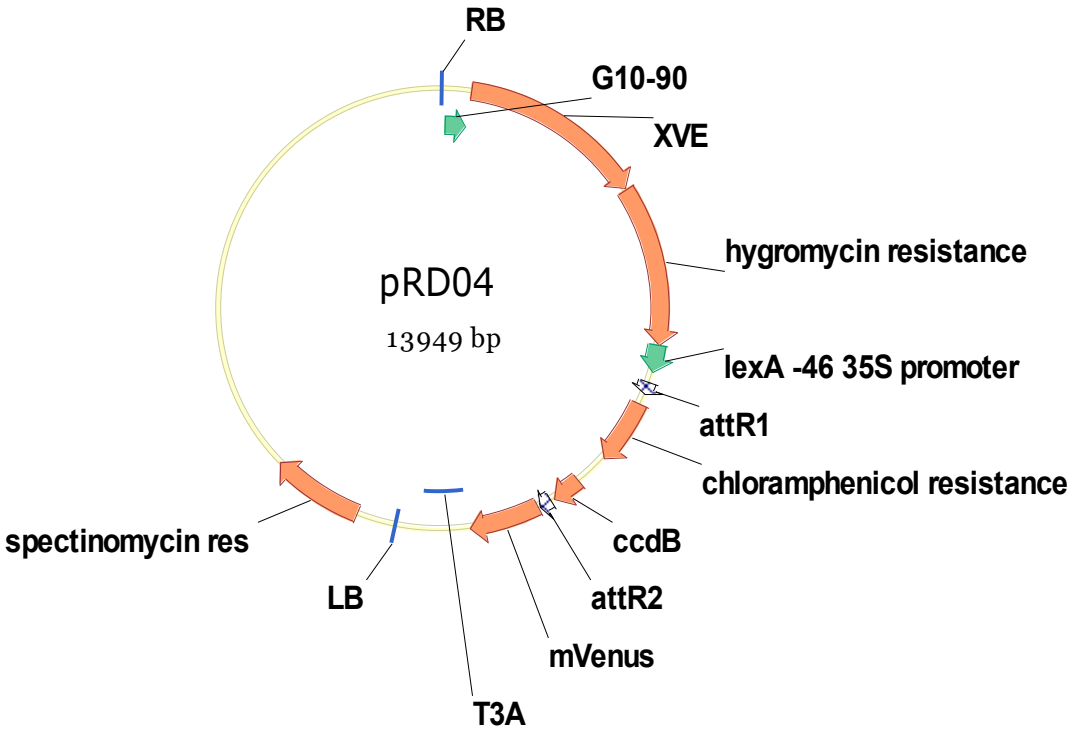

Plasmid map 3: Exemplary Gateway™ destination vector with mVenus

Empty Gateway™ destination vector for LR-reaction with the Gateway™ LR Clonase™ II Enzyme Mix (Invitrogen™, Thermo Fisher Scientific Inc.) to create expression plasmids for C-terminally mVenus-tagged fusion proteins. LB = left border; RB = right border; spectinomycin res = spectinomycin resistance; T3A: plant specific terminator. attR: Gateway™ recombination sites; ccdB: cytotoxic gene as negative selection marker, is removed after LR-reaction. G10-90: strong constitutive promoter drives XVE expression. XVE: chimeric transcriptional activator, is activated by β-estradiol and binds to its target promoter LexA -46 35S (consists of eight copies of the LexA operator upstream of the -46 35S minimal promoter).

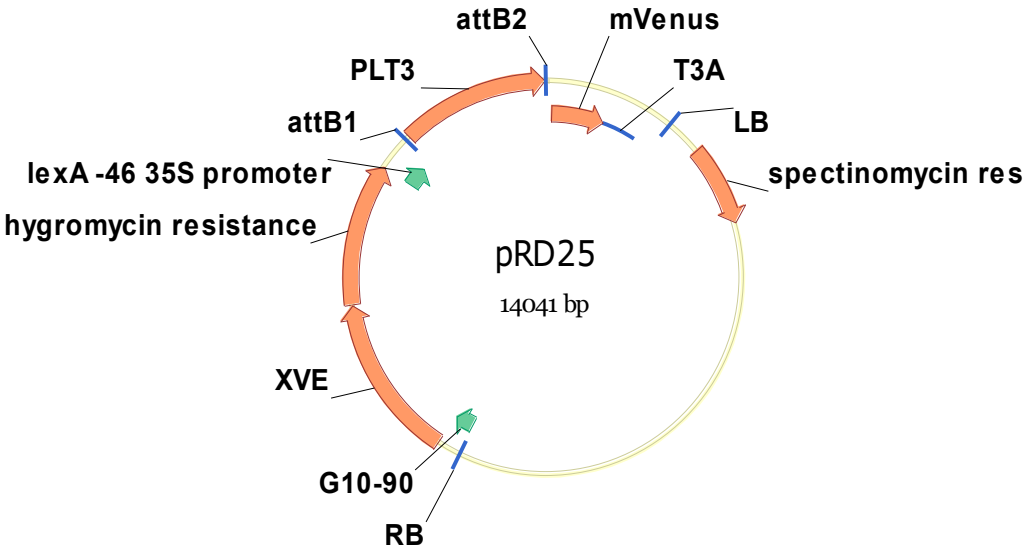

Plasmid map 4: Exemplary Gateway™ expression vector for β-estradiol inducible PLT3-mVenus

Expression vector for mVenus-tagged PLT3, resulted from an LR-reaction. PLT3 = PLETHORA3; LB = left border; RB = right border; spectinomycin res = spectinomycin resistance; T3A: plant specific terminator. attB: Gateway™ recombination sites. G10-90: strong constitutive promoter drives XVE expression. XVE: chimeric transcriptional activator, is activated by β-estradiol and binds to its target promoter LexA -46 35S (consists of eight copies of the LexA operator upstream of the -46 35S minimal promoter).

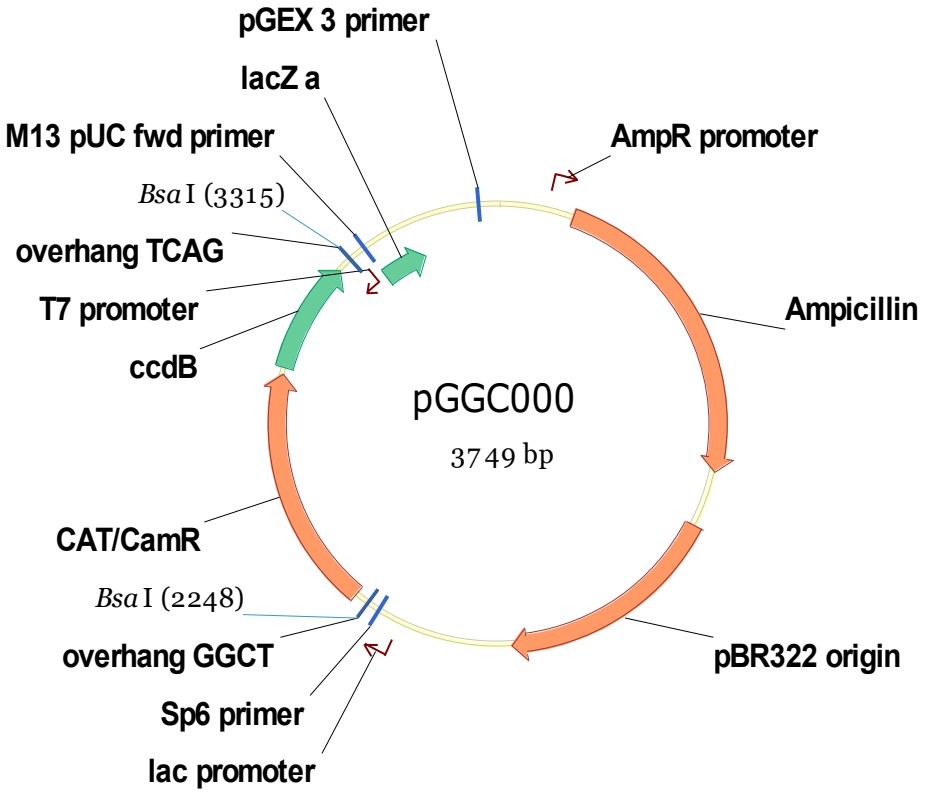

Plasmid map 5: Empty GreenGate entry vector pGGC000

Empty GreenGate entry vector for introduction of a gene of interest with *BsaI* restriction/ligation. AmpR = Ampicillin resistance; CAT/CamR = Chloramphenicol resistance; lac promoter = lactose promoter; *BsaI*: recognition sites for the *BsaI* restriction enzyme. SP6 primer, M13 primer, pGEX 3 primer and T7 promoter are primer binding sites for sequencing. The overhangs (GGCT and TCAG) are needed for the directed ligation of a PCR product after *BsaI* digestion. ccdB: cytotoxic gene as negative selection marker, is removed after *BsaI* restriction. pBR322: origin of replication. lacZ: gene that encodes for β-galactosidase.

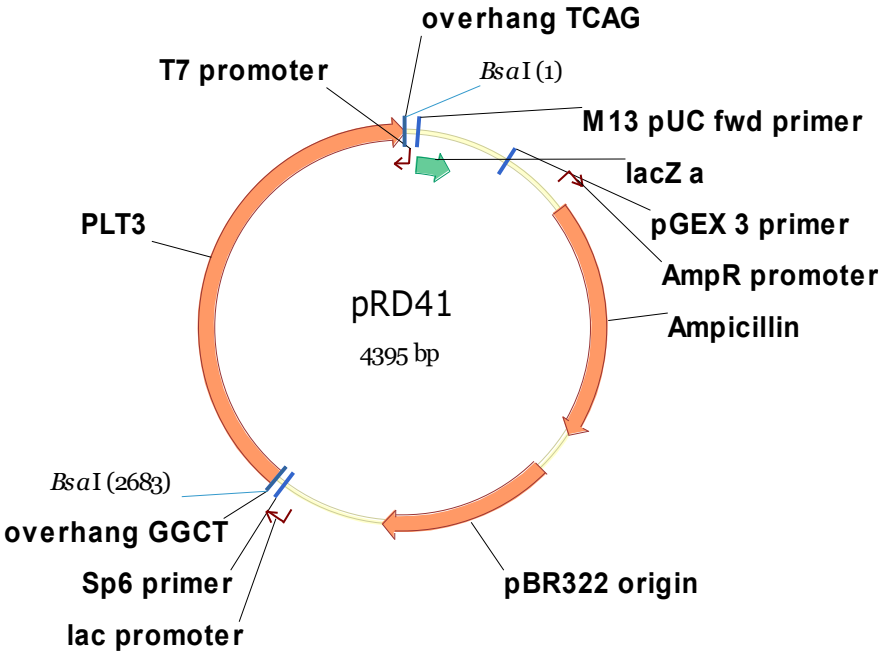

Plasmid map 6: Exemplary GreenGate CDS-module entry vector with PLT3

The entry vector was used for a GreenGate reaction, where six modules from six different entry vectors are assembled in one destination vector. PLT3 = PLETHORA3; AmpR = Ampicillin resistance; lac promoter = lactose promoter; *BsaI*: recognition sites for the *BsaI* restriction enzyme. SP6 primer, M13 primer, pGEX 3 primer and T7 promoter are primer binding sites for sequencing. The overhangs (GGCT and TCAG) were used for the directed ligation of PLT3 after *BsaI* digestion. pBR322: origin of replication. lacZ: gene that encodes for β-galactosidase.

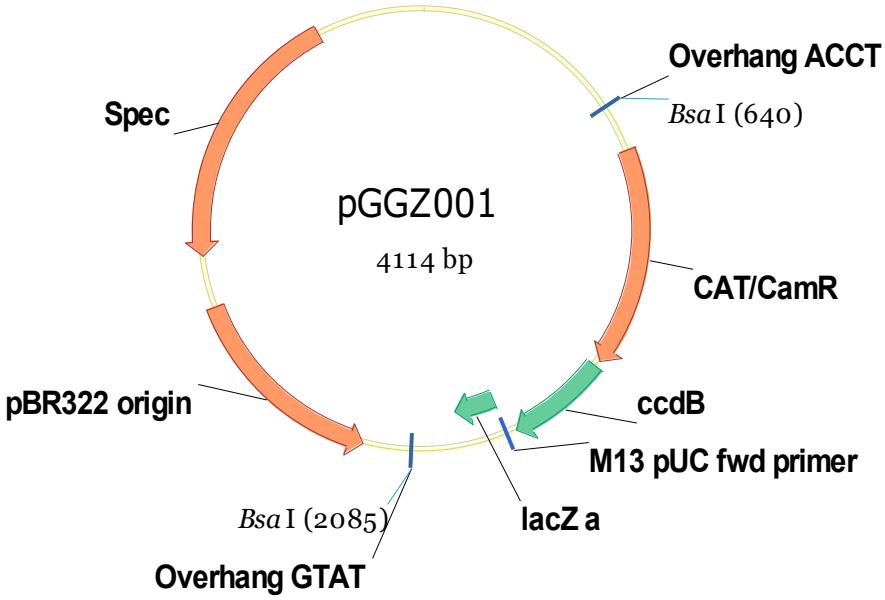

Plasmid map 7: Empty GreenGate destination vector pGGZ001

Empty GreenGate destination vector for the introduction of an expression cassette by GreenGate reaction. Spec = Spectinomycin resistance; CAT/CamR = Chloramphenicol resistance; *BsaI*: recognition sites for the *BsaI* restriction enzyme. M13 primer is a primer binding site for sequencing. The overhangs (AACT and GTAT) are needed for the directed ligation of the expression cassette after *BsaI* digestion. ccdB: cytotoxic gene as negative selection marker, is removed after *BsaI* restriction. pBR322: origin of replication. lacZ: gene that encodes for β-galactosidase.

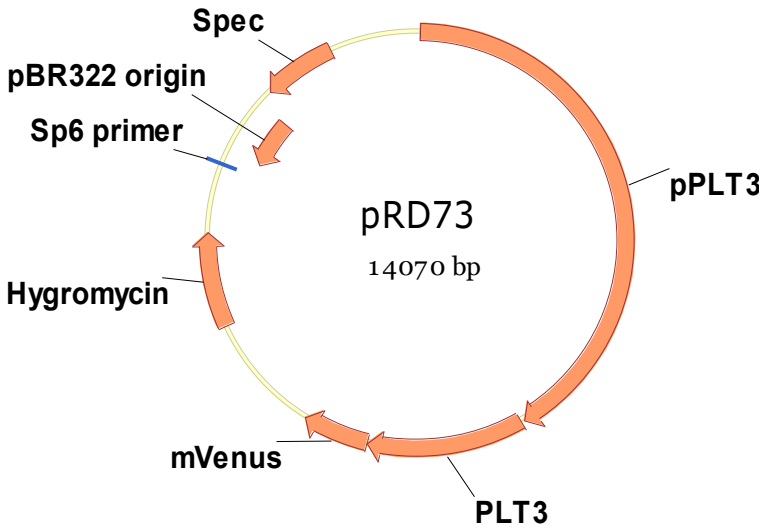

Plasmid map 8: Exemplary GreenGate expression vector with pPLT3::PLT3-mVenus

GreenGate expression vector for expression of mVenus-tagged PLT3 under the control of the endogenous PLT3 promoter. PLT3 = PLETHORA3; pPLT3 = promoter of PLT3; Spec = Spectinomycin resistance; Hygromycin = Hygromycin resistance; SP6 primer is a primer binding site for sequencing. pBR322 origin: origin of replication.

3. List of figures

Figure I-1:	Arabidopsis meristematic zone organization and regulation of WOX5 expression in the QC	11
Figure II-1:	BRI1/BAK1 (SERK3) and FLS2/BAK1 (SERK3) receptor complexes in PM microdomains	21
Figure II-2:	CLV1/CLV2/CRN receptor complexes in PM microdomains	23
Figure III-1:	BRAVO and WOX5 are required for the QC identity and stem cells maintenance	29
Figure III-2:	BRAVO and WOX5 reinforce each other at the root stem cell niche	31
Figure III-3:	WOX5 activates BRAVO which in turn alleviates WOX5 self-inhibition in the stem cell niche	34
Figure III-4:	BRAVO interacts with WOX5	36
Figure III-5:	BRAVO and WOX5 have a joint role in repressing QC divisions	38
Figure IV-1:	WOX5 positively regulates *PLT3* expression	69
Figure IV-2:	PLTs constrain the WOX5 expression domain	70
Figure IV-3:	*plt* and *wox5* mutants show more CSC differentiation and QC divisions	72
Figure IV-4:	QC divisions correlate negatively with the number of CSC layers	75
Figure IV-5:	PLT3 localises to NBs in *Arabidopsis thaliana* LRPs and CSCs	76
Figure IV-6:	PLT3 PrDs influence its subnuclear localisation	77
Figure IV-7:	WOX5 can interact with PLTs	80
Figure IV-8:	Model of PLT and WOX5 transcriptional regulation, interaction and subnuclear localisation during distal root stem cell maintenance	84
Figure V-1:	Localisation of PLT3 and ELF3 in the SCN of *Arabidopsis thaliana*	114
Figure V-2:	CSC and QC phenotypes of *Col* wildtype and *elf3* and *plt3* single and double mutants	116
Figure V-3:	QC divisions correlate with the number of CSC layers	117
Figure V-4:	Domain-dependent subcellular (co)-localisation of ELF3 and PLT3 in *N. benthamiana*	120
Figure V-5:	PLT3-dependent nuclear recruitment of ELF3 is mediated by the PLT3 PrDs	122
Figure V-6:	Tracking reveals a higher mobility for ELF3 bodies than PLT3-bodies in *N. benthamiana*.	124

Figure V-7: ELF3 and PLT3 interaction is mediated by the PrDs in *N. benthamiana* 126

Figure V-8: PIF3 and PIF4 import ELF3 to the nucleus and co-localise with PLT3 in HEp-2 cells 128

Figure V-9: PLT3 co-localises and interacts with PIF proteins in *N. benthamiana* 130

Figure V-10: Model of *A. thaliana* distal root stem cell fate regulation via dynamic differential subnuclear localisation of transcription factor complexes, integrating external cues through ELF3 135

4. List of tables

Table I-1: Transcription factors (TFs) in RAM maintenance 12

Table II-1: Live cell imaging techniques used to study receptor complexes at the PM 20

5. List of supplementary figures

Supplementary figure III-1: Medial longitudinal view of the *Arabidopsis thaliana* primary root apex 54

Supplementary figure III-2: BRAVO and WOX5 promote primary root growth and lateral root development 55

Supplementary figure III-3: BRAVO and WOX5 expression patterns in overexpressor lines 56

Supplementary figure III-4: BRAVO expression in the *bravo wox5* mutant background 57

Supplementary figure III-5: BRAVO and WOX5 expression is BL regulated 58

Supplementary figure III-6: Biochemical interactions of BRAVO and WOX5 with BES1 and TPL 59

Supplementary figure III-7: ROIs used for the quantification of the GFP 60

Supplementary figure IV-2: Expression of WOX5-mVenus and PLT3-mVenus rescues the respective mutant phenotypes 97

Supplementary figure IV-1: *plt* and *wox5* mutants show more periclinal cell divisions in the QC 96

Supplementary figure IV-3: WOX5 does not interact with PLT3 in established *Arabidopsis* root meristems 98

Supplementary figure IV-4: Subnuclear localisation and PrD prediction of WOX5, PLT1, PLT2 and PLT3 99

Supplementary figure IV-5: PLT3-NB formation is concentration-dependent 100

Supplementary figure V-1: Localisation of ELF3-mV and ELF3ΔPrD-mV in the RAM of *A. thaliana* 148

Supplementary figure V-2: Phenotypes of *Col wild* type, elf3 mutant and transgenic rescue lines 149

6. List of supplementary tables

Supplementary table III-1: Parameter values for the model of BRAVO and WOX5, used to generate the data in Figure III-3 61

Supplementary table III-2: List of plant material lines used in this study 61

Supplementary table III-3: List of primers used in this study 62

Supplementary table IV-1: List of cloning primers 102

Supplementary table IV-2: List of genotyping primers 103

Supplementary table IV-3: List of expression vectors used in this study 104

Supplementary table IV-4: *Arabidopsis* mutants and transgenic lines 105

Supplementary table IV-5: Intensity values of transcriptional and translational FP tagged PLT3 expression experiments in *Col-0* and *wox5* related to Figure IV-1 106

Supplementary table IV-6: Quantification of transcriptional mVenus tagged WOX5 expression in the QC region of *Col* and *plt2, plt3* related to Figure IV-2 107

Supplementary table IV-7: Average QC and CSC phenotypes related to Figure IV-3 107

Supplementary table IV-8: Percentage of periclinal cell divisions in the QC shown in Supplementary figure IV-1 108

Supplementary table IV-9: Average QC and CSC phenotypes of rescue experiments 108

Supplementary table IV-11: FLIM results of subnuclear data analysis in WOX5-mV and PLT3-mCh co-expressing *N. benthamiana* epidermal cells related to Figure IV-7 109

Supplementary table V-1: List of primers for GreenGate cloning 150

Supplementary table V-2: List of primers for Gateway Cloning 151

Supplementary table V-3: List of genotyping primers 151

Supplementary table V-4: List of GreenGate expression vectors used in this study 152

Supplementary table V-5: List of Gateway expression vectors used in this study 153

Supplementary table V-6:	*Arabidopsis* mutants and transgenic lines	153
Supplementary table V-7:	Average QC and CSC phenotypes related to Figure V-3	154
Supplementary table V-8:	Average nuclear/cytoplasmic intensity ratio of ELF3-mVenus variant expressing *N. benthamiana* leaf epidermal cells with and without PLT3-mCherry variant co-expression (related to Figure V-5)	154
Supplementary Table V-9:	Average hypocotyl length in *elf3* rescue experiment (related to Supplementary figure V-2e)	154
Supplementary table V-10:	Average leaf area in *elf3* rescue experiments (related to Supplementary figure V-2f)	154
Supplementary table V-11:	Average number of leaves in *elf3* rescue experiments (related to Supplementary figure V-2k)	155
Supplementary table V-12:	Average speed and displacement length of the body-tracking in ELF3-mVenus and PLT3-mVenus expressing *N. benthamiana* epidermal leaf cells (related to Figure V-6)	155
Supplementary table V-13:	Average fluorescence lifetimes (τ) and standard deviation (st. dev.) obtained in FLIM experiments and corresponding lifetime changes (Δτ) in comparison to the donor only. The Δτ were calculated from each experiment separately.	156
Supplementary table V-14:	Average fluorescence lifetimes (τ) and standard deviation (st. dev.) obtained in FLIM experiments with PIF-proteins and corresponding lifetime changes (Δτ) in comparison to the donor only.	156

7. List of supplementary movies

Supplementary movie IV-1:	Dynamic formation of nuclear bodies in a PLT3-mVenus expressing LRP	101

Acknowledgements - Danksagung

First and most importantly, I want to thank Yvonne for the opportunity to do this PhD. Thank you for all the support you gave the last six (or seven?) years during my Master thesis and my PhD. Thank you for always being positive and confident, especially when I am not. Thank you for your patience when things didn't work. Thank you for giving me all flexibility I needed since the birth of my son Noah. Thank you for your understanding in terms of motherhood. Thank you for being the best boss one can have.

Thanks to Rüdiger for providing the lab and office space. Thank you also for being critical, sometimes this helps to progress. Thank you for ideas and discussion. And finally, thank you for the organisation of the lab retreats, they were fun.

Thanks to Georg Groth for being my co-supervisor. Unfortunately, we didn't have much contact, but this just means that everything went well.

Thanks to the Center for Advanced Imaging (CAi), especially Steffi and Sebastian, for being there in case of microscope issues and for advice regarding image analysis. Thank you both also for teaching me in mammalian cell culture.

Thanks to all lab members, including the technicians Cornelia, Silke and Carin, our lab manager Karine, the other PhDs Jenia, Patrick, Vivien, Mehdi and Isaia and the only currently available postdoc Vicky. You make this lab a wonderful working place with a great atmosphere. Thanks also to the ones that already left but I had the luck to know them: Maike (Of course you will be back soon!), Greg, Nozomi, Gwen, Adrian, Julia, Petra, Barbara, Avantika and all the bachelor and master students. Thanks for the great atmosphere and a great common time.

Thanks to my first master student Philipp for starting together with me in this project and for sharing the first year. Thank you for finding out with me, where all this leads to and how things work. Thank you for teaching me how to work with *Arabidopsis* and thanks for all the good conversations.

Thanks to Laura, my second master student. You made my second year. Thank you for your good mood and thanks for the work you've done. It helped to complete this thesis.

Thanks a lot to Vivien, who started as my third master student and is doing her own PhD now. Thank you for all the effort you made to complete my experiments in times when I couldn't do it. Not only during maternity but also afterwards. You stayed until the end.

Thanks to Cornelia for helping me with this big amount of plant work in the end.

Thanks to Abdullah for carrying out experiments again and again. Thank you for your support during my pregnancy and maternity. I know you doubt it, but you really helped. It's vollkommen okay. And thank you for having a good time together. I wish both of you and your little baby all the best.

Thanks to Gwen for the good preparatory work. I used some of your *Arabidopsis* lines. And thank you for our trip to India, I think in the end it was somehow fun (I know you don't think like this). I really appreciated your company.

Thanks to Avantika. Thank you that you have been part of this period in my life. Thank you for being a friend right from the start. Thanks for all the good tea times, I missed it when you left. And thank you for your invitation to India.

Thanks to Andrea Bleckmann for all the cloning work. I never met you, but I know your plasmids.

Thanks to Yvonne and Vicky for proof-reading and discussion.

Natürlich möchte ich meinen Eltern dafür danken, dass sie immer für mich da sind. Ohne euch wäre ich nicht dort, wo ich jetzt bin.

Außerdem möchte ich meinen Schwiegereltern Susanne und Volker dafür danken, dass sie Teil meines Lebens sind. Danke für all die Unterstützung, Anteilnahme und Liebe. Ihr seid meine Familie in Düsseldorf.

Ich möchte auch meinem Mann Thomas danken, der mit mir durch gute, schlechte und zermürbende Zeiten gegangen ist, der versucht hat meine Arbeit zu verstehen und der mich bis zum Ende ertragen hat. Danke fürs Spülmaschine ausräumen. Meine Vernachlässigung unserer häuslichen Umgebung während meiner Schreibphase tut mir leid. Und danke für den unvoreingenommenen Blick des Außenstehenden. Ich liebe dich.

Schließlich möchte ich meinem Sohn Noah danken.
Ich weiß, du bist noch zu klein, um das jetzt zu verstehen, aber du warst für mich der wichtigste Teil in diesem Lebensabschnitt.
Danke, dass du mich ablenkst, wenn ich zu versunken bin.
Danke, dass du mich in die Wirklichkeit zurückholst, wenn mein Kopf noch woanders ist, vor allem nach langen Schreibtagen.
Danke für die Liebe, die du in mein Leben und in die diese Arbeit gebracht hast.
Du machst jeden Tag zu etwas Besonderem.

Vor Noahs Mittagsschlaf:
"Noah, wir müssen erst neue Bezüge aufs Bett machen."
Noah reagiert mit Begeisterung und beginnt, seine neuen Brio-Züge auf Papas Bett zu stellen.